Frequency Agile Materials for Electronics

Final Report

Date: 11/11/02

Period covered in this report: 6/1/98 through 6/1/01

Program Title: Novel Ferroelectric Materials for Satellite Communications

Contract # DABT63-98-C-0046

Performing Organization: DuPont Superconductivity

Subcontractor: University of Colorado at Boulder

Summary and Highlights:

This report summarizes work performed by DuPont and the University of Colorado under the DARPA sponsored FAME program. The work was divided into seven key task areas which are summarized in the highlight sections below. Additional detail is provided in the twelve quarterly progress reports which are attached as part of this Final Report.

Task 1 Highlights - Large Area Sputtered Film Manufacturing for Cryogenic Temperature

The first generation material developed and optimized (by experimental design) for cryogenic operation was $Ba_xSr_{1-x}TiO_3$ (x=0.06). Consecutive runs on 2-inch $LaAlO_3$ substrates showed excellent uniformity across the wafer (~7% variation in ε) and run-to-run reproducibility (~6% variation in ε run to run). Typical temperature dependence of the figure of merit, K, measured at 1 MHz for these materials shows a maximum value of about 20 at about 77 K.

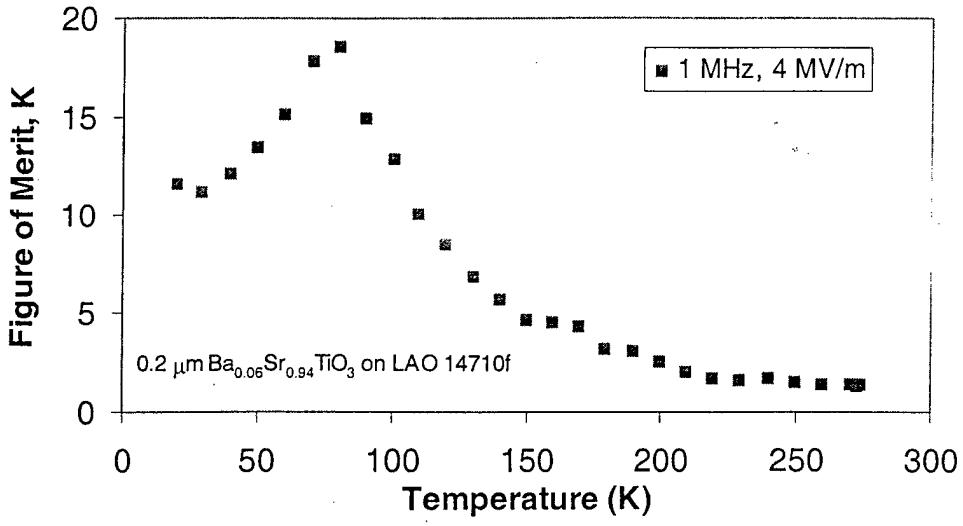

Figure 1 - Figure of merit K for optimized $Ba_xSr_{1-x}TiO_3$ (x=0.06) films on $LaAlO_3$.

The second generation material chosen for optimization on 2-inch wafers was $Ca_{0.05}Sr_{0.95}TiO_3$. Optimization of this material, including post deposition annealing in O_2 at 1000° C, showed similar performance to the first generation material, $Ba_xSr_{1-x}TiO_3$ (x=0.06).

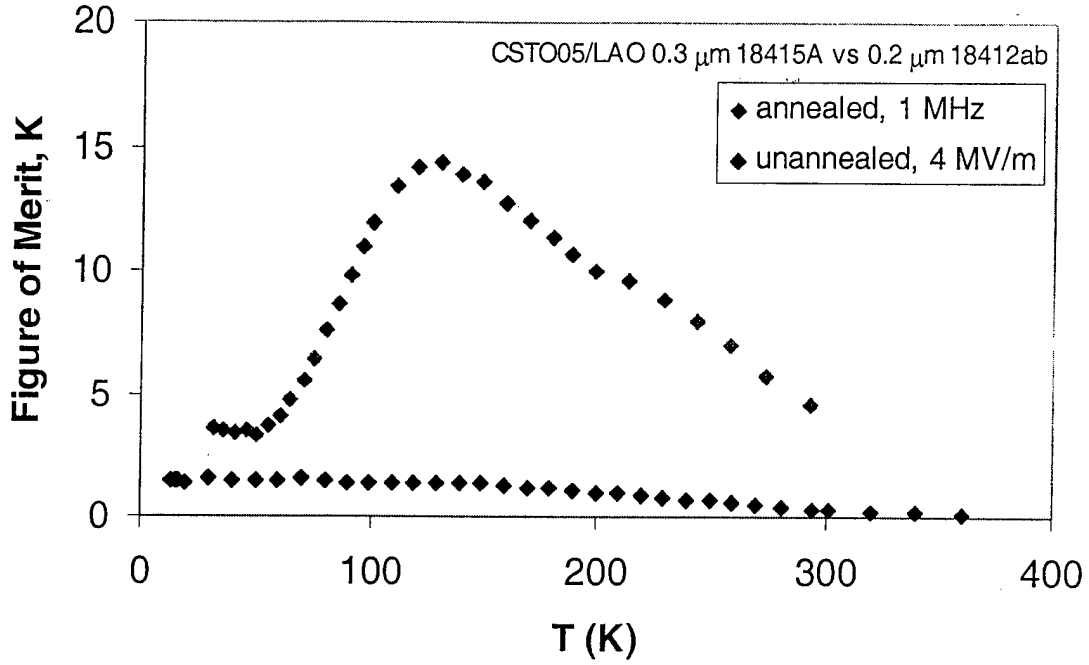

Figure 2 - Figure of merit, K, for optimized $Ca_{0.05}Sr_{0.95}TiO_3$ films on $LaAlO_3$

Task 2 Highlights - Large Area Sputtered Film Manufacturing for Ambient Temperature

The first generation material developed and optimized (by experimental design) for ambient temperature operation was $Ba_xSr_{1-x}TiO_3$ (x=0.6). Consecutive runs on 2-inch $LaAlO_3$ substrates showed excellent uniformity across the wafer (~6% variation in ε) and run-to-run reproducibility (~3% variation in ε run to run). Typical temperature dependence of the figure of merit, K, measured at 1 MHz for these materials shows a maximum value of about 2.5 (see figure 3 below). The second generation material developed for ambient temperature operation was $CaCu_3Ti_4O_{12}$. This material was initial explored in bulk form in Task 5 (Materials Discovery Research) and identified as a promising candidate for thin film development based on its extremely large dielectric constant (>10,000) albeit with high loss. The hope was that high quality thin films of this material would have reduced loss and an improved figure of merit.

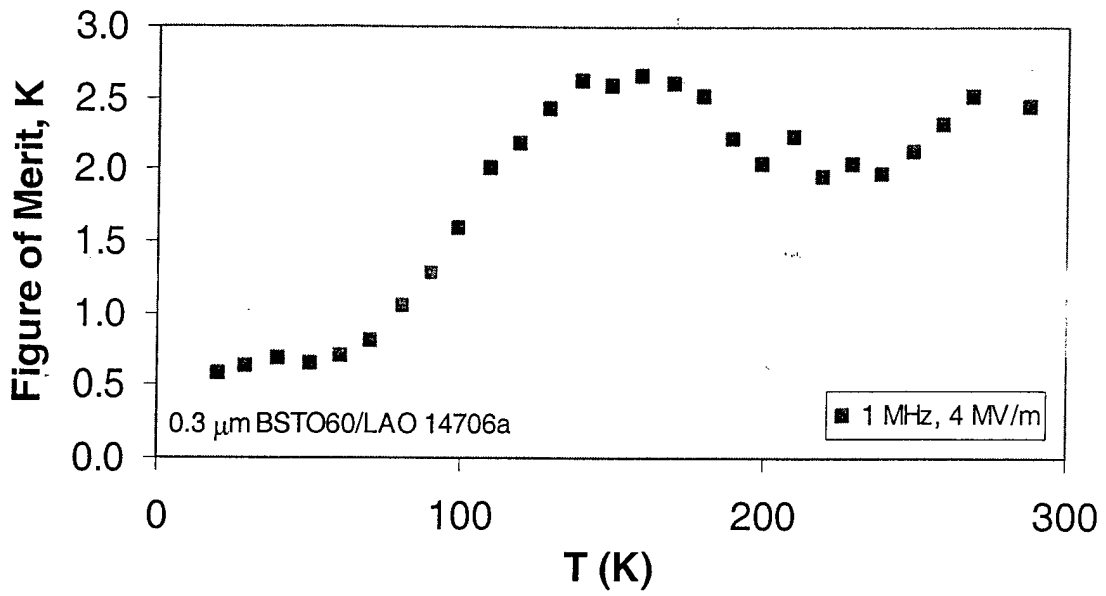

Figure 3 - Figure of merit K for optimized $Ba_xSr_{1-x}TiO_3$ (x=0.6) films on $LaAlO_3$.

While it was possible to achieve high values of permittivity and tunability for $CaCu_3Ti_4O_{12}$ thin films, the observed values of loss were also very high which resulted in K values in the range of 1 to 8.

Task 3 Highlights - Multilayer Film Development and Manufacturing

Multilayer film development has focused on the development of high quality YBCO films on top of thick (>0.5 μm) $Ba_xSr_{1-x}TiO_3$ (x=0.06) films. A series of experiments demonstrated that BSTO films up to 800 nm thick could be produced with a surface roughness of less than 2 nm. 350 nm thick YBCO produced on top of these thick BSTO films had good epitaxial alignment and low microwave surface resistance (< 600 μΩ).

Task 4 Highlights - Exploratory Laser Ablation Processing (University of Colorado)

The purpose of this task was to rapidly explore a wide range of material compositions for possible manufacturing implementation at DuPont. Materials explored and corresponding results are summarized in the following table.

Material	Results and Observations
$Ca_{0.05}Sr_{0.95}Ti_{0.98}Fe_{0.02}O_3$	No well defined ferroelectric transition. Negligible tunability but low loss (tan δ ~ $5x10^{-3}$)
$Ca_{0.05}Sr_{0.95}Ti_{0.98}Mn_{0.02}O_3$	T_c ~ 60 K (broad transition). Promising tunability and tan δ ~ $8x10^{-3}$
$Ba_{0.05}Sr_{0.95}TiO_3$	Small tunability and tan δ ~ $3x10^{-3}$
$Ba_{0.6}Sr_{0.4}Ti_{0.96}Mn_{0.04}O_3$	Tc~280 K, moderate tunability and tan δ ~1x10-3
$Ba_{0.6}Sr_{0.4}Ti_{0.98}Mn_{0.01}W_{0.01}O_3$	Tc~325 K, moderate tunability and tan δ ~1x10-2
$Ba_{0.6}Sr_{0.4}Ti_{0.99}Mn_{0.01}O_3$	Tc~325 K, moderate tunability and tan δ ~1x10-2
$Ba_{0.681}Sr_{0.281}Mg_{0.038}Ti_{0.962}Zr_{0.038}O_3$	Tc~300 K, 2% tunability, and tan δ ~$2x10^{-3}$
$Ba_{0.1}Sr_{0.9}TiO_3$	Tc~140 K, 7% tunability, and tan δ ~$1x10^{-2}$
$Ca_{0.05}Sr_{0.95}TiO_3$	Tc~70 K, 2% tunability, and tan δ ~$1x10^{-2}$
$KTaO_3$	No tunability, tan δ ~ $1x10^{-3}$

Table 1 - Summary of thin film materials investigated by Laser Ablation processing.

Task 5 Highlights - Materials Discovery Research

The purpose of this task was to search for new ferroelectric compounds and explore the effects of various elemental substitutions in the bulk phase. Promising candidate materials, such as $CaCu_3Ti_4O_{12}$, were identified for further exploration in thin film form. Some of the key materials investigated and their properties are summarized in Tables 2 and 3 below.

Compound	Relative Dielectric Constant (K)	Loss Tangent (D)	a (Å at 25°C)
$CaCu_3Ti_4O_{12}$	10286	0.067	7.391
$CdCu_3Ti_4O_{12}$	409	0.093	7.384
$La_{2/3}Cu_3Ti_4O_{12}$	418	0.060	7.427
$Sm_{2/3}Cu_3Ti_4O_{12}$	1665	0.048	7.400
$Dy_{2/3}Cu_3Ti_4O_{12}$	1633	0.040	7.386
$Y_{2/3}Cu_3Ti_4O_{12}$	1743	0.049	7.383
$Bi_{2/3}Cu_3Ti_4O_{12}$	1871	0.065	7.413
$BiCu_3Ti_3FeO_{12}$	692	0.082	7.445
$LaCu_3Ti_3FeO_{12}$	44	0.339	7.454
$NdCu_3Ti_3FeO_{12}$	52	0.325	7.426
$SmCu_3Ti_3FeO_{12}$	52	0.256	7.416
$GdCu_3Ti_3FeO_{12}$	94	0.327	7.409
$YCu_3Ti_3FeO_{12}$	33	0.308	7.394

[a]measured at 100 KHz.

Table 2 - Dielectric[a] and Cell Edge Data for $ACu_3M_4O_{12}$ Phases (at 25°C)

Composition	Electric Field (V/μm)	Dielectric Constant	Loss Tangent	Tunability (Percent)
$Ba_{.96}La_{.04}Ti_{.96}Al_{.04}O_3$	0.073	1713	0.0127	0.8
$Ba_{.96}La_{.04}Ti_{.96}Cr_{.04}O_3$	0.059	536	0.0060	1.6
$Ba_{.96}La_{.04}Ti_{.96}Fe_{.04}O_3$	0.053	4350	0.0130	4.2
$Ba_{.96}Sm_{.04}Ti_{.96}Fe_{.04}O_3$	0.061	1857	0.0180	1.2
$Ba_{.96}Gd_{.04}Ti_{.96}Fe_{.04}O_3$	0.063	929	0.0309	1.2
$Ba_{.96}Dy_{.04}Ti_{.96}Fe_{.04}O_3$	0.064	525	0.0225	0
$BaTiO_3$	0.065	1195	0.0080	0.1
$Ba_{0.6}Sr_{0.4}TiO_3$	0.060	2551	0.0115	2.7

Table 3 - Dielectric values of $Ba_{1-x}Ln^{3+}{}_xTi_{1-x}M^{3+}{}_xO_3$ at 1MHz and room temperature.

Task 6 Highlights - Rapid Test Method Development

The purpose of this task was to develop a rapid method for characterizing the dielectric properties (ε, tan δ, and tunability) of thin films without the need for patterning. The proposed technique was to press a coplanar HTS resonator into contact with a dielectric film to be tested. The resonator Q and frequency shift vs. bias voltage could then be used to determine the loss and dielectric constant vs. electric field of the film under test. After extensive investigation and experimentation, it was determined that air gaps present between the film under test severely limited the reproducibility and accuracy of this technique. This task was abandoned in the 5th quarter of the program and the resources applied to the multilayer film development (Task 3).

Task 7 Highlights - Demonstration Device Design and Test

Seven films manufactured under Tasks 1 and 3 were patterned into tunable ferroelectric/superconductor devices using the designs and masks developed in Q11 (one of the filter designs is shown in Figure 1). These devices were tested after the Q12 quarterly report was submitted. Below, we present the performance data to complete milestone 7.B.

The coplanar designs did not allow biasing of the individual resonators, which has the benefit of simplicity, but limits the performance attainable. Rather, the bias was applied between the two halves of the groundplane. Filters were designed for 3% bandwidth at 2 GHz relying on two assumptions: that the ferroelectric films 1.5 μm thick and had a permittivity $\varepsilon_r = 500$. The coupling coefficients between end-coupled resonators (hence the bandwidth and in-band return loss) depend strongly on the local dielectric environment between the resonators. If the fabricated dielectric environment is not as designed, adjustments have to be made (e.g. by applying a differential bias between resonators) to maintain performance.

The best results on tunable coplanar filters are plotted in Figure 2. The filters showed almost 8% tunability at 50 K with a 3 MV/m DC field, decreasing monotonically to 4% at 80 K. The ferroelectric layer was deposited from a $Ba_{0.06}Sr_{0.94}Ti_{0.98}O_x$ target. The center frequency is 1.3 GHz (0.7 GHz lower than design), the 3 dB bandwidth is about 5% (wider than the design). The insertion loss (around 5 dB for a 3 pole design) is very high, and the filter shape is poor. Results on the tunability and unloaded Q of individual resonators were generally consistent ($\Delta f/f$ = 5-7% and Q ~ 30 at 70 K) with measurements on the 3 pole filters. These results are explained to

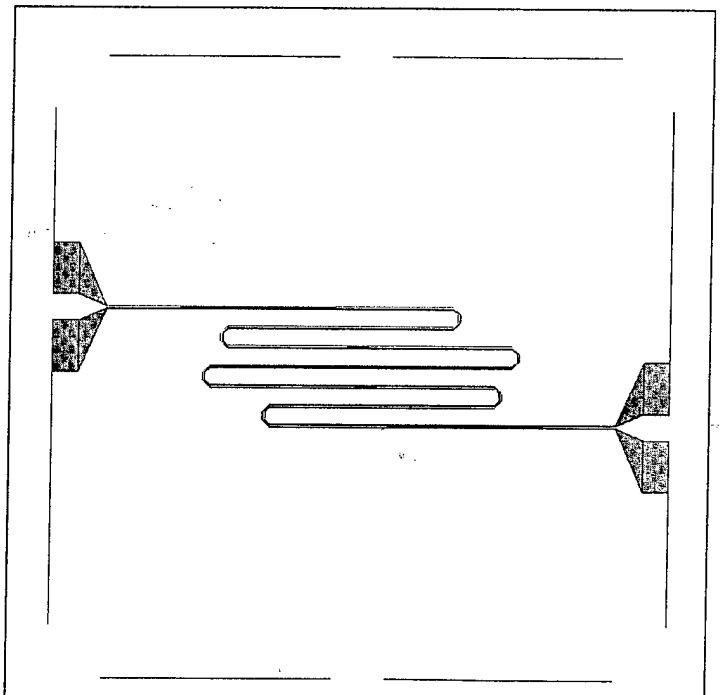

Figure 1. Mask layout of a 3 pole end-coupled coplanar waveguide bandpass filter. The dark areas are the gap in the superconducting layer. The chip is 12 x 12 mm.

some degree by the generally low figures of merit for even the best of our materials (leading to low unloaded resonator Q and high filter insertion loss) and by the fact that our fabricated films were not exactly as designed (in both thickness and permittivity).

Improvements in design could be made for two broad classes: for designs where the coupling coefficient depends on the dielectric (like the coplanar end-coupled ones used here) the resonators should be biased individually. This is the direction many others have pursued; another potentially more interesting class of design are those filters whose coupling coefficients do not depend strongly on the dielectric (resonators coupled by magnetic, rather than electric, fields). In these designs, the filter shape would be largely unaffected by tuning the permittivity. Stripline geometries, rather than microstrip, might lend themselves more readily to this type of design.

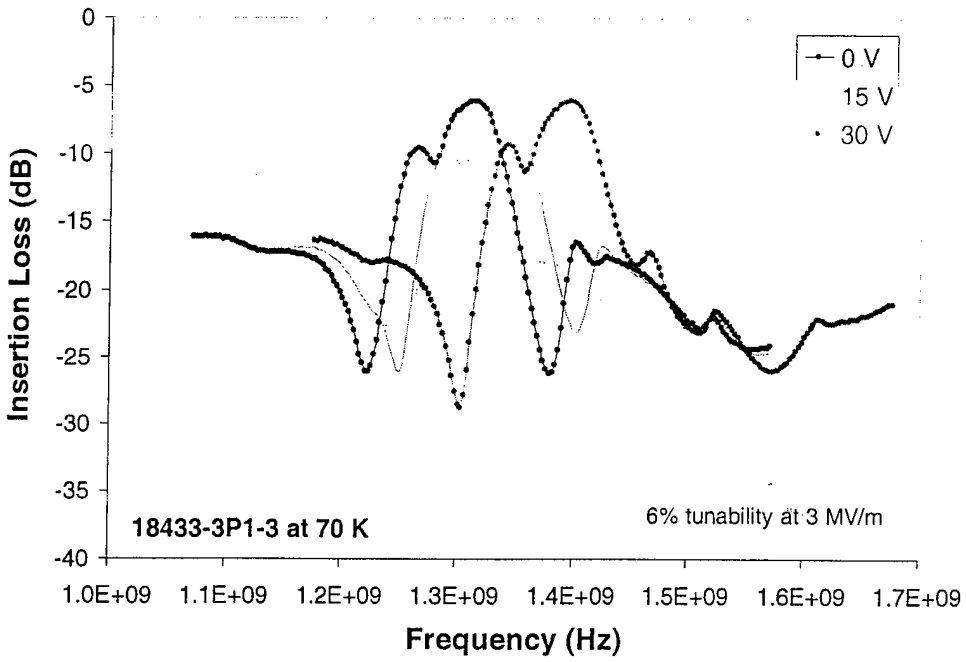

Figure 2. Tunability of a three pole coplanar filter (design shown in Figure 1). 0.4 μm YBCO on 0.9 μm Ti-deficient BSTO06 on 500 μm LAO. Design f_0 = 2 GHz, BW_{3dB} = 3%.

Frequency Agile Materials for Electronics

Q1

Date: October 14, 1998

Period covered in this report: 6/1/98 through 9/30/98

Program Title: Novel Ferroelectric Materials for Satellite Communications

Contract # DABT63-98-C-0046

Performing Organization: DuPont Superconductivity

Subcontractor: University of Colorado

Summary

During the first quarter of we demonstrated the uniform growth of large area ferroelectric thin films using $SrTiO_3$ as the model compound. We were able to deposit epitaxial STO on $LaAlO_3$ over a wide temperature range, 500 °C < T_{sub} < 625 °C. $Ba_xSr_{1-x}TiO_3$ (BSTO) targets with x=0.6 and 0.06 were obtained and installed for producing films with properties optimized for room temperature and cryogenic temperature operation. We plan to grow large area uniform films of BSTO early in the next quarter to complete the first two film deposition milestones. Exploratory thin films of $KTaO_3$ were produced by laser ablation, but further optimization is required to obtain single phase films of the desired structure. Exploratory films of $Ba_{0.6}Sr_{0.4}TiO_3$ were successfully prepared by laser ablation with the desired structure. Targets for the exploratory deposition of doped BSTO and $K_{1-x}Rb_xTaO_3$ are being developed for use in the next quarter. The development of a Rapid Intrinsic Film Test (RIFT) is on schedule and we completed the first milestone for this task.

Progress by Task

Task 1 & 2 - Large Area Sputtered Film Manufacturing for Cryogenic and Ambient Temperatures

We will report on the progress made on tasks 1 and 2 together, because we have not yet differentiated our efforts between the cryogenic and room temperature materials. We ordered four sputtering targets of the ferroelectric $Ba_xSr_{1-x}TiO_3$ (BSTO): two with x = 0.06 for low temperature applications and two with x = 0.60 for use near room temperature. We also

investigated a number of manufacturing issues relevant to making ferroelectric films using available materials and equipment.

Two sputtering systems were dedicated to the project. Both required modifications to meet the project needs. In system 1, L560-1, we deposited $SrTiO_3$ (STO) films and will shortly begin depositing BSTO films. We are also modifying a second system, L560-0, in order to test a new sputter source and eventually deposit ferroelectric films.

1.1 $SrTiO_3$ Films

We looked at the deposition of STO thin films on 51 mm diameter $LaAlO_3$ (LAO) substrates. This provided useful information about the deposition conditions for the doped material, BSTO. It also allowed us to evaluate a new style of radiant heater (vertical lamp type) which is being developed for the manufacture of uniform, large area oxide thin films. We started these concurrent investigations the first week of July and finished the last week of August.

We studied the role of substrate temperature T_{sub} during deposition and the use of a thin (~ 25 nm) CeO_2 buffer layer between the substrate and the film. We characterized these samples by x-ray diffraction (XRD). We looked for unwanted second phases and at the quality of the epitaxy (measured by in-plane and out-of-plane alignment between the film and substrate). In Figures 1.1-1 & 1.1-2, we show diffractometer data for sample 14168, a typical epitaxial sample. We demonstrated that we can deposit epitaxial STO on LAO over a wide temperature range, 500 °C < T_{sub} < 625 °C, though film crystallinity was degraded at the lowest temperatures. This process window is wider than the one for $YBa_2Cu_3O_{7-x}$ (YBCO). In Figure 1.1-3, we show the decrease of rocking curve width (narrower FWHM indicates better crystalline quality) with heater temperature. We could **not** find any substrate temperatures under which we could obtain an epitaxial film of STO if we used a buffer film of CeO_2 on LAO. We believe that the use of buffer layers is crucial to minimizing the stress created by lattice mismatches between the ferroelectric films and substrates; we intend to investigate them more thoroughly in the next quarter. Stress is known to decrease the tunability and increase the loss of ferroelectric thin films.

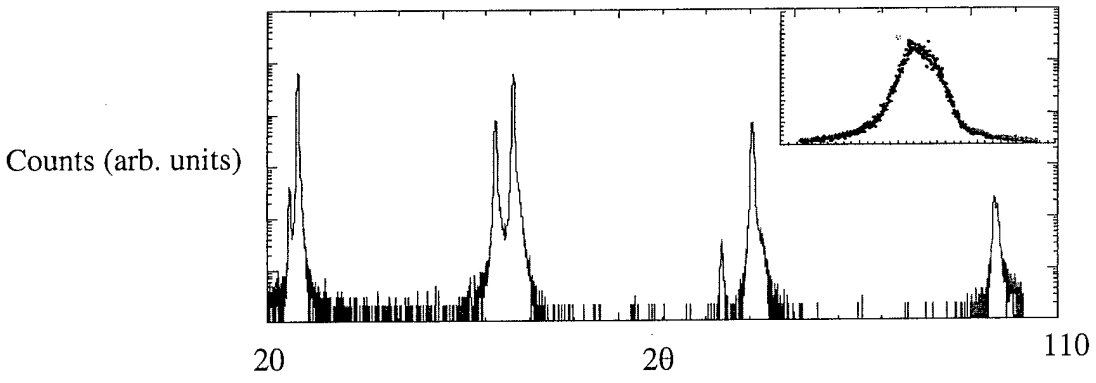

Figure 1.1-1. Phase scan of an STO film deposited on LAO at a heater temperature of 765 C. The film is oriented with $(00h)_{STO} \parallel (hh0)_{LAO}$. Inset: the rocking curve of the STO (200) peak.

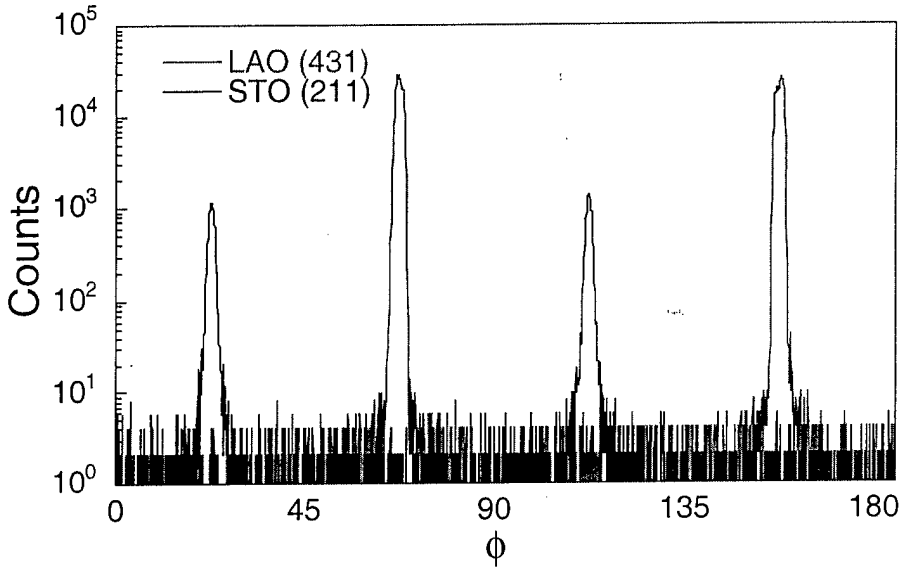

Figure 1.1-2. In-plane orientation of STO on LAO deposited at heater temperature of 765 °C. STO $(211)_{cubic}$ is rotated 45° from LAO $(431)_{rhomb}$. Combined with the phase scan data in Figure 1, we find the growth of STO on LAO is "cube-on-pseudo-cube".

To characterize the thickness and compositional uniformity of our STO depositions, we used the Rutherford Backscattered ion technique (RBS) on amorphous films deposited at ambient temperature on silicon wafers. In general, our RBS samples were slightly Sr-deficient. (Our extensive experience with similar studies on $YBa_2Cu_3O_{7-x}$ leads us to believe that the results from the amorphous films on silicon are not very different from the epitaxial films on LAO.) The other STO samples were deposited using the vertical lamp heater prototype. The prototype was not designed to allow sample rotation during deposition, which is a technique we usually use to improve thickness and temperature uniformity of the growing film. Nevertheless, we measured good epitaxial and compositional uniformity (4-9%) and fair temperature (uniform over central 40%) and thickness uniformity (5-12%) across the samples; this should improve markedly with substrate rotation.

We concluded our STO depositions and vertical lamp heater evaluation in system 1 (L560-1) after the BSTO targets arrived in late August. We replaced the non-rotating vertical lamp heater with our standard design quartz lamp heater, which can rotate the sample and has proven performance and reliability. We also installed the BSTO targets in the system. We completed the heater changeover and system reconfiguration in the last week of September. We have since tested the main system and are now ready to deposit BSTO films.

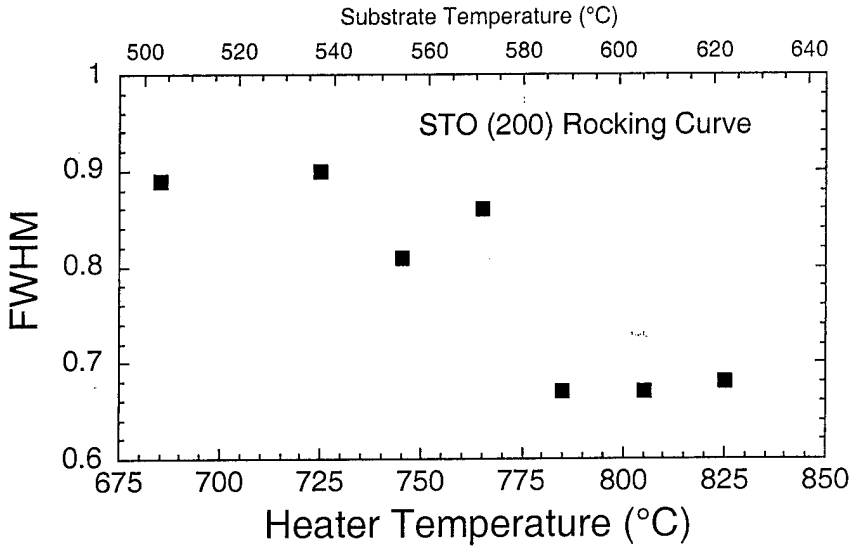

Figure 1.1-3. The full width half maximum of the (200) rocking curve of STO deposited on LAO versus heater temperature setpoint. The temperature of the center of the substrate (as measured with an imaging IR camera) is shown on the top axis.

1.2 - Rotating Magnetron Sputter Source Evaluation

We tested a new type of sputter source which holds the promise of higher uniformity and much higher rate than the traditional 3" or 4" diameter magnetron sputter guns we use in our research and manufacturing operations. In 1997, we purchased a 6" diameter rotating magnetron source. We also obtained a YBCO target for the 6" gun before the present program began. In a traditional magnetron source, the magnets which confine the sputter plasma are fixed in position. This means only a small fraction of the total target can be deposited, which is expensive. The target surface profile changes over time as the erosion gets deeper, hence the deposited composition changes as well. Because only a small volume of the target is used, the power density at a given deposition rate is very high. This leads to target cracking, limiting the ultimate rate.

Our new magnetron source should overcome these disadvantages because the confining magnets now rotate beneath the target: the full target surface is used for deposition. We predict the compositional and thickness uniformity will improve and we will be able to apply higher power to the target before cracking.

We installed the rotating magnetron sputter source in our system 2 (L560-0) in late August and have been evaluating its performance since mid-September. We plant to finish its characterization early in the second quarter of the program.

1.3 - Plans For Second Quarter

L560-0 (System 2)

Presently, system 2 has no substrate heater or rotation mechanism. We are designing a new heater and rotation unit (based on the prototype vertical lamp heater) to be installed in L560-0. The specifications for this new unit will be finished late in the second quarter. If the performance of the rotating magnetron sputter source looks promising, we will investigate its use in depositing large area films of BSTO or other ferroelectrics, perhaps in conjunction with the new vertical lamp heater.

L560-1 (System 1)

Given our experience with depositing STO films, we anticipate we will make rapid progress on demonstrating large area BSTO films. During the second quarter, we will concentrate primarily on optimizing the properties of BSTO films using all the characterization tools at our disposal. Of primary interest is finding the best substrate/buffer combination to grow high tunability, low loss BSTO. We have a number of candidates in mind: for substrates, we will look at LAO, sapphire, and MgO; for buffers, we will investigate CeO_2 initially, though probably not on LAO, given our experience with the STO films. One of the early second quarter tasks is to identify other promising buffer layers. Another area of investigation is the influence of stress caused by thermal expansion and lattice mismatch between the film and substrate/buffer on the ferroelectric properties.

Task 3 - Multilayer Film Development and Manufacturing

This development work will build on the materials technology developed in Tasks 1 and 2 and the measurement experience developed in Task 6. The first milestone under this task is scheduled for next quarter and calls for the design of a coplanar resonator and a coplanar transmission line. We anticipate completion of this milestone on schedule during the next quarter.

Task 4 - Exploratory Laser Ablation Processing (University of Colorado)

4.1 Potassium Tantalate ($KTaO_3$)

4.1.1 Target fabrication:

1" diameter and 4-5 mm thick $KTaO_3$ targets were prepared in air by sintering at 1320 °C for 6-12 h. We have observed that above 1350 °C $KTaO_3$ begins to melt. The XRD of the target revealed crystalline, cubic and single phase composition. The cubic phase has a lattice parameter a=3.989 Å.

4.1.2 Film fabrication:

$KTaO_3$ films were deposited on $LaAlO_3$ (001) substrates. The substrates were cleaned by methanol in an ultrasonic agitator for 30 minutes. The substrates were then heated at 900 °C in flowing oxygen atmosphere for 4 hours and cooled to room temperature under flowing oxygen.

Films were grown using a KrF excimer laser (248 nm) with a focused energy density of 1-2 J/cm^2 and a pulse rate of 7 Hz. The oxygen partial pressure during the deposition was varied to study the phase composition of the films. Thus, films were grown in an O_2 partial pressure of

100-200 mTorr, 300-400 mTorr, or 500-600 mTorr. For all the films the substrate temperature was maintained at 700 °C during the 30 minute deposition.

4.1.3 Results:

XRD of $KTaO_3$ films revealed deviations from the target phase. For an oxygen partial pressure in the range 100-200 and 300-400 mTorr, only peaks corresponding to (400) and (800) appeared in the XRD pattern. 'd' spacing matching revealed the possibility of a cubic defect pyrochlore '$K_2Ta_2O_6$' type phase formation. These films did not revert to the perovskite phase when annealed at 900 °C for 24 h under flowing O_2 followed by cooling to room temperature. XRD of the films deposited under 500-600 mTorr of oxygen pressure did not show epitaxial orientation. However, the reflections correspond to two different phases of $KTaO_3$ (phase i obtained by quenching from 1000 °C to 600 °C, lattice constant a=10.59 Å (K. Nassau et al, *J. Am. Ceram. Soc.*, 62, 74 (1979), phase ii achieved by slow cooling from high temperature).

The inconsistency in obtaining a single phase composition of $KTaO_3$ using above conditions has prompted us to look for alternate routes. New targets have been made by a) mixing preformed $KTaO_3$ and KNO_3 (50 wt% of $KTaO_3$), and b) segmented target, one-half of which is $KTaO_3$ perovskite, and the other half is KNO_3, to provide an extra reactive potassium and oxygen source during film formation. The deposition of films using these targets is presently under study.

4.2 Barium Strontium Titanate ($Ba_{0.6}Sr_{0.4}TiO_3$)

4.2.1 Target fabrication:

A target of the above composition was prepared by mixing a stoichiometric ratio of $BaCO_3$, $SrCO_3$, and TiO_2, and heating at 1000 °C for 72 hours with intermittent grindings. The powder was then compacted to a disc of 1" diameter and sintered at 1450 °C for 3-4 h and furnace cooled to room temperature. Phase formation and lattice parameter were confirmed by XRD.

4.2.2 Film fabrication:

Films of $Ba_{0.6}Sr_{0.4}TiO_3$ were grown on LAO (100) substrates with a similar procedure to that described above. Variations in the partial pressure of oxygen during deposition were also studied with respect to phase formation.

XRD of the films deposited in an oxygen partial pressure range of 100-300 mTorr, however, shows (unknown) impurity peaks. The films deposited in an oxygen partial pressure 500-600 mTorr have single phase cubic structure and are epitaxial in nature (Fig. 4.2-1). The lattice parameter calculated from the XRD is a=3.961 Å which is close to the reported value for bulk polycrystalline material. This indicates that the deposition conditions are optimized for the stoichiometric control on the composition of the BSTO film.

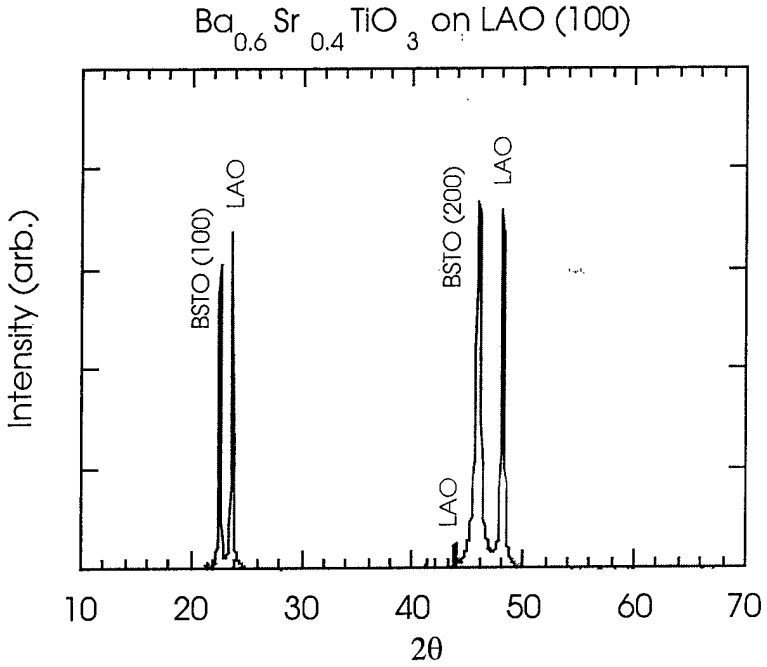

Fig. 4.2-1: XRD (Cu Kα1) pattern of Pulsed Laser Deposited $Ba_{0.6}Sr_{0.4}TiO_3$ film at 700°C, 600 mTorr oxygen pressure, on LAO (100) substrate.

4.3 Doped $Ba_{0.6}Sr_{0.4}TiO_3$

$Ba_{0.6}Sr_{0.4}Ti_{0.99}Mn_{0.01}O_3$ and $Ba_{0.6}Sr_{0.4}TiO_3$+30wt% MgO targets were made to study the effect of substitution and additives on the tunability. The deposition conditions and film properties will be evaluated in future.

4.4 $K_{1-x}Rb_xTaO_3$ system

It is well known that $KTaO_3$ often behaves as an incipient ferroelectric material. It has a very low value of tan δ ($\sim 10^{-4}$) at microwave frequencies. However, the dielectric constant is <2000. To increase the dielectric constant of $KTaO_3$ we have undertaken a solid solution study of the $K_{1-x}Rb_xTaO_3$ system. There are no reports on this solid solution study. The end member $RbTaO_3$ is, however, not a perovskite.

Compositions of x=0.05-0.6 have been synthesized at high temperatures. Preliminary results from XRD study reveal single phase formation for x=0.05-0.2. The lattice parameter indicates a systematic expansion in the unit cell as the Rb concentration increases (a=3.989 Å for x=0.0 and a=4.001 Å for x=0.2). For x>0.2 a mixture of $KTaO_3$ and $RbTaO_3$ phases is observed.

4.5 Mask Design for capacitance measurements

Following design studies at DuPont, we finalized a 4 capacitor shadow mask design with interdigitated capacitors. The mask has 6 contact pads, with finger widths and separation between the fingers of 100 micrometers. The mask was ordered and is expected to arrive next month.

4.6 Pressure apparatus for capacitance measurements using a press-on capacitor configuration

Following design studies at DuPont for microwave measurements, we have designed an apparatus for pressing metal capacitor electrodes (interdigitated) onto our PLD films. We have accepted the bid from the precision machine shop at CU. We expect the apparatus to be completed by November 1, 1998.

Task 5 - Materials Discovery Research

Due to prior research commitments, Dr. Mas Subramanian was not able to begin his materials discovery research this quarter. We anticipate that he will begin work during the next quarter of the program. During the next quarter we anticipate that Dr. Subramanian will identify candidate material compositions for further investigation. We also plan to hire a post-doc to work with Dr. Subramanian starting in 1999.

Task 6 - Rapid Intrinsic Film Test (RIFT) Development

The purpose of this task is to develop a non-destructive measurement technique for the rapid characterization of the electrical performance of ferroelectric films produced in Tasks 1-4. As discussed in our proposal and shown schematically below in figure 6-1, we plan to characterize ferroelectric film performance using a coplanar resonator which is pressed in contact with the ferroelectric film of interest.

During this past quarter we completed the design and modeling of all the parts needed to build the first generation RIFT probe. This completes the first milestone under this task. In addition, all mechanical parts of the probe have now been fabricated and are ready for assembly. Highlights of the mechanical design include: 1) a self aligning spring mechanism to assure uniform pressure between the substrates and; 2) a variable backside coupling to the resonator using laser-drilled vias. The coplanar resonator is designed to operate at ~ 6 GHz and has a dc bias line connected to the center of the resonator using a double choke structure to prevent rf leakage into the bias circuit. Several additional resonators were also designed to verify the performance of the double choke structure. Photomasks for fabrication of the biased coplanar resonator and choke test circuits were produced and are ready for use.

During the next quarter we will assemble and test the RIFT probe. We will also fabricate and test the 6 GHz coplanar resonators with bias circuits to verify the design. We also plan to design additional test circuits to verify the accuracy of the RIFT measurement technique.

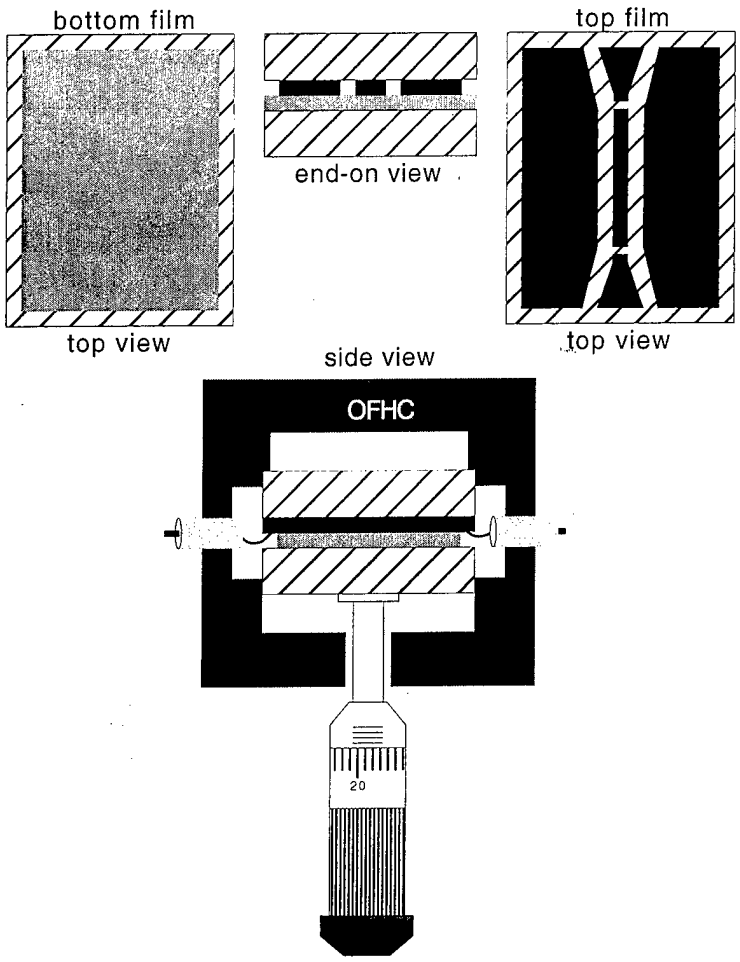

Figure 6-1 Rapid Intrinsic Film Test (RIFT). Two separate substrates are used: upper left, an unpatterned ferroelectric film; upper right, a patterned coplanar resonator. The resonator film would be semi-permanently mounted. The two substrate would be pressed together to eliminate any air gap in a microwave cavity and the Q measured. (The micromanipulator shown is only one of many possibilities for achieving intimate contact between the two films.)

Frequency Agile Materials for Electronics

Q2

Date: January 15, 1999

Period covered in this report: 10/1/98 through 12/31/98

Program Title: Novel Ferroelectric Materials for Satellite Communications

Contract # DABT63-98-C-0046

Performing Organization: DuPont Superconductivity

Subcontractor: University of Colorado

Summary

We demonstrated large area epitaxial growth of $Ba_xSr_{1-x}TiO_3$ (BSTO) thin films with both x=0.6 and 0.06 to complete the first two film deposition milestones for Tasks 1 and 2. Initial optimization of deposition conditions for x=0.6 using a statistical experimental design has shown important relationships between film crystallinity, composition, and deposition conditions. A coplanar resonator and several interdigital capacitors were designed, modeled, and fabricated to complete the first two milestones for Task 3. These devices will be used for extensive testing of the dielectric properties of ferroelectric films during the next quarter. Single phase $KTaO_3$ films were produced by exploratory pulsed laser deposition using excess potassium from a KNO_3 target to make up for potassium loss from the films at high temperature. The materials discovery research effort (Task 5) started this quarter with the investigation and synthesis of $ACu_3M_4O_{12}$ (A = Cd, Ca; M = Ti, Mn) phases which crystallize in a perovskite-like structure. The unusual feature of this structure is that it requires a Jahn-Teller ion, such as Cu^{2+}, Mn^{3+} in the A-site. No information is available in the literature regarding the dielectric properties of any member of this family of compounds.

Progress by Task

Task 1 - Large Area Sputtered Film Manufacturing for Low Temperature Applications

We deposited seven $Ba_{0.06}Sr_{0.94}TiO_3$ (BSTO x = 0.06) films on 51 mm diameter $LaAlO_3$ (LAO) and silicon substrates to verify that our results on the room temperature composition material BSTO x = 0.60 applied (see Task 2). Also, we concentrated on the room temperature material because we are still in the process of developing test methods for BSTO x = 0.06 at cryogenic temperatures (see Task 6). We continued to evaluate the rotating magnetron sputter

source and the new seven vertical lamp heater design for very large area/high throughput depositions.

1.1 BSTO x = 0.06 Films on LAO

In Figure 1.1-1 below, we plot the x-ray diffraction results of sample 16312, a BSTO x = 0.06 film on LAO, deposited at 875 °C. The θ-2θ scan shows c-axis orientation with no unwanted second phases or orientations. Inset is the rocking curve scan of the BSTO (002) peak, which is fairly narrow, indicating good crystalline quality of the ferroelectric film. The phi scans (not shown) also show good registration between the crystalline axes of the film and substrate in the plane: the growth of this film is cube-on-cube. Preliminary measurements such as these indicate that much of the general knowledge we gain from BSTO x = 0.60 is transferable to BSTO x = 0.06.

We plan to greatly expand our efforts on the BSTO x = 0.06 material in the third quarter. We will deposit the low temperature composition on MgO, ceria-buffered sapphire, and LAO. We will characterize the electrical and microstructural properties of all the films we deposit.

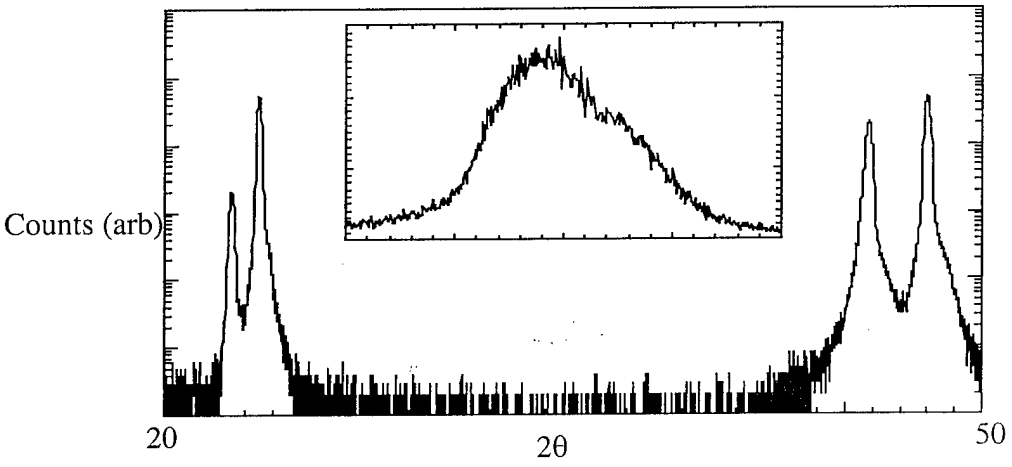

Figure 1.1-1 θ-2θ scan for sample 16312 ($Ba_{0.06}Sr_{0.94}TiO_3$ on LAO) showing good c-axis orientation and no unwanted second phases. Inset: rocking curve of the (002) peak, FWHM ~ 0.75°.

1.2 Rotating Magnetron Sputter Source

We concluded our low sputtering power tests (< 400 W) of the rotating magnetron source in our secondary sputtering system (L560-0) in mid December. Our intent was to evaluate the performance of the source with an eye to greatly improving our throughput of uniform, large area oxide films. We have been using the standard magnet system and a 6" diameter $YBa_2Cu_3O_x$ (YBCO) target, both of which were purchased before the program began. The results so far are encouraging: in the on-axis geometry, we believe we can achieve both very high rates (as high as 0.5 μm/hr) and good uniformity (both composition and rate) *without* substrate rotation. We plot our fit to the film thickness deposited per hour versus the height and radius from the target center (at 275 W and 82.5 mTorr) in Figure 1.2-1. Note that the rate is very uniform and very high near

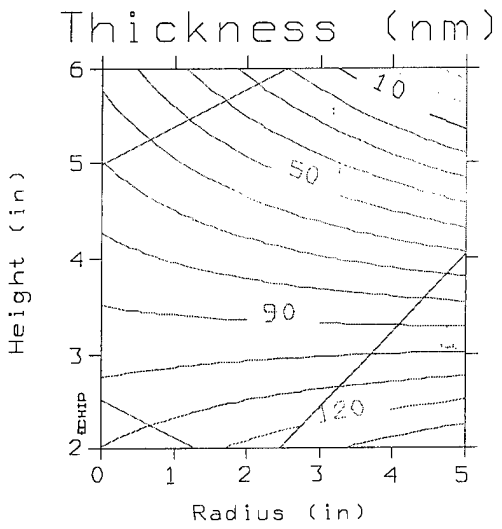

Figure 1.2-1. Predicted on-axis thickness (for a one hour deposition) of $YBa_2Cu_3O_x$ using the rotating magnetron sputter source at 275 W and 82.5 mTorr. Height and Radius are measured from the center of the target surface. Note the flat region near Height = 3.5 inches. The inscribed box indicates the region of highest confidence for the fit.

the center of the figure; our present deposition rates for YBCO are near 30 nm/hr. In the traditional off-axis geometry, the rates are also very high (up to 150 nm/hr at 400 W) but the uniformity is less impressive.

In the third quarter, we will investigate the high power performance of the rotating magnetron source for use with oxide materials. Because of the higher heat dissipation capability of this source, we expect we can increase the sputtering power at least a factor of 2 above what we have demonstrated (400 W). We also will begin design changes to the magnet system, which was originally optimized for metallic targets, to get higher target usage and improve uniformity further.

1.3 Seven Vertical Lamp Heater

We are currently finishing the design of a seven lamp heater and its rotating ferrofluidic feedthrough, which is also intended to increase our throughput of large area oxide films. This new heater is based on the 2 lamp prototype, which we tested in the first quarter of this program. The heater was designed for high temperature uniformity and ease of maintenance and repair. We intend to finish the design and begin building this heater for installation in L560-0 in late Q3/early Q4. This will give us a second fully capable deposition system and enable us to use the rotating magnetron source at high temperatures.

Task 2 Large Area Sputtered Film Manufacturing for Ambient Temperature Applications

We worked primarily on the deposition conditions for $Ba_{0.60}Sr_{0.40}TiO_3$ this quarter, because we have the capability to immediately test the electrical properties using deposited interdigitated capacitors. We deposited a total of 38 BSTO $x = 0.60$ on LAO, Si, and MgO in Q2. We implemented a statistically designed experiment to find the optimum deposition temperature,

pressure, and power for $Ba_{0.60}Sr_{0.40}TiO_3$ films on LAO; we believe that the results we obtain will be applicable across the range of substrates and buffer layers that we want to investigate. We did extensive frequency-domain electromagnetic simulations to model the influence of a ferroelectric layer on interdigitated capacitor structures. We measured the low frequency dielectric properties of interdigitated capacitors on bare LAO, sapphire, and the undoped $SrTiO_3$ on LAO films we made in Q1 to verify our test methods.

2.1 BSTO x = 0.60 Films on LAO

We completed the first BSTO x = 0.60 on LAO experiment at the end of December. It was designed to search our deposition parameters to find the best conditions for depositing high quality BSTO films. We have measured the orientations and lattice constants of these films, and are in the process of measuring the dielectric properties. We show a typical phase scan and rocking curve in Figure 2.1-1. The films were strongly c-axis oriented and grew cube-on-cube over all the conditions we tried. In Figure 2.1-2, we present some of the data extracted from this experiment. On the left is the atomic percentage of titanium in the film versus sputtering power and pressure. On the right is the thickness deposited in 3 hours. We desire high rate (for throughput) and good compositional uniformity; this restricts us to the lower right quadrant of the plot. The composition of our films seems to be Ti-rich over a broad processing range—we may have to use compensated targets to achieve stoichiometric films. We have omitted deposition temperature, since we found it to have negligible effect on the composition or rate.

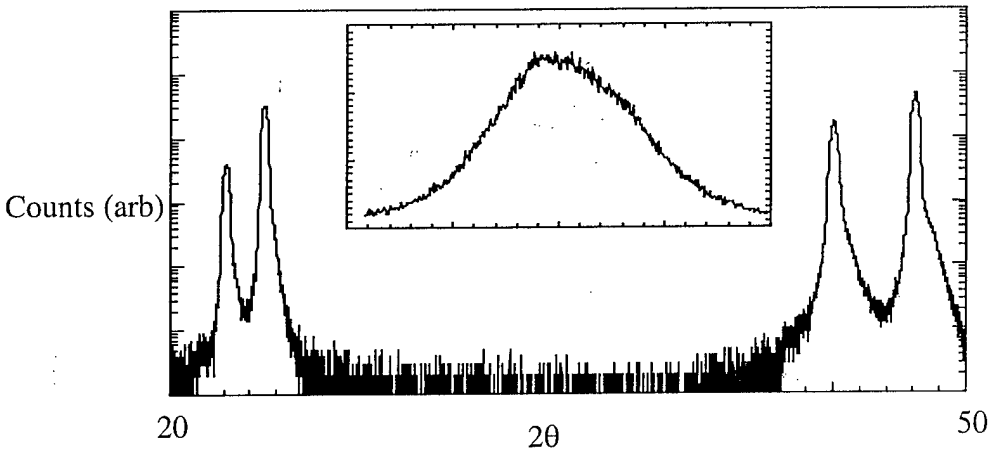

Figure 2.1-1 θ-2θ scan for sample 16297 ($Ba_{0.60}Sr_{0.40}TiO_3$ on LAO) showing good c-axis orientation and no unwanted second phases. Inset: rocking curve of the (002) peak, FWHM ~ 0.85°.

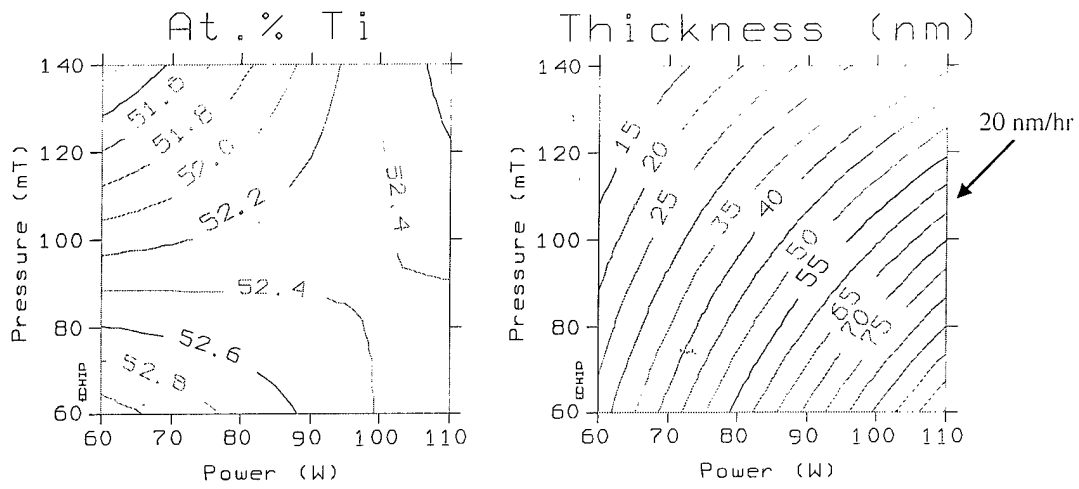

Figure 2.1-2 Fitted results of the deposition condition search. On the left is the concentration of Ti (in atomic %) in the BSTO x = 0.60 films on LAO. The desired concentration is 50%. On the right is the film thickness for a 3 hour deposition. We feel that deposition rates much below 20 nm/hr are unfeasible for manufacturing; this requires us to operate in the lower right corner of the plots. The deposition temperature did not have a strong effect on the rate or composition in BSTO films.

Using x-ray diffraction, we measured the orientation and lattice constants of the BSTO x = 0.60 films. The change in lattice constants gives a direct measure of the strain, which is of great importance to the dielectric tunability and loss. To obtain the lattice constants a and c, we measure a number of reflections (in- and out-of-plane) and assume a tetragonal distortion. In Figure 2.1-3, we plot the fitted rocking curve full at width half maximum against pressure, power, and temperature. Deposition temperature appears to have the most important influence on the rocking curve width, which is a measure of the crystalline quality in growth direction. In Figure 2.1-4, we plot the c-axis strain (c/a_0-1, where a_0 is the bulk cubic lattice constant) versus deposition power and pressure. We see that over the entire range, BSTO x = 0.60 films on LAO are in compressive stress (c > a), which is most likely due to lattice mismatch between the BSTO (a ~ 0.40 nm) and LAO (a = 0.38 nm). The deposition temperature did not have a large effect on the strain. Also note the similarity between the right plot in Figure 2.1-2 (film thickness vs. pressure and power) and Figure 2.1-4 (strain vs. pressure and power). It is possible that film thickness has the main effect on the strain in our films, rather than deposition power and pressure independently.

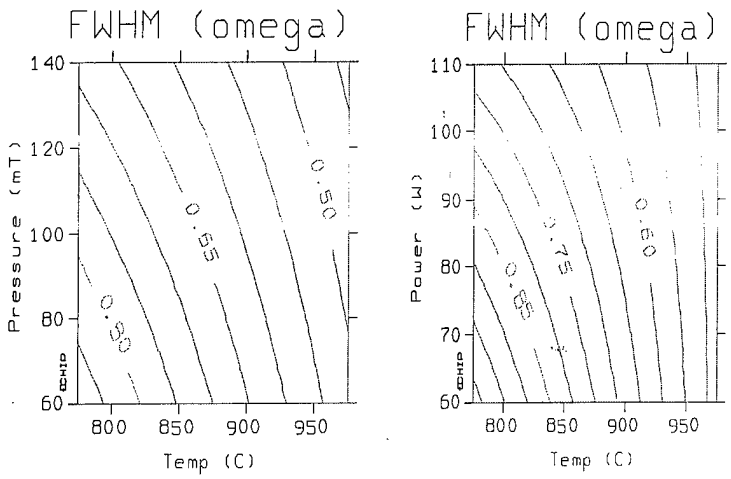

Figure 2.1-3 Fitted rocking curve width of BSTO x = 0.60 (002) on LAO versus deposition conditions. Deposition temperature is the most important factor. On the left, the power is set at 100 W. On the right, the pressure is set at 100 mTorr.

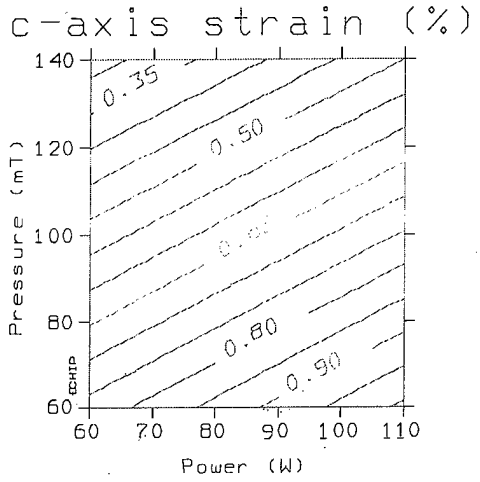

Figure 2.1-4 Fitted c-axis strain (normalized to the bulk lattice constant $a_0 = 0.398$ nm) versus deposition pressure and power. The temperature is set at 950 °C.

We are currently measuring the electrical properties of these films and beginning deposition on other substrates. In Q3, we plan to deposit BSTO x = 0.60 & 0.06 films on MgO, ceria-buffered sapphire, as well as on LAO. We hope to identify the optimum combination of film, buffer layer, and substrate to deliver high tunability and low loss.

2.2 Electromagnetic Modeling and Testing

We deposited interdigitated capacitors on top of some of our ferroelectric films in order to obtain low frequency dielectric property data—we are still in the process of qualifying the RIFT concept (see Task 6). We present a schematic of a interdigitated capacitor in Figure 2.2-1. To extract the dielectric permittivity and loss tangent of the ferroelectric layer, we modeled the capacitor structure using Sonnet, a highly accurate, frequency-domain electromagnetic simulation package. In Figure 2.2-2, we plot some of the results for the predicted capacitance per length (left) and device loss (right) for an interdigitated capacitor deposited on a ferroelectric

layer with a LAO substrate. We verified the correct behavior of our model by depositing capacitors on bare LAO and sapphire substrates.

We also deposited and measured capacitors on the STO films which we made in Q1 to test our model and measurement methods. We plot some of the results in Figure 2.2-3. We had not originally intended to characterize these films electrically, so they were not very thick. As a result, the sensitivity to permittivity changes is low.

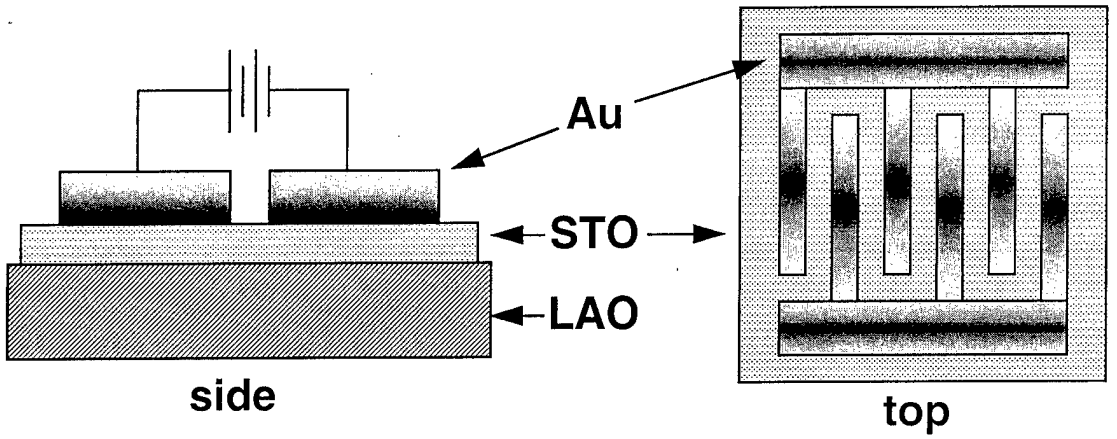

Figure 2.2-1 Schematic of interdigitated capacitor. Typical thicknesses: substrate (LAO) 500 μm. ferroelectric (STO) 0.4 μm, metal (Au) 1.2 μm.

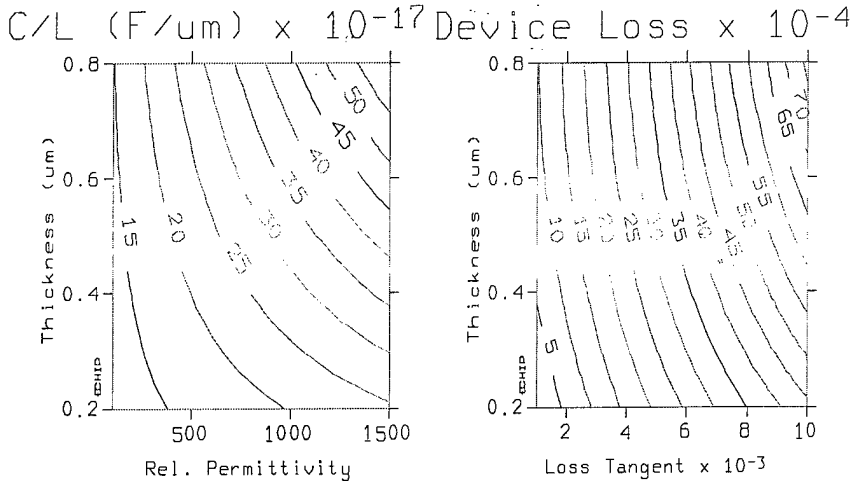

Figure 2.2-2 Results of electromagnetic modeling of interdigitated capacitor with 25 μm wide fingers and 20 μm wide gap between at 100 kHz. Left, the capacitance per length versus the ferroelectric layer thickness and permittivity. The predictions are independent of loss tangent. Right, the device loss at ε_r = 1000 versus film thickness and loss tangent. Best sensitivity is

achieved at high thickness and dielectric constant. The simulation neglects conductor and substrate losses.

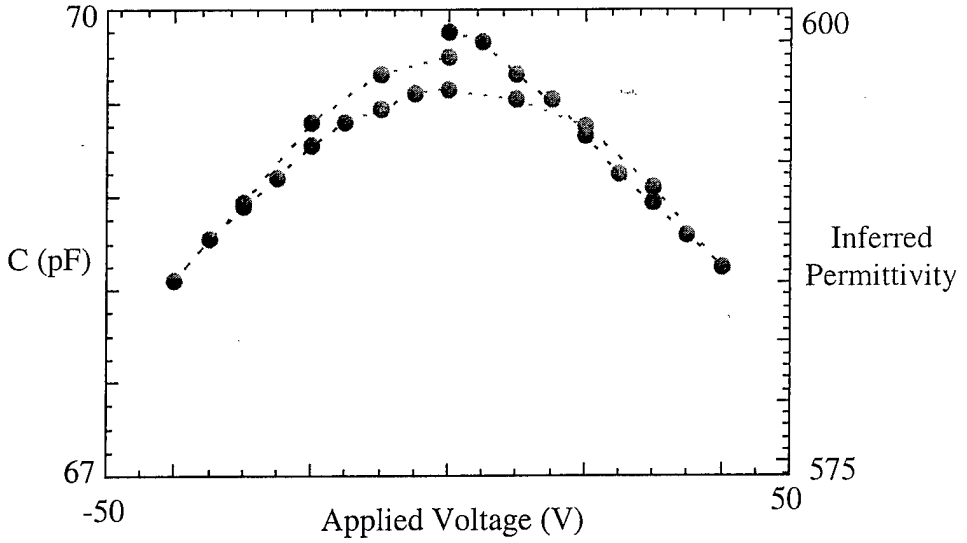

Figure 2.2-3 Capacitance versus applied voltage for an STO interdigitated capacitor at 100 kHz and 295 K. We used our simulation to deduce the change in permittivity, however, the accuracy is low because the STO film is fairly thin (~ 125 nm). The tunability did not change when we remeasured the sample at 77 K. The device loss was at the noise floor of the measurement.

In Q3, we plan to make extensive electrical measurements of both BSTO x = 0.06 and 0.60 films we have and will deposit, using a combination of deposited interdigital capacitors and the RIFT devices in Task 6.

Task 3 - Multilayer Film Development and Manufacturing

This development work will build on the materials technology developed in Tasks 1 and 2 and the measurement experience developed in Task 6. The first milestone under this task was to design a coplanar resonator and a coplanar transmission line to be produced with HTS/ferroelectric bilayers. We successfully completed the design of the coplanar resonator and have fabricated it using high quality $Tl_2Ba_2CaCu_2O_8$ films on MgO to verify the performance of the design. Testing of this design will take place next quarter. We decided to delay the design of the co-planar transmission line until testing of the co-planar resonator was complete to avoid a possible redesign effort. The second milestone under this task was to design a coplanar device and an interdigital capacitor to be produced with normal metal/ferroelectric bilayers for ambient temperature operation. For the coplanar device we decided to use the coplanar resonator design which was mentioned above. Several interdigital capacitors with electrode gaps of 10 and 20 μm were successfully designed and tested this quarter to complete this milestone of the program.

Task 4 - Exploratory Laser Ablation Processing (University of Colorado)

4.1 Potassium Tantalate ($KTaO_3$)

We have successfully optimized the conditions for reproducible growth of single phase KTaO3 films by pulsed laser deposition. Our earlier attempts using stoichiometric KTaO3 targets did not yield single phase KTaO3 films, however, excess potassium source (from KNO3) in the target helps to achieve single phase films.

Target:

Two types of targets were studied. Target #1 is a segmented circular disc with one-half of which is sintered KTaO3 perovskite and the other half is cold pressed KNO3 glued to the target holder assembly by silver paste at the bottom. Target #2 is a circular disc having thoroughly mixed 50 wt% of pre-formed KTaO3, and 50 wt% KNO3 and pelletized.

Film growth:

KTaO3 films were grown on MgO, LAO, and SrTiO3 single crystal substrates. The substrate temperature was maintained at 700°C. The oxygen pressure was kept at 300 mTorr before starting the deposition. However, the oxygen pressure started increasing during deposition due to the decomposition of KNO3 giving out oxygen. So the variation in oxygen pressure is 300-400 mTorr during deposition. The kV, and the time of deposition were kept at 17 kV and 30 min. respectively.

For the segmented target, Target #1, the pulse rate was kept at 1Hz. The target was manually rotated so that 2 pulses fall on KNO3 segment and 1 on KTaO3 half of the target. After deposition, the oxygen pressure was increased to 760 Torr and the film was cooled to room temperature by either shutting off the heater power or in 5h.

Results:

XRD showed that all KTaO3 films grown using both targets are single phase. For both type of targets, the films are oriented in (h00) direction showing epitaxial nature (Fig. 4.1-1). In cases where the film was cooled to room temperature slowly in 5h, additional reflection corresponding to (110) was also seen (Fig. 4.1-2). The lattice parameter calculated is a=3.989A.

The low frequency dielectric properties of these films will be studied in future.

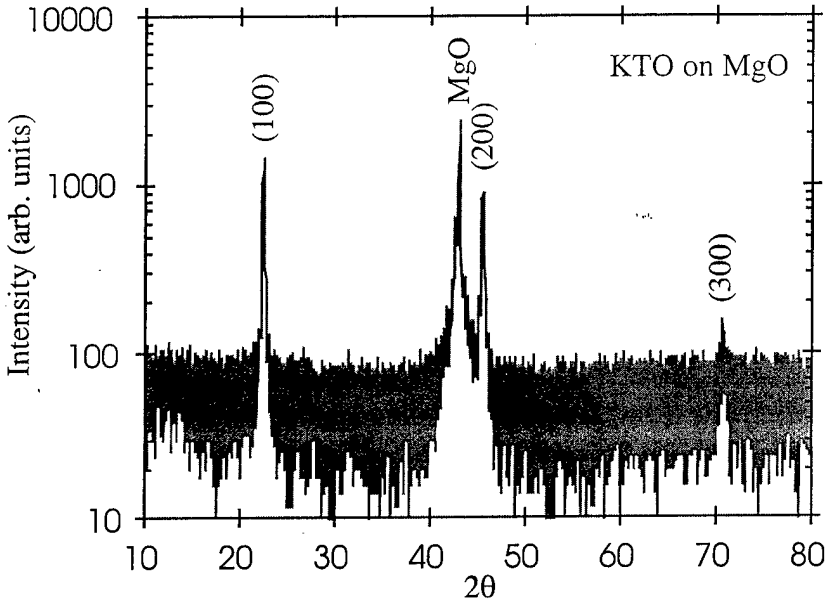

Fig. 4.1-1: XRD of $KTaO_3$ film on MgO using segmented target and cooled rapidly. The film shows epitaxial nature. Similar patterns were observed for the mixed target also.

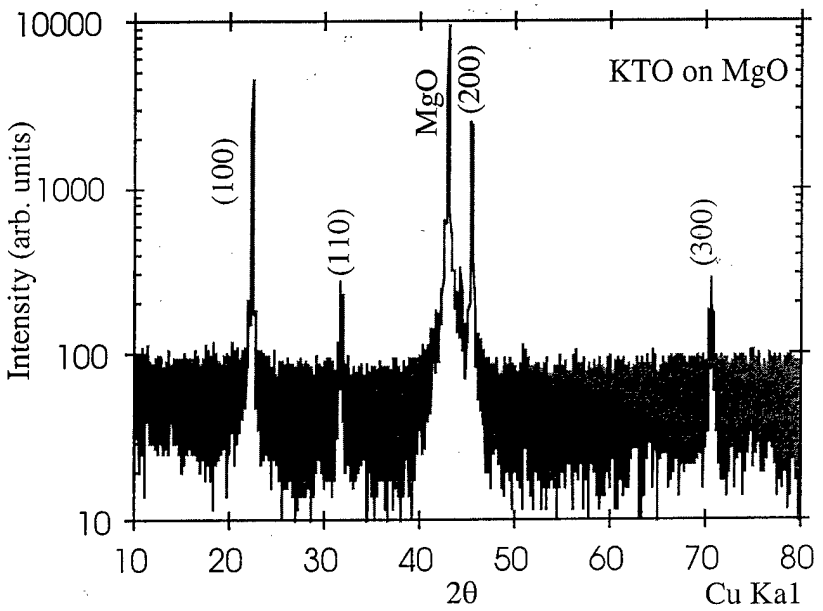

Fig. 4.1-2: XRD of $KTaO_3$ film deposited on MgO substrate using Target #2. After deposition the film was cooled to room temperature in 5h. Note the reflection due to (110) plane.

4.2 Contactless Microwave Measurements

We have enlisted the aid of Dr. Richard Geyer of NIST-Boulder to do contactless microwave dielectric measurements on some of our films. Dr. Geyer reports that he has made some preliminary room temperature microwave measurements, at 9GHz, on $Ba_{0.6}Sr_{0.4}TiO_3$ films, and $KTaO_3$ films that we have grown on LAO by PLD. He has found preliminary dielectric constants of 1330 and 325 for BSTO and $KTaO_3$ films, respectively. The latter value exceed room temperature values for $KTaO_3$ single crystals which he has studied. His only loss measurements to date give an upper limit for the tan δ at room temperature and 9GHz, a value of 0.014.

4.3 Other Targets

Targets with composition $SrTiO_3$, $Ca_{0.05}Sr_{0.95}TiO_3$ and $Ca_{0.1}Sr_{0.9}TiO_3$ were made by high temperature synthesis. XRD characterization indicated single phase formation.

4.4 Masks for capacitance measurements

The 4 capacitor shadow mask design with interdigitated capacitors were made. The mask has 6 contact pads and finger widths and separation between the fingers of 100 micrometers. The mask was originally designed to be held magnetically against the film, but initial experiments show that the fingers of the mask get magnetized by the magnet causing lifting of the fingers and poor definition of the consequent capacitor fingers. We intend to overcome this by mechanical attachment so that the whole mask is planar.

Task 5 - Materials Discovery Research

5.1 Investigation of $ACu_3Ti_4O_{12}$ perovskite-type phases

$ACu_3M_4O_{12}$ (A = Cd, Ca; M = Ti, Mn) phases crystallize in a perovskite-like phase $[A_{0.25}Cu_{0.75}MO_3]$ with cubic symmetry (space group *Im3*) at room temperature with a doubling of the ideal perovskite cell. The doubling of the unit cell is due to the ordering of the A^{2+} and Cu^{2+} ions and the distortion of the oxygen sublattice, which leads to a tilted three-dimensional network of MO_6 octahedra sharing corners as shown in Figure 5.1-1. The M-O-M bond angle is ~150∞ instead of 180∞, as in the ideal perovskite structure. This distortion creates two different polyhedra at the A site: a slightly distorted 12 oxygen-coordinated Ca site and a grossly distorted icosahedron at the Cu site. There are three sets of Cu-O distances at ~1.9, 2.8 and 3.2 Å, each forming an approximately square-planar coordination. The unusual feature of this structure is that it requires a Jahn-Teller ion, such as Cu^{2+}, Mn^{3+} in the A-site. No information is available in the literature regarding the dielectric properties of any member of this family of compounds. Recently, we have successfully synthesized high dense sintered samples of $CdCu_3Ti_4O_{12}$ and

$CaCu_3Ti_4O_{12}$ phases. Low temperature structural and dielectric property measurements are in progress to check for any ferroelectric transitions in the above compounds.

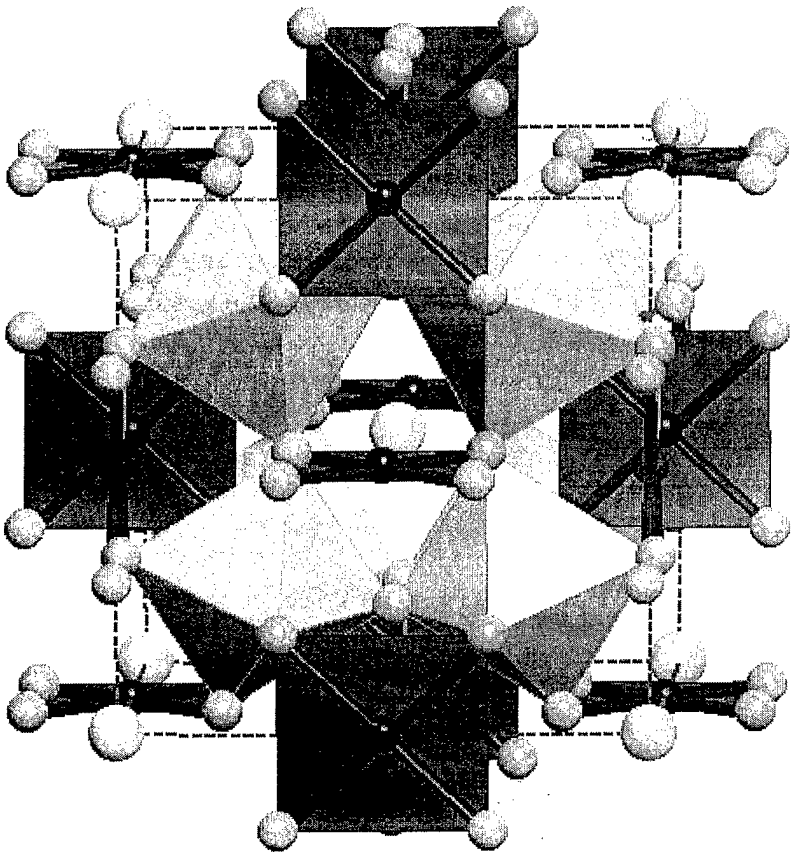

Figure 5.1-1 Perovskite-like crystal structure for $ACu_3M_4O_{12}$ (A = Cd, Ca; M = Ti, Mn) with cubic symmetry (space group *Im3*).

Task 6 - Rapid Intrinsic Film Test (RIFT) Development

We finished fabrication and began testing the first generation, low temperature RIFT package (RIFT 1). Using what we had learned in the construction of RIFT 1 and the testing of the deposited interdigitated capacitors, we designed a package to measure BSTO films near room temperature non-destructively (RIFT 2).

We completed the fabrication and assembly of RIFT 1 in late December. We have recently been testing the package to verify proper operation and identify design problems. We fabricated superconducting coplanar resonators which will be used in RIFT 1. These devices will be tested early in Q3 to complete the second milestone for this task. Also in December, we began designing a package (RIFT 2) which we will use to test room temperature ferroelectric materials using a clamped interdigitated capacitor. We made a number of small, but significant, design

improvements to improve ease-of-use, such as loosened tolerances on non-critical parts and a more robust clamping mechanism between sample and circuit. RIFT 2 is now being made. We designed, fabricated, and tested interdigital capacitors appropriate for use in RIFT 2 (see Task 2).

In the upcoming quarter, we will finish the testing of the RIFT 1 package and begin using it to test BSTO x = 0.06 films. We will design and manufacture a 2nd generation low temperature probe. RIFT 2 will be made and tested for proper operation. We will then use it to characterize BSTO x = 0.60 films and cross-check our results on deposited capacitors.

Frequency Agile Materials for Electronics

Q3

Date: April 28, 1999

Period covered in this report: 1/1/99 through 3/31/99

Program Title: Novel Ferroelectric Materials for Satellite Communications

Contract # DABT63-98-C-0046

Performing Organization: DuPont Superconductivity

Subcontractor: University of Colorado

Summary

We completed our first set of designed experiments to optimize large area $Ba_xSr_{1-x}TiO_3$ (BSTO) thin films for x=0.6. This completes the third required milestone for Task 2. The results of the designed experiments demonstrate quantitative relationships between film crystallinity, composition, deposition conditions, ε, and tan δ. Importantly, we found that reduced film strain correlates well with increased the tunability for $Ba_{0.6}Sr_{0.4}TiO_3$ films. We plan to complete a similar milestone for Task 1 during the next quarter. The single phase $KTaO_3$ films which were produced by exploratory pulsed laser deposition (Task 4) last quarter have been characterized for capacitance and tan δ versus temperature at 100 kHz. A tan δ as low as $1x10^{-3}$ was measured. Higher frequency measurements with applied bias will be carried out next quarter. In the materials discovery effort (Task 5), we synthesized a new series of perovskite oxides with the general formula $A^{3+}Cu_3Ti_3FeO_{12}$ (A = La-Gd). X-ray diffraction data indicated that the above compounds crystallize in body centered cubic unit cell with a ~ 7.5 Å. The Ti and Fe cations are disordered at the B-site of the perovskite structure. Low temperature structural and dielectric property measurements are in progress to check for any ferroelectric transitions in the above compounds.

Progress by Task

Task 1 - Large Area Sputtered Film Manufacturing for Low Temperature Applications

We deposited four $Ba_{0.06}Sr_{0.94}TiO_3$ (BSTO06 or BSTO x = 0.06) films on 51 mm diameter Si and $LaAlO_3$ (LAO) substrates to continue cross-checking the intercomparability of the low temperature composition with the room temperature composition. We discovered in late February that both our BSTO06 and $Ba_{0.6}Sr_{0.4}TiO_3$ (BSTO60 or BSTO x = 0.6) sputtering targets were inadvertently doped with Fe and Zr; we decided to continue work on the doped BSTO60

material (since we have concentrated primarily on it in Q1 and Q2) and wait for undoped BSTO06 targets.

1.1 BSTO x = 0.06 Films on $LaAlO_3$

We deposited Au interdigitated capacitors on two BSTO06/LAO films to extract information on the dielectric properties at low frequencies, and to compare them to BSTO60 films deposited under similar conditions. In Table 1.1-1 below, we compare the electrical properties of the two films measured at room temperature. The true substrate temperature is ~ 200 °C below the heater setpoint, T_{dep}. The relative permittivity ε_r and loss tangent, tan δ, were extracted from the raw data using the electromagnetic simulation package Sonnet™. We define tunability $\Delta\varepsilon/\varepsilon = [\varepsilon_r(0\ V) - \varepsilon_r(40\ V)]/\ \varepsilon_r(0\ V)$. Additionally, we measured sample 16312 at 80 K in our cryogenic probe station. As expected, moving closer to the Curie temperature increased the permittivity and tunability while decreasing the loss. These data are qualitatively similar to the data obtained on BSTO60 (see section 2).

Table 1.1-1. Comparison of electrical properties of BSTO06 films at room temperature.

sample #	T_{dep} (°C)	ε_r(0 V)	tan δ (0 V)	$\Delta\varepsilon/\varepsilon$ (%)
16312	875[a]	318 (406)[b]	7.8 (3.4)[b] x10^{-3}	0.3 (0.5)[b]
16313	975[a]	230	4.7x10^{-3}	0.3

[a]deposited at 85 W_{rf} and 100 mTorr, film thickness ~ 300 nm
[b]measured at 80 K

1.2 Seven Vertical Lamp Heater

1.3 Rotating Magnetron Sputter Source

We completed the design of the seven lamp heater in Q3, as well as the related mounting fixtures and feedthroughs. We will begin its manufacture in Q4 and expect its completion late Q4/early Q5. We will then install it in our secondary deposition unit (L560-0). This heater should increase our throughput of ferroelectric thin films by a factor of 3-5. We also had to perform heavy maintenance on L560-0, including replacing the high vacuum pump. No work was performed on the rotating magnetron sputter source as a result.

Task 2 - Large Area Sputtered Film Manufacturing for Ambient Temperature Applications

We deposited 32 BSTO60 films on Si, LAO, MgO, and CeO_2 buffered sapphire substrates. We did extensive electrical testing of films deposited in Q2 using deposited interdigitated capacitors. We also improved our electromagnetic simulations of the capacitors to provide higher accuracy and reliability in the extracted dielectric data. As mentioned in section 1, we discovered that the sputter targets we were using were inadvertently doped with 0.25 at.% Fe and 0.25 at.% Zr. All the samples produced to date therefore have some slight Fe and Zr doping. We have received BSTO targets which will allow us to look at undoped samples, as well as samples with different cation ratios.

2.1 BSTO x = 0.60 Films on $LaAlO_3$

We continued to deposit BSTO60 films on LAO to confirm our earlier experiments as well as to examine the role of intrinsic stress as a function of processing conditions and its effects on the dielectric properties. We also extensively measured the low frequency dielectric properties of six of the BSTO60/LAO samples we made in Q2 as part of our statistically designed experiment to identify the optimum deposition conditions.

In Figure 2.1-1, we plot the (fitted) relative permittivity and loss tangent of the six films from the designed experiment. All were measured by depositing Au interdigitated capacitors and measuring the device capacitance and loss at 100 kHz and ambient temperature. From our earlier results on these same films, we conclude that the permittivity and loss correlate well with the crystalline quality: at a given sputtering power, higher deposition temperatures and lower rates yield better films. In Figure 2.1-2, we plot the tunability of these films, again as a function of heater setpoint temperature and deposition pressure. These results correlate well with the residual stress in the films, reported on in Q2.

To date, we have not done elevated temperature measurements of the electrical properties of BSTO60 films (we are developing that capability, see section 6). From our electrical and x-ray diffraction (XRD) measurements, we believe that all of the films in Figures 2.1-1 & 2 are in the ferroelectric (as opposed to the desired paraelectric) state. Although the composition in bulk is paraelectric at room temperature, we believe the Curie temperature is increased by strain effects. We believe measurements taken above the Curie temperature will show much improved tunability and lower loss. We will undertake those measurements in Q4.

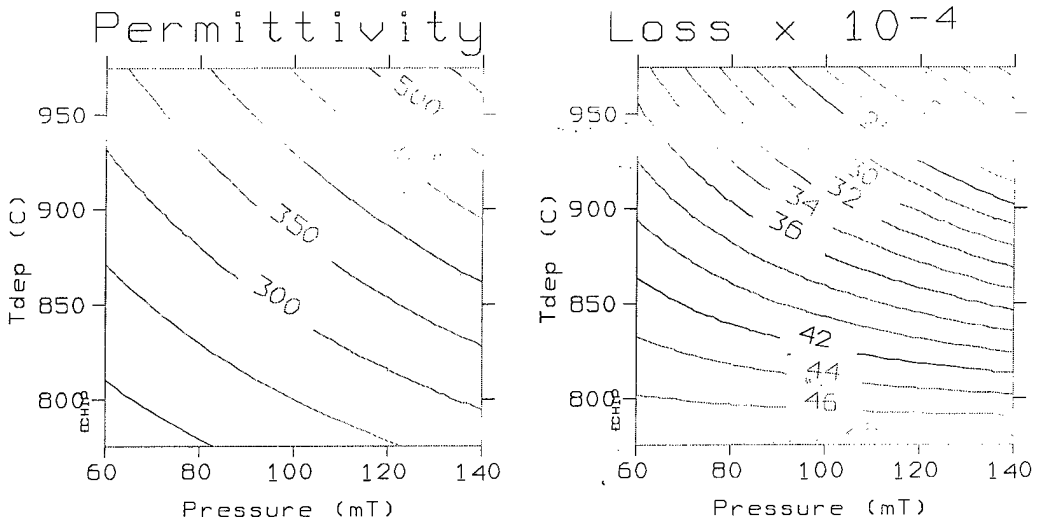

Figure 2.1-1. The relative permittivity (left) and loss tangent (right) of BSTO60/LAO films deposited at 110 W versus heater setpoint T_{dep} and gas pressure. Lowest loss, highest permittivity films are achieved at high pressures and temperatures, which correlates with overall crystalline quality (measured by rocking curves).

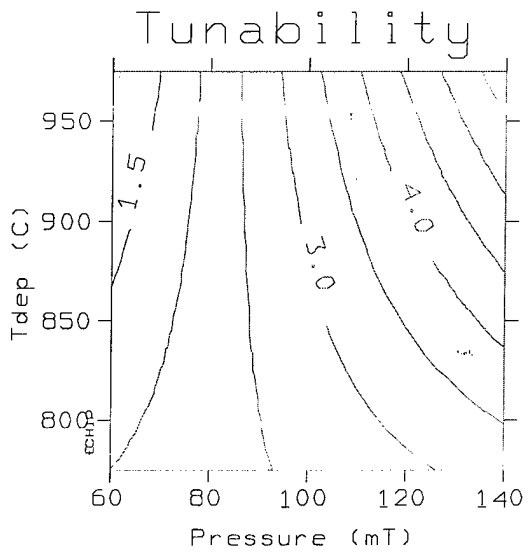

Figure 2.1-2. The tunability (percentage change in relative permittivity between 0-40 V dc) of the films in Figure 2.1-1. This correlates well with the earlier-measured c-axis strain of the films: the higher the strain, the lower the tunability.

2.2 BSTO x = 0.60 Films on MgO

We deposited nine BSTO60 films on 51 mm diameter MgO substrates. As opposed to LAO, we had some difficulty growing high quality films: we observed some misorientation peaks in XRD at all deposition temperatures. In Figure 2.2-1, we plot the phase scans and rocking curves for a BSTO60/MgO film deposited at high temperature (bottom, sample 17673) and at a lower temperature (top, sample 17532). Although the film quality is improving at the higher temperature, there is still some slight misorientation. We do not yet know what impact this has on the electrical properties. One encouraging indicator is that the strain is lower on MgO than on LAO (as measured by the elongation of the c-axis relative to the bulk). Under similar deposition conditions, the c-axis strain of BSTO60 is 1% on LAO but 0.5 % on MgO. Finally, in Figure 2.2-2, we plot the phi scans of the BSTO (112) and the MgO (202) peaks. The data shows that the growth of BSTO on MgO is "cube-on-cube", i.e. $(00l)_{BSTO} \parallel (00l)_{MgO}$ and $(h00)_{BSTO} \parallel (h00)_{MgO}$. In Q4, we will continue to examine the growth of BSTO on MgO, as well as investigate the electrical properties of the films.

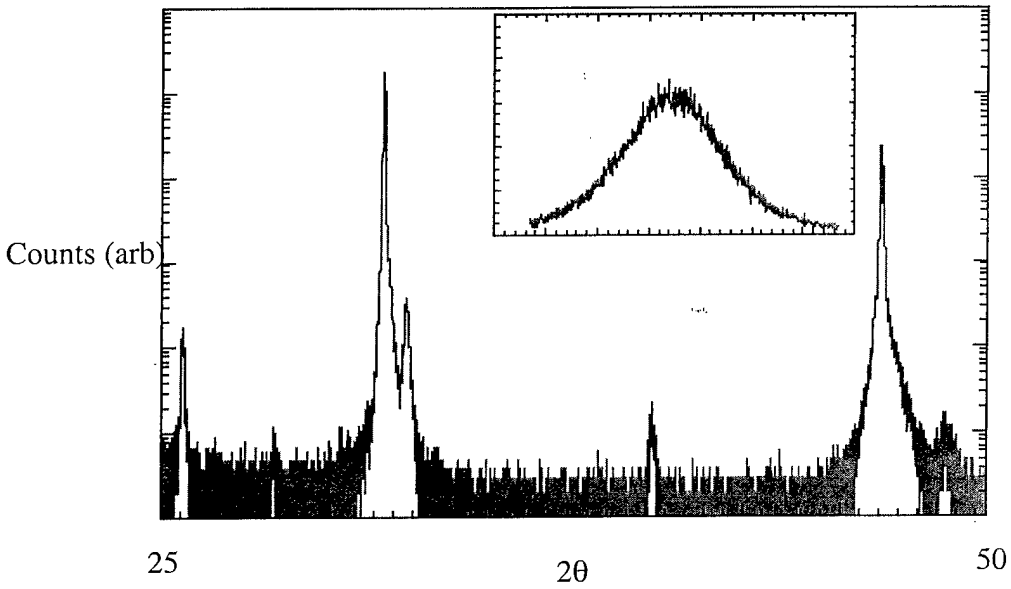

Figure 2.2-1a. BSTO60 on MgO, T_{dep} = 875 °C. Unindexed peaks are MgO. Note presence of small (110) peak, indicating some misorientation. Insets: BSTO60 (002) rocking curves. Note as the temperature increases the rocking curves narrows and the misorientation ratios (002)/(110) decrease.

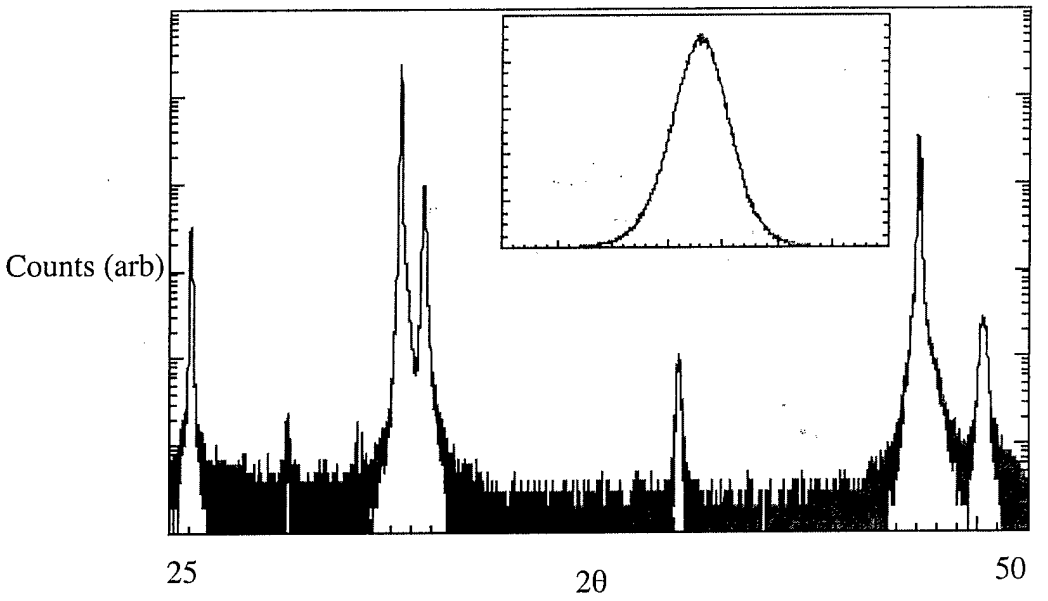

Figure 2.2-1b. BSTO60 on MgO, T_{dep} = 975 °C. Unindexed peaks are MgO. Note presence of small (110) peak, indicating some misorientation. Insets: BSTO60 (002) rocking curves. Note as the temperature increases the rocking curves narrows and the misorientation ratios (002)/(110) decrease.

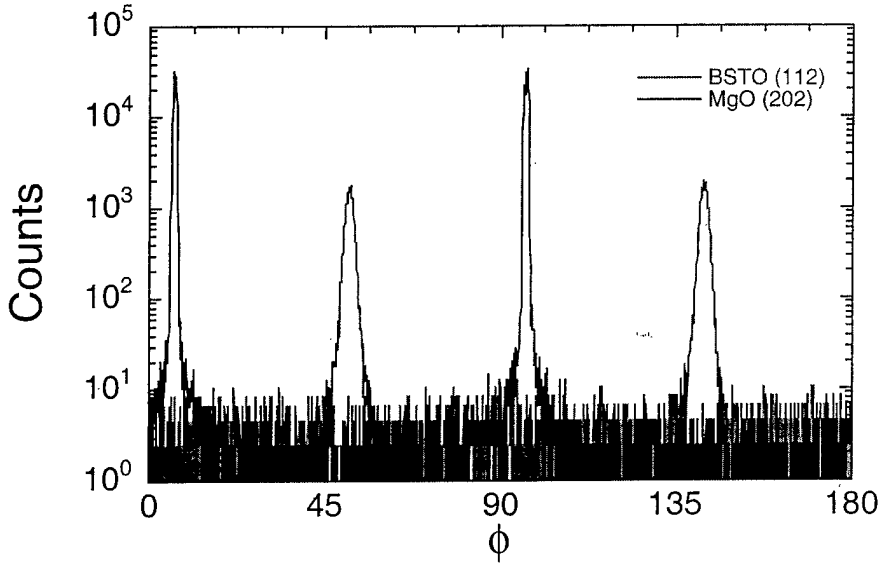

Figure 2.2-2. Phi scan of BSTO60 on MgO (deposited at 975 °C) indicating cube-on-cube growth.

2.3 BSTO x = 0.60 Films on CeO_2 Buffered Sapphire

We also began investigating the growth of BSTO60 on CeO_2 buffered sapphire. So far, we have not been able to achieve satisfactory epitaxy. We will pursue this further in Q4.

Electromagnetic Modeling and Testing

We are improving our models of the deposited interdigitated capacitor structures used to measure the low frequency dielectric properties. By simulating all the fingers of the capacitor, rather than extrapolating from a structure with a reduced number of fingers (to save memory and calculation time), we have increased the accuracy and reliability of our data on the relative permittivity and loss tangents of our BSTO films. Using our improved models, we now obtain less than 3% variation in the measured relative permittivity of a known substrate (MgO ε_r = 9.8, LAO ε_r = 23.8) across its entire diameter. This variation is probably caused by fabrication uncertainties. We are also extending our improved capacitor simulations to the room temperature RIFT package (see section 6).

Task 4. Exploratory Laser Ablation Processing (University of Colorado)

In the last quarterly progress we reported on the optimization of film growth conditions for BSTO and KTaO3 materials by pulsed laser deposition. In this quarterly progress we have successfully standardized the capacitance measurement technique. The capacitance and loss $1/\omega RC$ (tan δ) were measured using an LCR meter, HP 4192A, at 100kHz and 1MHz. The temperature variation of capacitance has also been performed in a closed cycle helium cryostat. A standard (2pF) capacitor was used to measure with $\leq$1% error for a given length of the probe cables.

4.1.Measurements on Polycrystalline pellets

A coplanar slot capacitor was used to test the bulk pellets. Pellets were prepared by sintering at 1450°C for 12 hours. Silver electrodes were deposited by thermal evaporation with a

mechanical mask to form a slot capacitor as shown in Fig. 4.1. The measurements were carried out in a closed cycle helium refrigerator at various temperatures.

Fig. 4.1 Coplanar Slot Capacitor for bulk polycrystalline pellets

Figures 4.2a, 4.2b, and 4.3 represent the measured capacitance and tan δ as a function of temperature and DC bias field at 100kHz and 1MHz frequencies, for bulk $Ba_{0.6}Sr_{0.4}TiO_3$, $Ba_{0.1}Sr_{0.9}TiO_3$ and $KTaO_3$, respectively.

As can be seen, the capacitance values did not vary significantly between 100 kHz and 1 MHz. The tan δ values for the BSTO samples are in the similar range of that reported in literature. However, the bias of 35 V has negligible effect on the tunability. We presume that the field is too low for the slot width of 1mm. We will construct a new shadow mask to produce slot widths in micron scale for studying tunability. The dielectric constant calculations using the conformal mapping procedure made by Wu et al. (IEEE transactions on applied superconductivity, Vol. 4, pp.156-160, 1994), for bulk materials is being carried out for our present investigation.

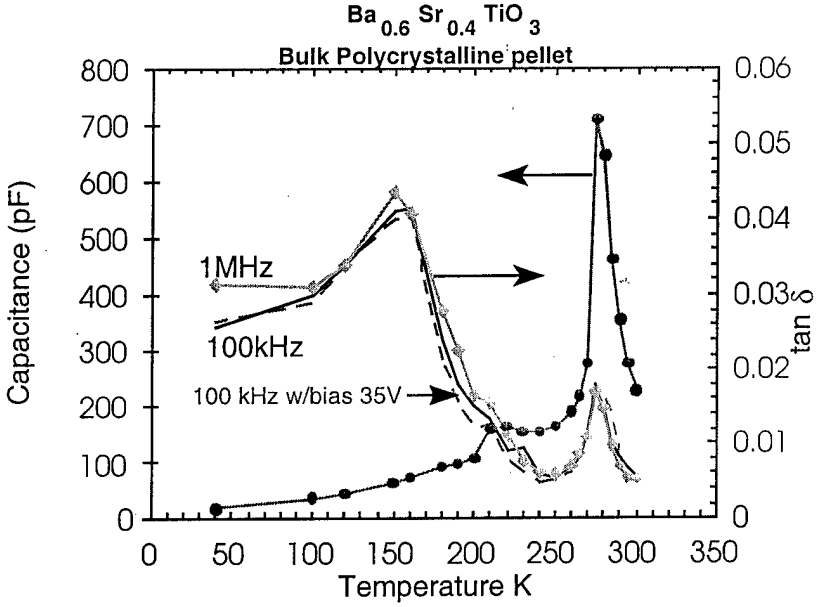

(a)

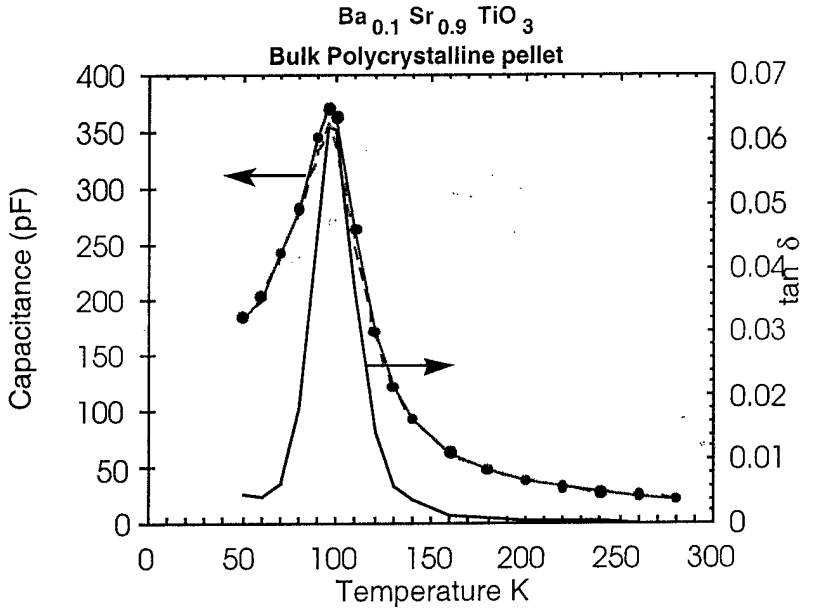

(b)

Fig. 4.2 Capacitance and Loss tangent versus temperature at 100 kHz and 1 MHz for (a) $Ba_{0.6}Sr_{0.4}TiO_3$, and (b) $Ba_{0.1}Sr_{0.9}TiO_3$ for coplanar slot capacitor on bulk polycrystalline pellets.

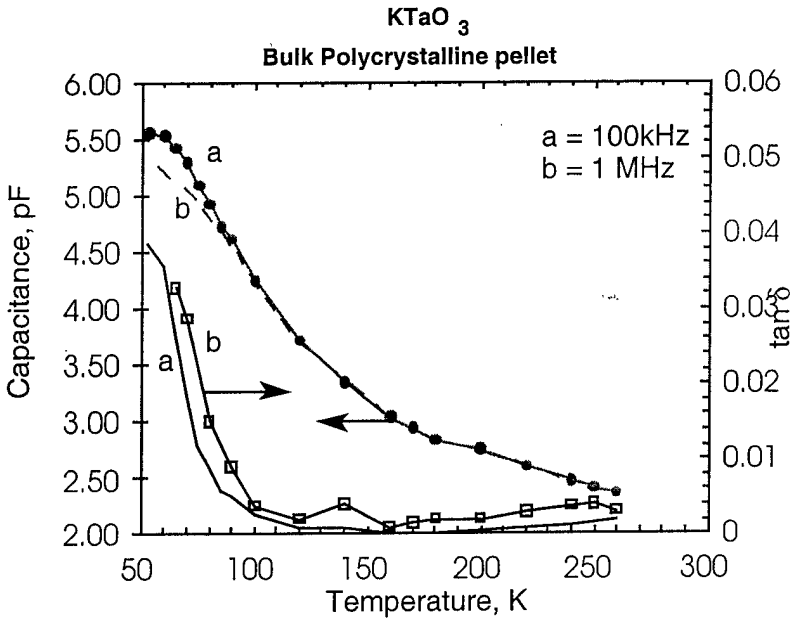

Fig. 4.3 Capacitance and tanδ for bulk $KTaO_3$ pellet.

The transition temperature for the pellet $Ba_{0.1}Sr_{0.9}TiO_3$ is 96K, which is 10K higher than that reported in the literature. However, at this low concentration of Ba, a change in 1% of Ba content in the grain varies the transition temperature by 8-10K (the T_c increases with increase in Ba content).

The capacitance C at Curie temperature T_c, and tan δ without DC bias is listed in Table 1.

TABLE 1. Capacitance, T_c, and tan δ for bulk polycrystalline pellets measured at f=100kHz and zero bias.

Compound	T_C (K)	Capacitance (pF)			tan δ	
		300K	T_C	77K	300K	77K
$Ba_{0.6}Sr_{0.4}TiO_3$	275K	227	709	--	0.0054	--
$Ba_{0.1}Sr_{0.9}TiO_3$	96K	23	370	260	0.0001	0.015
$KTaO_3$	--	2.60	--	5.00	0.0001	0.011

4.2. Measurements on $KTaO_3$ thin films

(00l) oriented, 250nm thick, $KTaO_3$ thin films were grown on single crystal LAO substrate by pulsed laser deposition using conditions described in our previous progress report. For capacitance measurement, we used a 4 capacitor shadow mask design with interdigitated capacitors. The mask has 6 contact pads, with finger widths and separation between the fingers of

100 microns. The stainless steel mask originally designed to be held magnetically against the film had problem of poor definition of capacitors caused by lifting of fingers with the magnetic poles, is overcome by using a non-magnetic mask, such as Mo, magnetically held at the edges.

The interdigitated capacitors were made using this mask by thermal evaporation of silver to a thickness of 200 nm. Fine gauge copper leads were attached to each capacitors using silver paste. The sample was then annealed at 250°C in air.

Figure 4.4 shows the capacitance and tan δ for KTaO3 film at 100 kHz at various temperature. The capacitance measured on two different capacitors and one on a different film are within 5% range. The plot shown below is an average on 2 different capacitors on the same film. However, application of DC bias has no significant effect on the capacitance. The LCR meter, HP 4192A, can supply internally a bias voltage of only ±35V. This generates a very low field to observe any tunability.

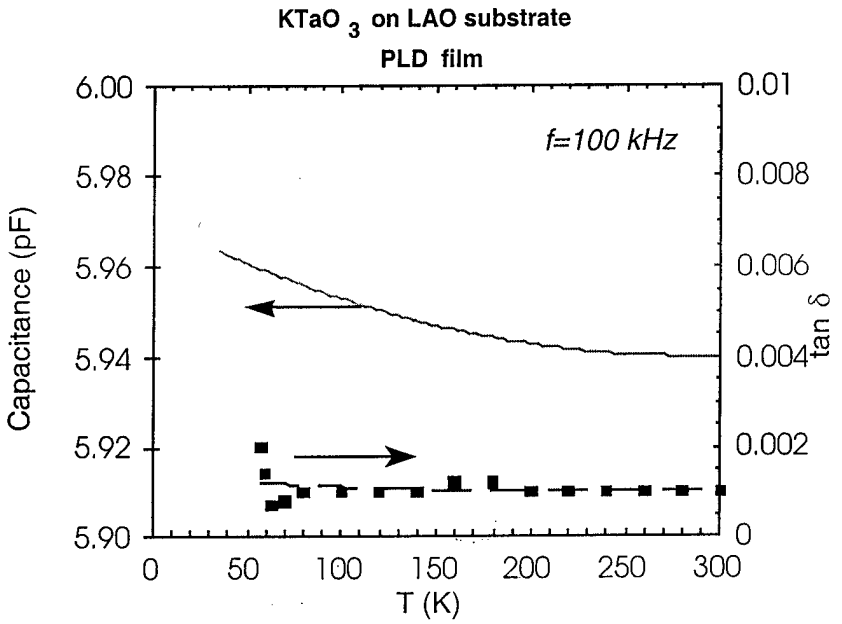

Fig. 4.4. Capacitance and tan δ versus temperature at 100 kHz for 250 nm KTaO3 film on LAO substrate. 200 nm silver electrodes for interdigitated capacitors was deposited by thermal evaporation using Mo shadow mask.

The dielectric constants of the film will be evaluated in future. These films will be further tested in the press-on capacitor electrodes with pressure rig (which is now complete) using the Au/Ti electrodes provided by DuPont.

Task 5 - Materials Discovery Research

Synthesis and characterization of $ACu_3M_4O_{12}$ pervoskite-type phases

$ACu_3M_4O_{12}$ (A = Cd, Ca; M = Ti, Mn) phases crystallize in a perovskite-like phase [$A_{0.25}Cu_{0.75}MO_3$] with cubic symmetry (space group *Im3*) at room temperature with a doubling of the ideal perovskite cell. The doubling of the unit cell is due to the ordering of the A^{2+} and Cu^{2+} ions and the distortion of the oxygen sublattice, which leads to a tilted three-dimensional network

of MO_6 octahedra sharing corners. The M-O-M bond angle is ~150° instead of 180°, as in the ideal perovskite structure. This distortion creates two different polyhedra at the A site: a slightly distorted 12 oxygen-coordinated Ca site and a grossly distorted icosahedron at the Cu site. There are three sets of Cu-O distances at ~1.9, 2.8 and 3.2 Å, each forming an approximately square-planar coordination. The unusual feature of this structure is that it requires a Jahn-Teller ion, such as Cu^{2+}, Mn^{3+} in the A-site.

Recently, we have synthesized a new series of perovskite oxides with the general formula $A^{3+}Cu_3Ti_3FeO_{12}$ (A = La-Gd). X-ray diffraction data indicated that the above compounds crystallize in body centered cubic unit cell with a ~ 7.5 Å. The Ti and Fe cations are disordered at the B-site of the perovskite structure. The crystallographic data is given in Table 5.1. Low temperature structural and dielectric property measurements are in progress to check for any ferroelectric transitions in the above compounds.

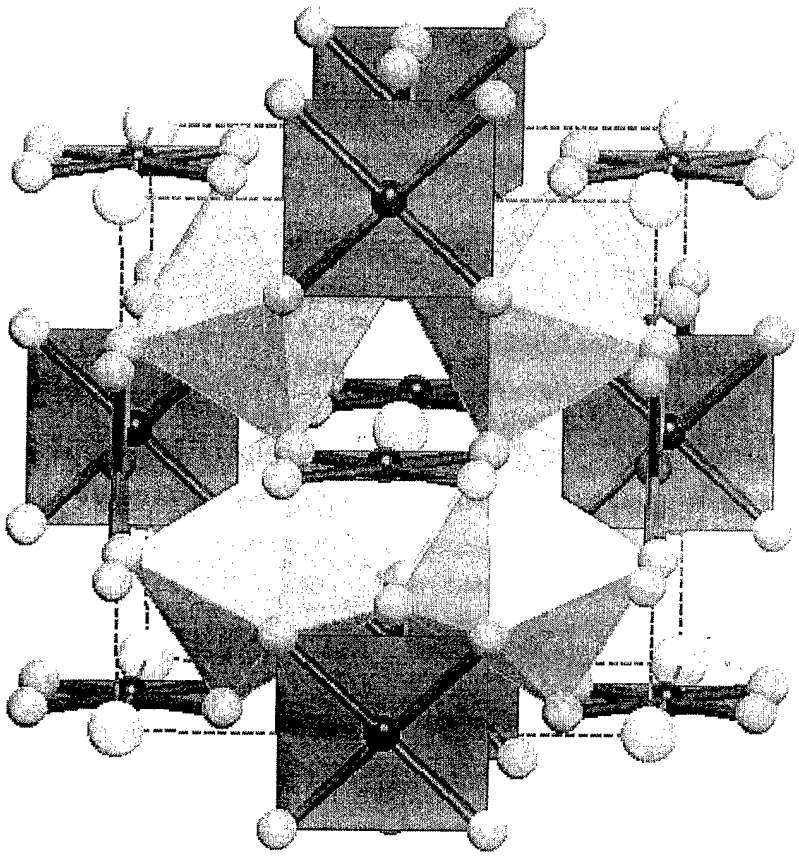

Table 5.1.

Compound	*a*, lattice parameter (Å)
$LaCu_3Ti_3FeO_{12}$	7.454
$NdCu_3Ti_3FeO_{12}$	7.430
$SmCu_3Ti_3FeO_{12}$	7.422
$GdCu_3Ti_3FeO_{12}$	7.408
$YCu_3Ti_3FeO_{12}$	7.393

Task 6 - Rapid Intrinsic Film Test (RIFT) Development

We completed the fabrication and began testing of the low (RIFT1) and high temperature (RIFT2) packages by mid-Q3. We are still in the process of understanding these packages for non-destructive testing of ferroelectric films.

We designed a novel, backside-coupled coplanar superconducting resonator with dc bias for use in RIFT1. We have assembled and tested a TlBaCaCuO on MgO resonator with an uncoated MgO test piece (presented in Table 6-1), using the minimum clamping force (~750 kPa). The designed resonant frequency was 5.441 GHz, assuming no airgap between the circuit and the test piece. We see one strong resonance (Q_u ~ 4000) at 2.906 GHz and a number of other resonances below 6 GHz. It is possible that there is an airgap between the two substrates, which could shift the resonant frequency far from the expected value. This hypothesis is partially supported by our data on the high temperature package, RIFT2.

Table 6-1. Summary of the initial resonator measurements in RIFT1.

T_{meas} (K)	Freq (GHz)	Ins Loss (dB)	Unloaded Q	Comments
38.5	1.155	-55	1408	
38.5	1.826	-28	5639	
38.5	2.906	-33	3946	
38.5	5.905	-30	~800	Filter-like response, not usable
48.1	1.155	-56	1113	
48.1	1.825	-29	5140	Q changes with coupling
48.1	2.906	-33	3750	
97.1	1.151	-60	754	Near T_c
97.1	1.795	-42	819	
97.1	2.863	-49	618	
97.1	5.867	-31	~400	Filter-like response
106.9				Above T_c, no resonances below 6 GHz

RIFT2 consists of an Au interdigitated capacitor (identical to the earlier designs) deposited on MgO clamped onto a test piece. We can measure the shift in the capacitance and device loss to obtain the dielectric permittivity and loss of the test piece. We assembled RIFT2 with a bare MgO test piece as well as shorting calibration piece (MgO wholly coated with a thick

layer of Au) and measured the impedance as a function of spring pressure. In Figure 6-1, we plot the impedance of the shorting calibration piece versus the applied spring pressure (from 11-40 kg on a 12 mm square area). Note there is a step change around 2000 kPa. Contrast this with the results of a bare MgO test piece over the same spring pressure range in Figure 6-2. Although the real part of the impedance is gradually increasing as the spring pressure is increased, it does not reach a steady value. There may still be an airgap present between the two MgO pieces. We will continue to investigate to determine whether our technique will be a viable one to repeatably measure bare films.

We have purchased an environmental chamber to make temperature-dependent measurements using RIFT2. Together with the RIFT1 probe, this will allow us to measure the dielectric properties of ferroelectric thin films non-destructively over a very wide temperature range (4.2-600 K).

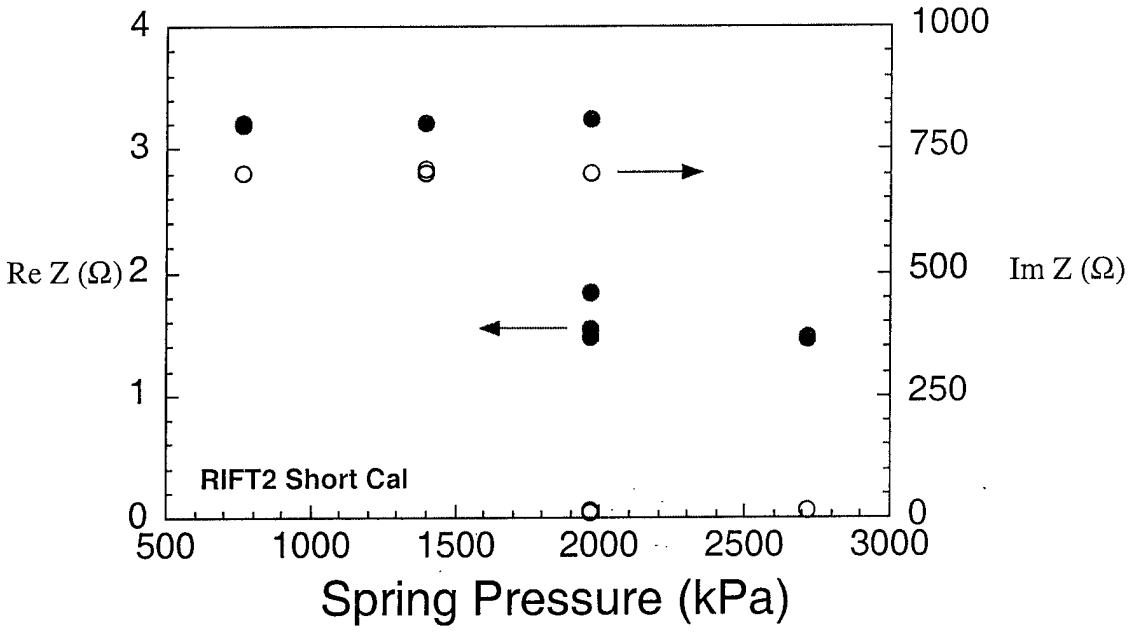

Figure 6-1. The complex impedance (closed symbols = real, open symbols = imaginary) of the short calibration piece as a function of spring pressure applied to the package. Note the step change to lower magnitude near 2000 kPa.

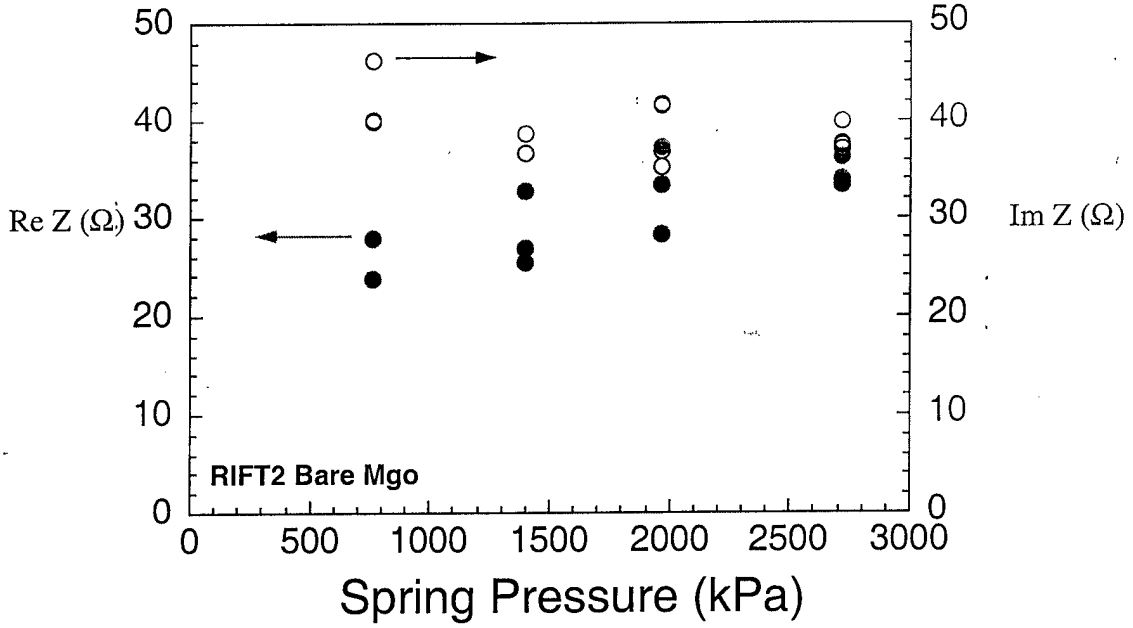

Figure 6-2. Impedance of RIFT2 capacitor with bare MgO test piece clamped on top as a function of applied spring pressure. It is not clear that a steady value has been reached over this range of pressures.

Frequency Agile Materials for Electronics

Q4

Date: July 30, 1999

Period covered in this report: 4/1/99 through 6/30/99

Program Title: Novel Ferroelectric Materials for Satellite Communications

Contract # DABT63-98-C-0046

Performing Organization: DuPont Superconductivity

Subcontractor: University of Colorado

Summary

We completed the fabrication of five process validation wafers using optimized conditions for large area $Ba_xSr_{1-x}TiO_3$ (BSTO) thin films with x=0.06 and for x=0.6. The reproducibility of the structural properties of these samples was excellent as measured by x-ray diffraction. Dielectric measurements of these samples will be completed in Q5 to finish the third milestone for Task 1 and 2. In Task 3, multilayer film development, we demonstrated the fabrication of a 0.35 μm thick YBCO film on a 0.2 μm BSTO film. The YBCO film had a microwave surface resistance of < 375 $\mu\Omega$ (at 77 K and 7.9 GHz) which is sufficient to produce high Q microwave devices and satisfy milestone 3C. Thin film samples of the following materials were fabricated by laser ablation and tested: 1) $Ba_{0.6}Sr_{0.4}TiO_3$, 2) $Ba_{0.6}Sr_{0.4}Ti_{0.99}Mn_{0.01}O_3$, 3) $Ba_{0.6}Sr_{0.4}TiO_3$ with 30wt% of MgO, 4) $BaTi_{0.85}Sn_{0.15}O_3$, 5) $Ba_{0.1}Sr_{0.9}TiO_3$, and 6) $Ca_{0.05}Sr_{0.95}TiO_3$. This work combined with the previously reported work on $KTaO_3$ completes the first milestone for Task 4. Under Task 5, work on $ACu_3M_4O_{12}$ phases was continued and extended to various new solid solution compositions. Some of these materials show unusually high relative dielectric constants (up to 15000) at room temperature. This completes the first milestone for Task 5. Under Task 6, work on the RIFT device demonstrated that air gaps less than 1 μm may be difficult to achieve and that this may limit the utility of this technique. Further work is underway to optimize the RIFT technique (i.e. achieve smaller air gaps) and quantify its performance.

Progress by Task

Task 1 - Large Area Sputtered Film Manufacturing for Low Temperature Applications

We deposited ten $Ba_{0.06}Sr_{0.94}TiO_3$ (BSTO06 or BSTO x = 0.06) films on 51 mm diameter Si and $LaAlO_3$ (LAO) substrates in Q4 to address manufacturability issues, such as reproducibility and quality.

1.1 BSTO x = 0.06 Films on $LaAlO_3$

We used the results of the designed experiments we carried out in Q2 and Q3 to find the optimum conditions for sputter depositing a low loss, high tunability ferroelectric film. We made nine ~ 0.4 μm thick BSTO06 films on 51 mm diameter LAO. The structural properties of these films have been characterized by x-ray diffraction and the results for five identically processed films are summarized in Table 1.1-1. These samples are being tested now for electrical performance and we will have results in early Q5 to complete milestone 1.C. of producing five large area, high quality ferroelectric films for cryogenic applications.

Material	Sample #	c-axis (Å)	Δc (Å)	Rocking Curve FWHM
BSTO06	14708	3.949	0.0009	0.31
BSTO06	14709	3.948	0.0003	0.27
BSTO06	14710	3.948	0.0004	n/a
BSTO06	14711	3.949	0.0003	n/a
BSTO06	14712	3.947	0.0005	n/a

Table 1.1-1 X-ray diffraction results for five identical 0.4 μm thick BSTO06 films on 51 mm diameter LAO.

Rotating Magnetron Sputter Source

The fabrication of the new high throughput, high uniformity heater (which was designed in Q3) is nearly complete. We are awaiting the delivery of the final components. Once they arrive, we will install the heater and its related feedthroughs in our secondary deposition unit. We have also been determining the specifications for a new magnet assembly for our high rate rotating magnetron (RM) sputter source which is currently mounted in the secondary deposition system. We believe the new magnet design will give improved target usage, higher throughput, better uniformity, and reduced particulates in our manufactured films. We should be specifying a new magnet system in Q5. We purchased a 150 mm diameter YBCO sputtering target to continue testing the RM source.

Task 2 - Large Area Sputtered Film Manufacturing for Ambient Temperature Applications

We deposited 17 BSTO60 films on Si, LAO, MgO, and buffered sapphire substrates in Q4. We also refined our electromagnetic simulations of the test devices.

2.1 BSTO x = 0.60 Films on $LaAlO_3$

We deposited ten 0.4 μm thick BSTO60 films on LAO in Q4 to demonstrate reproducible high performance film fabrication and to look at manufacturability issues. We used the results of the experiments we performed in Q3 to determine the optimum deposition conditions and best

substrate. . The structural properties of these films have been characterized by x-ray diffraction and the results for six identically processed films are summarized in Table 2.1-1. These films will be tested to determine the uniformity of their electrical properties early in Q5 to satisfy milestone 2.C. During these depositions, we began to have wafer breakage problems during the O_2 backfill and cooldown to room temperature. We suspect the breakage was the result of poor substrate quality. In response, we reduced the backfill pressure to 2 Torr for some of the affected runs, which alleviated the breakage problem, but necessitated a post-anneal to more fully oxygenate those samples.

Material	Sample #	c-axis (Å)	Δc (Å)	Rocking Curve FWHM
BSTO60	14699	4.007	0.0014	n/a
BSTO60	14701	4.006	0.0010	0.28
BSTO60	14703	4.007	0.0006	0.26
BSTO60	14704	4.008	0.0008	0.34
BSTO60	14705	4.006	0.0012	0.27
BSTO60	14707	4.006	0.0009	0.27

Table 2.1-1 X-ray diffraction results for five identical 0.4 μm thick BSTO60 films on 51 mm diameter LAO.

We also annealed and remeasured eleven samples made during Q2 and Q3 at 450-550 °C for 8 hours to see if we could improve the electrical properties by reducing oxygen vacancies. We found that there was little to no change in the structural or electrical properties as a result of the low temperature anneal. We plot the pre- and post-annealed c-axis lattice constants of the 11 samples in Figure 2.1-1.

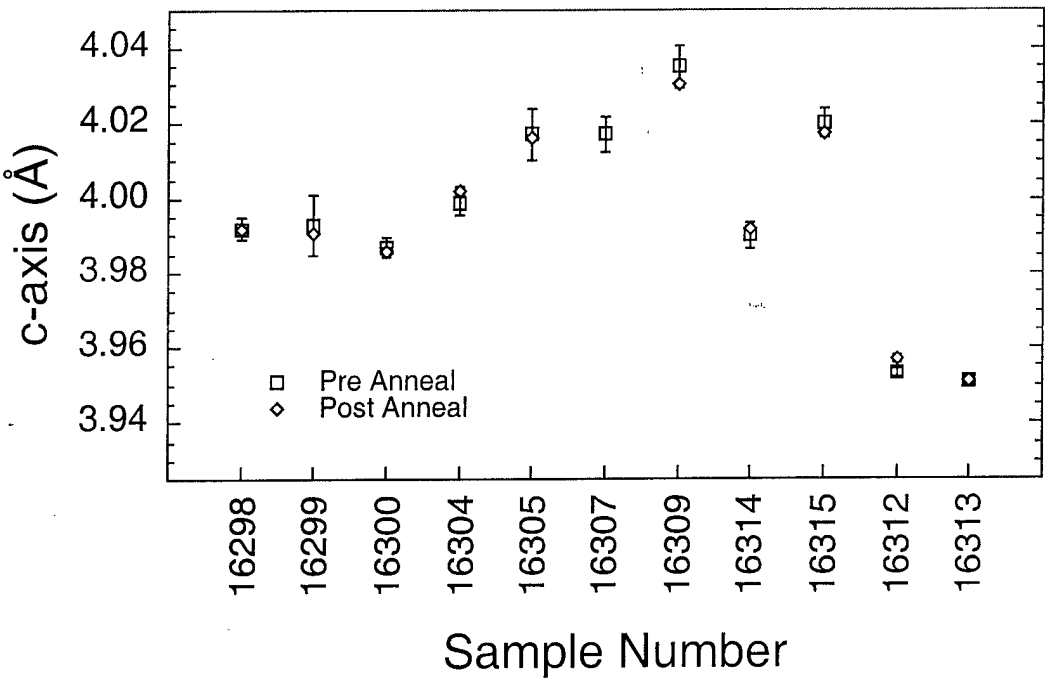

Fig. 2.1-1 The c-axis lattice constant of BSTO06 (16312-3) and BSTO60 (all others) films before and after low temperature annealing. No consistent change is observed in structural or electrical parameters.

2.2 BSTO x = 0.60 Films on MgO

We patterned and tested films made in Q3 on MgO and LAO to compare the electrical properties of films made under nominally identical conditions. We also compared the compositions of BSTO films deposited at ambient temperature on Si and at high temperature on MgO and sapphire: there was no difference in the compositions, but the high temperature films had higher (30-40%) measured rates. We found that the permittivity and loss of films deposited on LAO or MgO were comparable, but the tunability was generally lower on MgO. This may be caused by the poorer quality of the epitaxy of BSTO on bare MgO noted in Q3; we will investigate this further in Q5.

2.3 BSTO x = 0.60 Films on Buffered Sapphire

We investigated the growth of BSTO60 on buffered sapphire in Q4. Similar to our experiences with STO on CeO_2 buffered LAO (in Q1), we found BSTO60 did not grow epitaxially on CeO_2 buffered sapphire at the temperatures we were able to achieve (T_{sub} < 700 °C). We suspected that the CeO_2 surface was the culprit, so we then tried YBCO/CeO_2 buffers on sapphire. This worked quite well, as we show in Figure 2.3-1. BSTO60 films which were deposited directly on CeO_2 surfaces did not show epitaxy (sample 15179), while comparable films deposited on ~ 10 nm YBCO buffer layers on CeO_2 nucleated the desired phase.

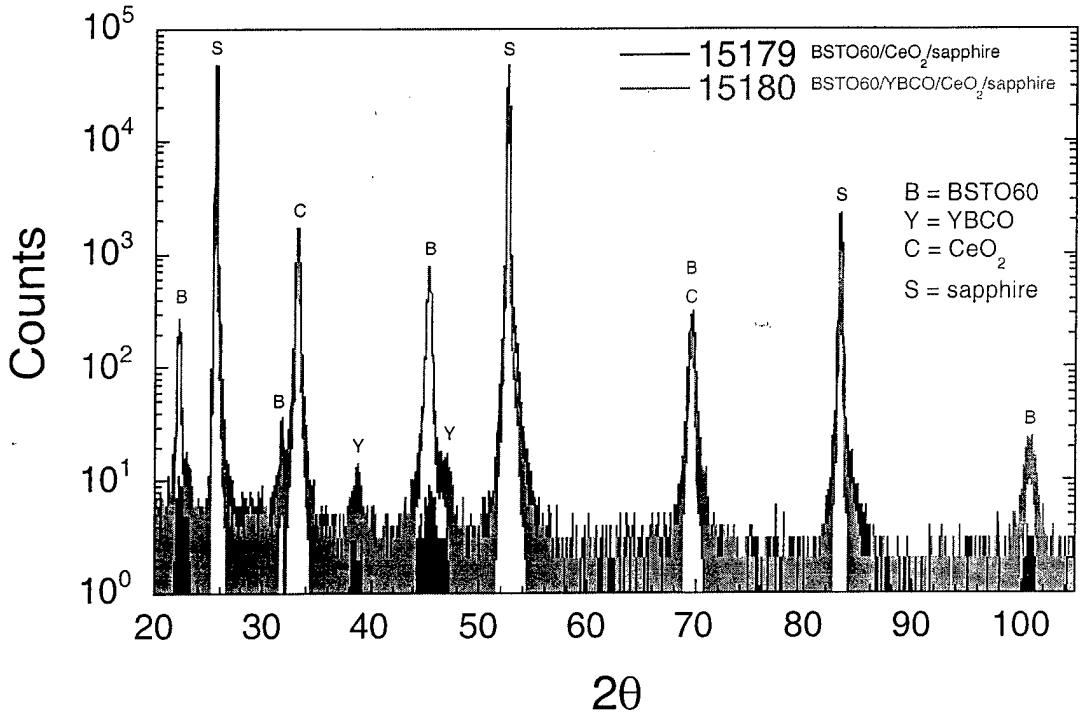

Fig. 2.3-1. Xray diffractograms of BSTO60 films on CeO_2 (15179) and YBCO/CeO_2 (15180) buffered sapphire. Notice that the prominent c-axis BSTO peaks near 22°, 45°, and 100° are missing or greatly reduced in sample 15179, indicating poor epitaxy.

2.4 Electromagnetic Modeling and Testing

In Q4, we purchased a license to the electromagnetic modeling software Sonnet™, which was used exclusively on this program. We continued to refine our models of the deposited interdigital capacitor structures used to measure the low frequency dielectric properties. We simulated each individual capacitor geometry and the corrections due to the finite gridsize. We also performed similar calculations for our collaborators at the University of Colorado for their test devices.

Task 3 - Multilayer Film Development and Manufacturing

We began investigating the growth of YBCO on top of BSTO, looking towards future coplanar device fabrication. We deposited 0.35 μm thick films of YBCO on a variety of BSTO60/LAO films. The structural and electrical properties of the films were then measured. The results are promising: all the YBCO films deposited were c-axis oriented (see Figure 3-1) and had low surface resistances (< 375 $\mu\Omega$ at 77 K and 7.9 GHz). This is sufficient superconducting quality to produce high Q microwave devices and satisfy milestone 3.C.

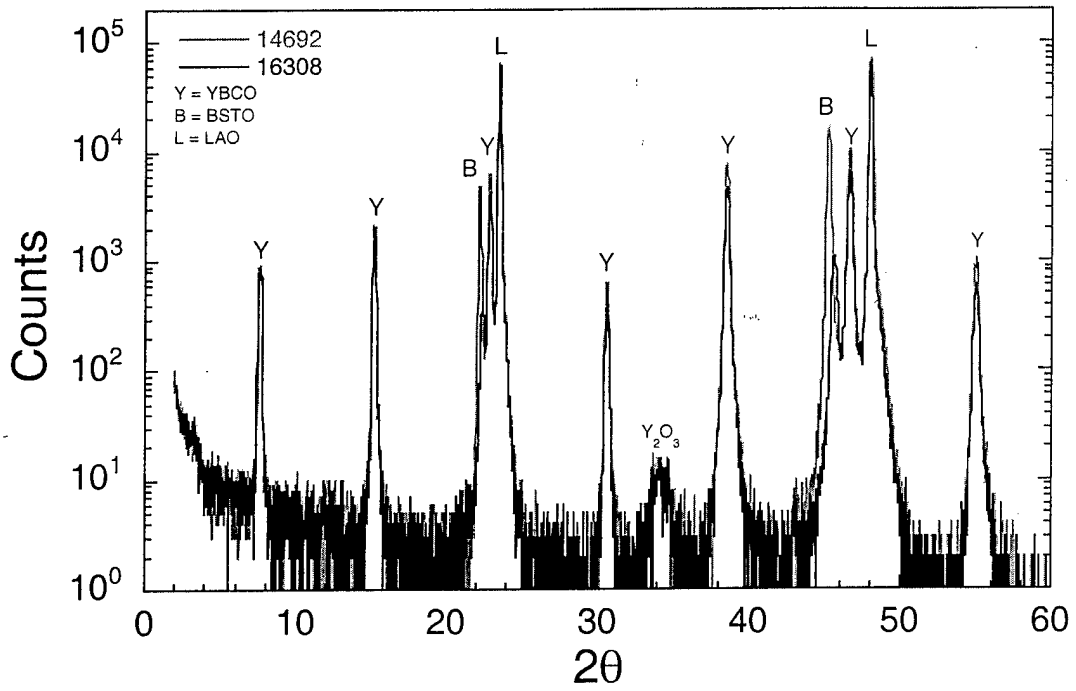

Fig. 3-1. Xray diffractogram of ~ 0.35 μm YBCO films grown on a 200 nm BSTO60/LAO film (14692) and a 25 nm BSTO60/LAO film (16308). Both are c-axis oriented and had R_s < 375 $\mu\Omega$ at 77 K. There is evidence for a slight amount of Y_2O_3 second phase in both films (peak at ~ 35°).

Task 4. Exploratory Laser Ablation Processing (University of Colorado)

We report the film fabrication and dielectric property measurements of both low and high temperature ferroelectric materials. Data on the following thin film materials are reported here: 1) $Ba_{0.6}Sr_{0.4}TiO_3$, 2) $Ba_{0.6}Sr_{0.4}Ti_{0.99}Mn_{0.01}O_3$, 3) $Ba_{0.6}Sr_{0.4}TiO_3$ with 30wt% of MgO, 4) $BaTi_{0.85}Sn_{0.15}O_3$, 5) $Ba_{0.1}Sr_{0.9}TiO_3$, and 6) $Ca_{0.05}Sr_{0.95}TiO_3$. Materials 1 to 4 were investigated for near room temperature operations, and 5 and 6 were studied for near 77K range. All films were deposited by pulsed laser ablation on <00l> $LaAlO_3$ substrates. Well-characterized stoichiometric targets were used. Oxygen post-annealing was carried out on all films to avoid any oxygen deficiency in the films. The films were heated at 900°C for 3h and cooled to RT at 1°C/min in flowing oxygen. The interdigitated capacitors were made using a shadow mask by thermal evaporation of Ag to a thickness of 200 nm. The mask has finger widths and separation between the fingers of 100 μm.

The capacitance and loss tangent were measured using HP 4192A LCR meter at 1 MHz. The temperature dependences were studied in a closed cycle helium refrigerator. A standard 2 pF capacitor was used for calibration giving $\leq$1% error at 1 MHz.

4.1. $Ba_{0.6}Sr_{0.4}TiO_3$ films

Coupled θ/2θ XRD scans showed only *h00* Bragg peaks for the $Ba_{0.6}Sr_{0.4}TiO_3$ film. Rocking curve (figure 4.1-1) shows that the FWHM is 0.84°. The instrumental and substrate broadening is estimated to be 0.25°. In figure 4.1-2 the capacitance and tan δ of the BSTO thin film is presented. The temperature dependence is significantly different from that of the bulk

material. The capacitance exhibits a much broader temperature variation with the maximum at 290 K, which is 20 K higher than the Curie temperature for the target which was separately measured. The tan δ values for thin films are much lower than those of the bulk. At 300 K, we obtained a tan δ of 0.002 at 1 MHz. Application of a dc bias voltage reduced the capacitance only by 1%. We can not observe significant tunability because of the low maximum electric field (3.5 kV/cm) possible with our shadow mask.

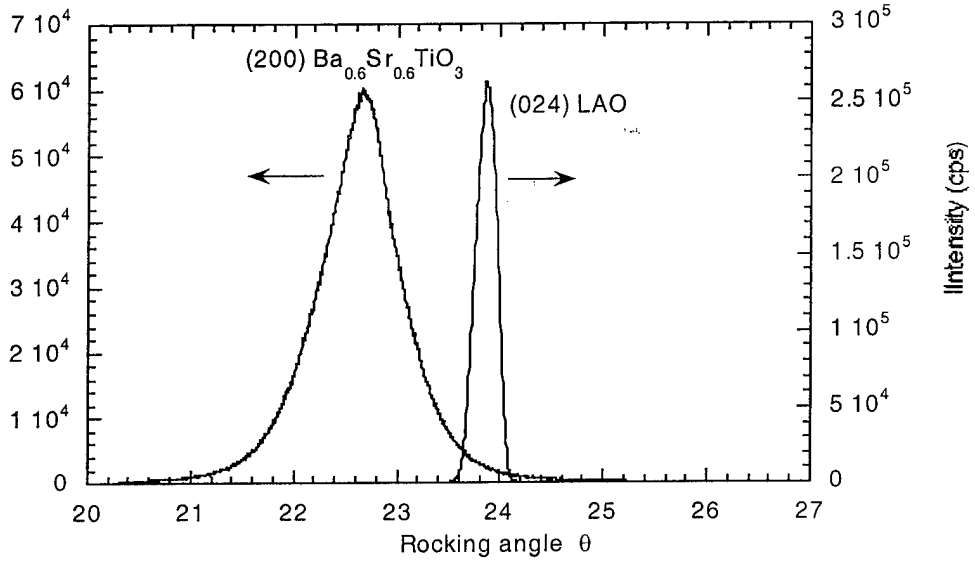

Fig. 4.1-1. Rocking curve for $Ba_{0.6}Sr_{0.4}TiO_3$ film on LAO substrate. FWHM is 0.84°.

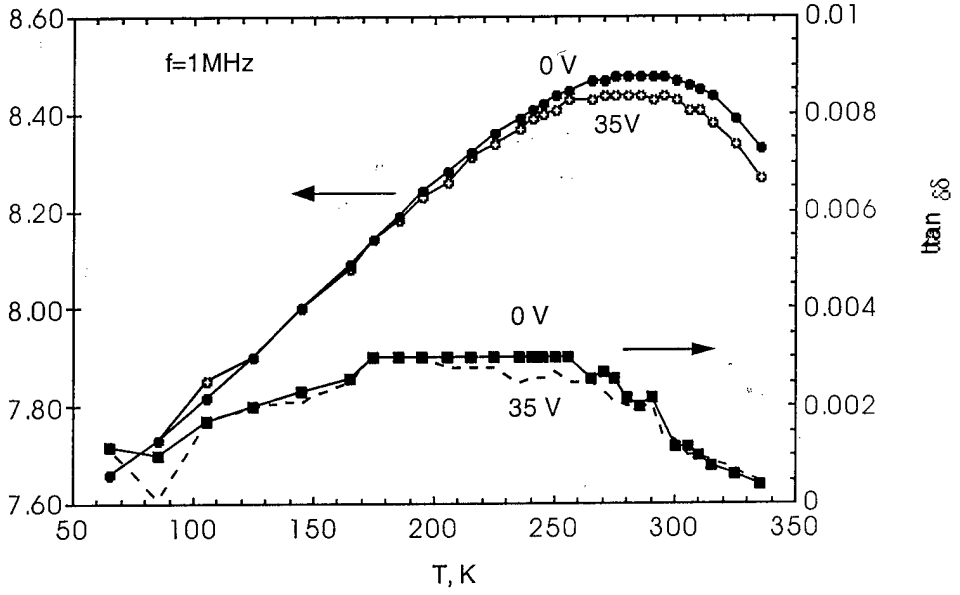

Fig. 4.1-2. C and tan δ versus T for $Ba_{0.6}Sr_{0.4}TiO_3$ film.

4.2. $Ba_{0.6}Sr_{0.4}Ti_{0.99}Mn_{0.01}O_3$ films

Doping at low levels of trivalent cations has been shown to be effective in reducing the loss tangent of BSTO at low frequencies. However, the exact mechanism of doping is unclear so

far. We have deposited thin films of Mn-doped $Ba_{0.6}Sr_{0.4}TiO_3$ from a target composition of $Ba_{0.6}Sr_{0.4}Ti_{0.99}Mn_{0.01}O_3$. Figure 4.2-1 shows the XRD pattern of the *(h00)* oriented Mn doped BSTO film deposited on LAO substrate. The dielectric property measurements on these films are underway.

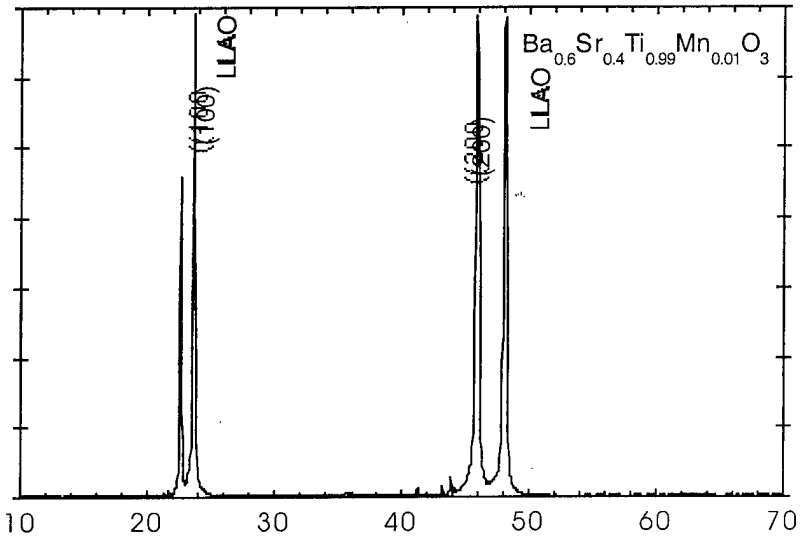

Fig. 4.2-1. XRD (CuK_α) of Mn doped BSTO film. The formula, $Ba_{0.6}Sr_{0.4}Ti_{0.99}Mn_{0.01}O_3$, indicates the starting composition of the target.

4.3. $Ba_{0.6}Sr_{0.4}TiO_3$ with 30 wt% of MgO films

In an another doping study of BSTO, we have added 30 wt% of MgO to the stoichiometric $Ba_{0.6}Sr_{0.4}TiO_3$. The XRD of the polycrystalline target showed lines corresponding to $Ba_{0.6}Sr_{0.4}TiO_3$ phase and MgO phase. PLD films show the *(h00)* oriented BSTO and MgO phases (figure 4.3-1). However, the BSTO peaks are broader compared to pristine $Ba_{0.6}Sr_{0.4}TiO_3$ films. The dielectric properties of these films will be measured in the future.

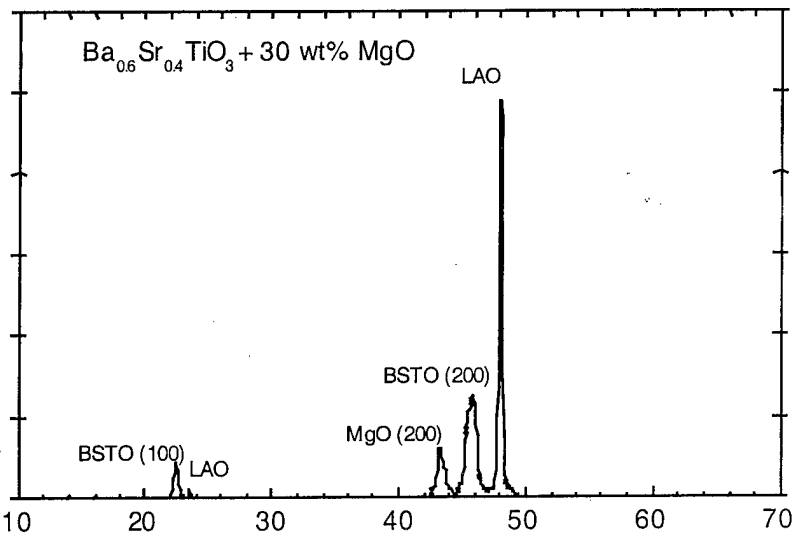

Fig. 4.3-1. XRD of $Ba_{0.6}Sr_{0.4}TiO_3$ with 30 wt% of MgO film. The perovskite lines are broader compared to pristine BSTO phase.

4.4. $BaTi_{0.85}Sn_{0.15}O_3$ films

Tin substitution at the Ti- site decreases the Curie temperature. For a 15% Sn substitution the T_C of the bulk polycrystalline material decreases to 291K. Stoichiometric $BaTi_{0.85}Sn_{0.15}O_3$ targets were synthesized for thin film deposition. Figure 4.4-1 shows the XRD of the (*h00*) oriented $BaTi_{0.85}Sn_{0.15}O_3$ phase. However, preliminary lattice parameter estimates indicate a lattice mismatch between the substrate and the film is about 5%.

Capacitance measurements on the epitaxial films indicate that the T_C is around 370 K (figure 4.4-2). The loss tangent is less than 0.01 at room temperature. The loss tangent decreases to a low value of 0.006 near T_C. In the future we will study a range of substitutions of Sn in BSTO phases.

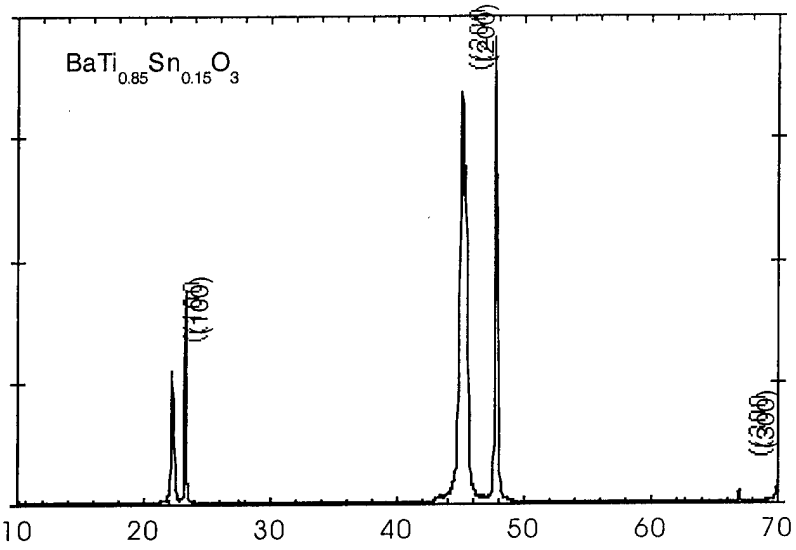

Fig. 4.4-1. XRD of $BaTi_{0.85}Sn_{0.15}O_3$ films.

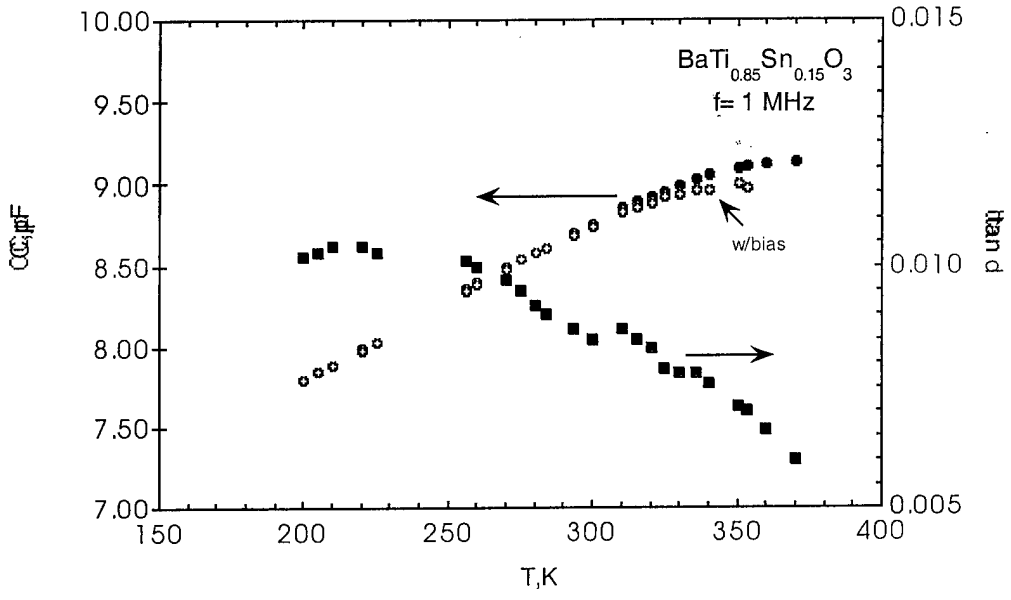

Fig. 4.4-2. C and tanδ of $BaTi_{0.85}Sn_{0.15}O_3$ film.

4.5. $Ba_{0.1}Sr_{0.9}TiO_3$ films

$Ba_{0.1}Sr_{0.9}TiO_3$ films were studied for low temperature operations. XRD of the as-grown film and oxygen annealed films do not show any significant phase modifications. Fig. 4.5-1 shows the oxygen annealed $Ba_{0.1}Sr_{0.9}TiO_3$ film pattern.

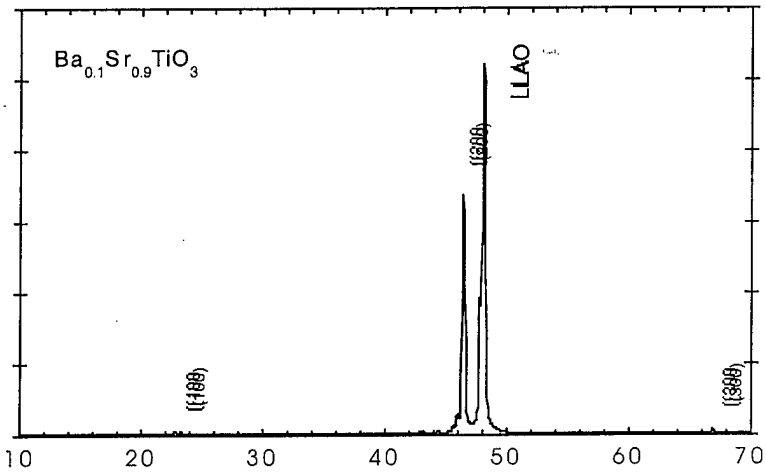

Fig. 4.5-1. XRD of $Ba_{0.1}Sr_{0.9}TiO_3$ film.

The capacitance measurement shows that the T_C is at 140K (figure 4.5-2). This is about 40 K higher than that of the target. At T_C a tunability of as high as 7% was observed for a maximum of 3.5kV/cm electric field which could be achieved in our study. However, the loss tangent values are much lower for the film compared to the bulk specimen. For example, loss tangent is 0.06 for the polycrystalline pellet at T_C while it is only 0.012 for the film. The higher T_C observed in the films will be studied in detail.

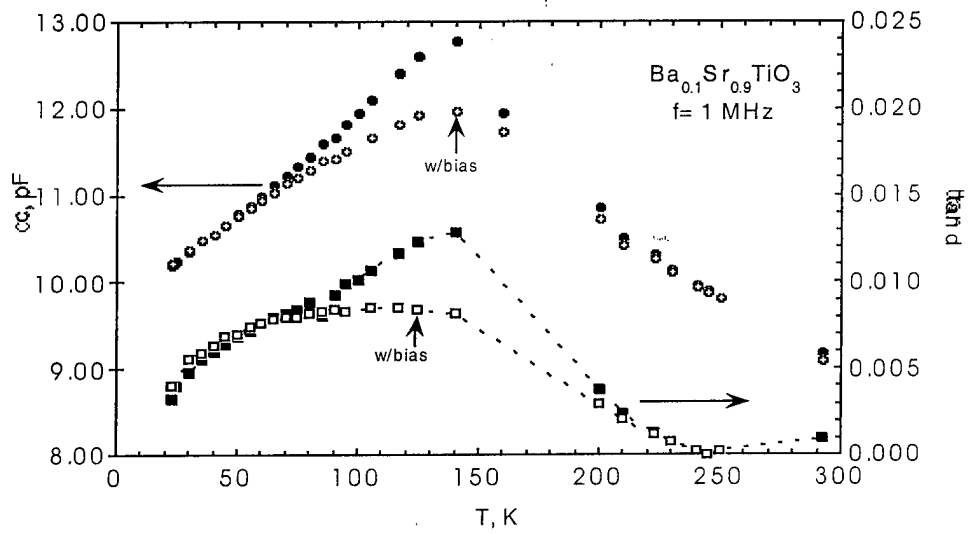

Fig. 4.5-2. C and tan δ for $Ba_{0.1}Sr_{0.9}TiO_3$ film.

4.6. $Ca_{0.05}Sr_{0.95}TiO_3$ films

The XRD, and C & tan δ, for the $Ca_{0.05}Sr_{0.95}TiO_3$ films are shown in the figure 4.6-1, and 4.6-2 respectively. The Curie temperature of the phase is near 70 K which is close to the desired 77 K operating range. The loss tangent shows a peak at 44 K. The loss tangent values are much lower compared to pristine films of $SrTiO_3$ reported in the literature. However, the tunability is only 2% compared to 7% in the $Ba_{0.1}Sr_{0.9}TiO_3$ films for the same electric field.

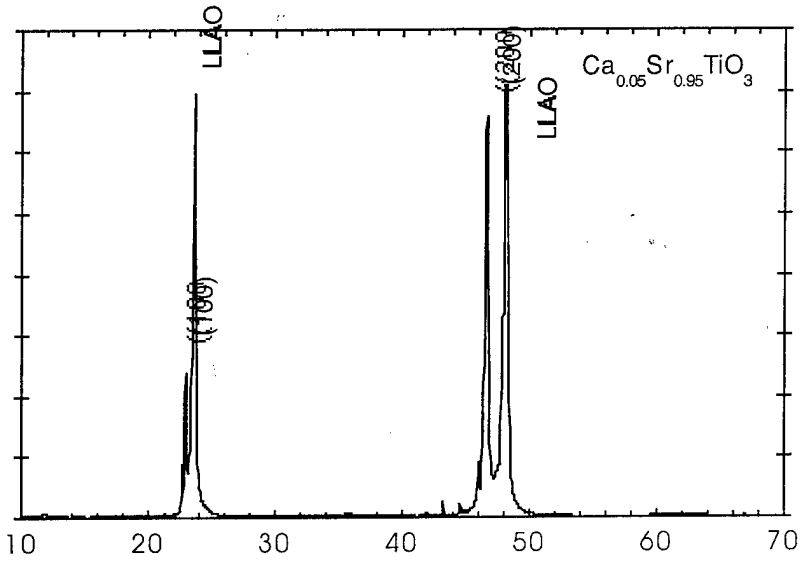

Fig. 4.6-1 XRD of Ca substituted $SrTiO_3$ film

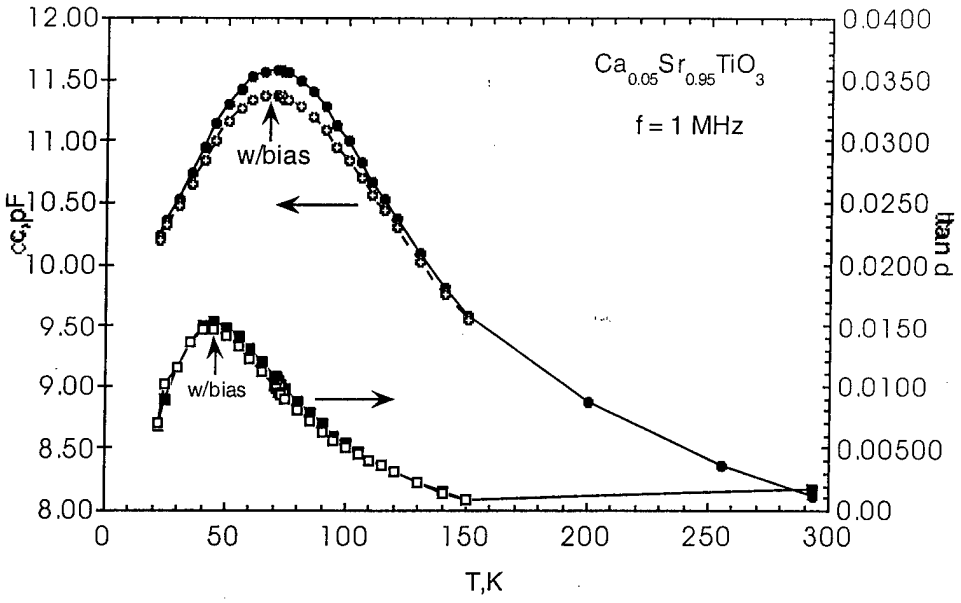

Fig. 4.6-2. C and tan δ for $Ca_{0.05}Sr_{0.95}TiO_3$ film showing a T_C of 70K.

Task 5 - Materials Discovery Research

Synthesis and characterization of solid solution of $CaCu_3Ti_4O_{12}$ and $LnCu_3Ti_3FeO_{12}$ (Ln = La, Sm, Dy, Y, and Bi).

Work on $ACu_3M_4O_{12}$ phases is continued and extended to various new solid solution compositions. X-ray diffraction data indicated that all these compounds crystallize in cubic phases. It is found some of these materials show unusually high relative dielectric constants, which are as high as 15000 at room temperature. Other properties of these materials, including dielectric constants at high and low temperature and agility are being determined.

A graphical interface programming language, HP-Vee, has been successfully used to control the measurement instruments. More instruments will be interfaced by HP-Vee. The lab automation will accelerate our progress in materials characterization.

New synthesized materials:

1. $Ca_{1-x}A_xCu_3Ti_4O_{12}$
2. $Ln_{2/3}Cu_3Ti_4O_{12}$ (Ln = La, Sm, Dy, Y, Bi)
3. $Ln_{0.}5Na_{0.5}Cu_3Ti_4O_{12}$ (Ln = La, Sm, Dy, Y, Bi)
4. $Ca_{0.5}Ln_{0.5}Cu_3Ti_{3.5}Fe_{0.5}O_{12}$ (Ln = La, Sm, Dy, Y, Bi)
5. $Bi_{(2+x)/3}Cu_3Ti_{4-x}Fe_xO_{12}$ (X = 0, 0.25, 0.5, 0.75, 1)
6. $Cu_3Ti_2Ta_2O_{12}$ and $Cu_2Ta_4O_{12}$

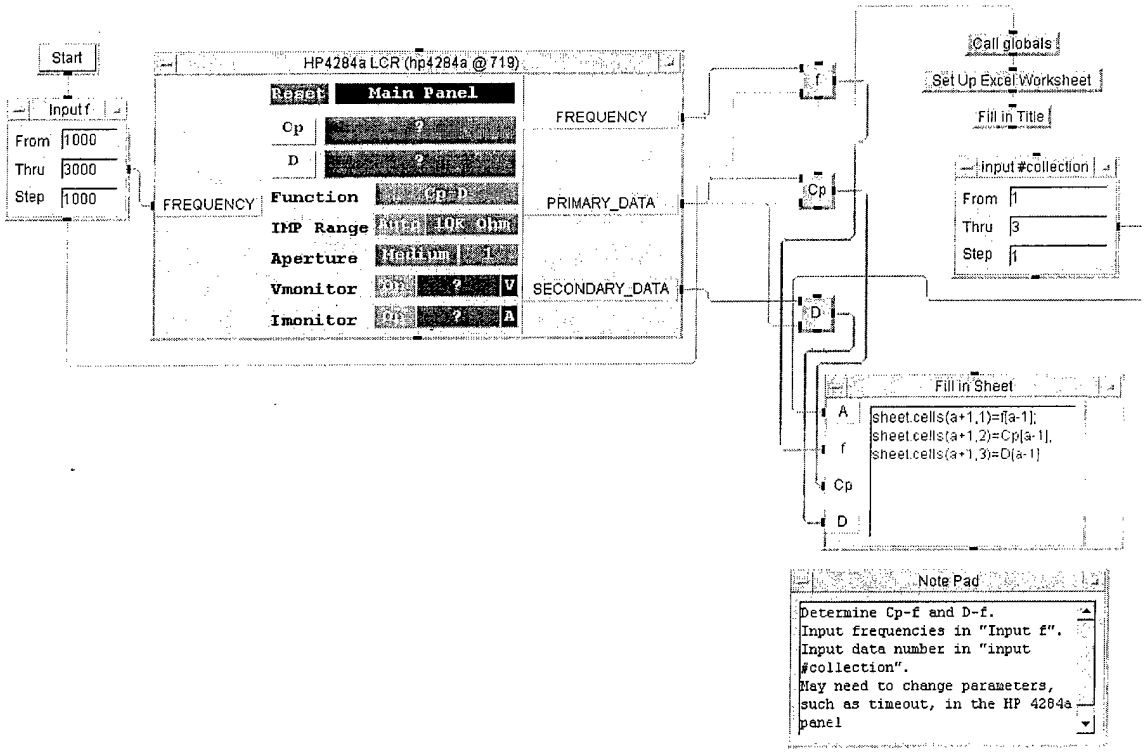

Fig. 5-1. Computer program to control measurement instrument.

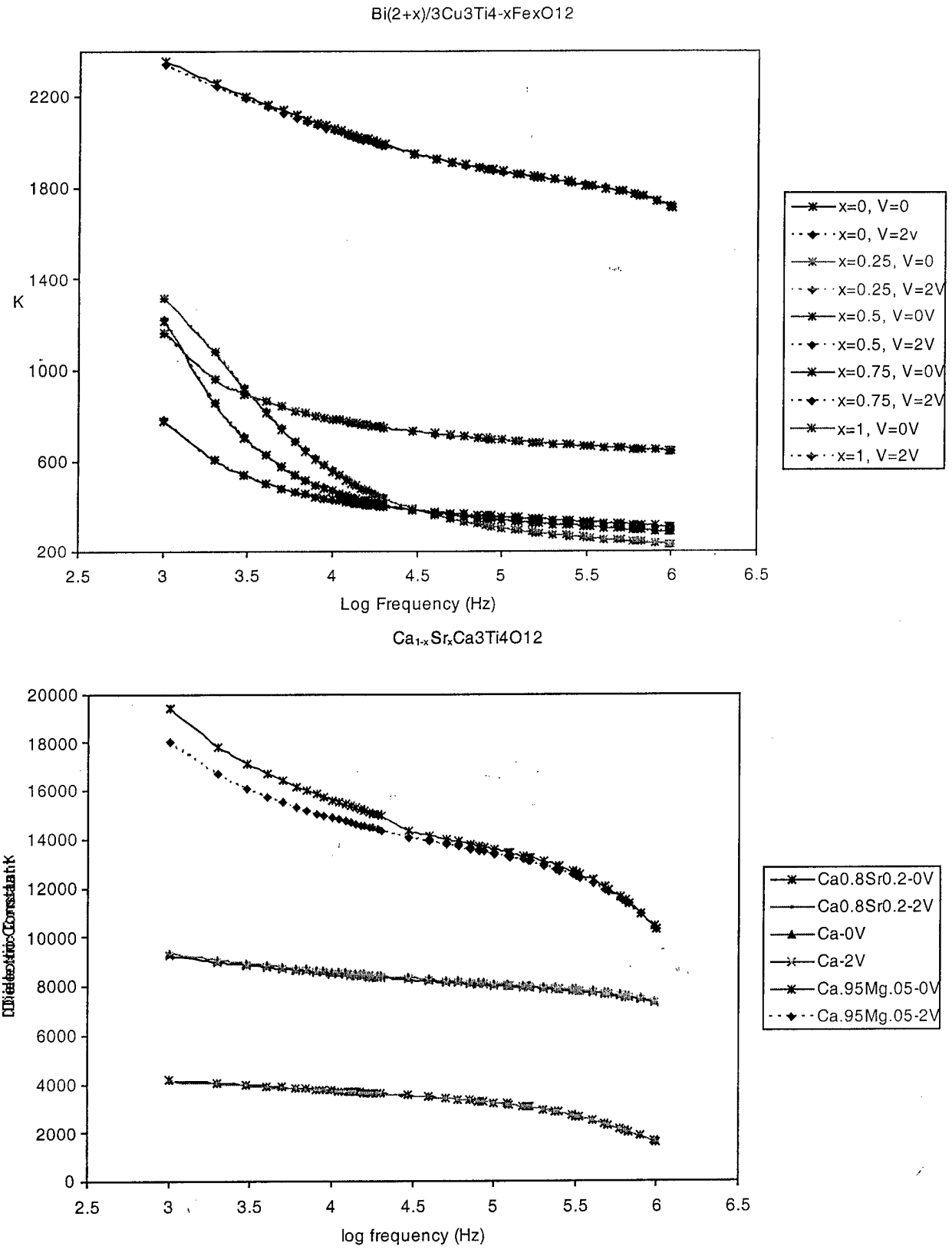

Fig. 5-2. Dielectric constants of some selected materials.

Task 6 - Rapid Intrinsic Film Test (RIFT) Development

We continued testing the low (RIFT1) and room temperature (RIFT2) packages in Q4 to understand and improve their behavior.

6.1. RIFT1

We continued our tests of the TBCCO resonator which we started in Q3. We again assembled the package with a bare MgO test chip and measured the microwave response as a function of the applied spring pressure and measurement temperature. Some of our results are plotted in Figure 6.1-1. If, as we suspect, there is an airgap between the chips, we should be able to decrease it by applying greater pressure to the package. The frequency of a particular resonance should be inversely proportional to the airgap: $f \sim c/(L\sqrt{\varepsilon_{eff}})$, where f is the frequency, c is the speed of light, L is the length of the resonating element, and ε_{eff} is the effective dielectric constant which surrounds the device. The effective dielectric constant depends on the separation of the two substrates: the farther apart the substrates, the lower the dielectric constant, hence the higher the resonant frequency. The data in Figure 6.1-1 are in general agreement with this hypothesis. We also tested a YBCO resonator in RIFT1 and verified its behavior was similar to the TBCCO resonator, though the unloaded Qs were lower.

6.2 RIFT2

We focused on RIFT2, because its results are easier to simulate and interpret. Figure 6.2-1 summarizes our difficulties to date with the RIFT technique: we plot the measured capacitance of the RIFT2 circuit with a bare MgO wafer clamped on top as a function of the applied spring pressure. No matter what spring pressure is applied, the capacitance is lower than expected from simulations and is not single valued. We attribute this behavior to airgaps between the interdigital capacitor chip and the test chip caused by dirt or debris on the chip surfaces. For this first set of experiments, we assembled the RIFT package without taking strong measures to ensure the cleanliness of the parts. We then assembled the RIFT2 package in a class 100 cleanroom using the cleanest chips we could manage—the measurements were foiled by chip cracking under the high pressure.

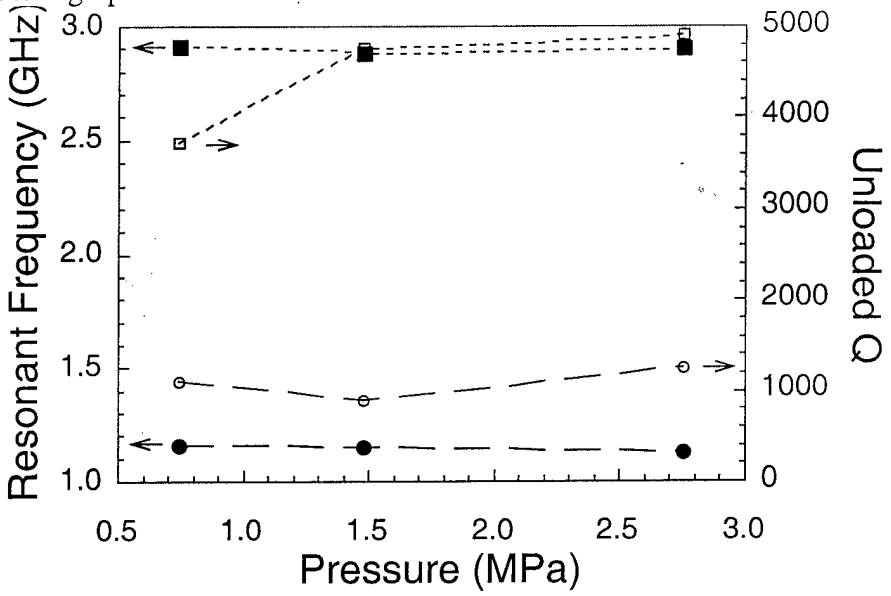

Fig. 6.1-1. Frequency and unloaded Q of two resonances of a TBCCO device in RIFT1 at ~ 45 K versus the applied spring pressure. If an airgap exists, and decreases with spring pressure, the resonant frequency should decrease and the Q should increase monotonically.

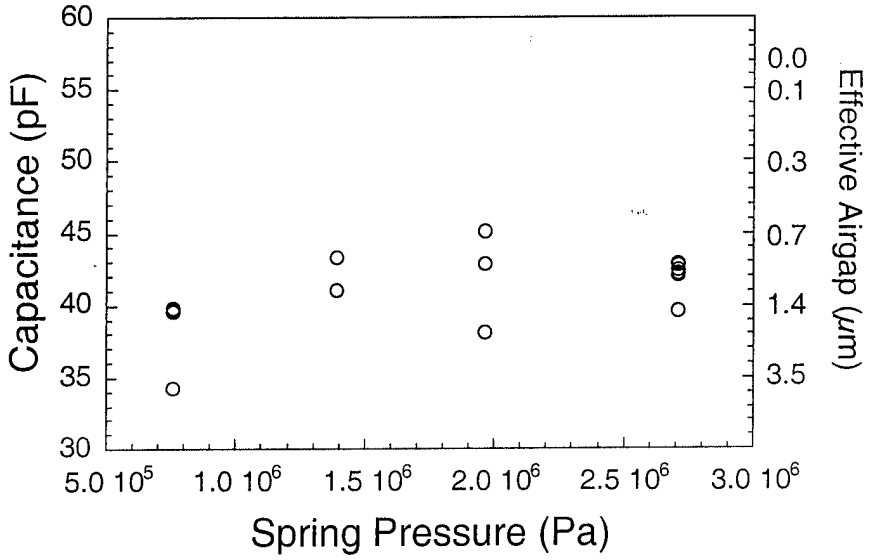

Fig. 6.2-1. The capacitance of the RIFT2 capacitor with a bare MgO wafer clamped on top versus the applied clamping pressure. On the right axis is the effective airgap (determined from simulations). Even at very high pressures (2.7 MPa), an equivalent airgap of ~ 1 μm still exists.

We will continue to study the feasibility of the RIFT technique for testing unpatterned ferroelectric chips, but as these results indicate, it may not be an easy road. We will investigate alternate means to obtain the necessary electrical data (frequency and temperature dependence of the permittivity, loss, and tunability) in parallel with our efforts to improve the performance of the RIFT packages. In order to meet milestone 6.C., we have sent BSTO samples to colleagues at Lawrence Berkeley Laboratories, NIST, the University of Pittsburgh, and the University of Boulder for measurement. These measurements will serve as a cross check and calibration for data obtained at DuPont.

Frequency Agile Materials for Electronics

Q5

Date: 10/18/99

Period covered in this report: 7/1/99 through 9/30/99

Program Title: Novel Ferroelectric Materials for Satellite Communications

Contract # DABT63-98-C-0046

Performing Organization: DuPont Superconductivity

Subcontractor: University of Colorado at Boulder

Summary

We completed the testing of five process validation wafers deposited under optimized conditions for both the cryogenic (x = 0.06) and room temperature (x = 0.60) $Ba_xSr_{1-x}TiO_3$ (BSTO) compositions. The electrical uniformity was excellent from run-to-run and across individual wafers. This completes the third milestone for Tasks 1 and 2. We chose $Ca_{0.05}Sr_{0.95}TiO_3$ (CSTO05) and $CaCu_3Ti_4O_{12}$ (CCTO) as our second generation materials for cryogenic and room temperature applications, respectively. Depositions of both should start by mid Q6, satisfying the fourth milestone of Tasks 1 and 2. We completed the design of the multilayer photomasks and began fabrication of Au/BSTO and YBCO/BSTO coplanar microwave devices, to finish the first and second milestones of Task 3. Under Task 4, we investigated the influence of Mn doping on the structural and electrical properties of BSTO60. We also began the study of the role of lattice mismatch strains in pulsed laser deposited $SrTiO_3$ (STO) films. We studied the effects of F-O substitution on bulk $BaTiO_3$ (BTO) and related compounds for room temperature applications, as well as looking at a number of tantalates and niobates for use at low temperatures under Task 5. Finally, in Task 6, we completed our evaluation of the rapid intrinsic film test (RIFT) technique. We determined that unavoidable substrate curvature was most likely responsible for the difficulties with the technique. We will end our development of RIFT and concentrate more effort on Task 3.

Progress By Task

Task 1. Large Area Sputtered Film Manufacturing for Low Temperature Applications

1.1. BSTO x = 0.06 on LAO

In Q5, we completed the electrical characterization of the manufacturing test samples produced in Q4. Combined with the structural characterization carried out in Q4, this completes milestone 1.C. Some of the results are presented in Table 1-1 and Figure 1-1. These results on the uniformity and reproducibility are very promising. From Table 1-1, we find the relative permittivity is repeatable run-to-run better than 6%. The losses (measured at 100 kHz) are repeatable to 10%. The tunability measured at room temperature is small, as expected, since T_c << 300 K. In Figure 1-1, we plot the relative permittivity of a 0.19 μm thick ferroelectric layer extracted from measurements on interdigitated capacitors deposited on top of the BSTO06 film.

Table 1-1. Summary of electrical and structural properties for select BSTO06/LAO films at room temperature (~ 300 K).

Sample	ε	tan δ	Δε/ε (%)	c-axis (nm)	Δω (FWHM)
14707	358	$8.1x10^{-3}$	0.6	0.3948	0.271
14710	323	$9.3x10^{-3}$	0.9	0.3948	0.294
14712	314	$9.6x10^{-3}$	0.6	0.3948	0.365
14713	342	$8.4x10^{-3}$	0.5	0.3948	0.299
17459	336	$8.5x10^{-3}$	0.7	0.3949	0.8*

*widened by substrate twinning

We described the technique for extracting the permittivity using electromagnetic modeling software in earlier reports. The measured on-wafer variability is 6.6%, of which ~3% is attributable to variations in lithography and the uncertainties of the modeling. The variability in the loss and tunability is comparable. We have also put in place the testing apparatus to obtain the cryogenic temperature dependence of the electrical properties and will continue characterization of these samples in Q6 and beyond.

1.2. Second Generation Material

Using the results of Tasks 4 & 5, we have chosen $Ca_{0.05}Sr_{0.95}TiO_3$ (CSTO) as a candidate for the second generation ferroelectric for cryogenic applications. Sputtering targets of this composition have been ordered and will be delivered early Q6, after which we will begin the

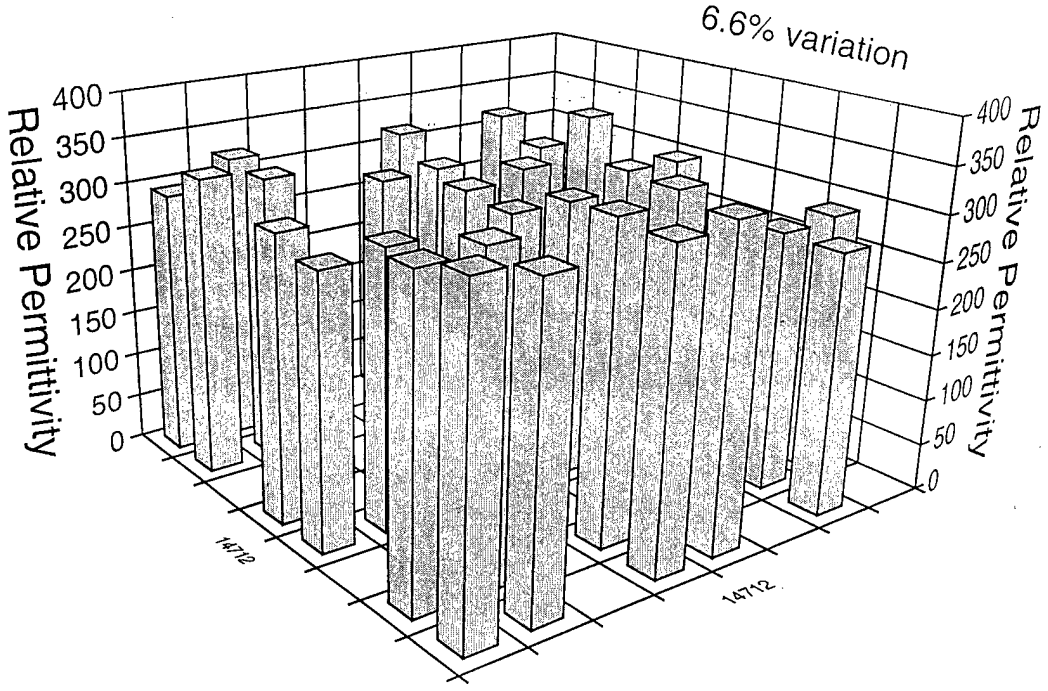

Figure 1-1. Map of the relative permittivity of a 0.19 μm thick BSTO06 film using 36 interdigitated Au capacitors of various sizes across a 51 mm diameter LAO wafer. Total variation of the permittivity across the wafer is 6.6%.

evaluation of CSTO. This will satisfy the requirements for milestone 1.D. We also have ordered non-stoichiometric BSTO targets to examine the effect of the Ti composition on the electrical properties. This work should begin in Q6. Lastly, we have received BSTO x = 0.05 targets from a second vendor which should not have the problems with inadvertent Zr and Fe doping that we have struggled with and will allow us to evaluate the influence of the Zr and Fe doping on the electrical properties.

1.3. Rotating Magnetron Sputter Source

We have ordered the materials and components necessary to modify the magnet system of our 150 mm diameter rotating magnetron sputter source. We will investigate the influence of the magnet geometry on high throughput/large area depositions; we are primarily concerned with uniformity and rate.

Task 2. Large Area Sputtered Film Manufacturing for Ambient Temperature Applications

2.1. BSTO x = 0.60 on LAO

We completed the room temperature characterization of the manufacturing repeatability runs of BSTO60 on 51 mm diameter LAO, to satisfy milestone 2.C. The run-to-run uniformity of the electrical results were very good. In Table 1-2, we summarize the results for seven runs under identical conditions. The relative permittivity of the ferroelectric layer was repeatable to 3%, which is within the uncertainty of the measurements. The tunabilities of the various samples are still low—our measurements, as well as measurements taken by the University of Colorado at Boulder, indicate that the Curie temperature of these films is above 300 K. In Q6, we will measure the T_c of these films to identify the correct operating range for both temperature and composition. In Figure 2-1, we show a map of the relative permittivity of the BSTO60 film across a 51 mm diameter wafer. The total variation is 6.3%, of which ~ 3% may be attributable to the measurement uncertainties. As mentioned above, we have finally obtained the testing apparatus to measure the electrical properties of the various devices from 40-500 K.

2.2. Second Generation Material

Using the information from Tasks 4 and 5 from previous reports, we have chosen $CaCu_3Ti_4O_{12}$ (CCTO) as a promising ferroelectric material for room temperature applications.

Table 1-2. Summary of ~ 300 K electrical and structural properties for select BSTO60/LAO films.

Sample	ε	tan δ	Δε/ε (%)	c-axis (nm)	Δω (FWHM)
14699	546	3.1×10^{-3}	2.9	0.4007	0.942*
14701	544	3.7×10^{-3}	2.8	0.4007	0.277
14703	517	3.1×10^{-3}	2.7	0.4007	0.256
14705	518	4.4×10^{-3}	2.7	0.4006	0.270
14709	531	3.7×10^{-3}	2.2	0.4006	0.267

*due to substrate twinning

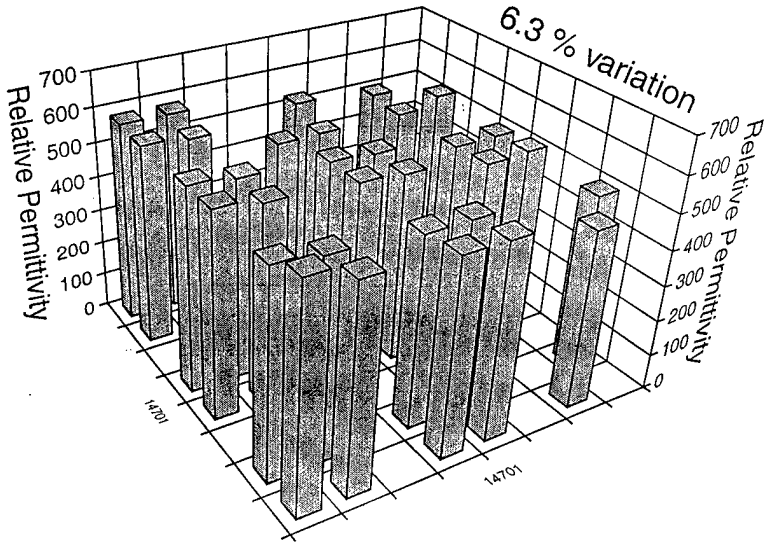

Figure 2-1. Map of the relative permittivity of a 0.29 μm thick BSTO60 film using 36 interdigitated Au capacitors of various sizes across a 51 mm diameter LAO wafer. Total variation of the permittivity across the wafer is 6.3%. Missing data caused by lithographic problems.

Targets have been ordered and should arrive in early Q6. We will then begin the investigation of the structural and electrical properties of CCTO to determine whether it holds more promise than BSTO as a material for tunable microwave applications. This will satisfy milestone 2.D. We also have received pure BSTO x = 0.50 targets which should produce films whose T_c will be lower than the current BSTO60 samples and more appropriate for room temperature applications.

2.3. Very Large Area Heater

The final parts for our high uniformity, very large area heater arrived in late Q5. We must now install the heater in our secondary deposition chamber and test it. We expect installation to take place sometime in late Q6/early Q7.

Task 3. Multilayer Film Development and Manufacturing

3.1. Bilayer Device Design

In Q5, we designed a Au/ferroelectric and YBCO/ferroelectric bilayer mask set and the associated packaging necessary to test the fabricated devices from 100 kHz to 20 GHz across the whole temperature range. The devices were based on designs used for Task 6, with some modifications. We included two single pole coplanar resonators with different resonant frequencies and couplings as well as phase shifters (coplanar transmission lines) with different characteristic impedances (to provide a better match to the test circuitry). We also designed a Through-Reflect-Line calibration set (a NIST standard) which should provide a highly accurate crosscheck of our measurements of the permittivity and loss. We have agreed to supply a number of these chips to NIST-Boulder for measurement. Finally, we included an interdigitated capacitor chip on the bilayer mask, to compare with our earlier measurements.

3.2. YBCO/BSTO multilayers

We have begun fabrication of YBCO/BSTO and Au/BSTO bilayers (and test devices on bare substrates) patterned using the new masks. Testing of these devices will begin in early Q6, to satisfy milestone 3.C. and 3.D.

Task 4. Exploratory Laser Ablation Processing (University of Colorado)

4.1. Mn Doped $Ba_{0.6}Sr_{0.4}TiO_3$ Thin Films

Mn doped BSTO films were fabricated using a target composition of $Ba_{0.6}Sr_{0.4}Ti_{0.99}Mn_{0.01}O_3$. The XRD of the film is shown in Figure 4-1 indicating the presence of (00l) oriented films. Capacitance and loss tangents were measured between 250-350 K and are shown in Figure 4-3. A Curie temperature of 292 K was observed for the Mn doped films, which is 10 K lower than that of the undoped $Ba_{0.6}Sr_{0.4}TiO_3$ films. Also the transition is narrower for the Mn doped films compared to the undoped films. The loss tangent, however, is higher by an order of magnitude for the Mn doped films. Calculations of the dielectric constants and tunability measurements of the films are underway. We plan to study various Mn dopant levels for low loss films.

4.2. $SrTiO_3$ Films

We have grown $SrTiO_3$ films on LAO substrate and $SrTiO_3/Sr_2TiO_4$ /LAO type films to study the effect of strain on the dielectric properties. The lattice constants for $SrTiO_3$ is a = 0.3905 nm, LAO a = 0.38 nm, and Sr_2TiO_4 a = 0.3886 nm & c = 1.259 nm. Films of $SrTiO_3$ were grown by pulsed laser deposition from the perovskite target. The XRD of the post-oxygen annealed films show (00l) orientation (Figure 4-2a). The multilayer $SrTiO_3/Sr_2TiO_4$ films were grown on LAO substrates by depositing 0.15 μm Sr_2TiO_4 followed by depositing 0.4 μm $SrTiO_3$. The XRD (Figure 4-2b) shows the (110) peak in addition to (00l) lines. The dielectric properties of both films are currently being measured.

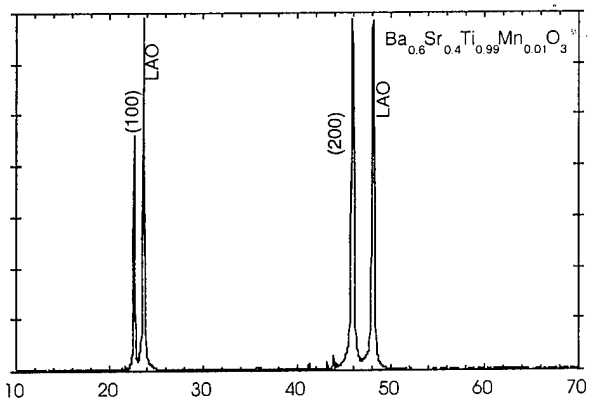

Figure 4-1. XRD scan (θ-2θ) of Mn doped BSTO film. The formula, $Ba_{0.6}Sr_{0.4}Ti_{0.99}Mn_{0.01}O_3$, indicates the starting composition of the target.

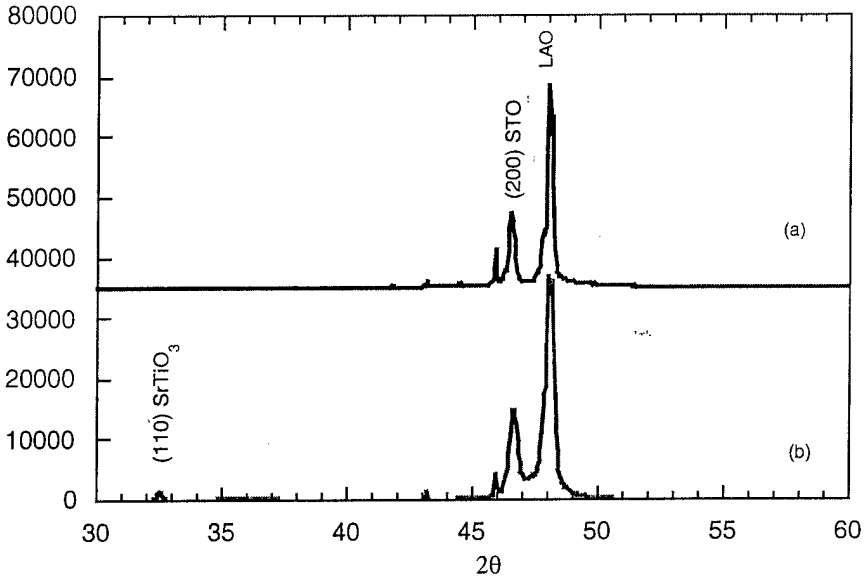

Figure 4-2. XRD of (a) $SrTiO_3$ film on LAO substrate, and (b) $SrTiO_3/Sr_2TiO_4$ films grown on LAO substrate. Note the presence of (110) line. Both films were annealed at 900°C in flowing O_2 for 6 hours.

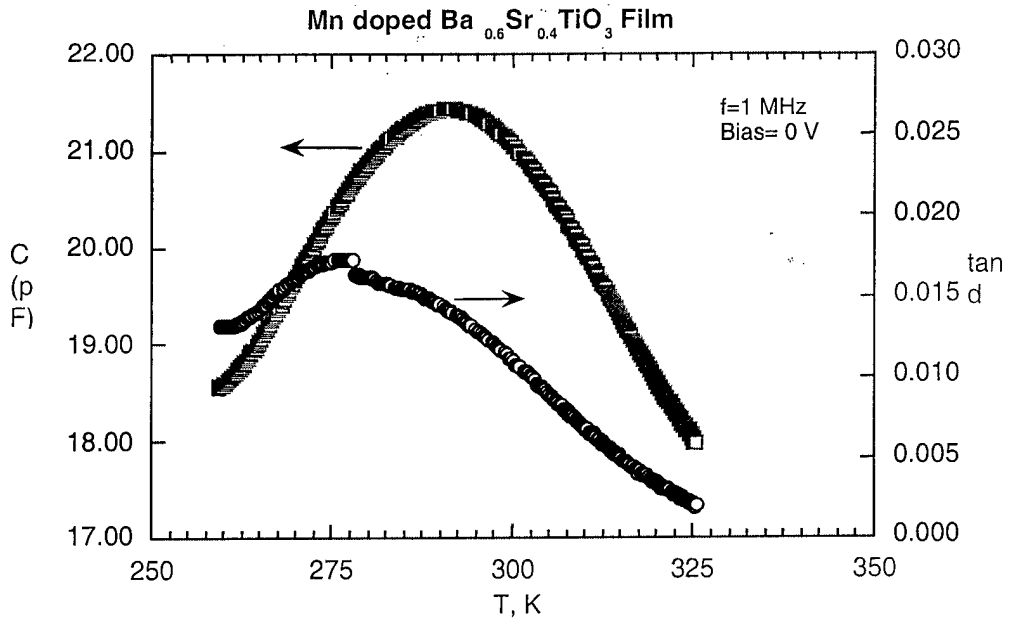

Figure 4-3. Capacitance and tan δ vs. T for Mn doped BSTO films, measured at 1 MHz with no bias.

Task 5. Materials Discovery Research

5.1. F Doping Effects on Tunability and T_c of $BaTiO_3$

F-O substitution is known to decrease the covalency of $BaTiO_3$ (BTO) and lead to the decrease of T_c. F is charge balanced by Li, K, Al, Ga, In, Fe, or Y. Except for Al, all the other ions can form solid solutions, although with different solubility. The materials we studied in Q5 are summarized in Table 5-1. Only the sample with 4% Li showed tunability at room temperature and the tunability is frequency dependent, as is shown in Figure 5-1 & Figure 5-2. However, the use of LiF dramatically decreases the sintering temperature from above 1300°C to below 1100°C. More experiments are being done to obtain better quality samples of LiF doped BTO. The 3+ co-dopant ions tend to lower the phase transition temperature (cubic to hexagonal). Charge balance by 3+ ions is not favored.

5.2. Materials With Low T_c

None of the materials we have prepared this quarter (summarized in

Table 5-2) show any sign of tuning at room temperature. The tunability at low temperatures will be measured in Q6.

Table 5-1. Materials studied with F-O substitution.

Parent Compound	Dopants (A)	Concentration (x)
$BaTi_{1-x}Li_xO_{3-3x}F_{3x}$		0.02, 0.04, 0.06, 0.08
$BaTi_{1-x}K_xO_{3-3x}F_{3x}$		0.04
$BaTi_{1-x}A_xO_{3-x}F_x$	Al, Ga, In, Fe, Y	0.02, 0.04, 0.06, 0.08

Table 5-2. Low T_c materials made in Q5.

Parent Compound	T_c (K)	Concentration (x)
$Pb(Ni_{1/3}Ta_{2/3})O_3$	93	
$Sr_2Ta_2O_7$	161	
$K_3Li_2Ta_5O_{15}$	7	
$BaNa_2Nb_5O_{14}F$	100	
$Cd_{2-x}Pb_xNb_2O_7$	185	0, 0.2, 0.4, 0.6

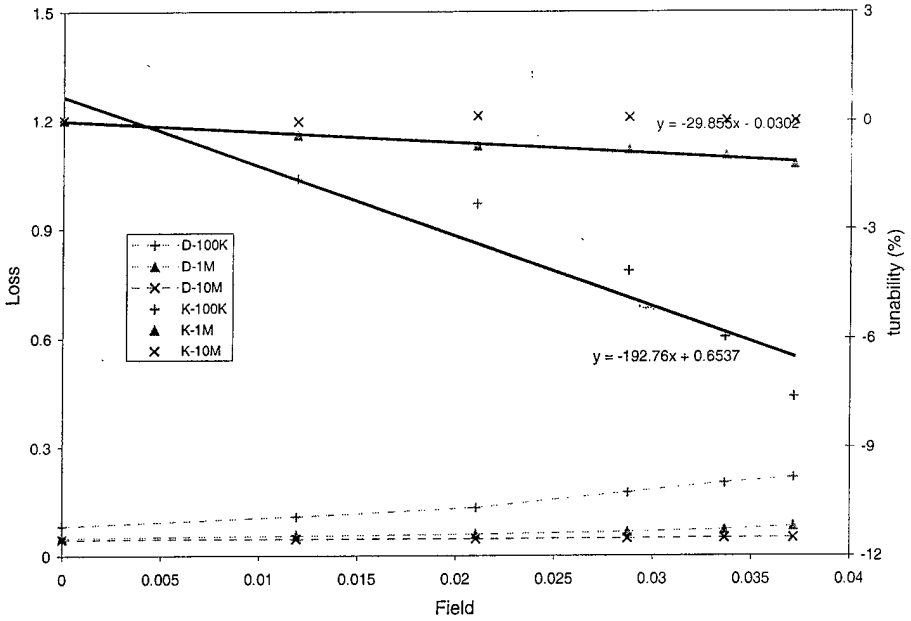

Figure 5-1. Tunability and loss of $BaTi_{0.96}Li_{0.04}O_{2.88}F_{0.12}$ measured at ~300 K.

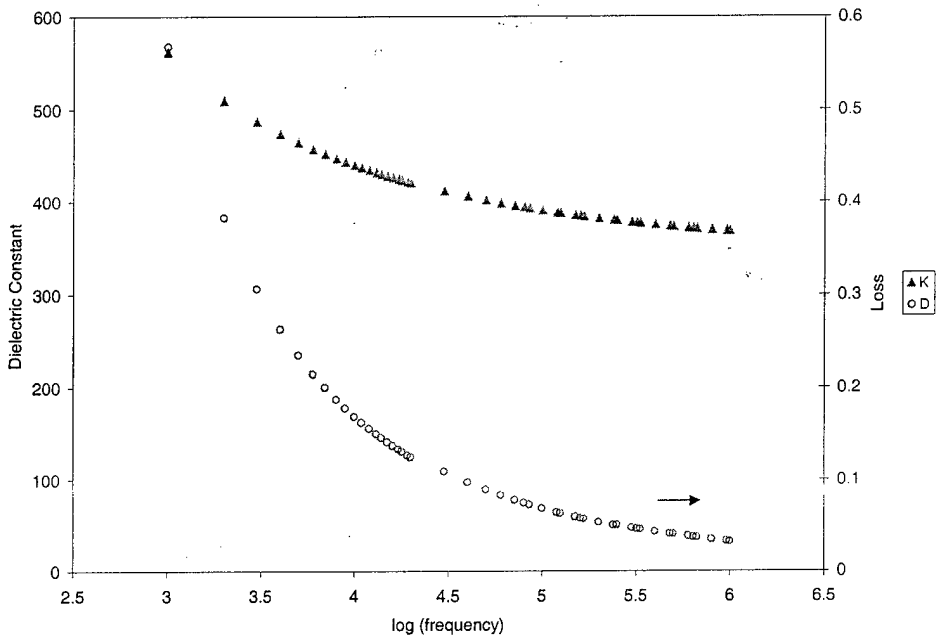

Figure 5-2. Frequency dependence of the tunability and the loss of $BaTi_{0.96}Li_{0.04}O_{2.88}F_{0.12}$ measured at ~ 300 K.

Task 6. Rapid Intrinsic Film Test (RIFT) Development

We continued to test the RIFT packages to understand (and possibly overcome) their limitations. In earlier reports, we described the results of the initial measurements which indicated an airgap of was present in our measurements. The airgap was not reproducible, which prevented reliable measurements of the dielectric properties. In Q5 we conducted tests to further characterize the influence of the airgap and its cause(s).

6.1. Dirt or Curvature?

We suspected two possible causes for the airgap: dirt or debris caught between the substrates or intrinsic curvature of the samples. In Figure 6-1 we show the results of measurements on a single pole coplanar resonator "sandwiched" between two 500 μm thick MgO substrates. The microwave package and its contents were cleaned and assembled in a class 100 cleanroom. In Figure 6-2, we plot the simulated resonant frequency of this structure versus the gap between the substrates. By comparing the two, it is evident that there is a gap of greater than 3 μm between the two MgO chips. This is consistent with earlier measurements in which we did not clean assemble the package. It seemed that no matter how cleanly we made the measurements, the results were the same.

We then investigated the curvature of the samples using an optical flat. In Figure 6-3, we show an image of a 12 mm x 12 mm chip on top of the optical flat, illuminated with 546 nm light. The height deviation from the chip center to edge is approximately 4 μm. This radius of curvature is typical of all of the samples we measured, including the untouched 51 mm diameter MgO substrates. It is consistent with radius of curvature measurements carried out on bare MgO substrates with a profilometer in Q1. We had initially assumed that a small amount of substrate curvature could be overcome by applying greater pressure, but we have had considerable wafer breakage above ~ 1.5 MPa.

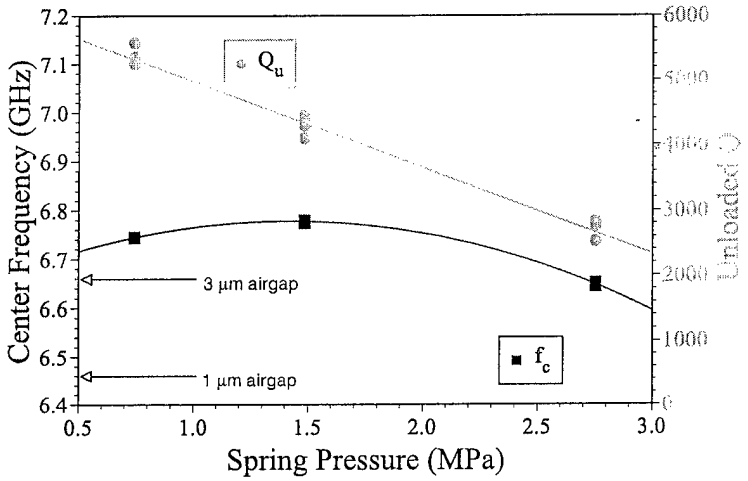

Figure 6-1. Center frequency and unloaded Q of a simple TBCCO/MgO resonator in the RIFT1 package, measured at ~ 45 K. At spring pressures above 1.5 MPa, we suffered heavy sample loss through substrate cracking.

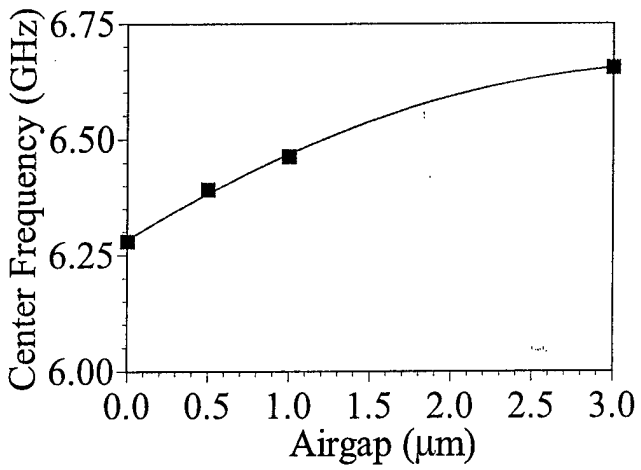

Figure 6-2. Simulated resonator center frequency versus airgap.

We initially proposed the RIFT technique as a rapid, reliable way to obtain the dielectric properties of unpatterned ferroelectric films. The current technique is unreliable and slow. We do not believe we can make RIFT a viable testing technique within the monetary and time constraints of the FAME program. Consequently, we would like to concentrate our film measurement efforts on Task 3, multilayer growth and microwave devices, which will provide the necessary sensitivity to the ferroelectric tunability and loss.

6.2. Cross Check With Accepted Techniques

We are continuing our efforts to cross check the measurements carried out at DuPont with other laboratories. We have recently sent off a number of samples to FAME participants at the University of Colorado at Boulder, the University of Pittsburgh, and Lawrence Berkeley National Labs. We hope to get results back by mid Q6. As mentioned in Task 3, we have also made arrangements to send samples to NIST-Boulder in the near future.

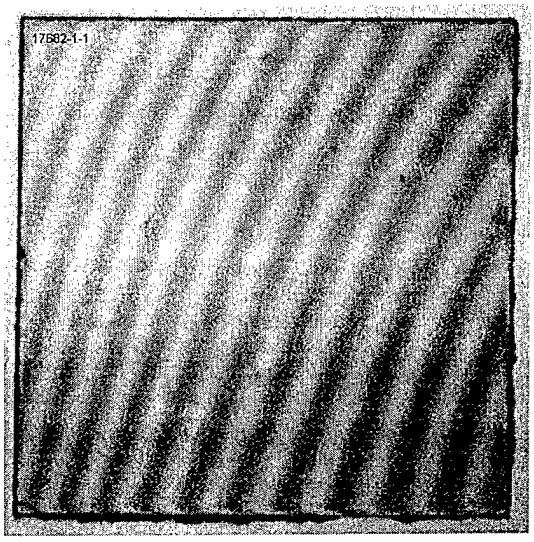

Figure 6-3. Interference pattern of 12 mm x 12 mm MgO chip on top of an optical flat, using 546 nm illumination. Assuming the curvature is uniform, the height deviation is ~ 4 μm from edge to center.

Frequency Agile Materials for Electronics

Q6

Date: 01/31/00

Period covered in this report: 10/01/99 through 12/31/99

Program Title: Novel Ferroelectric Materials for Satellite Communications

Contract # DABT63-98-C-0046

Performing Organization: DuPont Superconductivity

Subcontractor: University of Colorado at Boulder

Summary

A computer controlled cryogenic measurement station was completed and put into service for testing the temperature and frequency dependent performance of ferroelectric films and multilayers produced in this program. Initial depositions of 2nd generation materials were completed for both ambient and cryogenic temperature operation thus completing the fourth milestone for both Tasks 1 and 2. For cryogenic operation, $Ca_{0.05}Sr_{0.95}TiO_3$ (CSTO x = 0.05) was deposited with good epitaxial alignment on $LaAlO_3$, MgO, and LSAT substrates. For ambient temperature operation, $CaCu_3Ti_4O_{12}$ (CCTO) was deposited on $LaAlO_3$, MgO, and LSAT. Although growth of this more complex material system was cube-on-cube, epitaxial alignment was relatively poor and the loss tangent was relatively high. Further experiments are in progress to improve the epitaxial quality of CCTO films. Exploratory laser ablation processing under Task 4 has been used to investigate several doped BSTO compositions including $Ba_{0.6}Sr_{0.4}Ti_{0.98}Mn_{0.02}O_3$, $Ba_{0.6}Sr_{0.4}Ti_{0.99}Fe_{0.01}O_3$, $Ba_{0.6}Sr_{0.4}Ti_{0.98}Mn_{0.01}W_{0.01}O_3$, $Ba_{0.681}Sr_{0.281}Mg_{0.038}Ti_{0.962}Zr_{0.038}O_3$ for room temperature applications and $Ba_{0.05}Sr_{0.95}TiO_3$ for cryogenic applications. Under Task 5, materials discovery research, a wide range of acceptor-donor codoped $BaTiO_3$ samples were prepared in this quarter and their dielectric properties were measured. One system was identified with high tunability (>70% at 1 V/μm). Patent applications are being filed for some of these materials.

Progress By Task

Task 1. Large Area Sputtered Film Manufacturing for Low Temperature Applications

1.1. BSTO x = 0.06

In Q6, we completed the installation of a computer controlled, cryocooled measurement station suitable for low and high frequency measurements between 20-300 K. In Figures 1-1 and 1-2, we present some of the first data obtained with this setup. Figure 1-1 shows the dielectric permittivity and loss tangent of a 0.2 μm thick film of $Ba_{0.06}Sr_{0.94}TiO_3$ (BSTO x = 0.06) grown on a 51 mm diameter $LaAlO_3$ (LAO) wafer. The Curie temperature $T_c \sim 40$ K. The measurement was made with a deposited interdigital capacitor at 100 kHz. Figure 1-2 shows the tunability of

the permittivity for a 4 V/μm electric field applied between the fingers of the capacitor. In Q7, we will expand the use of this apparatus to characterize BSTO as well as the second generation material, $Ca_{0.05}Sr_{0.95}TiO_3$ (CSTO x = 0.05), over a broader range of frequencies.

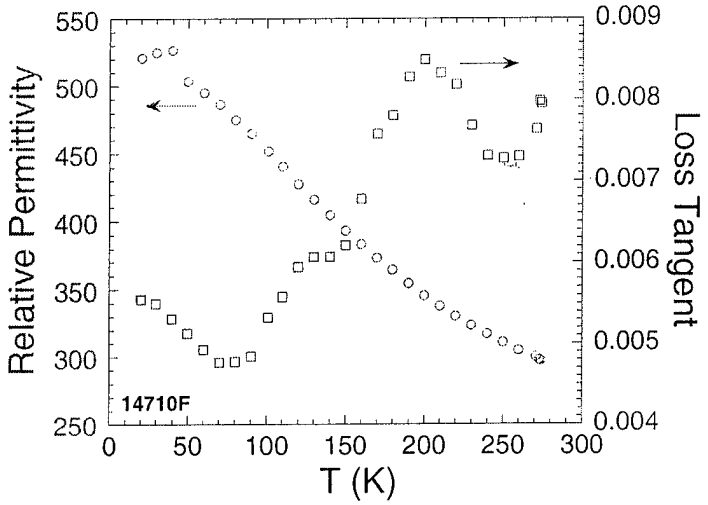

Figure 1-1. The relative permittivity and loss of a 0.19 μm thick BSTO x = 0.06 film on LAO, measured with an interdigitated capacitor at 100 kHz. The Curie temperature of this film is near 40 K.

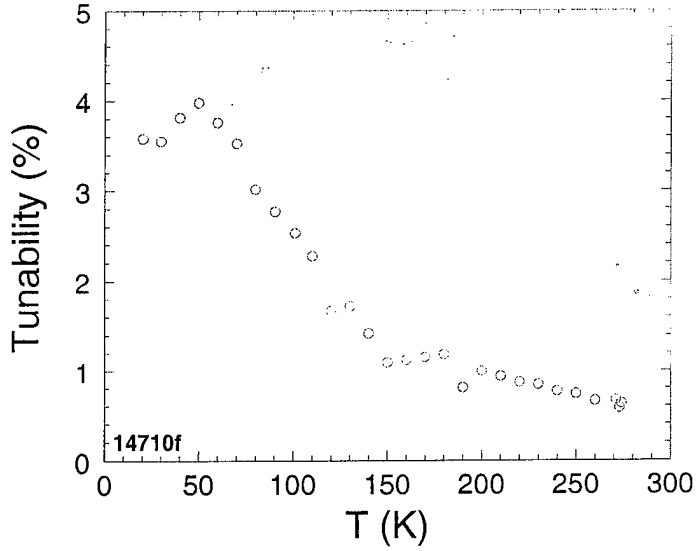

Figure 1-2. The tunability of the permittivity of the sample in Figure 1-1 for 40 V applied across a 10 μm gap (E ~ 4 V/μm).

1.2. CSTO x = 0.05 on LAO, MgO, & LSAT

In Q6, we began our exploration of CSTO x = 0.05, which we chose to evaluate as our second generation material. Twelve samples of CSTO were deposited on LAO, MgO, and Si. In addition, we also began investigating the use of solid-solution $LaAlO_3$-Sr_2AlTaO_6 (LSAT) substrates, with some success.

Figure 1-3 is a θ–2θ scan of a CSTO film on LAO. We find CSTO to be very similar to BSTO: for similar processing conditions, films of similar quality and orientation are produced. Preliminary room temperature electrical measurements of CSTO x = 0.05 show properties similar to BSTO x = 0.06 ($\varepsilon \sim 250$, $\tan\delta \sim 10^{-3}$, $\Delta\varepsilon/\varepsilon < 1\%$). We will obtain cryogenic measurements of the dielectric properties in early Q7. Figure 1-4 is a θ–2θ scan of CSTO grown on LSAT. Like films on LAO, the CSTO/LSAT films grow cube-on-cube with high quality. The lattice parameter in the c direction is between 0.393-0.395 nm. In Q7, we will implement XRD strain measurements and annealing studies on these films.

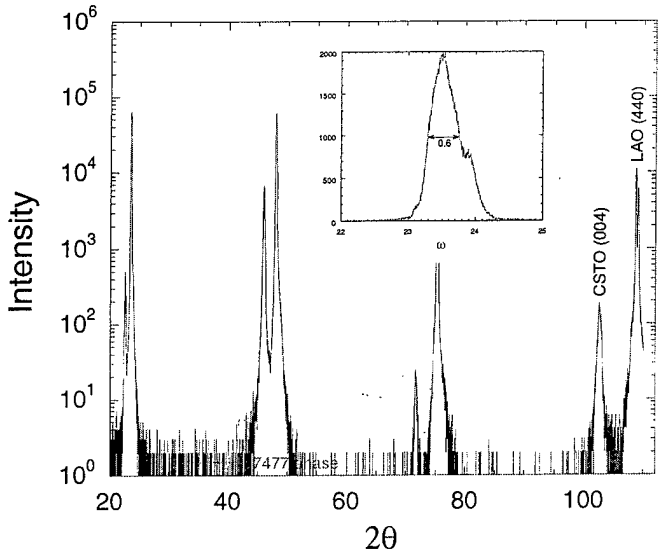

Figure 1-3. Phase scan of a 0.1 μm CSTO x = 0.05 film on LAO deposited at T_{set} = 950 °C. The film is c-axis oriented. Inset: rocking curve of CSTO (002), FWHM ~ 0.6°. Phi scans (not shown) indicate cube-on-cube growth.

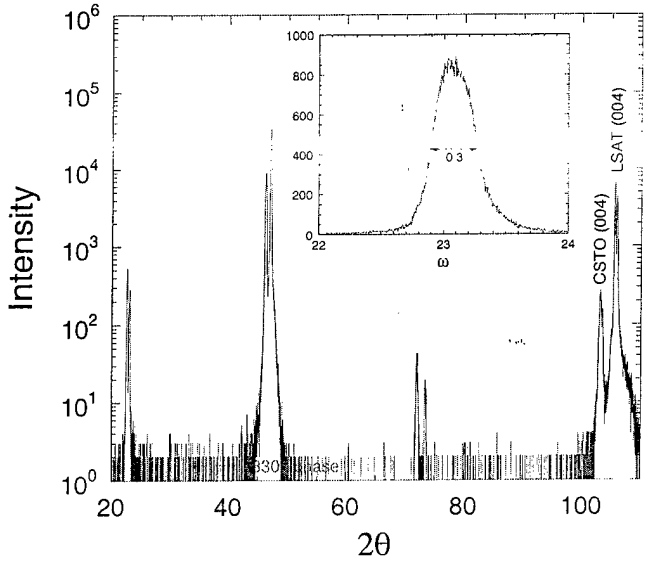

Figure 1-4. Phase scan of a 0.21 μm CSTO x = 0.05 film on LSAT at 950 °C. The film is c-axis oriented. Inset: the CSTO (002) rocking curve, FWHM ~ 0.3°. Phi scans (not shown) indicate cube-on-cube growth.

1.3. Very Large Area Heater & Rotating Magnetron Sputter Source

We have begun assembly of the very large area (VLA) heater. If no problems are encountered, we will install and test this new heater design by early Q8. It will enable much higher throughput compared to our present designs. We also received a second magnet assembly for the rotating magnetron sputter source. We will modify this magnet assembly to improve deposition uniformity and target usage of the source after the VLA heater is installed.

Task 2. Large Area Sputtered Film Manufacturing for Ambient Temperature Applications

2.1. BSTO x = 0.60

In addition to the cryogenic test rig installed and tested in Q6, we designed and installed a test station for measurements between 200-400 K. We completed preliminary testing of the station in Q6 and will begin characterizing BSTO x = 0.60 as well as $CaCu_3Ti_4O_{12}$ (CCTO), our chosen second generation room temperature material, versus temperature in early Q7.

2.2. *CCTO on LAO, MgO, & LSAT*

In Q6, we began our investigation of CCTO, a second generation material which showed promise as a nonlinear dielectric material in bulk measurements. We deposited 19 samples of CCTO on LAO, MgO, LSAT, and Si wafers. In Figure 2-1, we present a phase scan of a typical CCTO film grown on LAO at 950 °C. The films grow cube-on-cube, but with fairly low quality. Attempts to grow CCTO on MgO failed—the films were amorphous and did not adhere to the substrate. In the inset of Figure 2-1, we show the CCTO (004) rocking curve, which has a width of 2.8°. The width of the peaks in the phi scans (not shown) are also broader than usually seen with other materials (like BSTO or CSTO).

Preliminary electrical measurements (frequencies below 3 MHz) show these epitaxial films have very high loss at room temperature ($\tan \delta > 0.5$) and frequency-dependent tuning. Although these results are consistent with the bulk measurements performed in Q4, there is some concern (arising from the XRD data) that the poor performance of the thin film samples may be due to the low film quality. We have begun exploring the deposition conditions more fully to find a more promising process region. In Figure 2-2, we plot the results of an RBS study of the rate (Figure 2-2a) and compositional deviation (Figure 2-2b) for different deposition powers and pressures. Our first samples were deposited at 75 W_{RF} and 140 mT. From Figure 2-2b we can see that improvements in film stoichiometry can be had by moving to lower deposition pressures. In Q7, we will see if higher epitaxial quality films lead to better electrical performance.

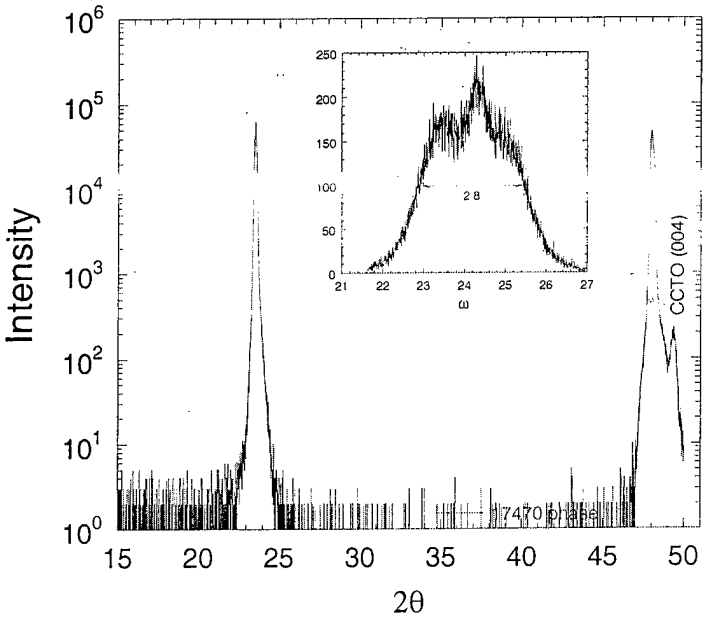

Figure 2-1. Phase scan of a 0.16 μm CCTO film on LAO. The film is c-axis oriented. Inset: CCTO (004) rocking curve, FWHM ~ 2.8°. Phi scans (not shown) indicate cube-on-cube growth. The widths of the rocking curve and phi scans are unusually broad.

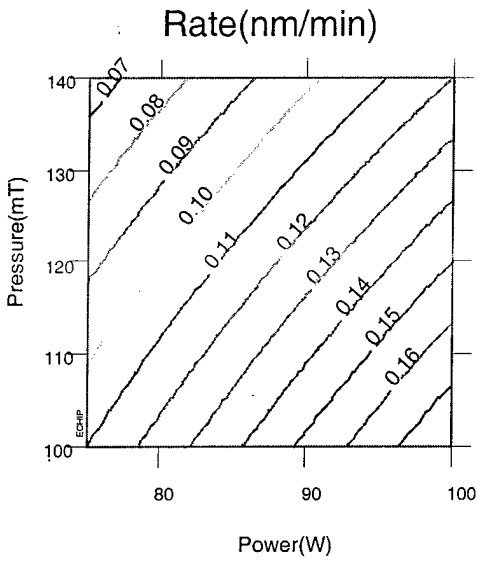

Figure 2-2a. Deposition rate vs. RF power and Ar + O_2 pressure for CCTO.

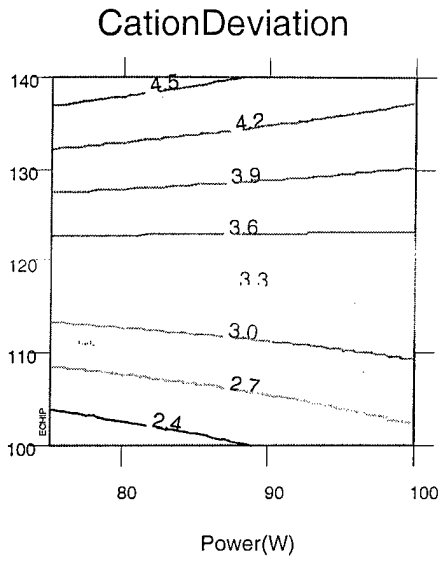

Figure 2-2b. Average percentage deviation from stoichiometry ($CaCu_3Ti_4O_x$) vs. deposition parameters.

Task 3. Multilayer Film Development and Manufacturing

3.1. Multilayer Devices

This quarter we fabricated 17 wafers using the photomasks designed in Q5. These consisted of both test wafers (Au or superconductor on bare substrates, to check our modeling of known geometries) and YBCO/BSTO or Au/BSTO bilayers. We also designed and fabricated fast-assembly microwave packages to ease testing of these samples in the variable temperature test rigs. Testing of these devices will begin in Q7 to satisfy milestones 3.D & E.

Task 4. Exploratory Laser Ablation Processing (University of Colorado)

In this quarterly progress, we report the preparation of some new bulk materials and targets, growth of epitaxial films of two new films and their dielectric characterization. We also report the XRD measurements carried out to understand the strain in the thin films and strain/dielectric property correlation.

4.1. Preparation of bulk materials and targets.

Bulk materials with compositions, $Ba_{0.6}Sr_{0.4}Ti_{0.98}Mn_{0.02}O_3$, $Ba_{0.6}Sr_{0.4}Ti_{0.99}Fe_{0.01}O_3$, $Ba_{0.6}Sr_{0.4}Ti_{0.98}Mn_{0.01}W_{0.01}O_3$, $Ba_{0.681}Sr_{0.281}Mg_{0.038}Ti_{0.962}Zr_{0.038}O_3$ (or 68.1% $BaTiO_3$ + 28.1% $SrTiO_3$ + 3.8% $MgZrO_3$) for room temperature applications and $Ba_{0.05}Sr_{0.95}TiO_3$ for cryogenic applications were prepared. Single phase materials could be obtained, as confirmed by powder X-ray diffraction (Typical XRD patterns are shown in figs. 4.1.1 and 4.1.2).

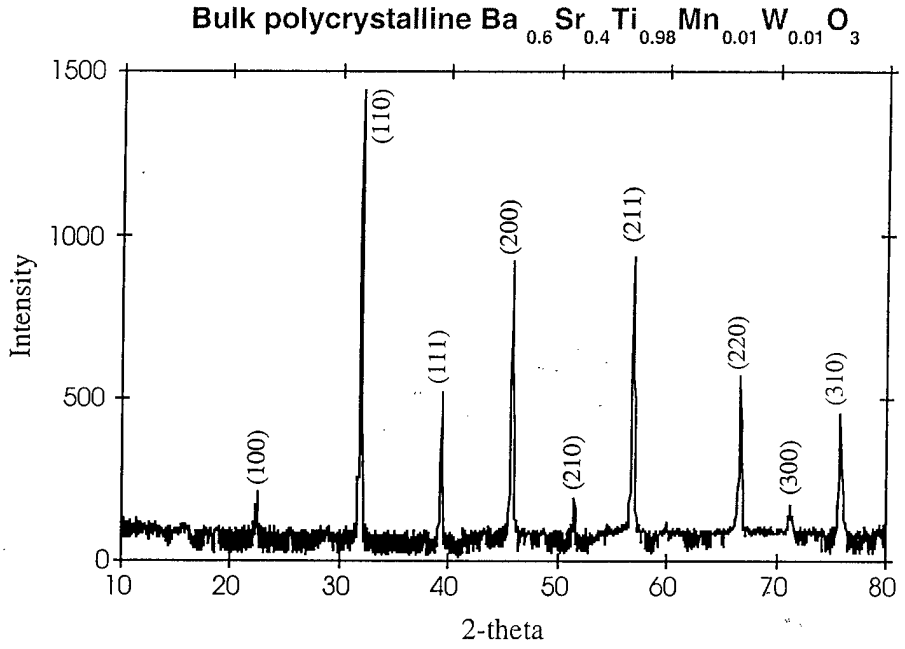

Fig. 4.1.1. Powder X-ray diffraction pattern for bulk $Ba_{0.6}Sr_{0.4}Ti_{0.99}Mn_{0.01}W_{0.01}O_3$

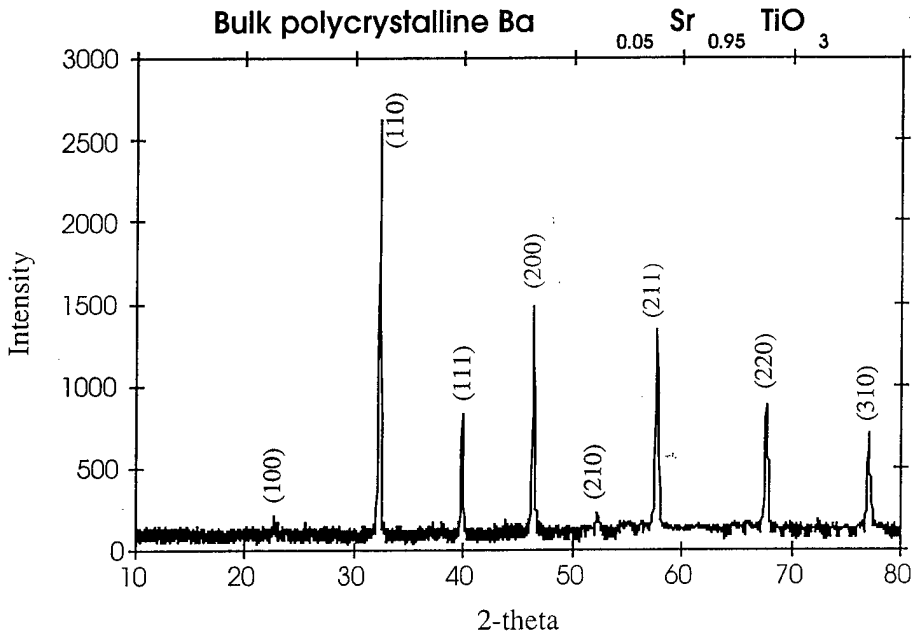

Fig. 4.1.2. Powder X-ray diffraction pattern of bulk $Ba_{0.05}Sr_{0.95}TiO_3$

4.2. Thin film deposition and dielectric studies

Thin films of co-doped BSTO ($Ba_{0.6}Sr_{0.4}Ti_{0.98}Mn_{0.01}W_{0.01}O_3$) and $Ba_{0.681}Sr_{0.281}Mg_{0.038}Ti_{0.962}Zr_{0.038}O_3$ were grown on LAO substrate using pulsed laser deposition. The unannealed as well as the post-oxygen annealed (950 °C for 6h) films showed *h00* orientation (figs. 4.2.1 and 4.2.2).

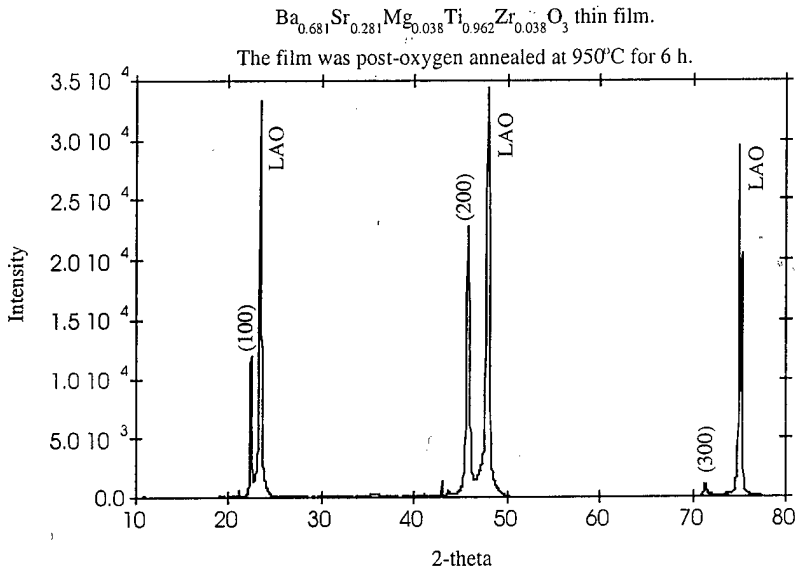

Fig. 4.2.1. XRD pattern of $Ba_{0.681}Sr_{0.281}Mg_{0.038}Ti_{0.962}Zr_{0.038}O_3$ thin film grown by PLD. The epitaxial nature of the film is clearly revealed.

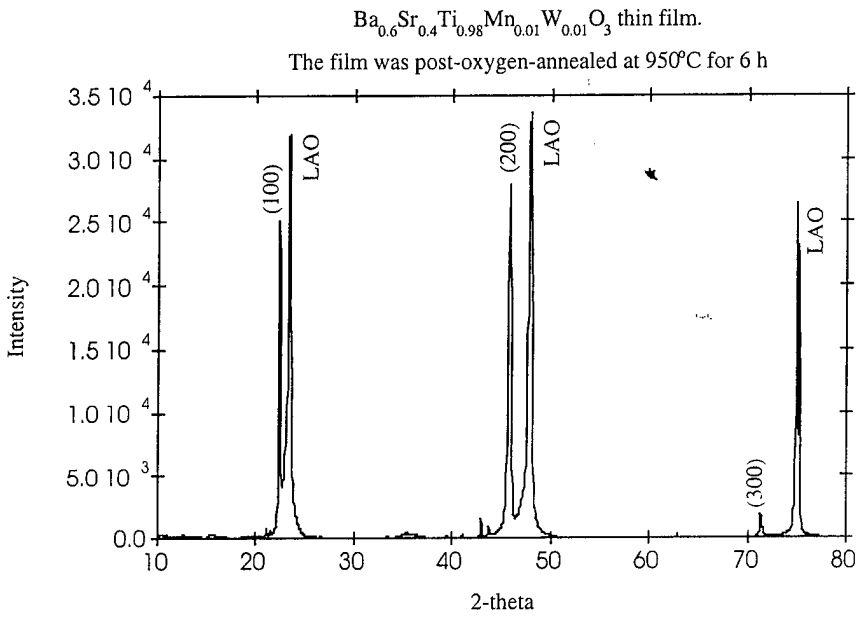

Fig. 4.2.2. X-ray pattern of co-doped BSTO film revealing the epitaxial nature of the film

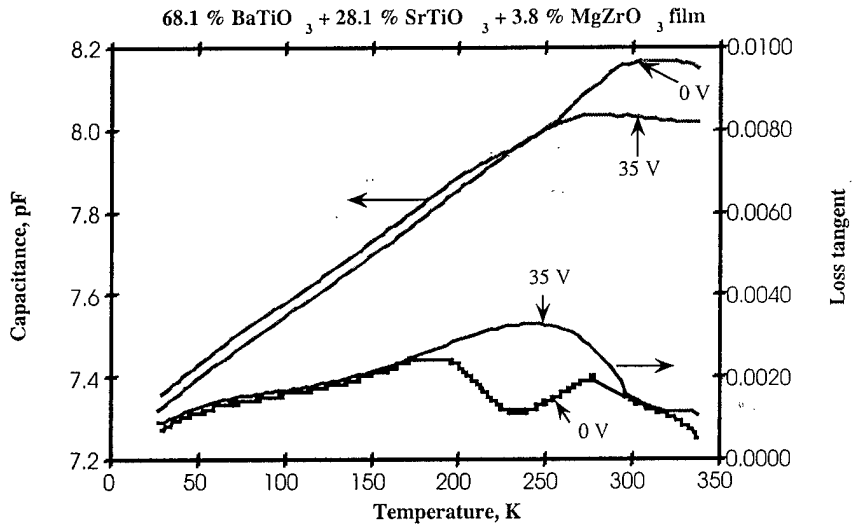

Fig. 4.2.3. Capacitance and loss tangent as a function of temperature for $Ba_{0.681}Sr_{0.281}Mg_{0.038}Ti_{0.962}Zr_{0.038}O_3$ thin film. The measurements were done at 1 MHz. The ferroelectric-paraelectric transition is broad around 300 K. The film exhibits a tunability of about 2% for a field of 0.5 V/μm and moderately low loss.

Interdigitated capacitors were made using a shadow mask by thermal evaporation of Ag to a thickness of 150 nm. The capacitance and loss tangent were measured using HP 4192A LCR meter at 1MHz. $Ba_{0.681}Sr_{0.281}Mg_{0.038}Ti_{0.962}Zr_{0.038}O_3$ showed a broad peak and a tunability of about 2% (for a field of ~ 0.5 V/μm). The dielectric loss was moderately low (<2 x 10^{-3} at 300 K). (fig. 4.2.3)

Preliminary measurements on co-doped (1% Mn and W) BSTO showed low tunability, although the film exhibited very low dielectric loss (~$6x10^{-4}$) at 295 K. Dielectric measurements were also done on W-doped BSTO, which shows a tunability of about 1% and moderately low loss (fig. 4.2.4)

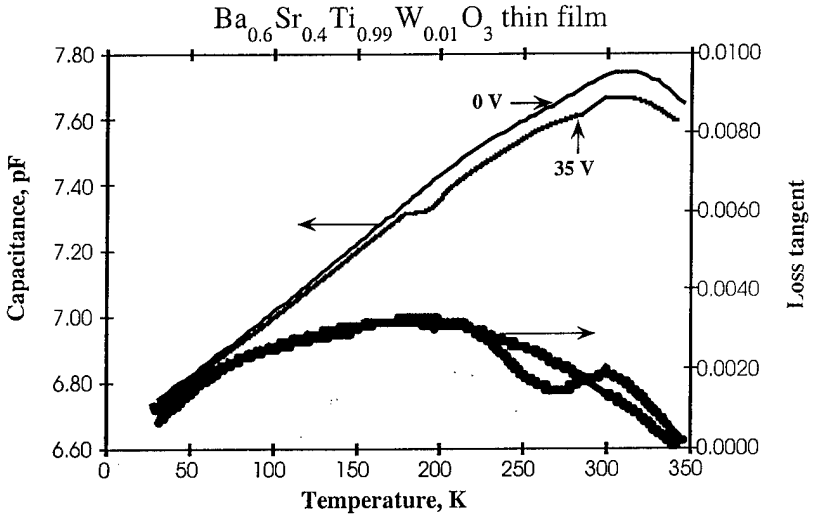

Fig. 4.2.4. Capacitance and dielectric loss as a function of temperature for W-doped BSTO thin film. The Curie temperature is about 310 K. The film shows about 1.2 % tunability for a field of 0.5 V/μm and moderately low losses at the T_c

4.3. XRD Measurements of $Ba_{0.6}Sr_{0.4}Ti_{0.99}M_{0.01}O_3$ (M = Ti, Mn, W) Thin Films

A key factor that can influence mechanical, dielectric, thermodynamic, and optical properties of non-linear dielectrics is stress. For instance, film stresses limit the maximum thickness of epitaxial films, alter ferroelectric domain structure, the Curie temperature, and tunability. Sources of thin-film stresses are numerous: differences in thermal-expansion

coefficients and lattice parameters between the substrate and thin film, increase in density due to formation of an amorphous phase, and some lattice defects, notably dislocations and vacancies.

We obtained x-ray diffraction patterns of three specimens: $Ba_{0.6}Sr_{0.4}Ti_{0.99}M_{0.01}O_3$ (M = Ti, Mn, W). Coupled $\theta/2\theta$ scans showed only *h*00 Bragg peaks for all three phases. A good epitaxy with the substrate was confirmed by the azimuthal (ϕ) scans. To thoroughly investigate the misfit relationship at the film-substrate interface, we recorded reciprocal space maps for all three films. Reciprocal space maps of the symmetric 002 Bragg reflection for the pristine $Ba_{0.6}Sr_{0.4}TiO_3$ and $Ba_{0.6}Sr_{0.4}Ti_{0.99}W_{0.01}O_3$ are shown in the Fig. 4.3.1. It is clear that the pristine film shows very little mosaicity, in contrast to $Ba_{0.6}Sr_{0.4}Ti_{0.99}W_{0.01}O_3$, where the misfit largely relaxes by introduction of misfit dislocations and a larger mosaic spread. Both films show broadening perpendicular to the interface, which could be caused by small correlation lengths, inhomogeneous strain, and the depth-dependent stoichiometry variations. To investigate this further, we conducted a careful study of line broadening perpendicular to the interface. The analysis takes into account multiple Bragg reflections, thus allowing for an unequivocal separation of correlation-length and inhomogeneous-strain effects on line broadening. The results indicate that both effects are present; however, increase in inhomogeneous strain in the W-doped thin film is much more important. The Mn-doped thin film also shows a relatively modest increase in inhomogeneous strain over the pristine film, but the correlation length is unchanged. Reciprocal space maps confirm this behavior, because the Mn-doped film shows little or no increase of mosaicity. The understanding of W-substitution on strain and dielectric properties is not yet totally clear but a different-size substitution atom may facilitate introduction of line defects and subsequently the relaxation of lattice-mismatch strains.

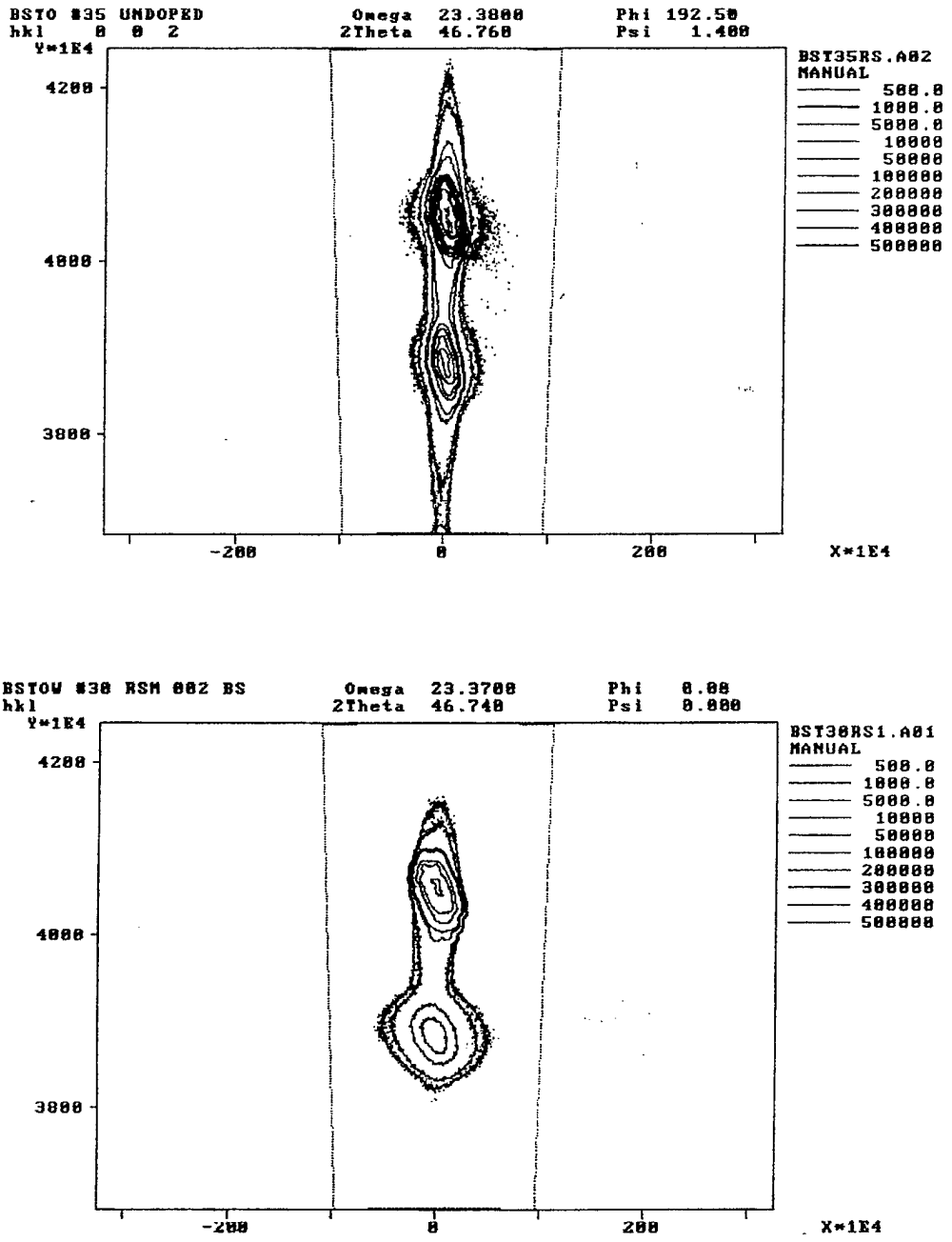

Figure 4.3.1. Reciprocal space maps of symmetric 002 Bragg reflections: $Ba_{0.6}Sr_{0.4}TiO_3$ (upper) and $Ba_{0.6}Sr_{0.4}Ti_{0.99}W_{0.01}O_3$ (lower).

Task 5 - Materials Discovery Research

A wide range of acceptor-donor codoped $BaTiO_3$ samples were prepared in this quarter and their dielectric properties were measured. One system has been identified with high tunability (>70% at 1V/μm). Patent applications are being filed for some of these materials. More detailed information will be provided once the patents are filed.

Frequency Agile Materials for Electronics

Quarterly Report 7

Date: 04/20/00

Period covered in this report: 1/1/00 through 3/31/00

Program Title: Novel Ferroelectric Materials for Satellite Communications

Contract # DABT63-98-C-0046

Performing Organization: DuPont Superconductivity

Subcontractor: University of Colorado at Boulder

Progress By Task

Task 1. Large Area Sputtered Film Manufacturing for Low Temperature Applications

In Q7, we concentrated on making variable temperature measurements of the low frequency (0.1-10 MHz) dielectric properties of both $Ba_{0.06}Sr_{0.94}TiO_3$ (BSTO06 or BSTO x = 0.06) and $Ca_{0.05}Sr_{0.95}TiO_3$ (CSTO05) films. We designed and began using a spring-loaded contact fixture for rapid characterization of our interdigitated capacitors (IDCs). We also added an additional cryocooled microwave testing station specifically for use on the FAME program.

1.1. BSTO x = 0.06 on LAO

We measured a number of Fe doped BSTO06 films on $LaAlO_3$ (LAO). Representative data extracted from an Au IDC at 1 MHz are shown in Figure 1-1. (All the materials properties presented in this report were measured in the same way.) The Curie temperature of these films is suppressed somewhat from the bulk value; this is consistent with the degree of Fe doping (< 0.5 at.%) observed in these films. This doping, as mentioned previously, was inadvertent. The measured T_c is appropriate for cryogenic applications. We also will attempt to deposit undoped BSTO05 films to evaluate the effect of doping.

1.2. CSTO x = 0.05 on LAO, MgO, and LSAT

We also measured the dielectric properties of the putative second generation cryogenic material CSTO05. A total of 12 films were deposited on LAO, MgO, and LSAT in Q6. Typical results for films on LAO are shown in Figure 1-2. The relative permittivity of this material is quite high compared to BSTO06. However, the tunability is lower and the losses are higher, which does not make CSTO a good candidate for replacing BSTO at low temperatures. We are therefore postponing milestone 1.E., the optimization of the second generation material, until a better candidate can be identified.

1.3. Very Large Area Heater & Rotating Magnetron Sputter Source

We are preparing to move our laboratories to a new building in Q8, so work on the VLA heater and the new sputter source have been postponed until all the equipment has been moved. We expect to resume evaluation on the heater and source in late Q8/early Q9.

Task 2. Large Area Sputtered Film Manufacturing for Ambient Temperature Applications

We also concentrated on making variable temperature measurements on the nominal ambient (or room) temperature materials: BSTO50, BSTO60, and $CaCu_3Ti_4O_{12}$ (CCTO). We used the various cryocooler test stations (which cover the range 20-290 K) as well as building a dedicated environmental chamber to examine their properties from 150-450 K.

2.1. BSTO x = 0.60

In Figure 2-1 below, we plot the dielectric properties of ~ 0.5 at.% Fe doped BSTO60 on LAO at 1 MHz versus temperature. An interesting feature is the double peak in the figure of merit, perhaps indicating phase segregation of the Fe dopants. We desired the undoped composition to have a T_c near 270 K. T_c for the Fe doped material is much lower, around 100 K, although the second peak in K falls in a useful region for ambient temperature operations.

2.2. BSTO x = 0.50

In an attempt to quantify the effect of the Fe doping on the initial targets and films, we deposited a number of films from a nominally clean BSTO50 target purchased from our primary target vendor. The electrical data are shown in Figure 2-2. To our surprise, the Curie temperature for this material is suppressed (our T_c ~ 70 K, bulk T_c ~ 250 K), like the BSTO06 and BSTO60 before it. This indicates that the Fe contamination may not have been eliminated; we also have BSTO50 targets purchased from another vendor which we will use to compare to the present data in Q8.

2.3. CCTO on LAO

We continued our investigation of CCTO to determine its suitability for use as a non-linear dielectric near room temperature. As noted in Q6, initial measurements on CCTO films showed very high loss. In the present measurements, the loss is no better. Although the films show strong dielectric non-linearity for T > 300 K, the loss is prohibitively high. We are therefore also postponing the completion of milestone 2.E., the optimization of a second generation ferroelectric material for room temperature applications.

Task 3. Multilayer Film Development and Manufacturing

3.1. Multilayer Devices

In Q7, we fabricated an additional five coplanar ferroelectric structures, however our wirebonder (which is necessary to enable high frequency testing) was not available for use until late Q7 because of repairs. Therefore, we will begin testing of our multilayer devices in early Q8 to satisfy milestones 3.D & E. We also hope to satisfy milestone 3.F. in late Q8.

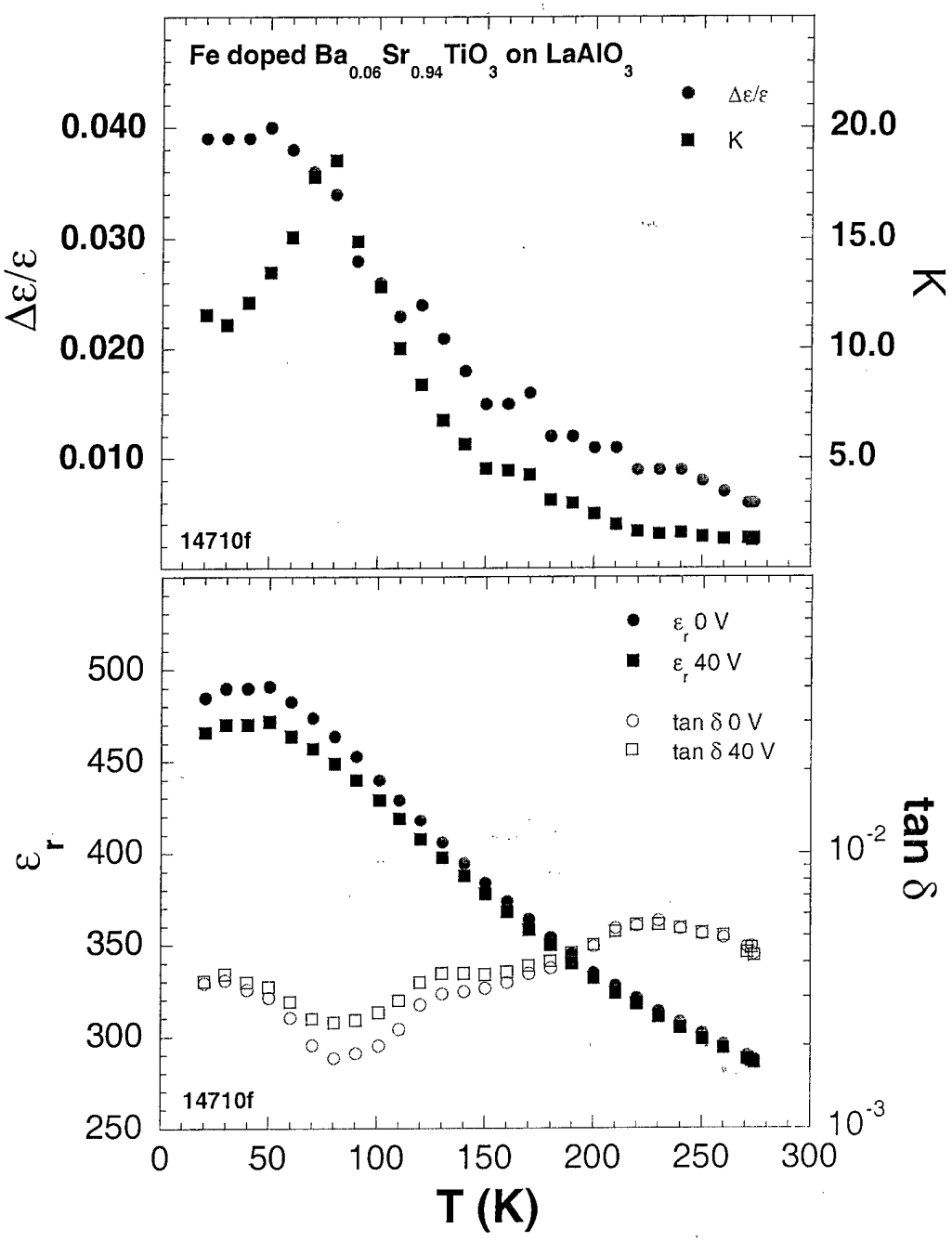

Figure 1-1. The dielectric properties of a 0.2 μm thick ~ 0.5 at.% Fe doped BSTO06 film on LAO, measured using a 10 μm gap intedigitated capacitor at 1 MHz. Top: the tunability Δε/ε and figure of merit K at 4 V/μm. Bottom: the relative permittivity ε_r and loss tangent tan δ.

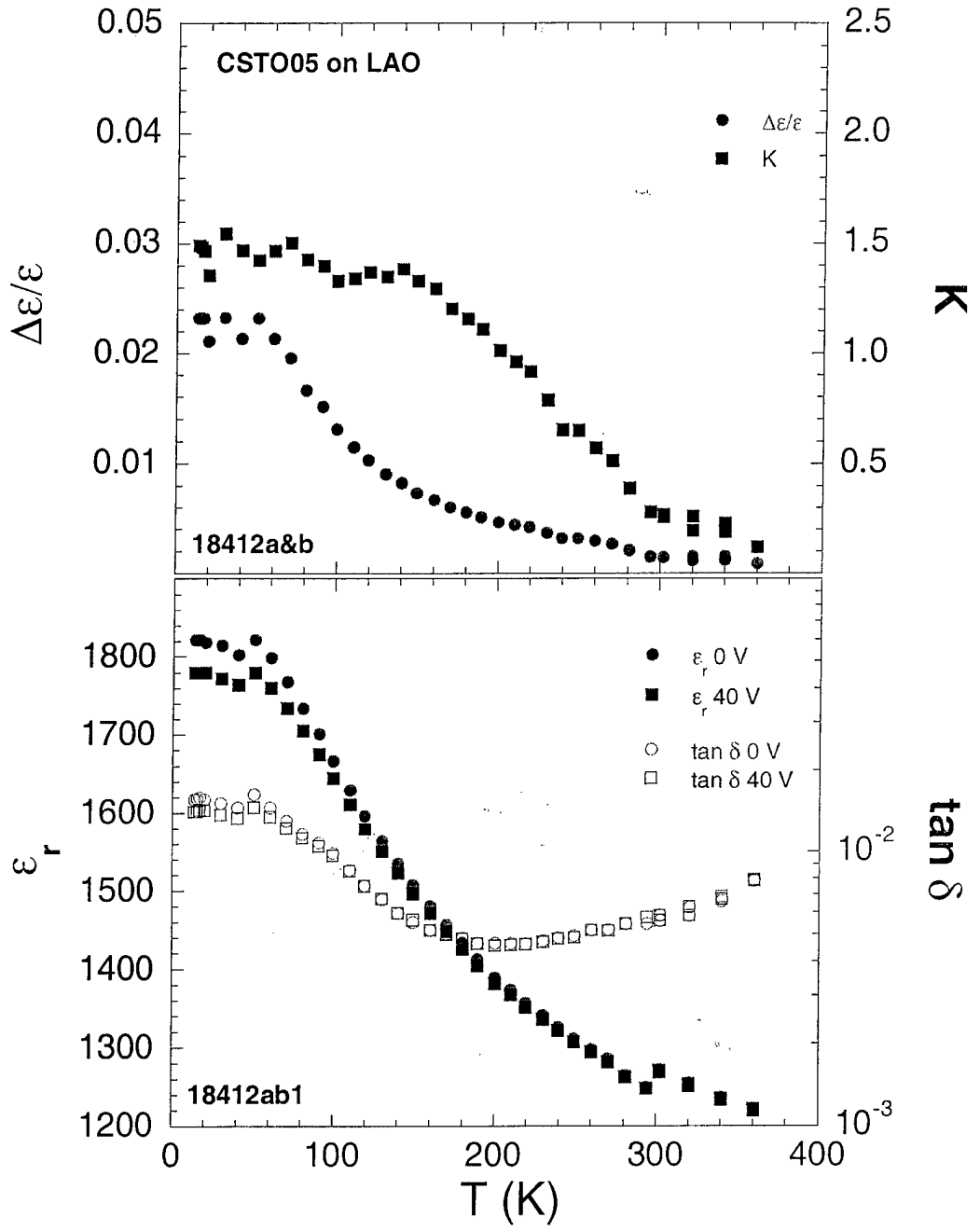

Figure 1-2. Dielectric properties of a 0.14 μm CSTO05 film on LAO. Measurement setup identical to Figure 1-1. The tunability and loss are worse than our BSTO06 films, making this a poor choice as a second generation material.

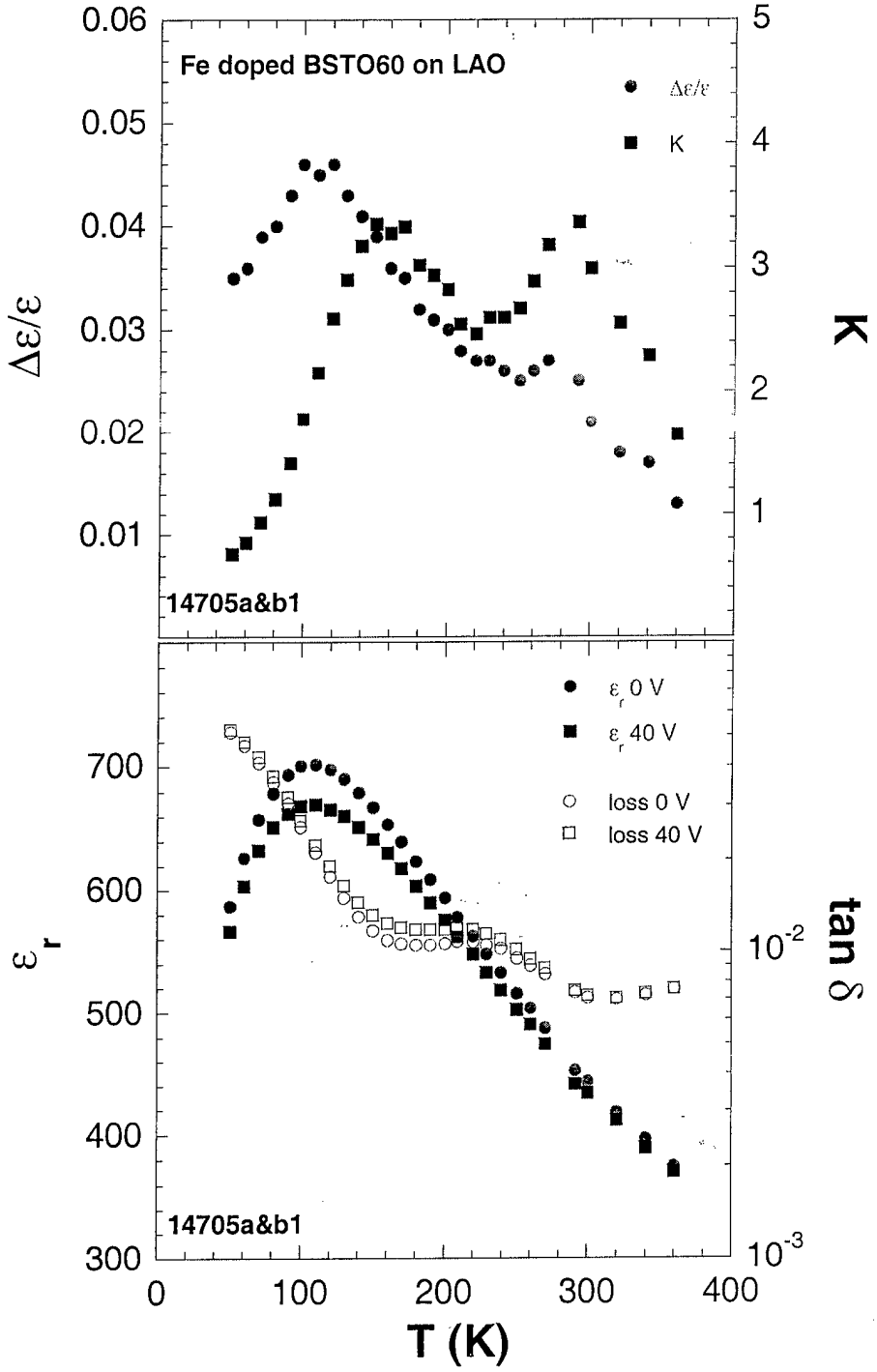

Figure 2-1. Dielectric properties of a 0.3 μm thick ~ 0.5 at.% Fe doped BSTO60 film on LAO. T_c is greatly suppressed from the bulk value. However, K has a second peak near 300 K, ideal for room temperature applications.

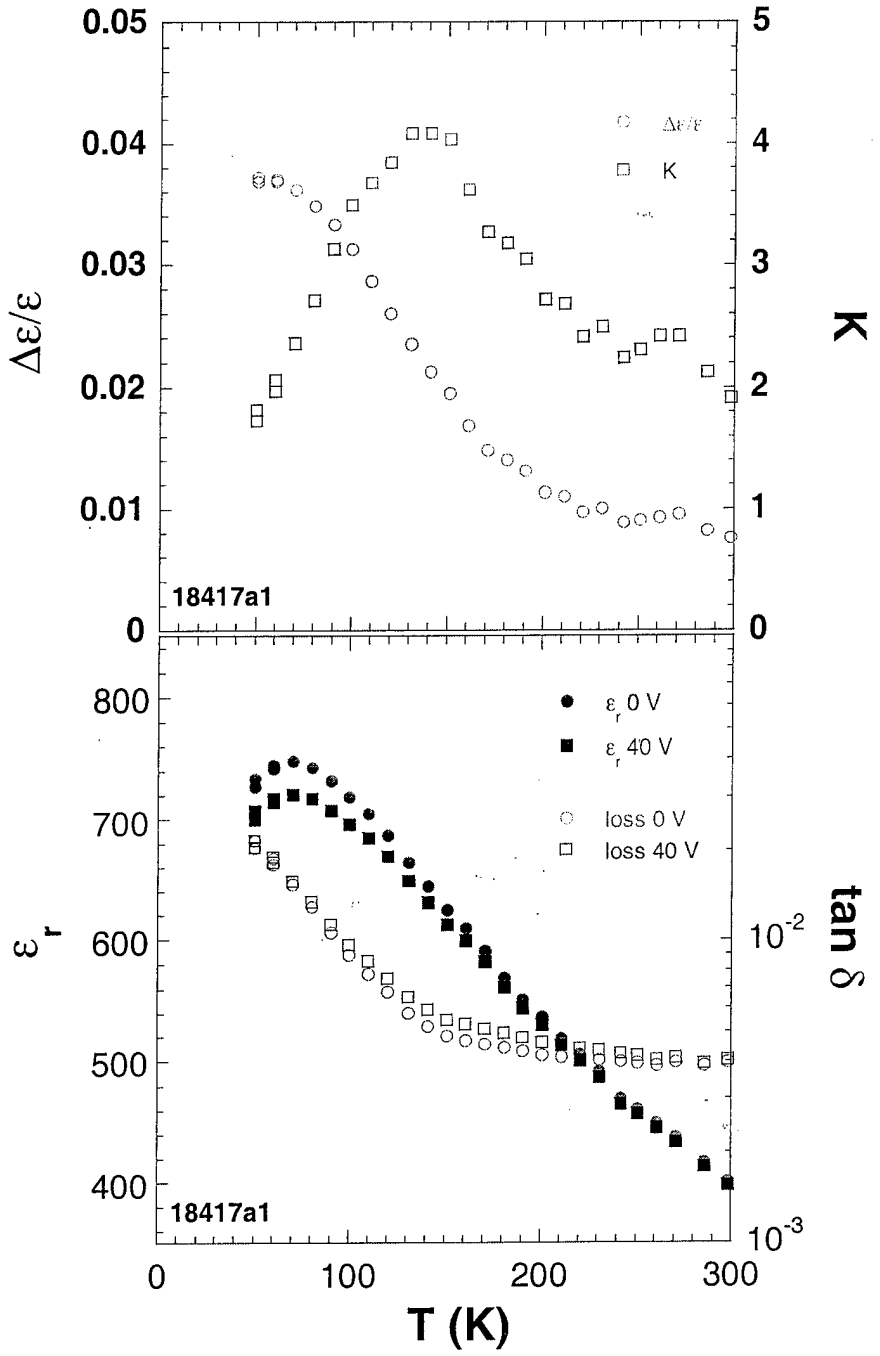

Figure 2-2. 0.74 μm thick BSTO50 film on LAO. Note T_c is far below the bulk value, probably indicating inadvertent Fe doping, as in the BSTO06 and BSTO60 films.

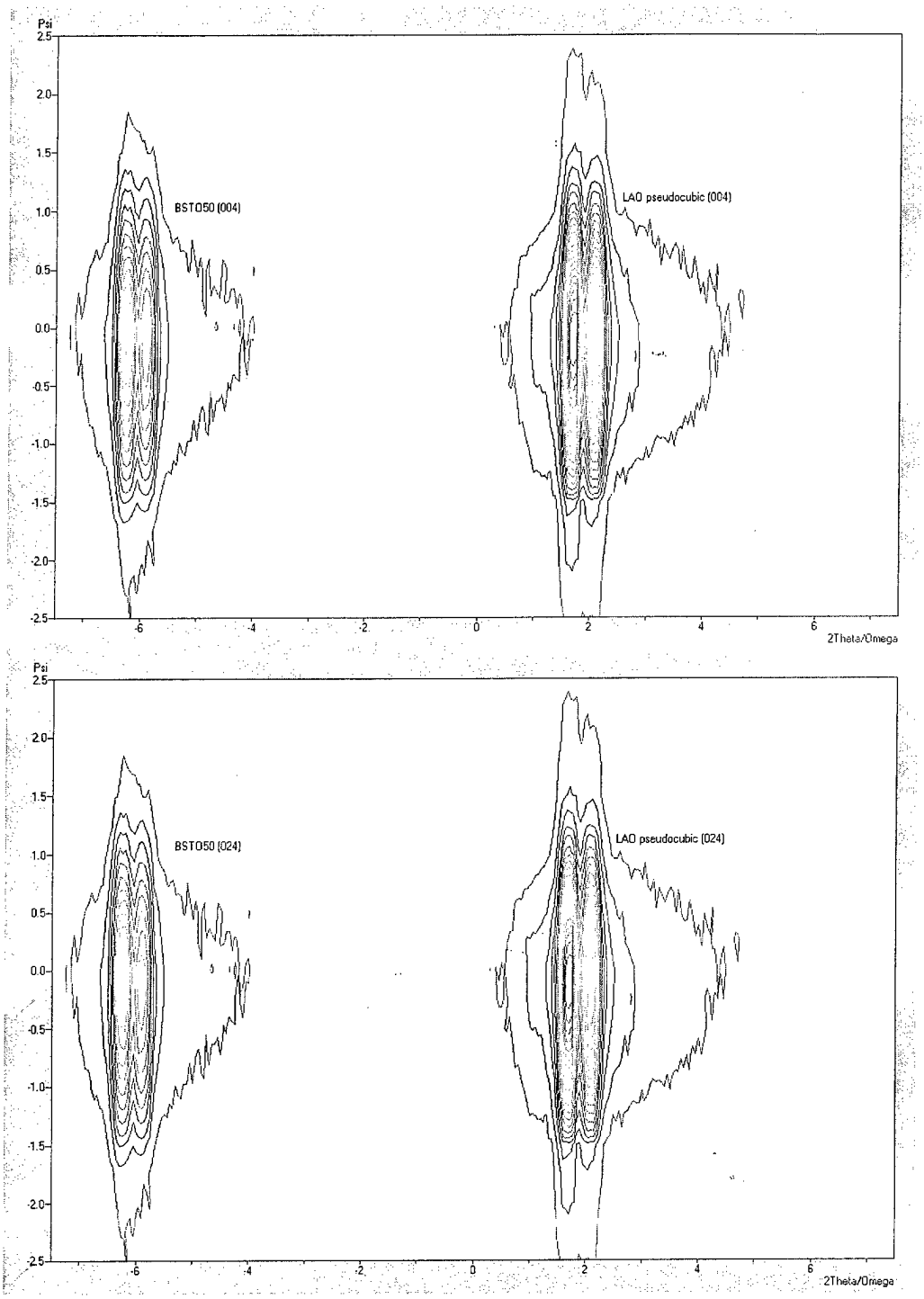

Figure 2-3. Reciprocal lattice scans of the cubic (004), top plot, and (024), bottom, reflections of the BSTO50 film from Figure 2-2. These data indicate that BSTO50 grows cube-on-cube with high quality and slight compressive strain at 295 K.

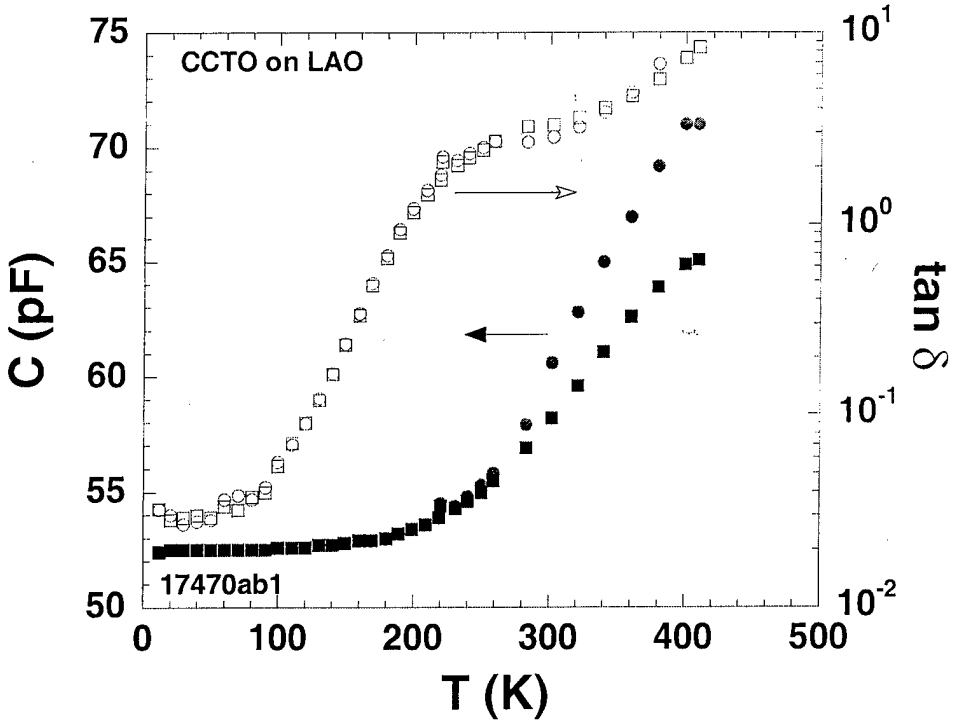

Figure 2-4. 0.1 μm thick CCTO film on LAO. The losses at 1 MHz are so high, it is difficult to extract the dielectric properties properly. Note tan δ > 1 when there is appreciable tunability of the capacitance. The non-linearity is strongly frequency dependent, increasing as the frequency decreases below 300 kHz. This material does not appear to be a good second generation ferroelectric candidate for room temperature applications.

Task 4. Exploratory Laser Ablation Processing (University of Colorado)

In this quarterly progress, we report the preparation of some new bulk materials, their dielectric characterization, and dielectric characterization of epitaxial films of Mn-doped BSTO.

4.1. Synthesis and dielectric characterization of $Ba_{0.6}Sr_{0.4-x}Mg_xTi_{1-x}Zr_xO_3$ bulk materials

We had reported in the previous report the dielectric properties of $Ba_{0.681}Sr_{0.281}Mg_{0.038}Ti_{0.962}Zr_{0.038}O_3$ epitaxial films. The films showed a 7% drop in the dielectric constant value for a field of 0.5 V/μm. Encouraged by this, we undertook a systematic study of Mg, Zr doped BSTO materials. We prepared the compositions, $Ba_{0.6}Sr_{0.4-x}Mg_xTi_{1-x}Zr_xO_3$ (x = 0.01-0.04). Single phase materials could be obtained as confirmed by powder X-ray diffraction (fig. 4.1.1).

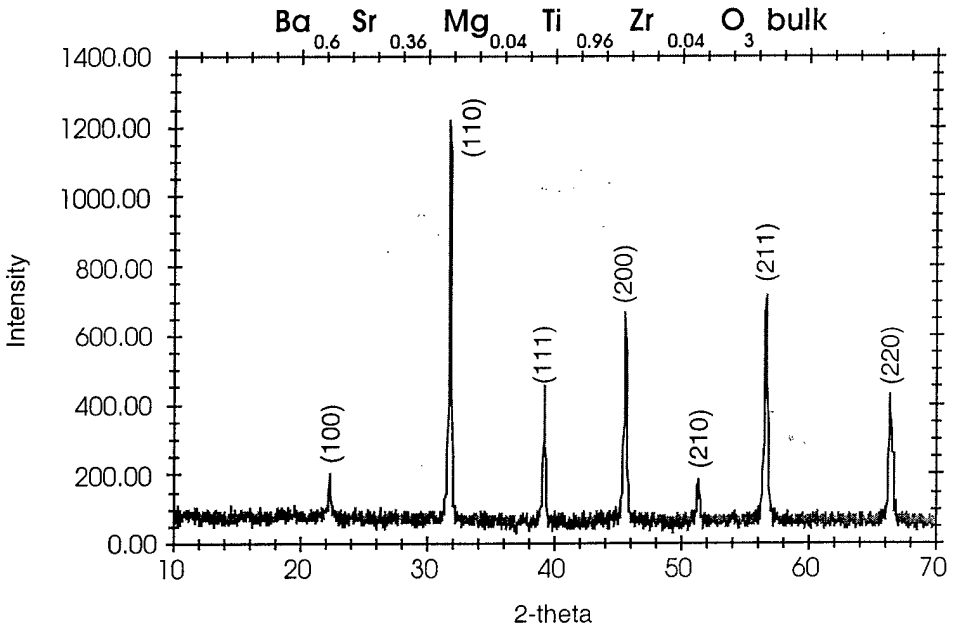

Fi.g. 4.1.1. Powder X-ray diffraction pattern of 4% Mg, Zr doped BSTO bulk material

Dielectric constant measurements were carried out on 1 and 2% Mg, Zr - doped samples using slotted capacitor configuration at a constant frequency of 1 MHz. The observed Curie temperature was around 265 K for both the samples (fig. 4.1.2 and 4.1.3).

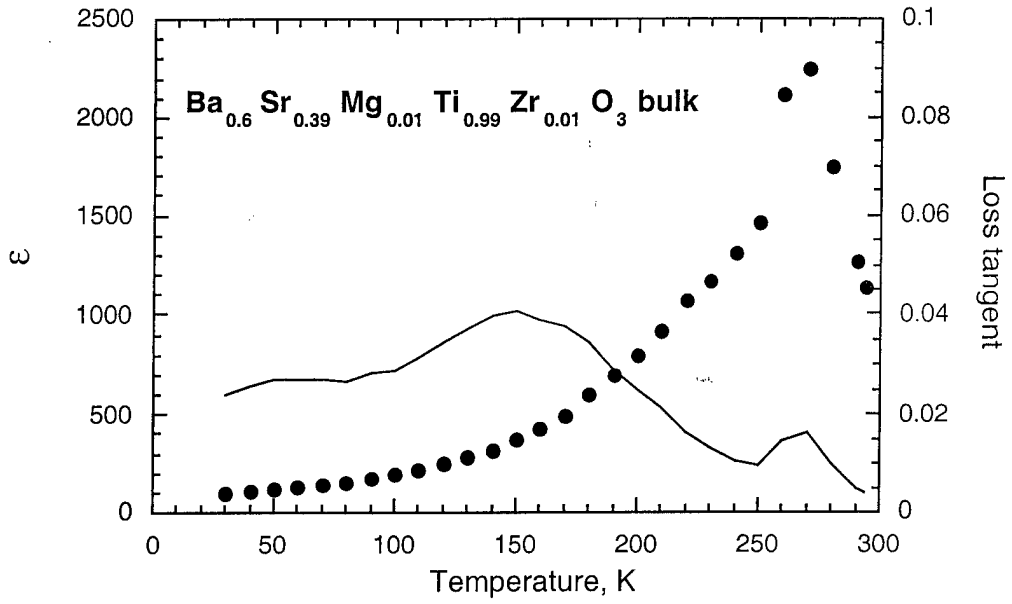

Fig. 4.1.2 Dielectric property variation with temperature for bulk $Ba_{0.6}Sr_{0.39}Mg_{0.01}Ti_{0.99}Zr_{0.01}O_3$

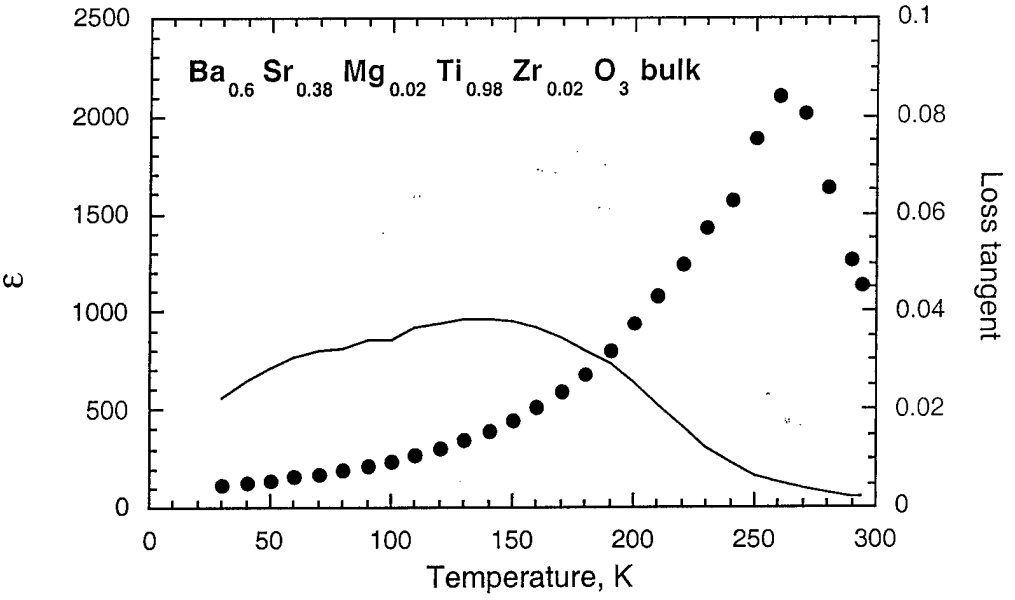

Fig. 4.1.3 Dielectric property variation with temperature for bulk $Ba_{0.6}Sr_{0.38}Mg_{0.02}Ti_{0.98}Zr_{0.02}O_3$

This Curie temperature is almost the same as what we observe for pristine BSTO bulk samples. The loss showed a peak at T_c for the 1% doped sample, whereas for the 2% doped sample, this peak is not present. The dielectric loss for 2% doped sample is lower

at ambient temperature. Dielectric characterization of 3 and 4% doped samples are underway.

4.2. Synthesis and dielectric characterization of Rb-doped KTO bulk materials

Our earlier studies on $KTaO_3$ (KTO) bulk as well as epitaxial films showed that there was no ferroelectric transition and KTO behaves as an incipient ferroelectric material. It has very low dielectric loss (10^{-4}) at microwave frequencies, but the dielectric constant value is <2000. Also, there was negligible tunability. To improve the dielectric properties and to induce well-defined ferroelectric transition, we undertook the synthesis of a series of Rb-doped KTO bulk materials. We found that single phase materials could be obtained up to x = 0.1 in the $K_{1-x}Rb_xTaO_3$ system (fig. 4.2.1). For x= 0.2, we see small impurity peaks and for x > 0.2, there is a phase segregation of $KTaO_3$ and $RbTaO_3$ (fig. 4.2.2).

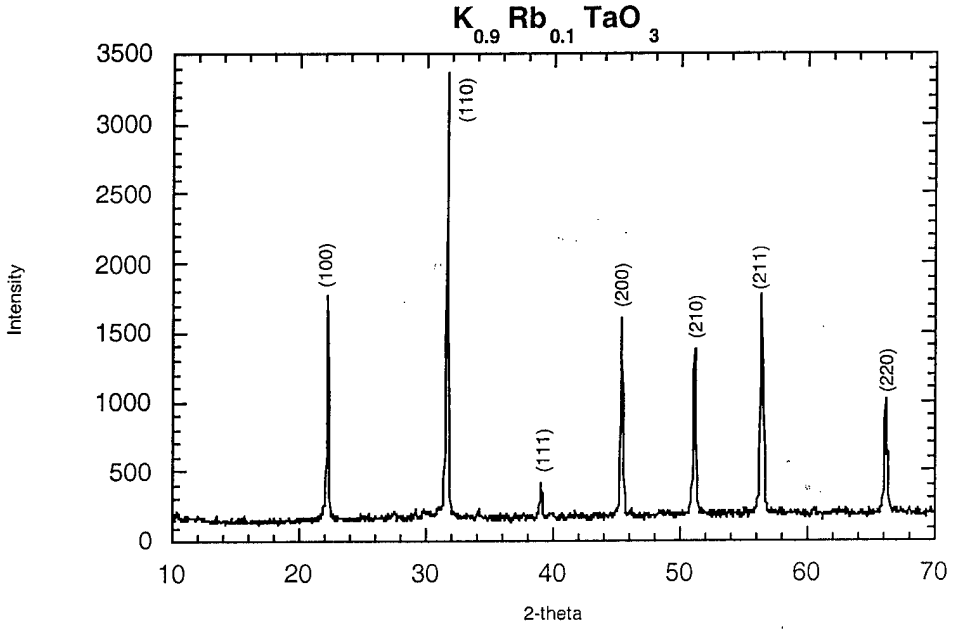

Fig. 4.2.1. Powder X-ray diffraction pattern of bulk $K_{0.9}Rb_{0.1}TaO_3$. Single phase material could be obtained.

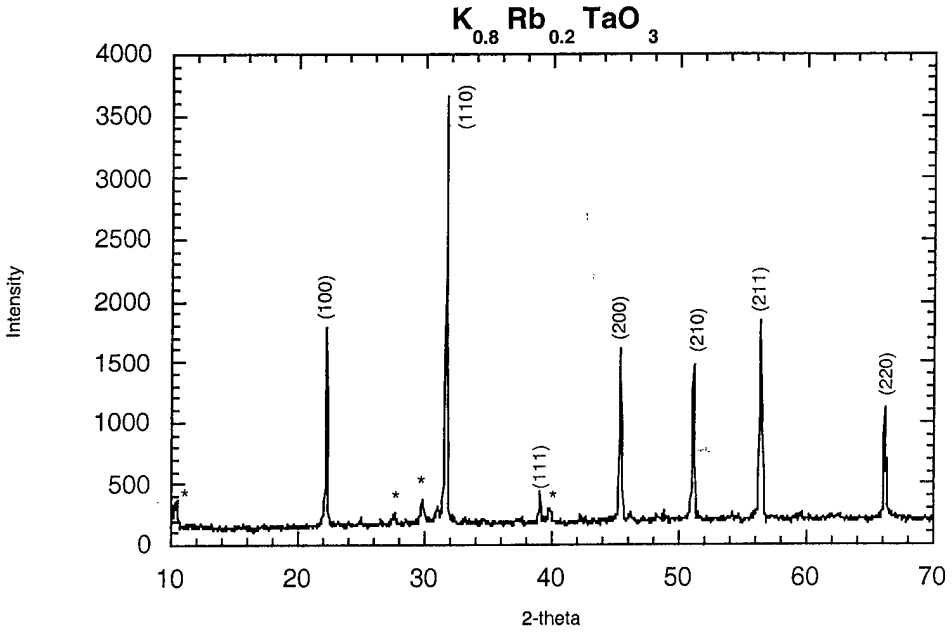

Fig. 4.2.2. Powder X-ray diffraction pattern of $K_{0.8}Rb_{0.2}TaO_3$ bulk material. Asterisks indicate impurity peaks.

Dielectric measurements at a constant frequency of 1 MHz were carried out on $K_{0.95}Rb_{0.05}TaO_3$ bulk sample using slotted capacitor configuration. The material does not show any ferroelectric transition down to 25 K (fig. 4.2.3). The dielectric loss shows a peak around 70 K. This peak was absent in pristine $KTaO_3$ studied earlier. Dielectric studies on bulk $K_{0.9}Rb_{0.1}TaO_3$ are underway.

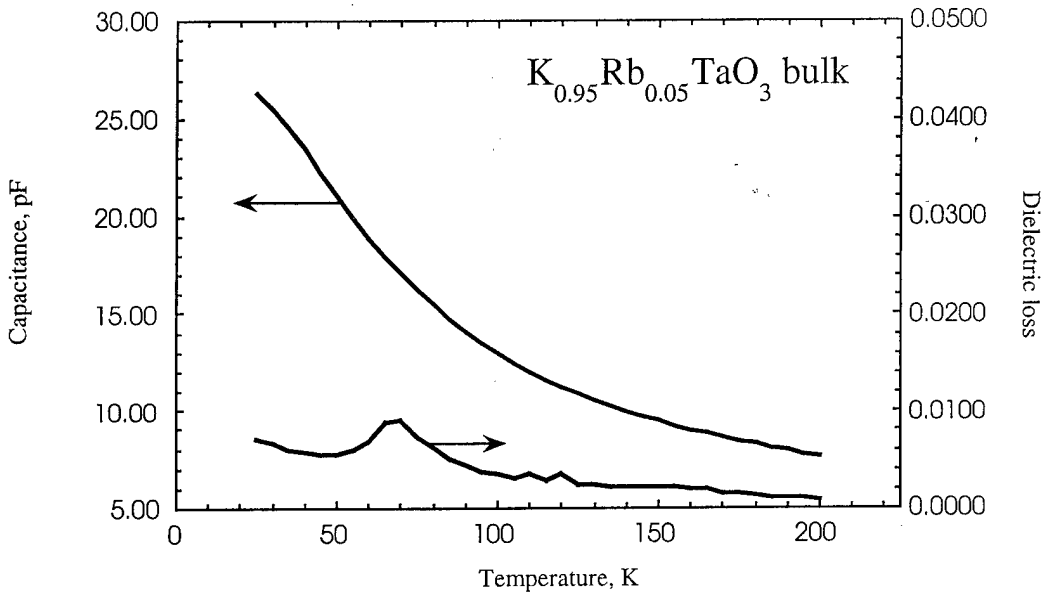

Fig. 4.2.3. Dielectric properties of bulk $K_{0.95}Rb_{0.05}TaO_3$

4.3. Dielectric studies on Mn- doped BSTO epitaxial films

Dielectric measurements were carried out on Mn-doped BSTO epitaxial films using interdigitated capacitor configuration. The measurements were done at 1 MHz. The film showed a Tc of about 325 K, which is higher than that of pristine BSTO. This could be strain related, as evident from our strain studies carried out on pristine and Mn-doped BSTO films. The Mn-doped film showed increased inhomogeneous strain than the pristine film. This increased strain is also reflected in the increased loss, which is about an order of higher than that observed for pristine film. The capacitance values are, surprisingly, higher than those observed in any of our other films. The reason for this is not clear yet. The film exhibits promising tunability behavior.

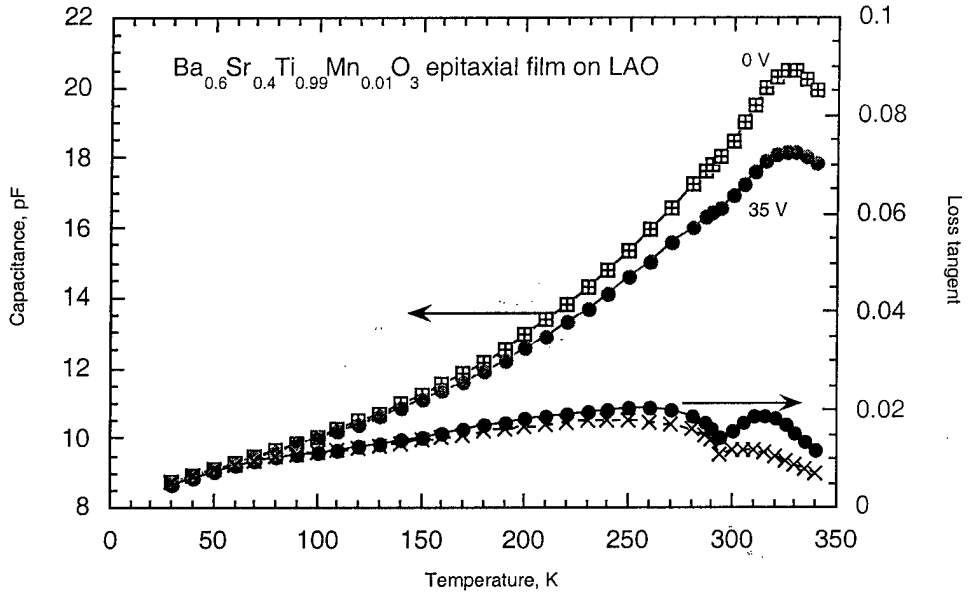

Fig. 4.3.1 Capacitance and loss tangent as a function of temperature of Mn-doped BSTO epitaxial thin film on LAO substrate

Task 5 - Materials Discovery Research

A wide range of acceptor-donor codoped $BaTiO_3$ were prepared in this quarter and their dielectric properties were measured. One system, $BaTiO_3$-$LaFeO_3$, has been identified with high tunability. In this report, the phase change, loss tangent, and tunability in this system and dielectric properties of other acceptor-donor codoped $BaTiO_3$ are reported.

<1> La doping

La is co-doped with Al, Ga, Fe, and Cr. Fe codoped samples show very pronounced tunability at room temperature followed by Cr and Al. There is almost no tunning observed for Ga samples. The 4% [La, Fe] sample shows the highest tunability (Fig.5-1). The T_C is decreased from about 130°C of $BaTiO_3$ to below room temperature (Fig. 5-2). There exists whole range solid solution between $BaTiO_3$ and $LaFeO_3$ (Fig. 5-3). The doping tends to change the phase of $BaTiO_3$ from tetragonal to cubic at room temperature. $(Ba,La)(Ti,Fe)O_3$ solid solution remained as tetragonal up to about 5% $LaFeO_3$. For higher concentration of La and Fe, the solid solutions are cubic. This phase change contributes to the lowering of T_C. In comparison, only about 4% $LaCrO_3$ can be dissolved in $BaTiO_3$ at current preparing condition whereas $LaAlO_3$ solubility is about 15mol%. They all show less tunability.

<2> Fe doping

Fe is co-doped with La, Sm, Gd, Dy, Bi, Nb, and Ta at 4% concentration. Except for Dy, Nb, and Ta, all other ions show some kind of tunning at room temperature.

<3> Other transient metal ions doping

Mn^{2+}, Co^{2+}, Ni^{2+}, Cu^{2+}, and Zn^{2+} ions are doped in $BaTiO_3$ together with W. The Mn^{2+} sample shows noticiable tunning, however there is $BaWO_4$ impurity in the sample. Other samples do not show appreciable tunning.

Studied materials:

1. $Ba_{1-x}La_xTi_{1-x}A_xO_3$: A=Al, Ga, Fe, Cr. x=0.02, 0.04, 0.06, 0.08
2. $Ba_{1-x}La_xTi_{1-x}Fe_xO_3$: x=0.01, 0.02, 0.03, 0.04, 0.05, 0.06, 0.07, 0.08, 0.2, 0.4, 0.6, 0.8, 0.9, 0.95.
3. $BaTi_{0.92}W_{0.04}A_{0.04}O_3$: A= Mn^{2+}, Co^{2+}, Ni^{2+}, Cu^{2+}, and Zn^{2+}.

Table 5-1: Relative dielectric constants and loss of $BaTiO_3$: x%LaFe at 1MHz

X	Dielectric Constant	Loss Tangent
0	1195	0.0080
0.02	1495	0.0091
0.04	4540	0.0144
0.05	1491	0.0243
0.06	954	0.0237
0.08	770	0.0802
0.2	127	0.3518

Table 5-2: Fitted tunability equation of selected materials.

Composition	Tunability Equation. (T: tunability in %, E: electric field in V/μm)
$Ba_{.96}La_{.04}Ti_{.96}Al_{.04}O_3$	T = 11.4 x (E)
$Ba_{.96}La_{.04}Ti_{.96}Cr_{.04}O_3$	T = 27.2 x (E)
$Ba_{.96}La_{.04}Ti_{.96}Fe_{.04}O_3$	T = 74.3 x (E)
$Ba_{.96}Sm_{.04}Ti_{.96}Fe_{.04}O_3$	T = 21.0 x (E)
$Ba_{.96}Gd_{.04}Ti_{.96}Fe_{.04}O_3$	Frequency dependent, tetragonal
$Ba_{.96}Dy_{.04}Ti_{.96}Fe_{.04}O_3$	**No tuning**
$BaTi_{0.92}Mn_{0.04}W_{0.04}O_3$	T = 20.5 x (E)
$BaTiO_3$	T = -6.67 x (E) (10k Hz)
$Ba_{0.6}Sr_{0.4}TiO_3$	T = 38.4 x (E)

Tunability, $T = 100 \times [K(v=0) - K(v\neq0)] / K(v=0)]$

Table 5-3: Dielectric values of $Ba_{1-x}Ln^{3+}{}_xTi_{1-x}M^{3+}{}_xO_3$ at 1 MHz and room temperature.

Composition	Electric Field (V/μm)	Dielectric Constant	Loss Tangent	Tunability (Percent)
$Ba_{.96}La_{.04}Ti_{.96}Al_{.04}O_3$	0.073	1713	0.0127	0.8
$Ba_{.96}La_{.04}Ti_{.96}Cr_{.04}O_3$	0.059	536	0.0060	1.6
$Ba_{.96}La_{.04}Ti_{.96}Fe_{.04}O_3$	0.053	4350	0.0130	4.2
$Ba_{.96}Sm_{.04}Ti_{.96}Fe_{.04}O_3$	0.061	1857	0.0180	1.2
$Ba_{.96}Gd_{.04}Ti_{.96}Fe_{.04}O_3$	0.063	929	0.0309	1.2
$Ba_{.96}Dy_{.04}Ti_{.96}Fe_{.04}O_3$	0.064	525	0.0225	0
$BaTiO_3$	0.065	1195	0.0080	0.1
$Ba_{0.6}Sr_{0.4}TiO_3$	0.060	2551	0.0115	2.7

Figure 5-1: Tunability and loss tangent of $BaTiO_3$: 4%LaFe at room temperature.

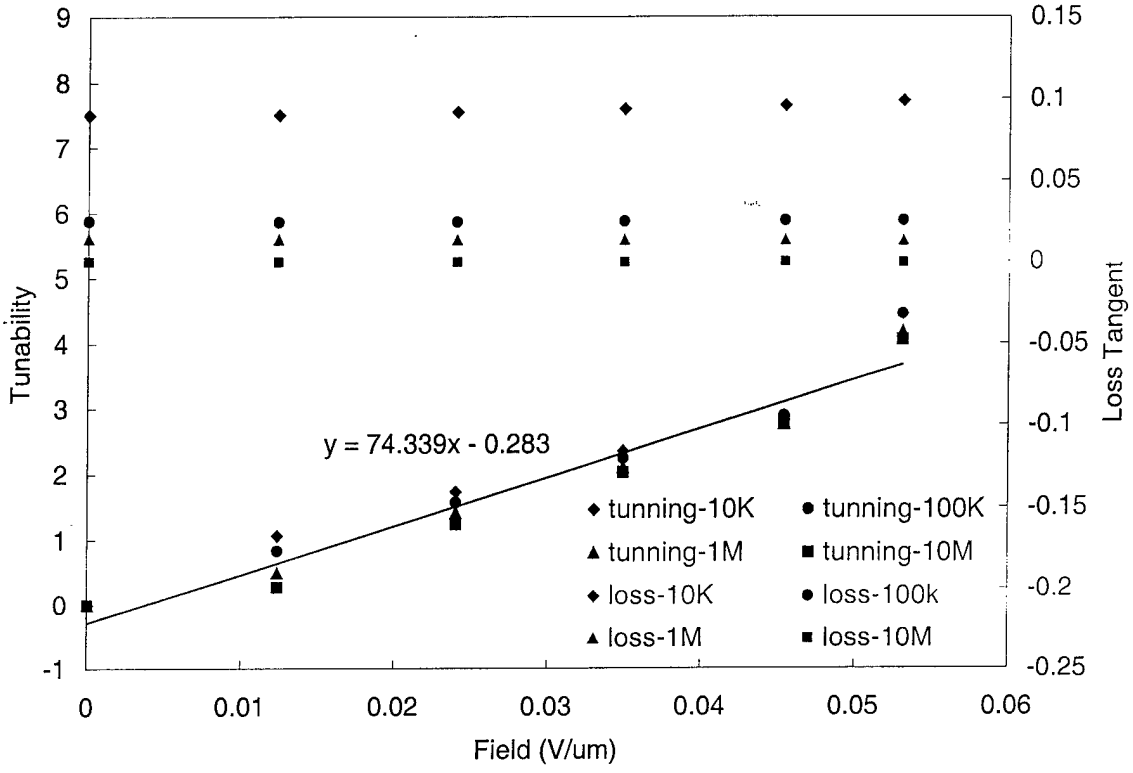

Figure 5-2: Temperature dependence of relative dielectric constants of $BaTiO_3$: x%LaFe.

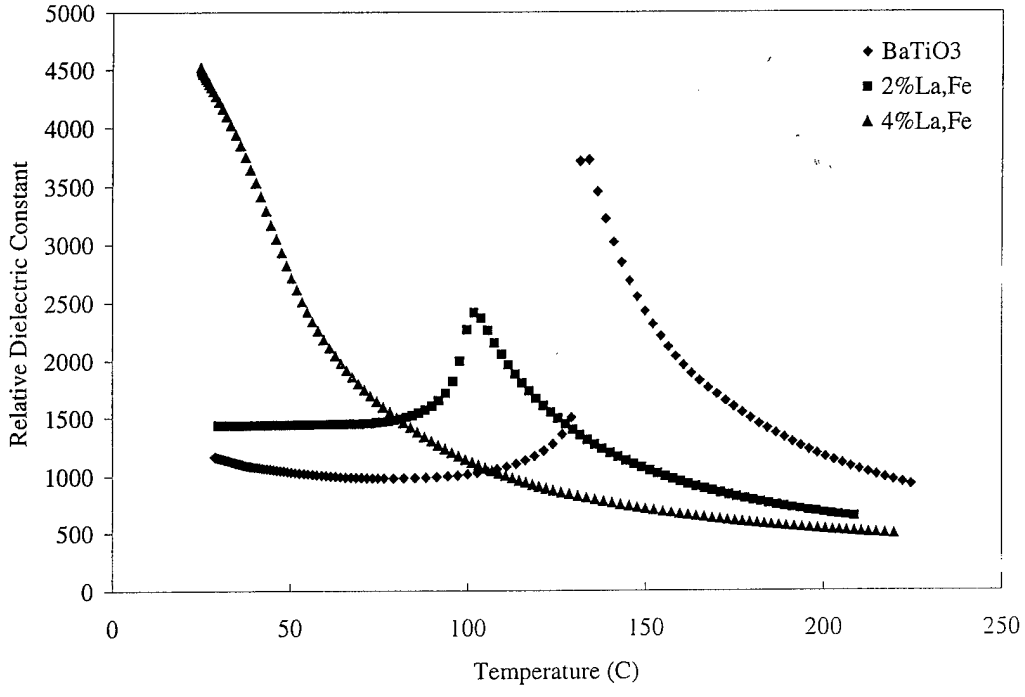

Figure 5-3: Cell parameters of $Ba_{1-x}La_xTi_{1-x}Fe_xO_3$.

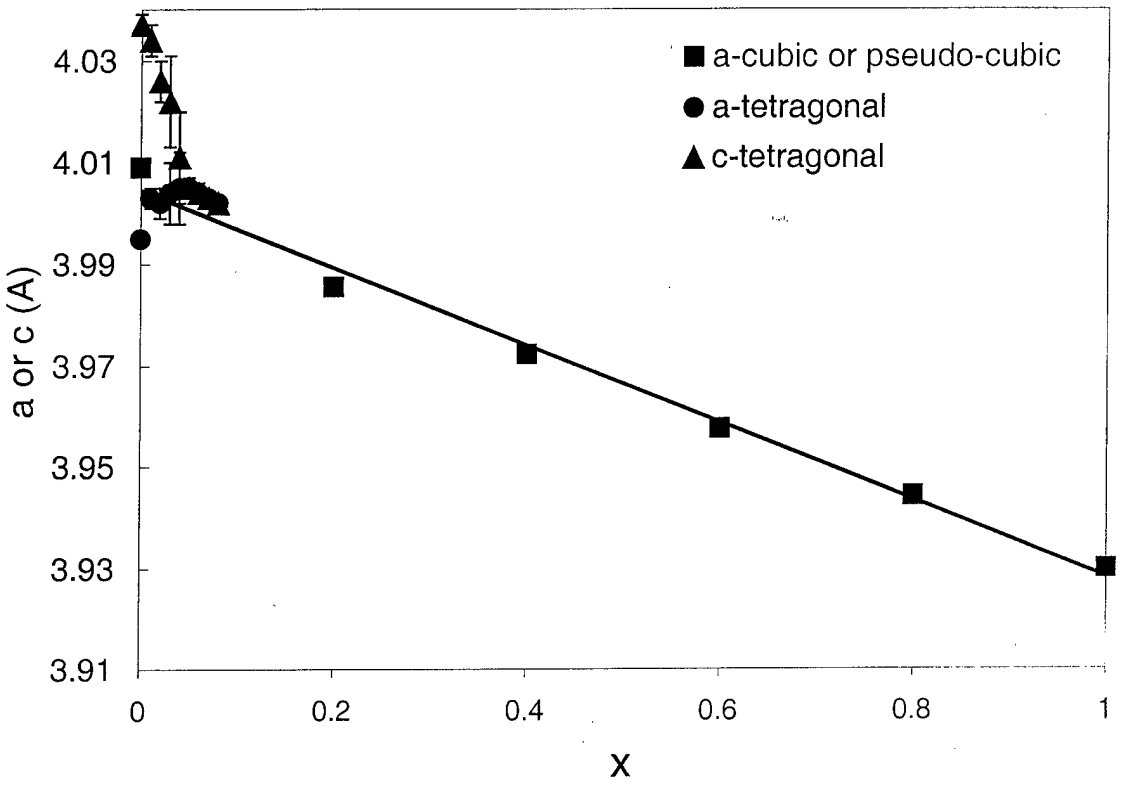

Frequency Agile Materials for Electronics

Quarterly Report 8

Date: 08/16/00

Period covered in this report: 4/1/00 through 6/31/00

Program Title: Novel Ferroelectric Materials for Satellite Communications

Contract # DABT63-98-C-0046

Performing Organization: DuPont Superconductivity

Subcontractor: University of Colorado at Boulder

Summary

The optimization of 2nd generation materials was completed for both ambient and cryogenic temperature operation thus completing milestones 1E and 2E. For cryogenic operation, $Ca_{0.05}Sr_{0.95}TiO_3$ (CSTO x = 0.05) films were deposited with good epitaxial alignment on $LaAlO_3$, MgO, and LSAT substrates. Annealing of the films increased the tunability, but also increased the loss with no net improvement in the figure of merit. For ambient temperature operation, the composition of $CaCu_3Ti_4O_{12}$ (CCTO) films was optimized with the hope of reducing the loss tangent. Unfortunately, all compositions that were evaluated resulted in an unacceptably high loss. No further work will be done on the CCTO system. Exploratory laser ablation processing under Task 4 has been used to investigate epitaxial films several doped BSTO compositions including $Ba_{0.6}Sr_{0.4}Ti_{0.99}Fe_{0.01}O_3$, $Ba_{0.6}Sr_{0.38}Mg_{0.02}Ti_{0.98}Zr_{0.02}O_3$ and $Ba_{0.6}Sr_{0.36}Mg_{0.04}Ti_{0.96}Zr_{0.04}O_3$. This work combined with previously reported work under Task 4 completes milestone 4B. Under Task 5, materials discovery research, a wide range of acceptor-donor codoped $BaTiO_3$ samples were prepared in this quarter and their dielectric properties were measured to complete milestone 5B.

Progress By Task

Tasks 1 & 2. Large Area Sputtered Film Manufacturing

In Q8 our efforts on the program were hampered somewhat by the relocation of our office and laboratory space to a new building. Consequently, we were unable to deposit thin film samples during a about six weeks of this report period as the systems required were shut down and people were busy with the move. Also, material testing was slowed because the new laboratory area was not complete. We will combine our descriptions of tasks 1 and 2 in one section since we are concentrating on films for cryogenic applications.

BSTO x = 0.50

We continued to investigate the source and extent of unintentional doping of our $BaSrTiO_3$ samples. Sputtering targets were purchased from a second vendor (Puretech) to compare electrical behavior and composition to our original samples (Praxair Specialty Ceramics). We deposited a total of eleven (11) films of nominal BSTO x = 0.50 composition on Si and LAO substrates from the two different targets: both had suppressed Curie temperatures (T_c < 100K). Overall, the electrical and material properties of films made from either target were similar. The Praxair samples were measured by RBS and x-ray fluorescence spectroscopy (XRF) and found to contain Fe (and possibly W doping as well) between 0.5-1 at.%. Although we have not completed our characterization of the Puretech films, we believe they also suffer from unintentional doping. It appears that the vendors quality control is an issue for the fabrication of clean BSTO targets; however, the Curie temperatures achieved from both targets are in the appropriate range for cryogenic applications.

BSTO x = 0.60

We continued our characterization of the properties of nominal BSTO60 films on both LAO and MgO. In Figure 1-1, we compare the electrical performance of similar films deposited on both substrates. The relative permittivity and loss are very similar, but the tunability (not shown) of the film on MgO is much lower. In Figure 1-2, we present a transmission x-ray diffractogram of a BSTO60 film on MgO taken at the Advanced Photon Source at Argonne National Labs. The presence of undesired orientations, like {110} & {111}, and the diffraction rings indicate low epitaxial quality. This may contribute to the reduced tunability of these films. In Q9, we will continue to investigate the structural properties of our films at the APS.

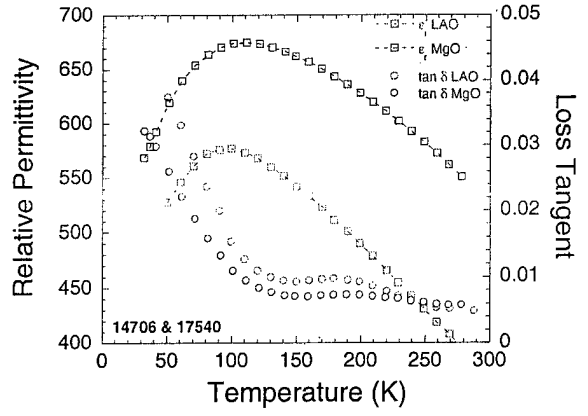

Fig. 1-1. Dielectric properties of Fe-doped BSTO60 on LAO and MgO at 100kHz. The permittivity and loss are essentially unchanged, but the tunability is decreased on MgO.

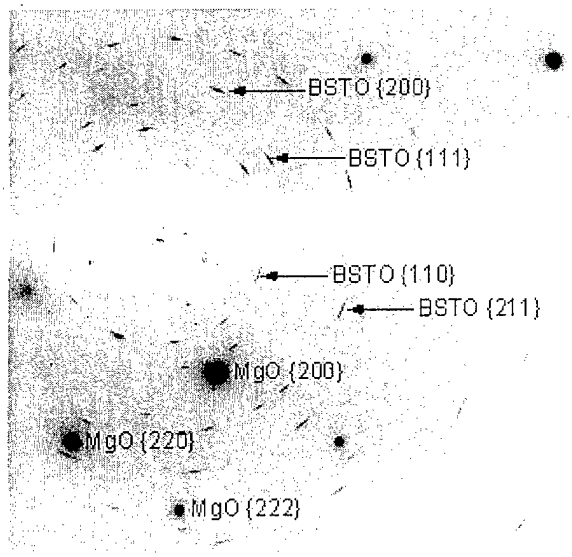

Fig. 1-2. Transmission synchrotron x-ray diffractogram of Fe-doped BSTO60 on MgO. Note the presence of unwanted orientations and the diffraction rings from the film, indicating poor epitaxial quality.

CSTO x = 0.05

Chosen as our second-generation material, $Ca_{0.05}Sr_{0.95}TiO_3$, has not shown exceptional promise as a replacement for BSTO. Initially, the dielectric properties were not an improvement over BSTO (see Figure 1-3). To improve the properties of our films we tried high temperature annealing. Samples were annealed up to 8 hours in flowing O_2 at 1200K. We then measured the ferroelectric properties of these annealed films. We plot typical results in Figure 1-4. The tunability and loss at low temperatures dramatically increased over the as-deposited films; however, no improvement in the figure of merit over what we have achieved with the first generation material BSTO was observed. This satisfies milestone 1.E.

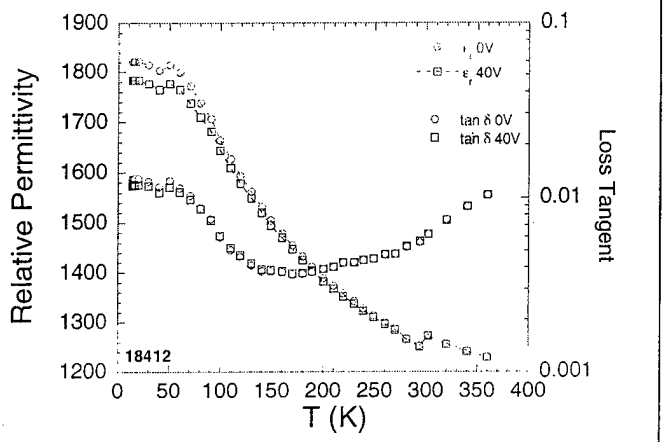

Fig. 1-3. Permittivity and tan δ at 100kHz of as-deposited CSTO film on LAO. The dielectric properties are similar to BSTO.

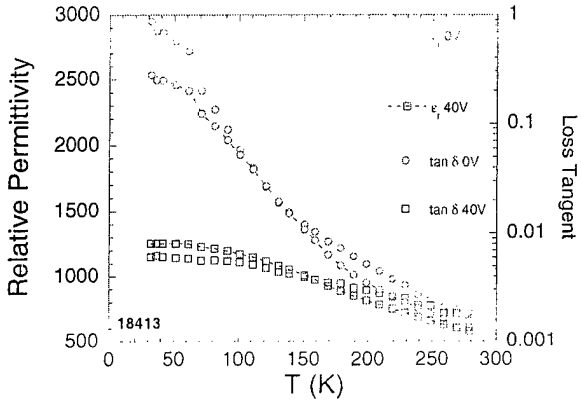

Figure 1-4. Dielectric properties of annealed CSTO on LAO. The tunability and loss are greatly increased below 150K, however the figure of merit is not improved over BSTO.

CCTO

In Q8, we continued to characterize and improve our second-generation material for room temperature use, CCTO. Initial results were disappointing: although the dielectric response was strongly nonlinear, the thin films were extremely lossy and the tunability was frequency dependent. We suspected that making films with compositions closer to stoichiometric would improve the ferroelectric performance. To that end, we mapped out the dependence of composition on deposition parameters (see Fig. 1-5). We then deposited films with the optimum composition to satisfy milestone 2.E. and tested their electrical performance. The results are displayed in Figure 1-6: the films are no better than our earlier results. We will cease our work on CCTO.

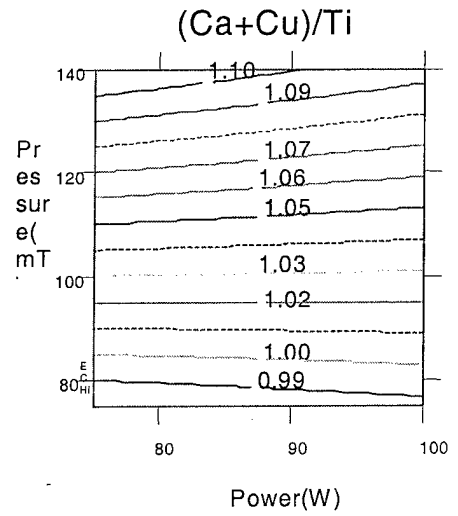

Figure 1-5. The variation of composition with deposition conditions for $CaCu_3Ti_4O_{12}$. The proper stoichiometry is obtained near 80mTorr.

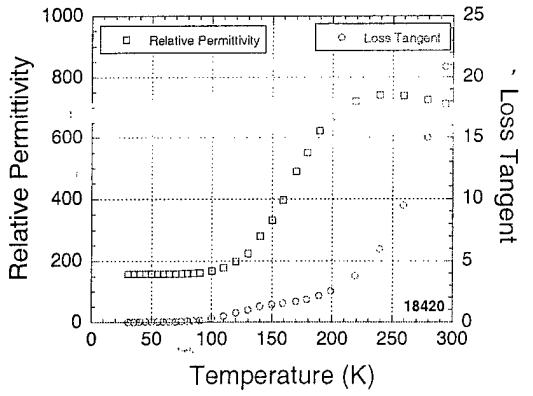

Figure 1-6. Dielectric properties of compositionally optimized CCTO. The properties are not improved over our initial results; the loss is very high.

Task 3. Multilayer Film Development and Manufacturing

Our progress on the development of multilayers was slowed in Q8 by our move to new facilities, but we did begin testing of samples we produced in Q7. We tested a number of simple YBCO resonator and phase shifter designs which we will use to measure ferroelectric films. The YBCO phase shifters on bare LAO worked well, but the coplanar resonators had surprisingly low Qs. We will endeavor to understand why the resonators performed poorly and redesign them in Q9 if necessary. We hope to complete the measurements of ferroelectric films using our devices (to satisfy milestones 3.D. & E.) in Q9.

Task 5 - Materials Discovery Research

Acceptor-donor codoped $SrTiO_3$ were prepared last quarter. Their tunability, T_C and loss properties at low temperature were measured during this quarter with the new low temperature measurement setup. The studies of the dielectric properties of solid solution system based on $KTaO_3$ were initiated.

<1> Doping of $SrTiO_3$

(Bi, Fe) and (Bi, Ga) codoped samples were measured. Although T_Cs are likely to be increased, no high tunabilities were observed on these samples, which might be due to the low electric field. Last quarter, we found $SrTiO_3$:4%BiFe has low loss among this system. This is confirmed by the figure of merit, although it is still too low. (see figure 5.1)

The dielectric properties of other doped STO will continue to be measured.

<2> Solid solution of $KTaO_3$

Several $KTaO_3$ based solutions were prepared. a. $KTaO_3$-$PbTiO_3$ b. $KTaO_3$-$SrTiO_3$ c. $KTaO_3$-$BaTiO_3$ d. $KTaO_3$-BiA (A=Fe, Cr, Al, Ga).

The dielectric properties of $KTaO_3$-$PbTiO_3$ at low temperature were measured. It seems the T_C can be shifted due to the doping. However due to the relaxation, the peaks are too broad. No tunabilities are observed. The cell parameters are shown in figure 5.2 and tunabilities are shown in figure 5.3. The tunability data are measured at about 40K above T_C or 80K when the T_C is low enough.

Studied materials:

1. $K_{1-x}Pb_xTa_{1-x}Ti_xO_3$: (x=0.05, 0.1, 0.2, 0.3, 0.4, 0.5, 0.55, 0.6, 0.7, 0.8, 0.9)
2. $K_{1-x}Sr_xTa_{1-x}Ti_xO_3$: (x=0.2, 0.4, 0.6, 0.8)
3. $K_{1-x}Ba_xTa_{1-x}Ti_xO_3$: (x=0.1, 0.2, 0.8, 0.9)
4. $K_{1-x}Bi_xTa_{1-x}A_xO_3$: A=Al, Ga, Fe, Cr.

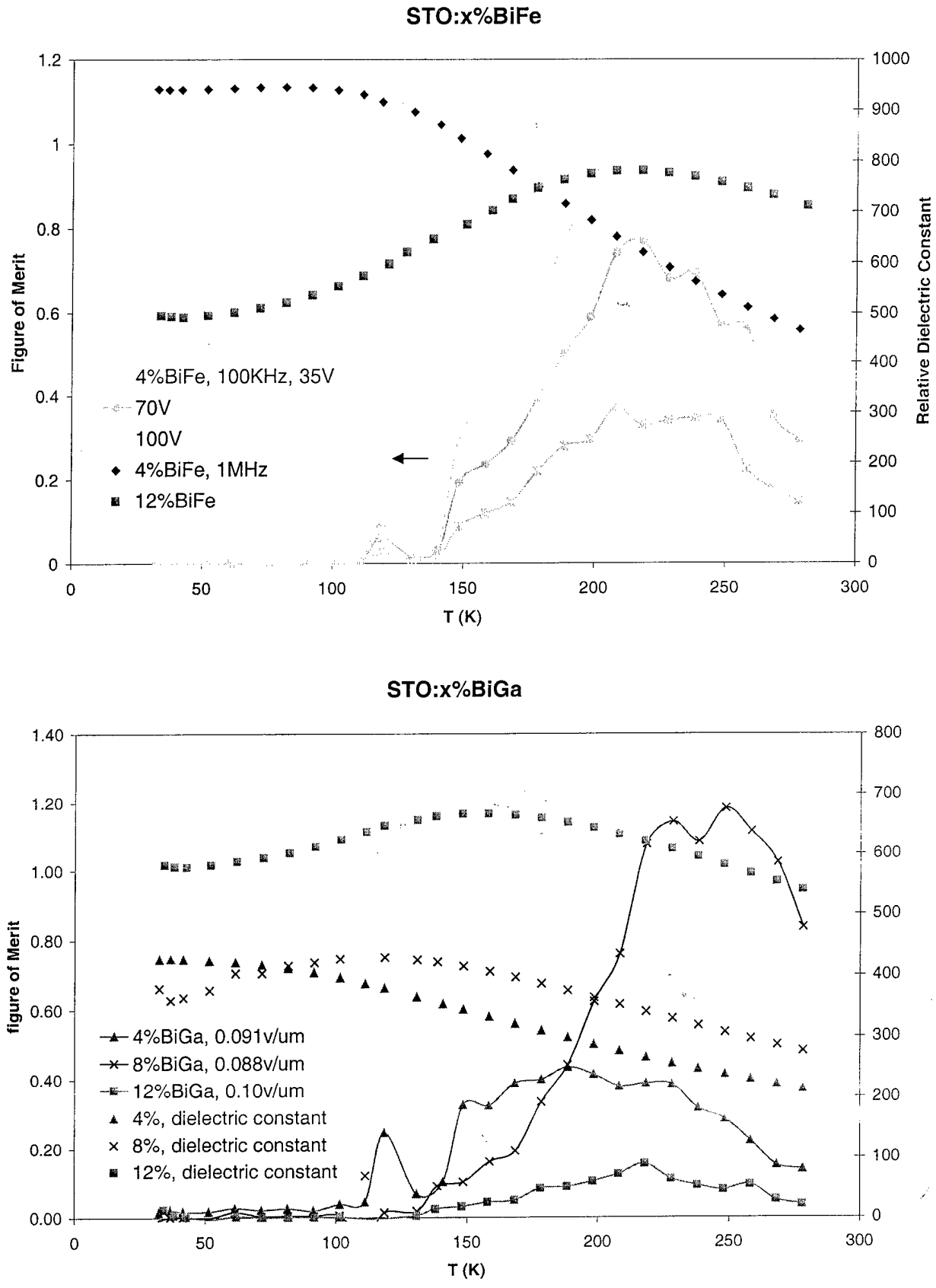

Figure 5.1: Dielectric properties of STO:BiFe and STO:BiGa

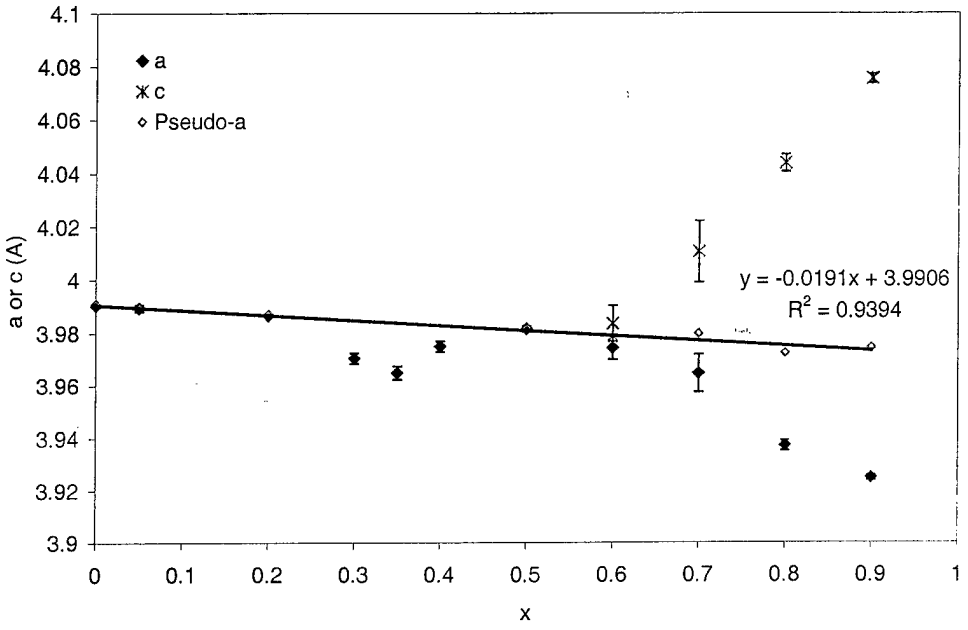

Figure 5.2: Cell parameters of $K_{1-x}Pb_xTa_{1-x}Ti_xO_3$

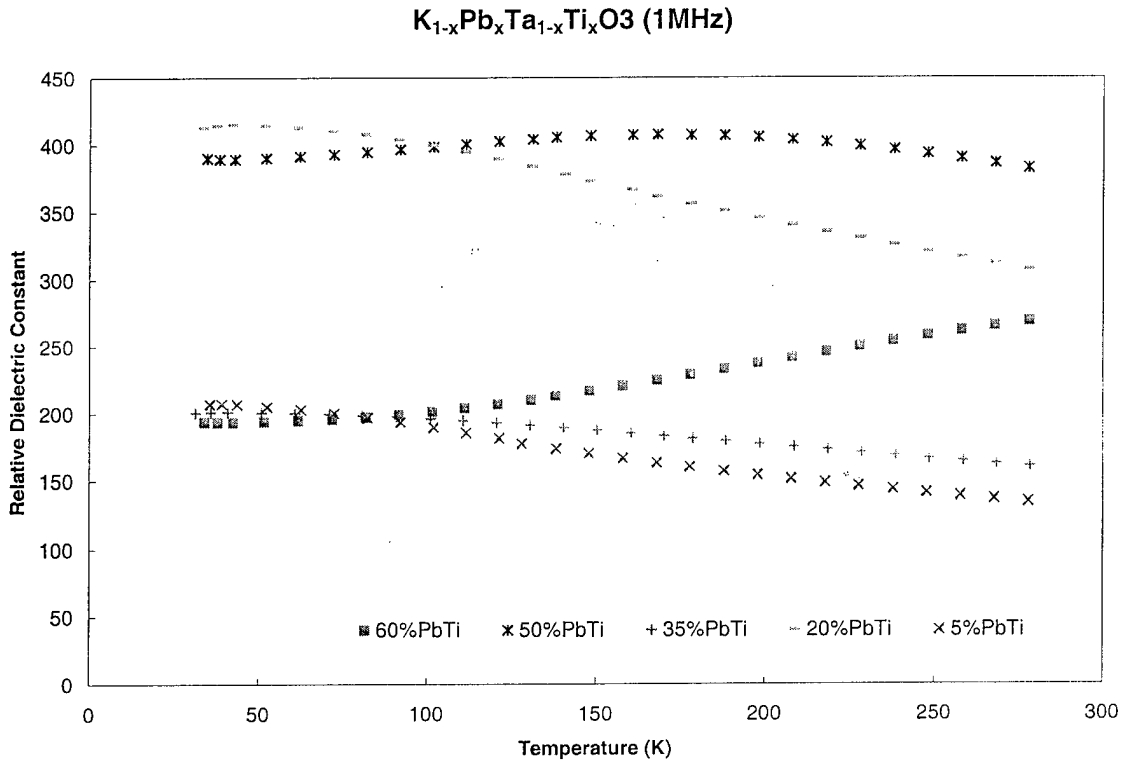

Figure 5.3: Dielectric properties of $K_{1-x}Pb_xTa_{1-x}Ti_xO_3$

Task 4. Exploratory Laser Ablation Processing (University of Colorado)

In this quarterly progress, we report the preparation of several new bulk materials, and growth of epitaxial films of new materials and their dielectric characterization. We also report the results of microwave dielectric studies on pristine and Mn and W doped BSTO conducted at NRL.

4.1 Synthesis of bulk BSTO materials

Our earlier studies on new materials were focused on 1% doping and observed tunability values were low. The exception was the Mg,Zr doped BSTO materials, in which we observed significant tunability for 0.5 V/μm. In view of this, we have synthesized a series of new bulk materials where the dopant concentration is increased. All the compounds were prepared by standard high temperature solid state reaction. The compositions of these new materials are shown below.

1. $Ba_{0.6}Sr_{0.4}Ti_{1-x}M_xO_3$ (M = Mn, W, Fe; x = 0.02-0.04)
2. $Ba_{0.6}Sr_{0.4}Ti_{0.96}Mn_{0.02}W_{0.02}O_3$

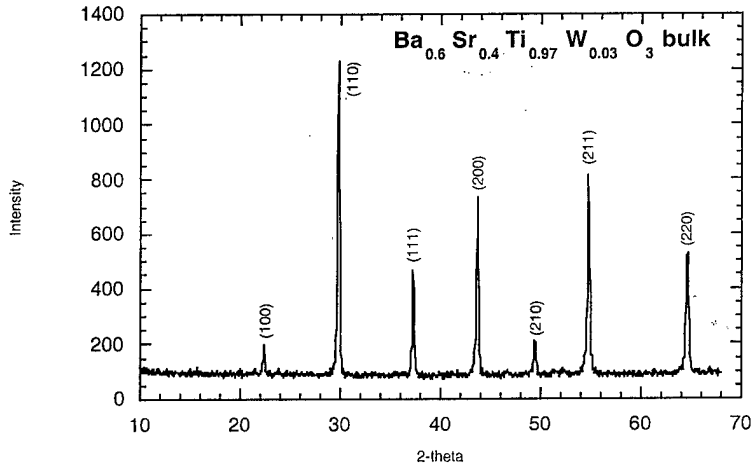

Fig. 4.1.1 Powder X-ray diffraction pattern of BSTO doped with 3% W. Doping with 4% W resulted in impurities.

In the case of W doping, the XRD pattern of x = 0.04 composition showed impurity peaks. All the other compositions formed single phase. We have also presently investigated Fe doping in BSTO system and doping up to 4% forms single phase. Typical XRD patterns of these new materials are shown figs. 4.1.1 and 4.1.2.

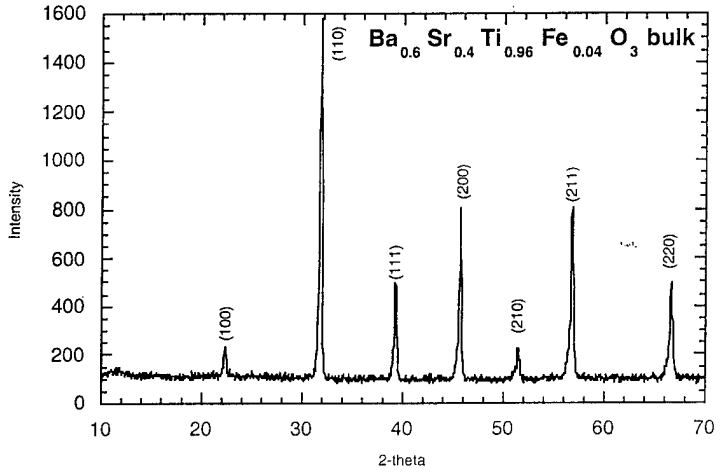

Fig. 4.1.2 Powder X-ray diffraction pattern of $Ba_{0.6}Sr_{0.4}Ti_{0.96}Fe_{0.04}O_3$ bulk material

4.2 Growth of epitaxial thin films and dielectric characterization

Epitaxial films of $Ba_{0.6}Sr_{0.4}Ti_{0.99}Fe_{0.01}O_3$, $Ba_{0.6}Sr_{0.38}Mg_{0.02}Ti_{0.98}Zr_{0.02}O_3$ and $Ba_{0.6}Sr_{0.36}Mg_{0.04}Ti_{0.96}Zr_{0.04}O_3$were grown on $LaAlO_3$ (LAO) single crystal substrates using pulsed laser deposition. The deposition was carried out in 300 mTorr of oxygen. and the

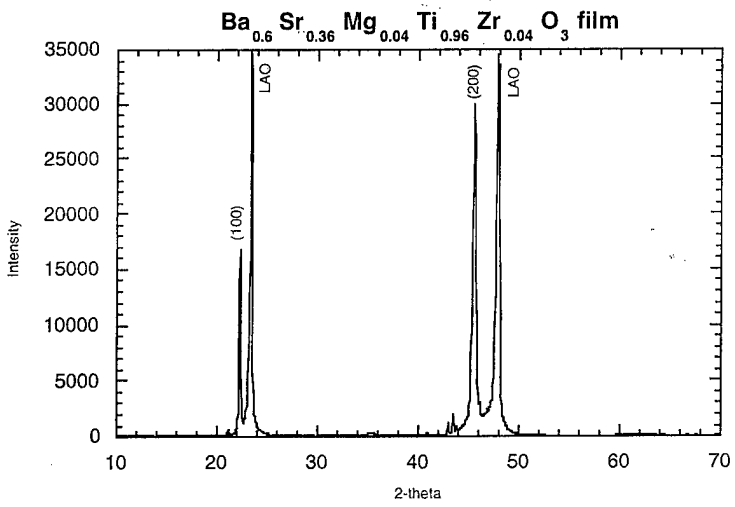

Fig. 4.2.1 θ-2θ scan of epitaxial $Ba_{0.6}Sr_{0.36}Mg_{0.04}Ti_{0.96}Zr_{0.04}O_3$ film

substrate temperature was maintained at 700 °C. The films were post annealed in flowing oxygen at 950 °C for 6 h. Epitaxy of the films was confirmed by powder X-ray diffraction (figs. 4.2.1 and 4.2.2).

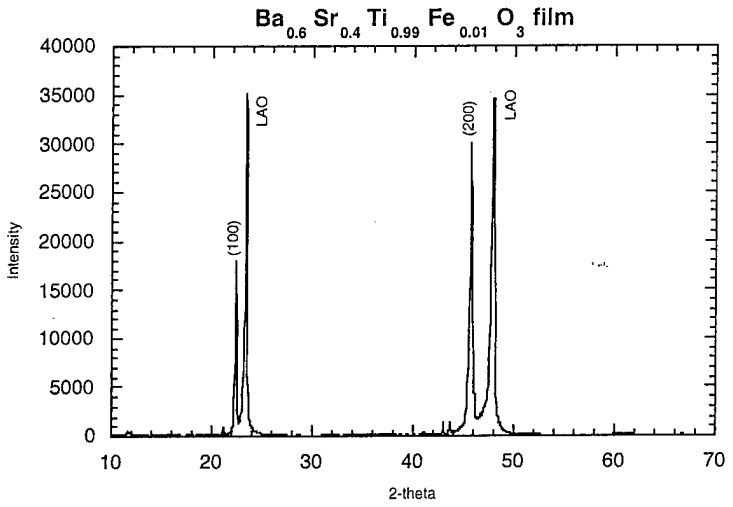

Fig. 4.2.2 θ-2θ scan of $Ba_{0.6}Sr_{0.4}Ti_{0.99}Fe_{0.01}O_3$ film confirming epitaxy of the film

The dielectric measurements were carried out using interdigitated capacitor configuration for the Fe doped epitaxial film. The capacitance and loss tangent were measured using HP 4192A LCR meter at 1MHz. The observed Tc is around the ambient

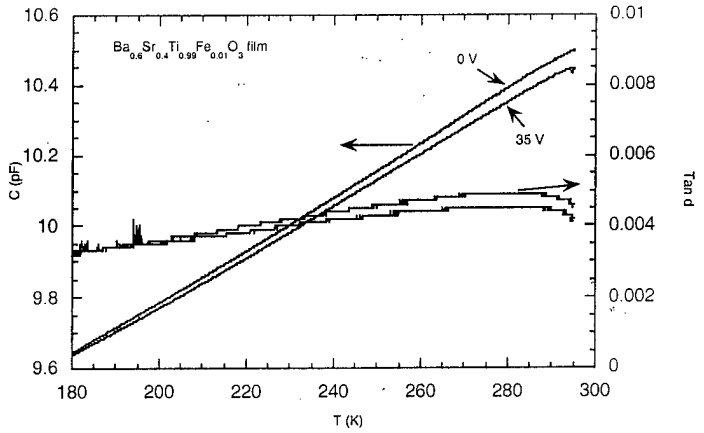

Fig. 4.2.3 Dielectric properties of $Ba_{0.6}Sr_{0.4}Ti_{0.99}Fe_{0.01}O_3$ epitaxial film

temperature (294 K) and the tunability is low. The dielectric loss remained almost constant over the entire temperature regime and was moderately low (< 0.005) at 294 K. Dielectric studies on the other epitaxial films are underway.

4.3 Microwave dielectric properties of pristine and doped BSTO films

The results of microwave dielectric studies on pristine and 1% Mn and W doped epitaxial films are shown below.

Microwave dielectric properties of pristine and 1% Mn and 1% W doped BSTO ($Ba_{0.6}Sr_{0.4}TiO_3$) films (Measured at NRL)

Film #	Capacitor #	gap (μm)	finger length(μm)	Q(0) - Q(40V)	Cap (40V) - Cap (0) (pf)	ε (40V) - ε (0V)
BSTO-W	3f1c-a	6	80	10-22	.194-.253	128 – 174
	5f3c-a	10	80	5-10	.161-.183	163 – 194
	7d2c-a	8	80	12-19	.146-.170	118 – 136
	7f3c-a	10	80	11-17	.164-.186	167 – 197
BSTO	2e2c-a	8	80	7-17	.221-.305	184 – 277
	4c2b-a	8	60	6-12	.196-.282	199 – 320
	5d2c-a	8	80	6-15	.237-.356	200 – 340
BSTO-Mn	1d1c-a	6	80	7-18	.258-.385	178 – 300
	2c1c-a	6	80	7-20	.266-.419	185 – 334
	3b1b-a	6	60	7-15	.209-.318	169 – 297

Frequency Agile Materials for Electronics

Quarterly Report 9

Date: 10/15/00

Period covered in this report: 7/1/00 through 9/31/00

Program Title: Novel Ferroelectric Materials for Satellite Communications

Contract # DABT63-98-C-0046

Performing Organization: DuPont Superconductivity

Subcontractor: University of Colorado at Boulder

Summary

We performed additional characterization of our second-generation material, $Ca_{0.05}Sr_{0.95}TiO_3$ and found that films on $LaAlO_3$ and LSAT have the best epitaxial alignment. The role of low level Fe doping in $Ba_{0.5}Sr_{0.5}TiO_3$ films was also investigated further using targets from two different vendors. La, Fe co-doped BSTO was identified as our third generation material and targets were ordered. We also began deposition studies of thicker BSTO films for integration with YBCO layers. In the exploratory laser ablation effort (Task 4), Mn and W co-doped BSTO films were investigated by laser ablation. Of great interest was the fact that the peak in loss occurred at a lower temperature than the peak in tunability. In the materials discovery effort (Task 5), a number of new materials were investigated including additional co-doped BSTO compositions and compounds with the $CaCu_3Ti_4O_{12}$ structure. For the tunable filter demonstration, a co-planar end-coupled filter design was selected.

Progress By Task

Tasks 2. Large Area Sputtered Film Manufacturing

In Q9, we concentrated on the characterization of the temperature-dependent electrical properties of ferroelectrics for liquid nitrogen temperatures and higher, though we did continue to examine the detailed nature of the epitaxy of our films using XRD.

CSTO x = 0.05

We continued to characterize CSTO05 by examining the epitaxy & stress of CSTO05 films grown on LAO, MgO, and LSAT earlier in the program. We are still interested in this material since its microstructure is closely related to BSTO. We have deposited CSTO05 films on a number of lattice-matched substrates: LAO, MgO, and LSAT. The x-ray phase scans are summarized in Figure 2.1. We plot the θ-2θ data and the rocking curves for the (002) reflection on all three substrates with films deposited under similar conditions. We believe the results are comparable on LAO and LSAT: the rocking curves on LAO are sometimes artificially broadened by twinning. Results on MgO mirror our earlier results for BSTO on MgO—the films grow with some misorientation and the rocking curves are quite broad. We also measured the stress in these films by measuring symmetric and asymmetric Bragg reflections [i.e. the (004) and (024)] and

finding the in and out-of-plane lattice constants for the films. Table 2.1 summarizes our data for the three films above: all grow with slight compressive strain, with LAO under the most compression. We are in the process of testing the electrical properties of these films to elucidate the importance of strain to the tunability and loss.

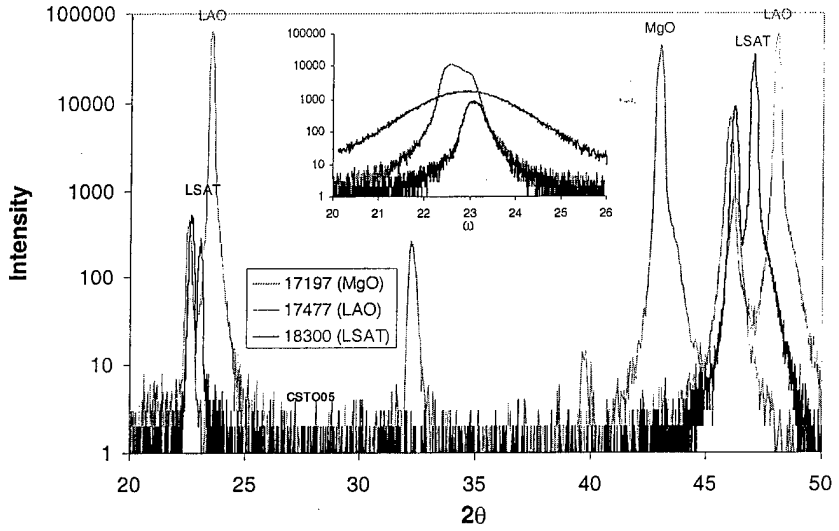

Figure 2.1. θ-2θ scans for CSTO05 on MgO, LAO, and LSAT. Note the misorientation on MgO: (110) near 32° and (111) near 40°. Inset: the rocking curves of the CSTO05 (002) line. MgO is broadest, LAO is artificially broadened by twinning and is probably comparable to LSAT, which is narrowest.

Table 2.1. The tetragonal distortion of CSTO05 on nearly lattice-matched substrates.

Substrate	1-c/a
LSAT	$-3x10^{-4}$
MgO	$-9x10^{-4}$
LAO	$-1x10^{-3}$

BSTO x = 0.50

We continued to investigate the role of Fe doping in our BSTO targets. We purchased BSTO50 targets from Praxair and Puretech to see if either could provide targets with reduced levels of iron. We were able to obtain XRF data on films from the Praxair targets which still showed Fe contamination, though at a lower level than earlier films (0.3 at.% vs. 0.8 at.%). The films also showed evidence for W contamination at the ~0.5 at.% level. We tested the electrical properties of these films and found the T_c suppressed as expected. We have not yet been able to

obtain XRF data on the Puretech films or targets, but we have measured their electrical properties. Both films are shown in Figure 2.2 and 2.3. There are slight differences in their permittivities and losses at 1 MHz, but essentially none in their figures of merit

$$K = \frac{\varepsilon_r(0) - \varepsilon_r(V)}{\varepsilon_r(0) \cdot \tan\delta(0)}$$

where we typically apply an electric field of 4 V/μm. These facts indicate that the films made from the Puretech targets have a similar level of contamination. This conclusion remains to be confirmed by XRF.

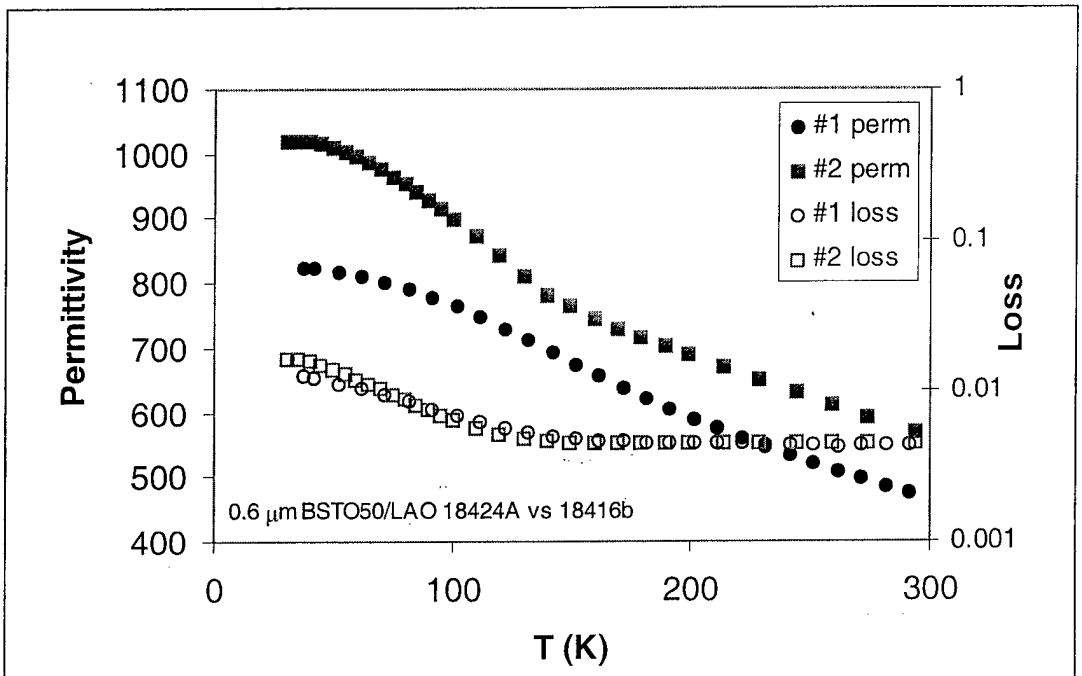

Figure 2.2. Zero field permittivity and loss for Praxair (#1) and Puretech (#2) films, nominally BSTO50 on LAO. There are slight differences in their electrical behavior—we know the Praxair sample to have ~0.3 at.% Fe.

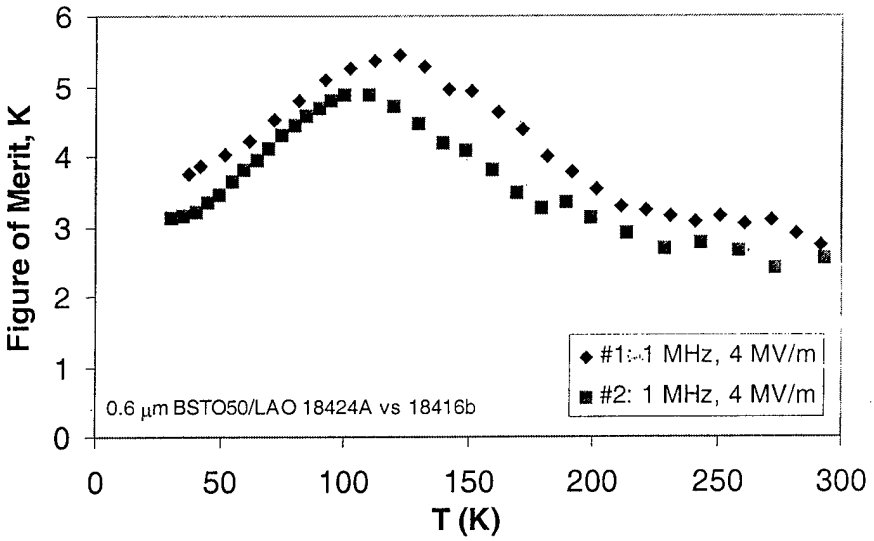

Figure 2.3. The ferroelectric figure of merit vs. temperature for the Praxair (#1) and Puretech (#2) BSTO50/LAO films. There is no significant difference between the performances of these two samples.

GWU Data

We received data from our colleagues at George Washington University in Q9. Drs. Mark Reeves and Yuguo Wang performed measurements on a number of our films at C-band (2 GHz) using a scanning coaxial resonant probe. Their data on our films is summarized below in Table 2.2. The DuPont data is the average of all capacitors at 100 kHz on a particular wafer at room temperature.

The trends are somewhat consistent: the permittivities agree fairly well between the two measurements, while the losses measured at GWU are about an order of magnitude higher. Considering the difference in the measurement frequency, this is not too surprising. However, if the losses in the microwave range are really greater than 10^{-2} it will be difficult to make successful frequency agile devices using these materials. We will continue to collaborate with GWU to crosscheck and improve our estimates of our material properties.

Table 2. Comparison of dielectric properties measured at DuPont and GWU at 300 K.

Substrate #	Film/Substrate	ε_{GWU}	$\tan\delta_{GWU}$	ε_{DuPont}	$\tan\delta_{DuPont}$
14703	BSTO60/LAO	370	$6x10^{-2}$	517	$3x10^{-3}$
14705	BSTO60/LAO	500	$1x10^{-1}$	*453	$*7x10^{-3}$
14710	BSTO06/LAO	290	$4x10^{-2}$	*280	$*4x10^{-3}$
16316	BSTO60/LAO	225	$1x10^{-1}$	193	$6x10^{-3}$
16317	BSTO60/LAO	320	$7x10^{-2}$	258	$8x10^{-3}$
17689	BSTO60/MgO	165	$7x10^{-2}$	262	$9x10^{-3}$
17690	BSTO60/MgO	165	$8x10^{-2}$	296	$6x10^{-3}$

*data taken from variable temperature scans on individual device at 1 MHz, T nearest 295 K

Third Generation Material

We chose La, Fe co-doped BSTO as the most promising candidate for our third generation ferroelectric material for cryogenic applications. Results from our new materials discovery research program indicate that the tunability and loss of these compounds may be better than either Fe-doped or pristine BSTO. We ordered 4% La, Fe doped sputtering targets with x = 0.2-0.6 to achieve Curie temperatures in the range 20-50 K. We will begin depositing these materials by mid Q10 to satisfy milestone 1.F.

Task 3. Multilayer Film Development and Manufacturing

Our efforts on task 3 were slowed in Q9 because of our move to new laboratory space, as mentioned in the last quarterly report.

Thick Film Deposition

We began work on depositing thick (>0.5 mm) ferroelectric films for use as the active layer in multilayered superconducting devices. We chose BSTO06 as the first material to try, since it has given us the best cryogenic performance of all the materials we have examined. We do not have structural or electrical data as yet. Our plan is to explore the epitaxial and ferroelectric quality of the thickest BSTO06 films that we can grow. We will also grow YBCO overlayers and examine their epitaxial and superconducting quality to determine the optimum device parameters. We will also look at optimizing high temperature annealing of the single and bilayers to improve and control their electrical properties to satisfy milestone 3.F.

Task 4. Exploratory Laser Ablation Processing (University of Colorado)

In this quarterly progress, we report growth of epitaxial films of new materials and their dielectric characterization. We also report the results of strain studies on (Mn,W) co-doped BSTO.

4.1 Growth of epitaxial thin films and dielectric characterization

Epitaxial films of $Ba_{0.6}Sr_{0.4}Ti_{0.96}Mn_{0.04}O_3$ and $Ba_{0.05}Sr_{0.95}TiO_3$ were grown on $LaAlO_3$ (LAO) single crystal substrates using pulsed laser deposition. The deposition was carried out in 300 mTorr of oxygen pressure and the substrate temperature was maintained at 700 °C. The films were post annealed in flowing oxygen at 950 °C for 6 h. Epitaxy of the films was confirmed by powder X-ray diffraction (fig. 4.1.1 shows the XRD pattern for $Ba_{0.05}Sr_{0.95}TiO_3$ epitaxial film).

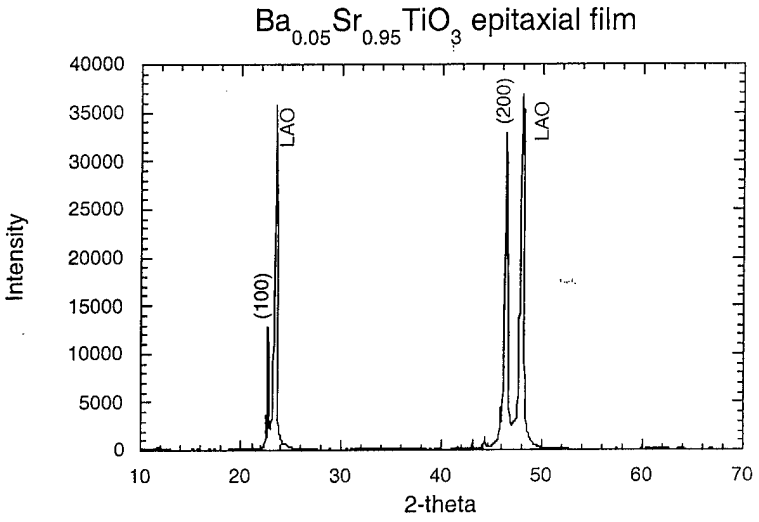

Fig. 4.1.1 θ-2θ X-ray scan for $Ba_{0.05}Sr_{0.95}TiO_3$ film. The film was post annealed at 950° C for 6 h in flowing oxygen.

Dielectric measurements on the $Ba_{0.6}Sr_{0.4}Ti_{0.96}Mn_{0.04}O_3$ film were carried out using interdigitated capacitor configuration. We also carried out measurements on $Ba_{0.6}Sr_{0.4}Ti_{0.98}Mn_{0.01}W_{0.01}O_3$ film. The capacitance and loss tangent were measured using HP 4192A LCR meter at 1MHz. The observed Tc for 4% Mn doped BSTO is around 280 K, although the dielectric constant did not show a well-defined peak and the transition looked diffuse. There is moderate tunability and the observed loss is quite low. This may be compared with the 1% Mn doped BSTO film, where the losses were higher than the pristine sample and the Tc was also enhanced (325 K). and the tunability is low. The dielectric loss remained almost constant over the entire temperature regime and was moderately low (< 0.005) at 294 K. The (Mn,W) co-doped film did not show a well-defined ferroelectric-paraelectric transition. There is moderate tunability and the loss was moderately low.

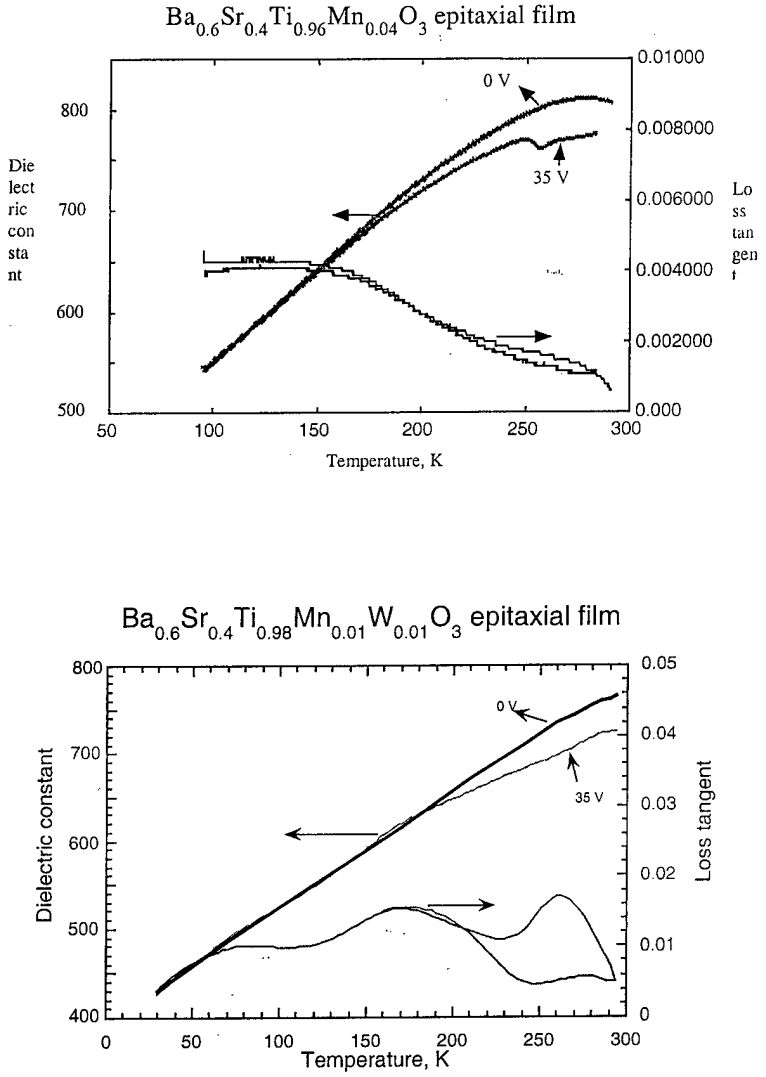

Fig. 4.1.2. Dielectric measurements on $Ba_{0.6}Sr_{0.4}Ti_{0.96}Mn_{0.04}O_3$ and $Ba_{0.6}Sr_{0.4}Ti_{0.98}Mn_{0.01}W_{0.01}O_3$ epitaxial films

Dielectric measurements were also carried out on bulk polycrystalline $Ba_{0.05}Sr_{0.95}TiO_3$ using slotted capacitor configuration at 1 MHz to determine the Tc for this material. The results are shown in fig. 4.1.3. The observed Tc is 64 K, which is lower than that observed for $Ba_{0.1}Sr_{0.9}TiO_3$ bulk (which showed a Tc of 96 K). The dielectric loss showed a peak around 50 K and there was no peak at Tc. Films of $Ba_{0.1}Sr_{0.9}TiO_3$ showed a Tc of 140 K, far above the cryogenic operating temperature. We expect the films of $Ba_{0.05}Sr_{0.95}TiO_3$ to show a Tc around 77K.

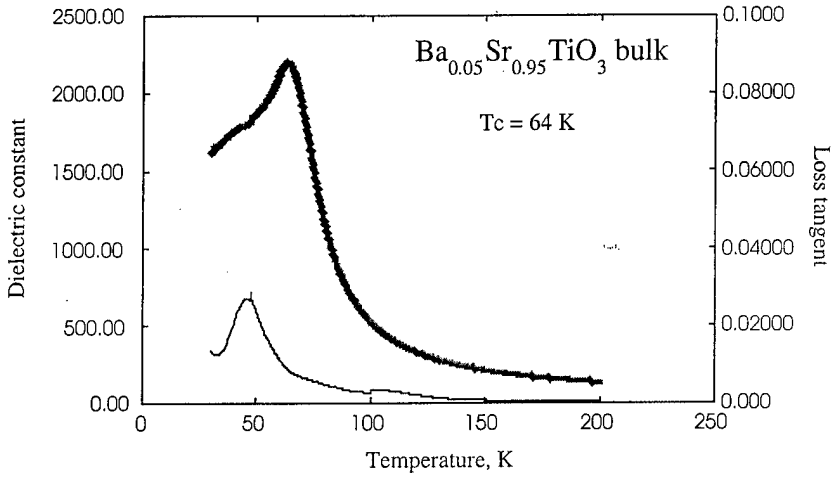

Fig. 4.1.3 Dielectric properties of bulk polycrystalline Ba0.05Sr0.95TiO3. The measurements were done at 1 MHz

4.2. XRD Measurements of $Ba_{0.6}Sr_{0.4}Ti_{0.99}M_{0.01}O_3$ (M = Ti, Mn, W) Thin Films

In order to understand the strain-dielectric property correlation, we obtained x-ray diffraction pattern of $Ba_{0.6}Sr_{0.4}Ti_{0.98}Mn_{0.01}W_{0.01}O_3$ film. Coupled $\theta/2\theta$ scans showed only *h*00 Bragg peaks for all three phases. A good epitaxy with the substrate was confirmed by the azimuthal (ϕ) scans. To thoroughly investigate the misfit relationship at the film-substrate interface, we recorded reciprocal space maps for all three films. Reciprocal space maps of the symmetric 002 and asymmetric 013 Bragg reflections obtained for the film is shown in the Fig. 4.2.1.

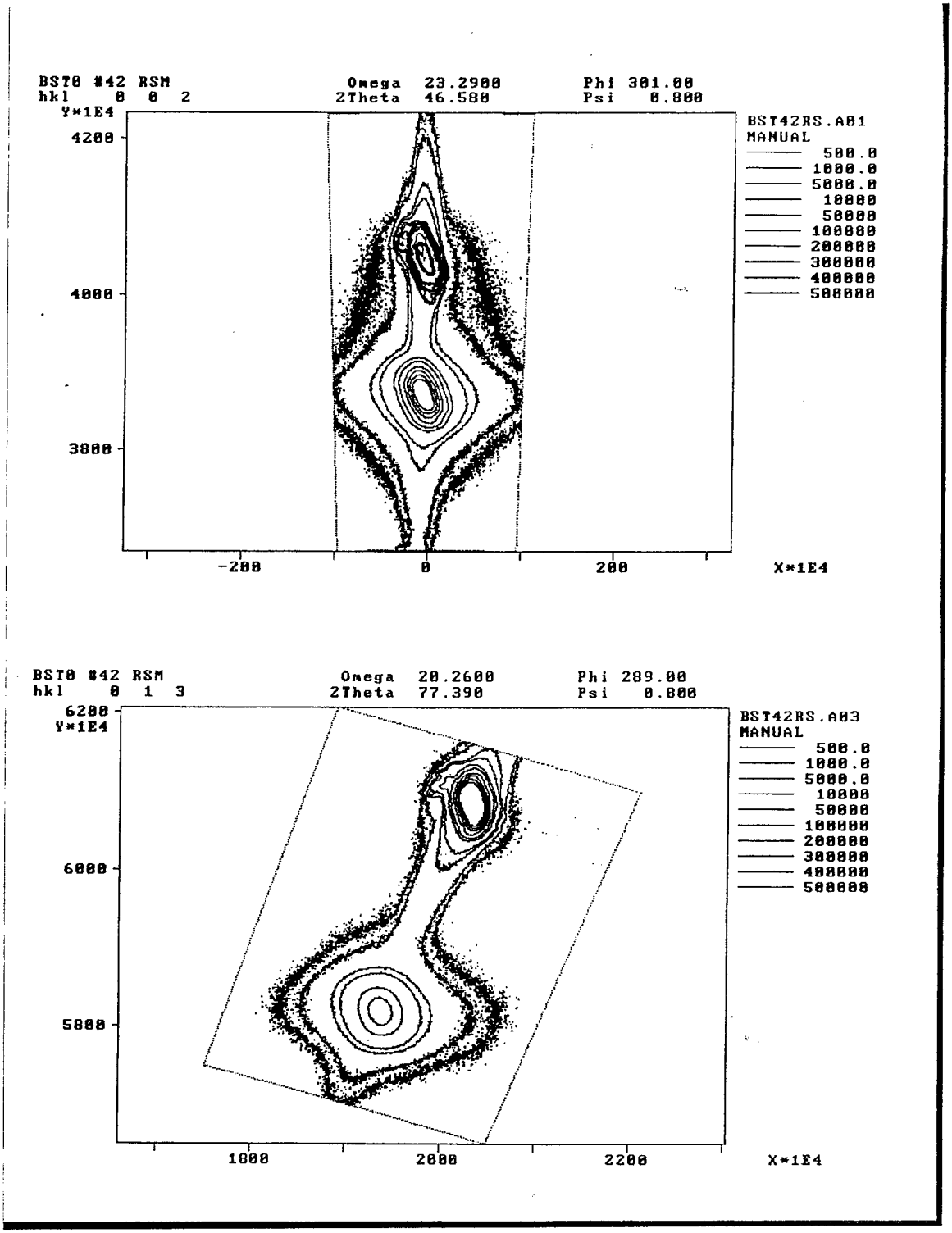

Fig. 4.2.1. 002 and 013 reciprocal space maps of (Mn,W) co-doped BSTO film

A comparative analysis of the results obtained with the (Mn,W) co-doped BSTO film with those of pristine and Mn-doped BSTO films, along with the dielectric properties of the films is shown in fig. 4.2.2.

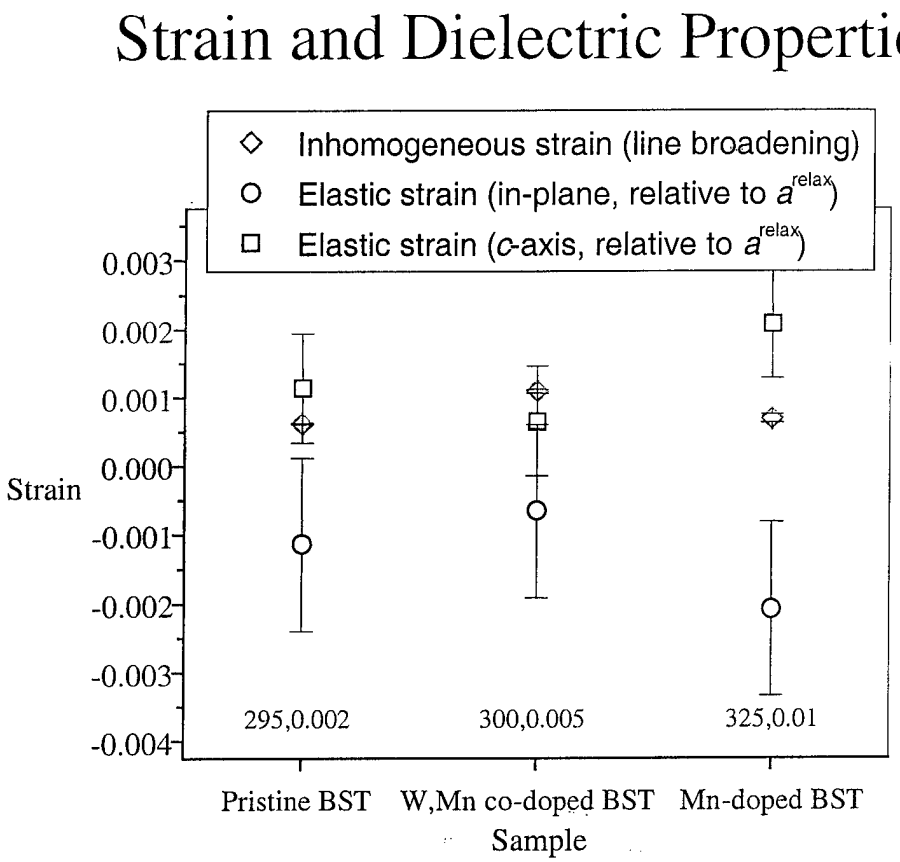

Fig. 4.2.2 Comparative strain results on pristine BSTO (left), (Mn,W) co-doped BSTO (middle) and Mn-doped BSTO (right) films. Also indicated are the observed Tc and dielectric loss.

Task 5. Materials Discovery Research

5.1. In this quarter, we finished the dielectric measurement of doped $SrTiO_3$. Similar to the cases of (Bi, Fe) and (Bi, Ga), the T_Cs of (Bi, Al) doped STO are likely to be increased due to doping. However, no tunabilities were observed on these samples.

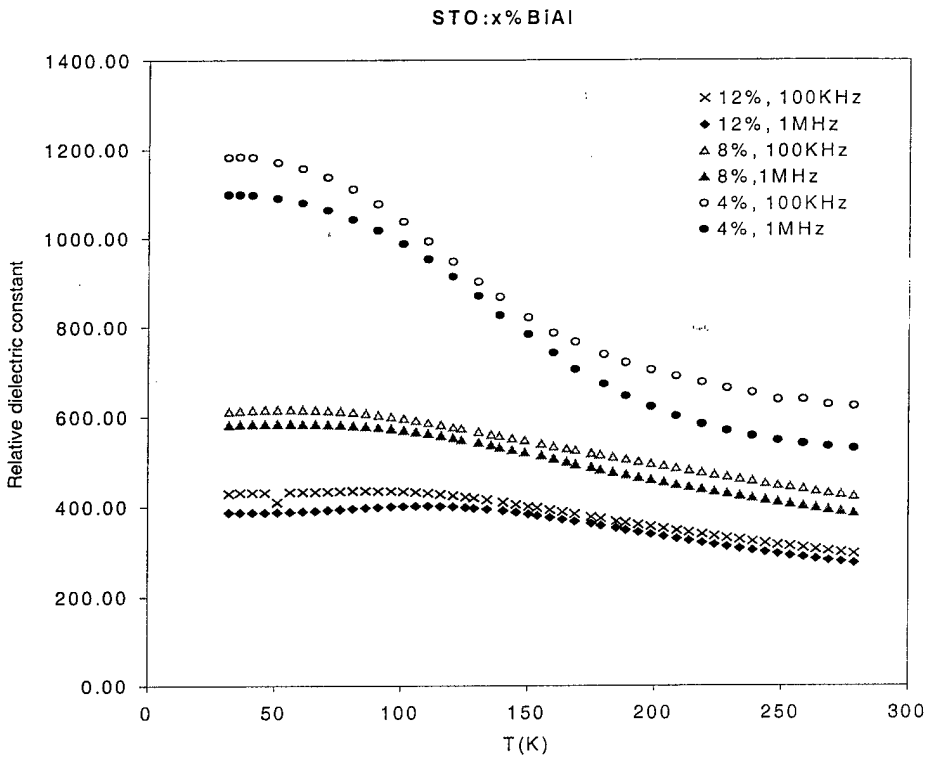

5.2. Prepare Compounds with $CaCu_3Ti_4O_{12}$ structure

<1> Sol-gel reaction have been tried to obtain better quality samples of $ACu_3Ti_4O_{12}$ (A=Ca, Cd, and Sr) and try to form $Sn_2Nb_2O_7$ and $Sn_2Ta_2O_7$ at low temperature.

$CaCu_3Ti_4O_{12}$ and $CdCu_3Ti_4O_{12}$ can be formed by this reaction while others failed. The dielectric measurements on $CaCu_3Ti_4O_{12}$ and $CdCu_3Ti_4O_{12}$ showed the same results as those measured on the samples prepared by solid state reaction.

<2> We also attempted to prepare $ACu_3Sn_4O_{12}$ and $ACu_3Hf_4O_{12}$ with A=Ca, Sr, Ba. However none of them can be prepared.

5.3 Oxynitride

In this quarter, we initiate the research on the dielectric properties on the oxynitride. The first attempt was to prepare a series compounds with the pyrochlore formula, $LnCaNb_2O_6N$ (Ln=La, Sm, Gd, Dy, Y). However none of them can be formed. The research on other oxynitride will be continued to the next quarter.

Task 7. Demonstration Device Design and Test

We spent considerable time in Q9 examining various bandpass filter structures to use as a testbed for our ferroelectric materials. We looked at microstrip designs, but decided that the proper design of bias chokes for each resonator to achieve acceptable performance was beyond the scope of this program. We settled on a coplanar end-coupled resonator scheme as the most practical, since it holds out the hope of applying a single bias to control the multipole device and its fabrication is relatively straightforward. We are in the process of designing these filters which will use a bilayer of ferroelectric material and HTS (either YBCO or TBCCO) and will report on their final design in Q10.

Frequency Agile Materials for Electronics

Quarterly Report 10

Date: 02/20/01

Period covered in this report: 10/1/00 through 12/31/00

Program Title: Novel Ferroelectric Materials for Satellite Communications

Contract # DABT63-98-C-0046

Performing Organization: DuPont Superconductivity

Subcontractor: University of Colorado at Boulder

Progress By Task

Task 2. Large Area Sputtered Film Manufacturing

In Q10, we continued our search for better ferroelectrics by looking at new materials and attempting to find connections between the microstructural and dielectric properties of known materials.

Third Generation Material: La, Fe co-doped BSTO

Our earlier work on bulk La, Fe co-doped BSTO showed promise for improving the ferroelectric figure of merit. During this quarter, we successfully deposited thin films of these new materials on 51 mm diameter Si and LAO substrates to complete milestone 2.F. We chose three compositions with different Ba:Sr ratios to find at least one whose T_c was in the appropriate range. The targets were 4% La, Fe doped BSTO x = 0.20, 0.39, 0.58. All three grew well on LAO, with very slight compressive strain (ranging between 0.1-0.3%). Figure 2.1 shows diffraction data for the x = 0.20 film, which is representative of the results of the others. No misorientation was observed and the rocking curves were fairly narrow. Our microfabrication facilities are still down; as soon as we can fabricate devices, we'll check the electrical properties of these films.

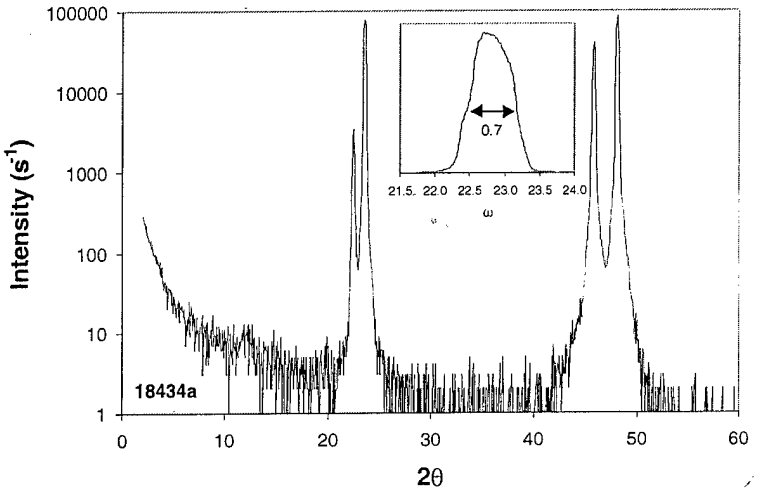

Figure 2.1. X-ray diffraction data for a 0.25 μm thick 4% La, Fe doped BSTO x = 0.20 film on LAO showing excellent (00l) orientation. Inset: FWHM of BSTO (002). Other compositions had similar quality data.

Synchrotron Measurements at the APS

Encouraged by our earlier results showing transmission diffraction measurements on our samples were possible using a synchrotron source, we returned to the DuPont-Northwestern-Dow Collaborative Access Team beamline at the Advanced Photon Source at Argonne National Labs to measure more samples: thin films from DuPont and the University of Colorado as well as bulk samples made at DuPont. Ferroelectricity is normally associated with a structural phase transition. This transition is seen in bulk samples. We wish to know whether the same effect is seen in thin film samples which show ferroelectric behavior. By taking transmission diffraction data as a function of sample temperature, we hope to extract the lattice parameters of the samples, which will give us evidence for a structural phase transition to compare with the electrical data already measured. We have not completed our analysis of the synchrotron data.

Inaccuracies of Conformal Mapping

In Q10 we also took a closer look at the differences between conformal mapping techniques and electromagnetic solvers for determining the dielectric properties of ferroelectric thin films. Many groups on the FAME program use the conformal mapping approximation for interdigitated capacitors to determine the intrinsic film permittivity. We have been using Sonnet™ (an EM field solver) to extract both the intrinsic permittivity **and** loss of our films from the measured capacitance and Q. In Figure 2.2 we compare the results of the conformal mapping technique (as implemented by Moeckly and Zhang at Conductus) with Sonnet™ for an interdigitated capacitor. The Sonnet™ calculations have been corrected for finite size effects (cellsize = 0) to give the most accurate answer possible.

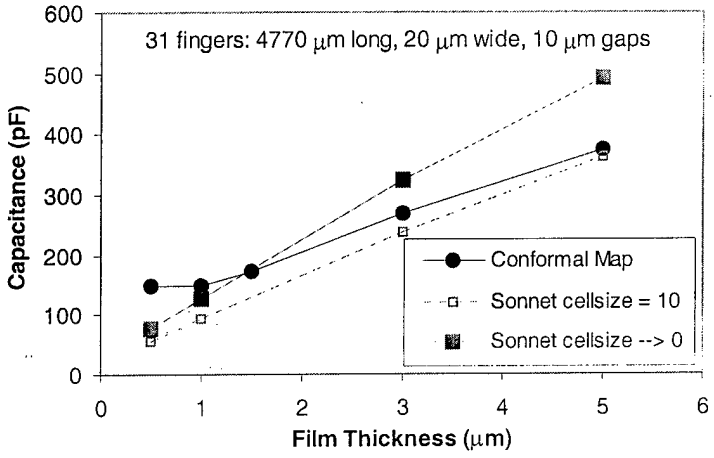

Figure 2.2. Calculated capacitance versus ferroelectric film thickness (with ε_r = 300) for an interdigital capacitor on LAO using conformal mapping and Sonnet™. Cellsize = 0 is the true value. The conformal mapping technique is insensitive to the properties of films less than 1 μm thick, precisely the region of interest .

The conformal mapping technique is not well suited for films below 1 μm thick: it predicts the same capacitance for a film of infinitesimal thickness as it does a film 1 μm thick! Additionally, without using an EM solver to analyze thin film data, the intrinsic loss cannot be obtained. The film loss is therefore underestimated, since the device loss is always higher than the film loss.

Task 3. Multilayer Film Development and Manufacturing

In Q10 we continued our efforts to develop a multilayer film process suitable for producing tunable microwave devices. We concentrated on the deposition of very thick BSTO films.

Thick Film Deposition

We deposited twelve BSTO06 films on both Si and LAO using two sputtering guns simultaneously to see how thick we could produce high quality ferroelectric material. Films ranged in thickness from 0.3-1.3 μm. Initial RBS results indicate some deviation from the target stoichiometry: in contrast to films produced from a single target, these films appear to be Ti deficient. However, x-ray diffractometry shows no evidence for second phase formation, as shown in Figure 3.1. These films also grow with low tetragonal distortion (< 0.1%), as might be expected for very thick films since the top layers do not feel any influence of the substrate. Optical micrographs of these films show no evidence for microcracking. The electrical characteristics of these films remain to be studied, but the microstructural results indicate that they will be useful for device fabrication.

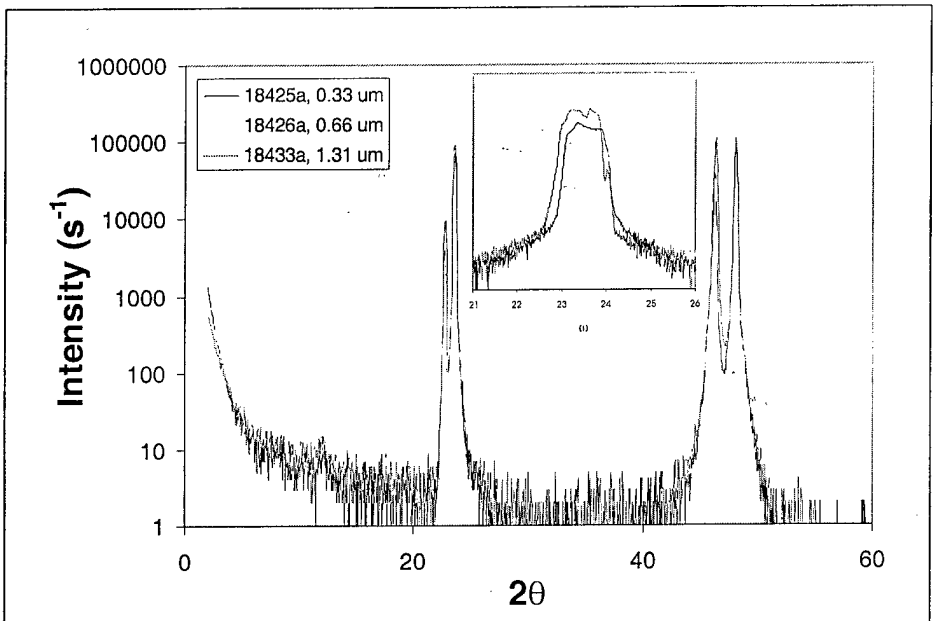

Figure 3.1. X-ray data for three BSTO06/LAO films of progressively greater thickness. There is no evidence for second phase formation. Inset: rocking curve width of the (002) reflection, log scale. The quality of the films is not very different between the thinnest and thickest.

Task 4. Exploratory Laser Ablation Processing (University of Colorado)

In this task, we report the growth of epitaxial films of cryogenic materials and their dielectric characterization. We also report the preliminary results of phase shifter dielectric studies on (Mg,Zr)-doped $Ba_{0.6}Sr_{0.4}TiO_3$ films, carried out in collaboration with NASA-Glenn.

4.1 Growth of epitaxial films

We carried out growth of films of Ba- and Ca- substituted $SrTiO_3$. Our earlier studies on $Ba_{0.1}Sr_{0.9}TiO_3$ epitaxial films showed that the Tc of the material was much above 77 K. Therefore, we chose a composition with less Ba content. The dielectric measurements on bulk material showed that the Tc is around 64 K. Presently, we have carried out growth of epitaxial films of $Ba_{0.05}Sr_{0.95}TiO_3$ (pristine and Mn-doped) and $Ca_{0.1}Sr_{0.9}TiO_3$.

Epitaxial films were grown on $LaAlO_3$ (LAO) single crystal substrates using pulsed laser deposition. The deposition was carried out in 300 mTorr of oxygen pressure and the substrate temperature was maintained at 700 °C. The films were post annealed in flowing oxygen at 950 °C for 6 h. Epitaxy of the films was confirmed by powder X-ray diffraction. A typical XRD pattern is shown in fig. 4.1.1.

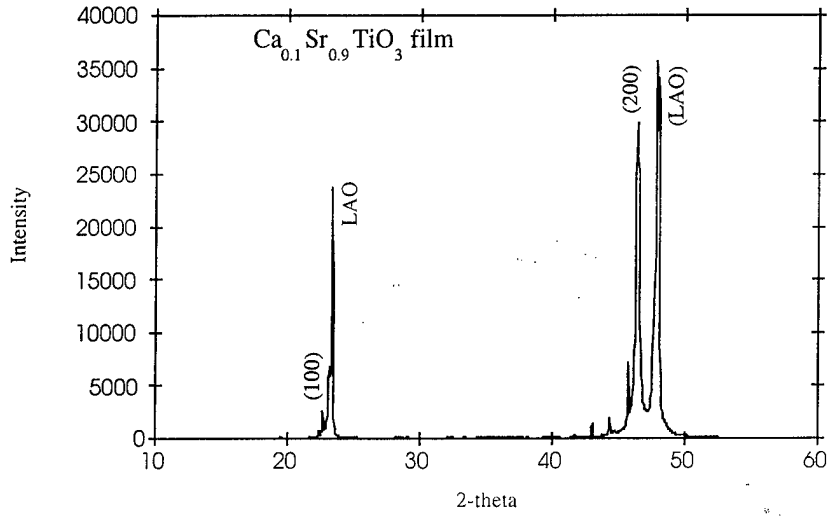

Figure 4.1.1. Powder XRD pattern of $Ca_{0.1}Sr_{0.9}TiO_3$ film. Presence of only (h00) reflections confirms epitaxy of the film

4.2. Dielectric measurements

The dielectric measurements were carried out using interdigitated capacitor configuration for the pristine and Mn-doped $Ba_{0.05}Sr_{0.95}TiO_3$ films. The capacitance and loss tangent were measured using HP 4192A LCR meter at 1MHz at low temperatures using closed cycle He refrigerator.

The results of dielectric measurements on $Ba_{0.05}Sr_{0.95}TiO_3$ epitaxial film are shown in fig. 4.2.1. The observed T_c is around 45 K, although the transition is very broad. This value of T_c is

lower than that observed for the bulk material. However, the dielectric loss for the bulk material showed a peak around 45 K The dielectric loss observed for the film is quite low (~0.003) and remained almost constant over the temperature range of measurements. These properties make this material promising if the tunability could be improved.

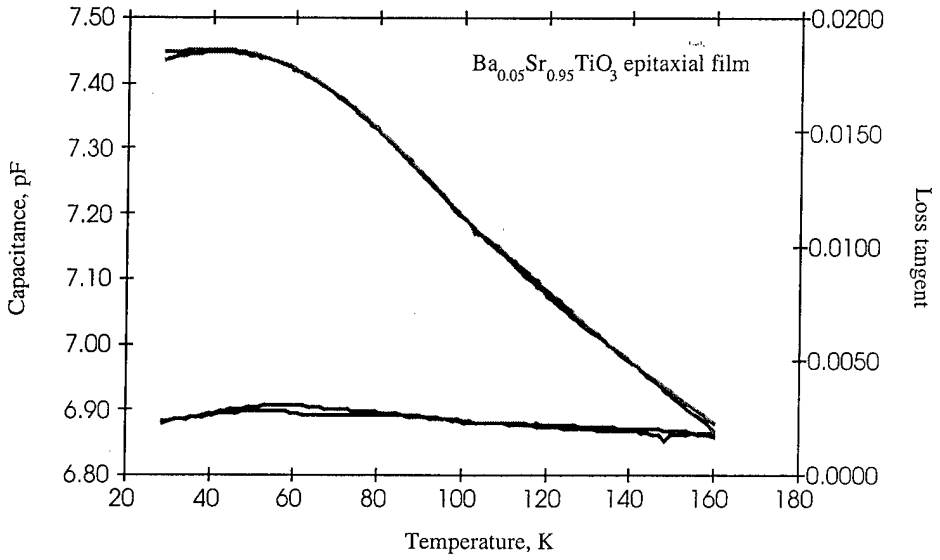

Figure 4.2.1. Dielectric properties of $Ba_{0.05}Sr_{0.95}TiO_3$ epitaxial film

Dielectric properties of $Ba_{0.05}Sr_{0.95}Ti_{0.98}Mn_{0.02}O_3$ film are shown in fig. 4.2.2. The ferroelectric-to-paraelectric transition was quite well-defined at around 115 K. This value of Tc is much higher than that observed for the pristine film. The dielectric loss also increased considerably compared the pristine film. This material, however, promise in terms of tunability. The effect of Mn doping on dielectric properties on $Ba_{0.05}Sr_{0.95}TiO_3$, such as increased Tc, higher dielectric loss and better tunability, is similar to that observed for the room temperature material, $Ba_{0.6}Sr_{0.4}TiO_3$.

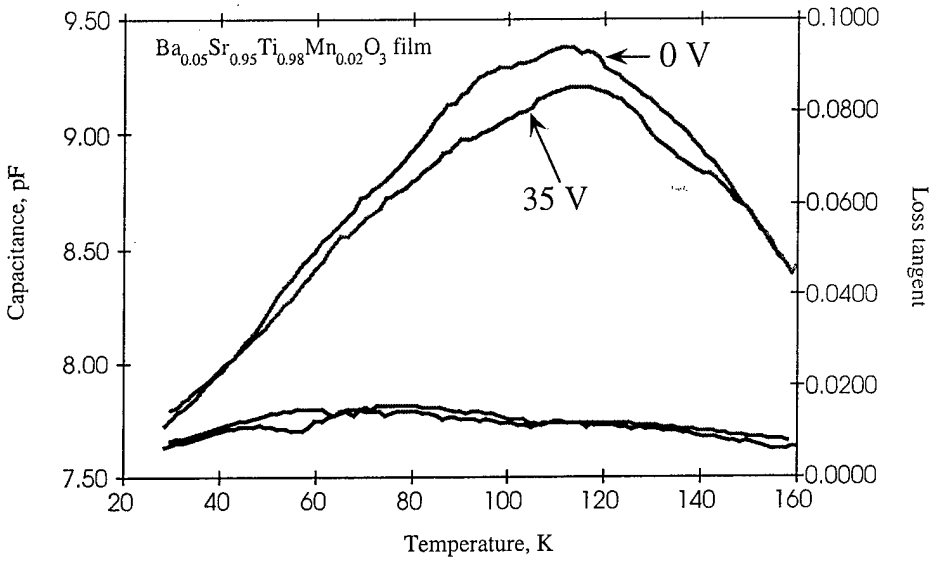

Figure 4.2.2. Dielectric properties of Mn-doped Ba0.05Sr0.95TiO3. The material shows promising tunability.

4.3. Phase shifter measurements

Preliminary data on the magnitude and phase corresponding to the coupled microstrip phase shifters (CMPS) fabricated with two $Ba_{0,6}Sr_{0.36}Mg_{0.04}Ti_{0.96}Zr_{0.04}O_3$ epitaxial films (designated A & B) were collected. It was found that the samples burnt out at relatively low voltages. The data for selective frequencies are shown below.

Sample	freq(GHz)	Loss(dB)	Phase Shift (deg)	Vmeas for PS	K (deg/dB)
A	18	-8.304	93.17	105.5	11.22
A	19	-7.766	80.51	105.5	10.37
B	17	-7.408	127.32	140	17.187
B	18	-6.784	105.21	140	15.508

The K values (defined as maximum phase shift/worst case loss) should be considered cautiously since the samples burnt out at relatively low voltages. The data obtained from the measurements are shown in fig. 4.3.1.

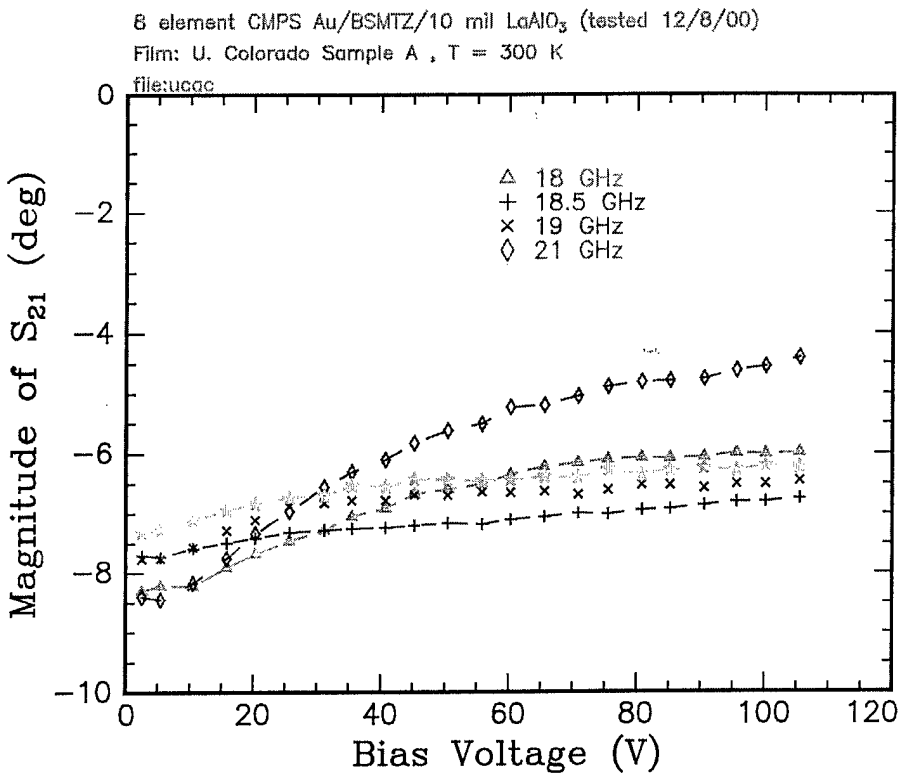

Figure 4.3.1. Data from coupled microstrip phase shifters fabricated using pulsed laser deposited $Ba_{0.6}Sr_{0.36}Mg_{0.04}Ti_{0.96}Zr_{0.04}O_3$ films.

Task 5 Materials Discovery Research

Effects of La, Fe and La, Al codoping on the dielectric properties of barium strontium titanate for tuning application have been studied. The doping shifts the Curie temperature to lower value and increases the tunability of the high Ba content samples at the cryogenic temperature. La and Al codoping also lower the loss tangent. Although the loss tangents of La, Fe codoped samples are lower at low temperature, they are higher at room temperature. The applied electric field shows little effect on the loss tangent. 6%La with 2%Al codoped $Ba_{0.6}Sr_{0.4}TiO_3$ shows the best figure of merit among the samples we prepared. Its tunability is comparable to that of the undoped $Ba_{0.2}Sr_{0.8}TiO_3$ at 80K

Studied materials:

1. 4%La4%Fe doped $Ba_{1-x}Sr_xTiO_3$ (x=0.2, 0.4, 0.6, 0.8)
2. 4%La4%Al doped $Ba_{1-x}Sr_xTiO_3$ (x=0.2, 0.4, 0.6, 0.8)
3. 6%La2%Al doped $Ba_{1-x}Sr_xTiO_3$ (x=0.1, 0.2, 0.3, 0.4)
4. pure BSTO for comparison

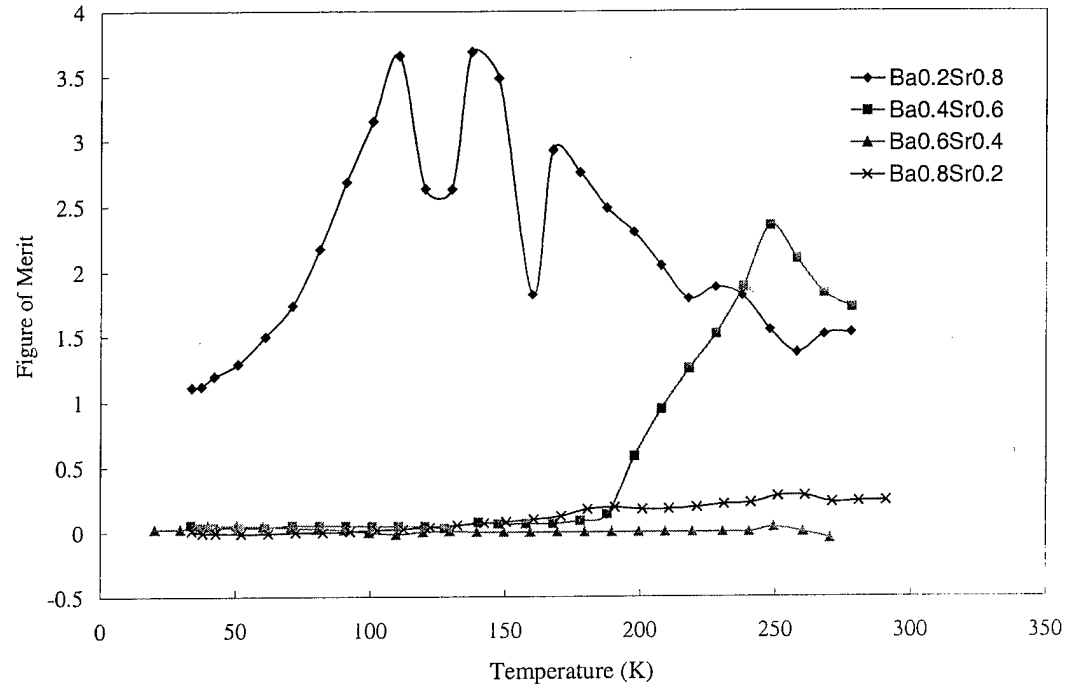

Figure 5.1. Figure of merit vs. temperature (@ 1MHz) for pure BSTO.

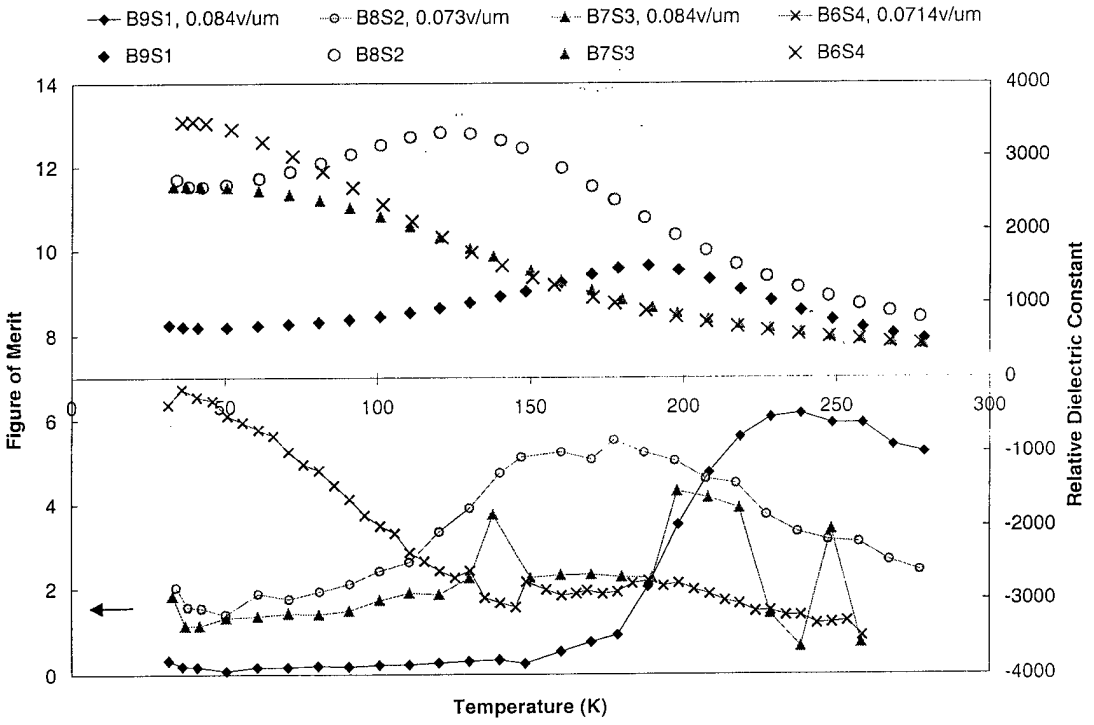

Figure 5.2. Figure of merit vs. temperature (@ 1MHz) for La, Fe doped BSTO.

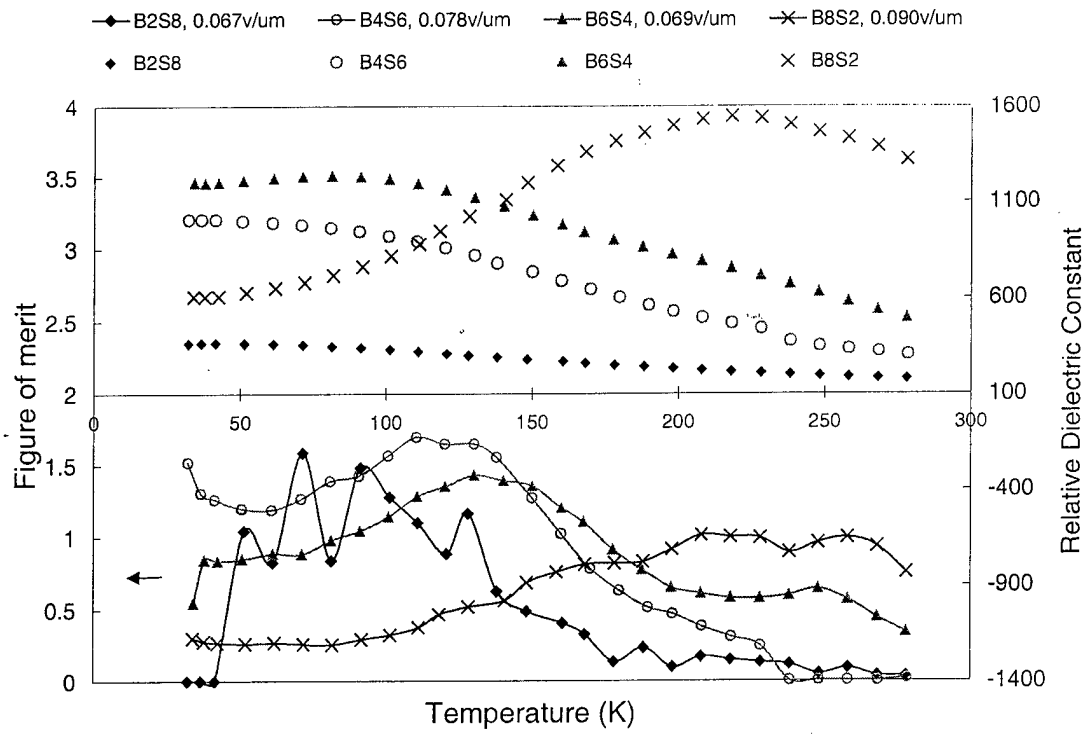

Figure 5.3. Figure of merit vs. temperature (@ 100 KHz) 6%La, 2%Al doped BSTO.

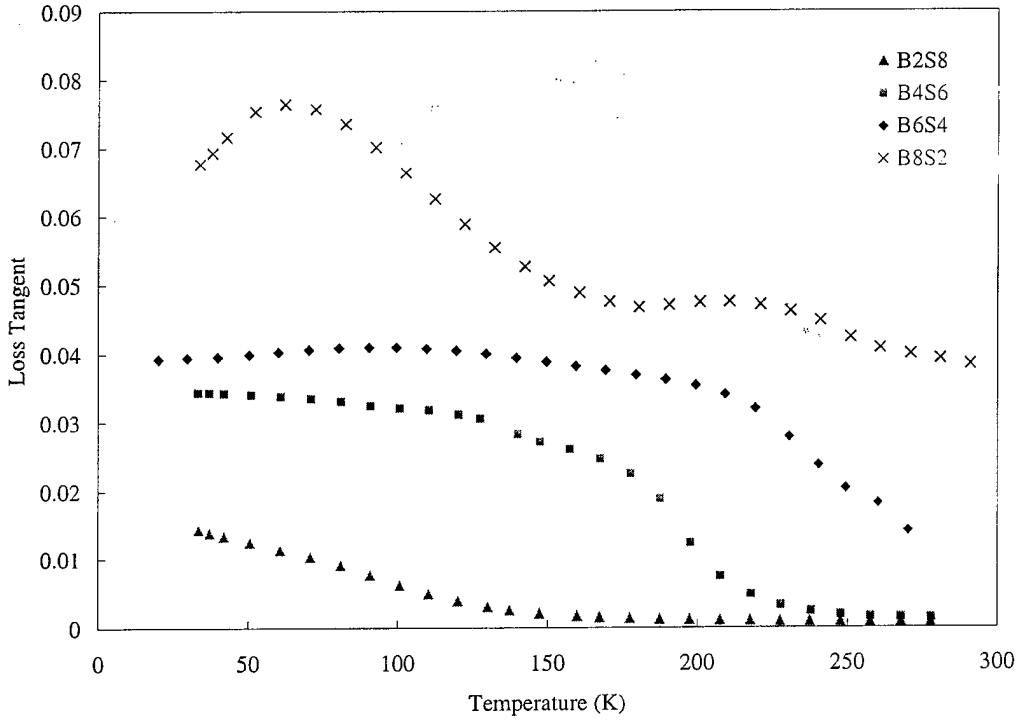

Figure 5.4. Loss tangents of pure BSTO at 1MHz.

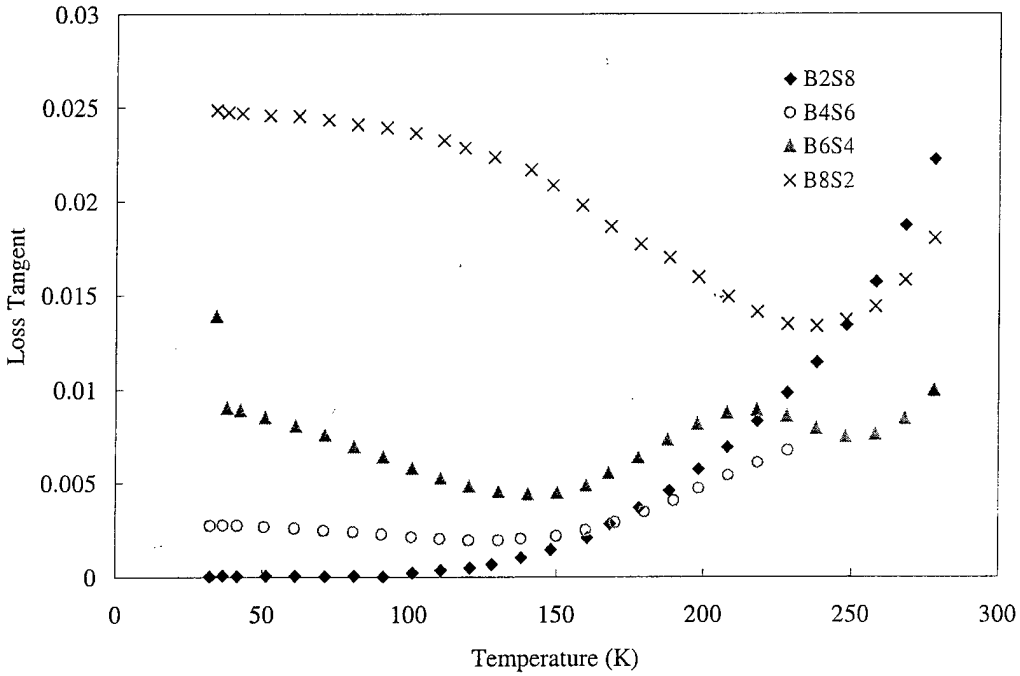

Figure 5.5. Loss tangents of La, Fe doped BSTO at 1MHz.

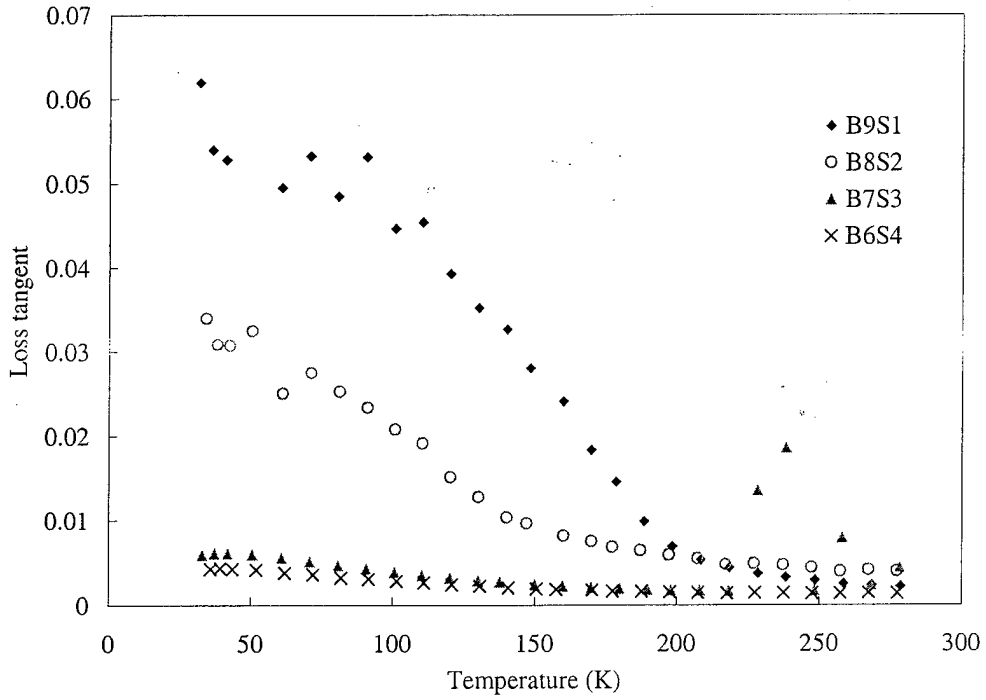

Figure 5.6. Loss tangents of 6%La, 2%Al doped (bottom) BSTO at 1MHz.

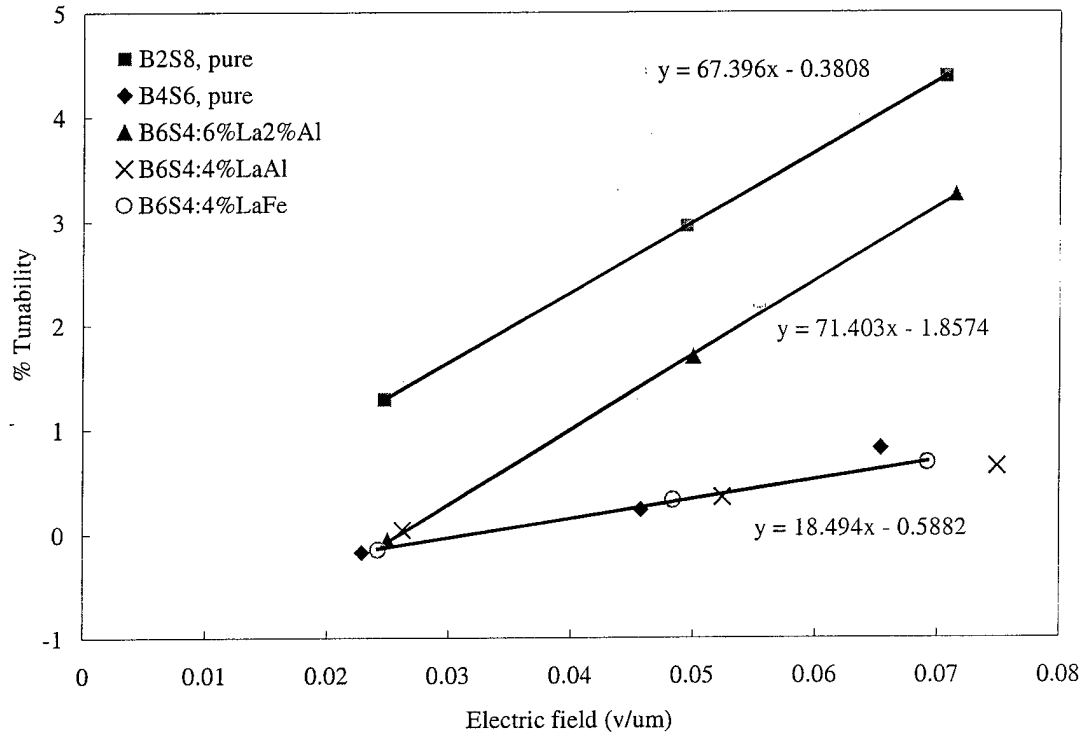

Figure 5.7. Tunability of selected doped and undoped BSTO

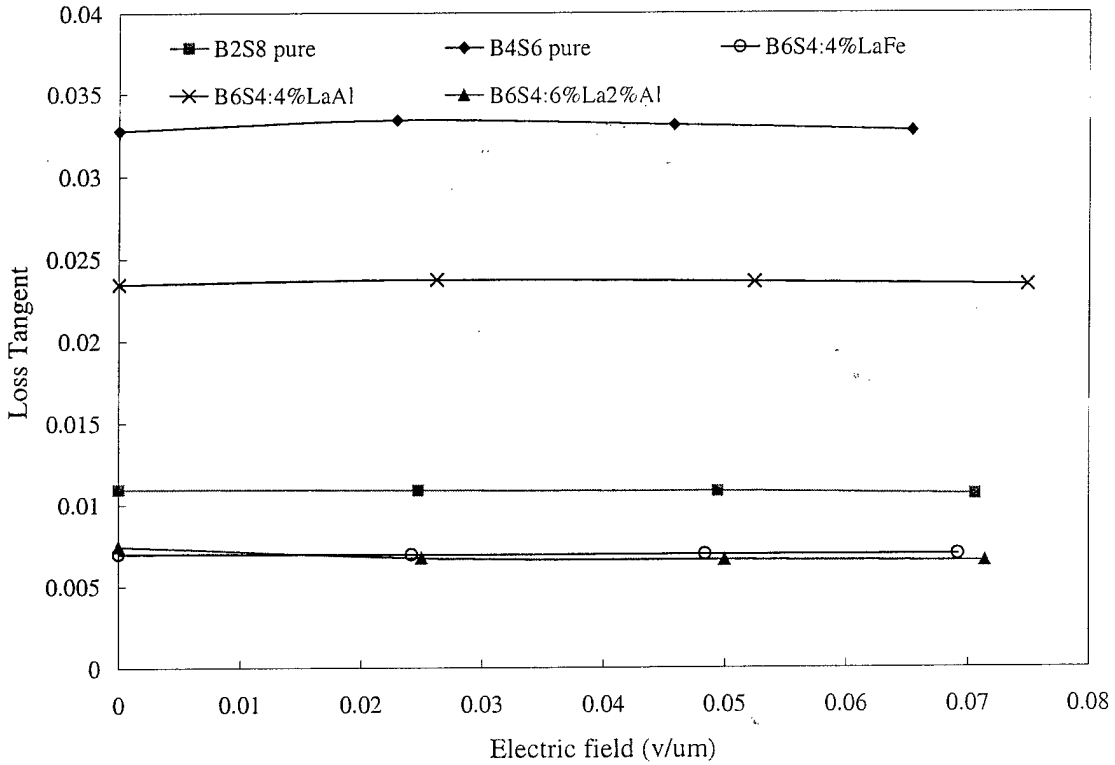

Figure 5.8. Electric field dependence of loss tangent

Table 5.1: Tunability of pure and doped BSTO at 80K (1 MHz).

	Tunability Equation
$Ba_{0.2}Sr_{0.8}TiO_3$	$T = 67.9 \times (E)$
$Ba_{0.4}Sr_{0.6}TiO_3$	$T = 23.3 \times (E)$
$Ba_{0.6}Sr_{0.4}TiO_3$: 6%La, 2%Al	$T = 71.4 \times (E)$
$Ba_{0.6}Sr_{0.4}TiO_3$: 4%La, 4%Al	$T = 12.3 \times (E)$
$Ba_{0.6}Sr_{0.4}TiO_3$: 4%La, 4%Fe	$T = 18.5 \times (E)$

Task 7. Demonstration Device Design and Test

We focussed much of our efforts in Q10 on designing a multipole coplanar filter, examining different design techniques, and attempting to improve the software tools available to us.

Semi-analytic 3 Pole Filter Design

We decided that the best geometry for a multipole bandpass filter using ferroelectrics was coplanar, with a narrow gap between the groundplanes and the center conductor to maximize the DC electric field that could be applied across the ferroelectric layer underneath the superconductor. This layout would also eliminate bias chokes to the different poles necessary in a microstrip design.

For our first design, we decided to use a technique described by Matthaei *et al.*[1] and more

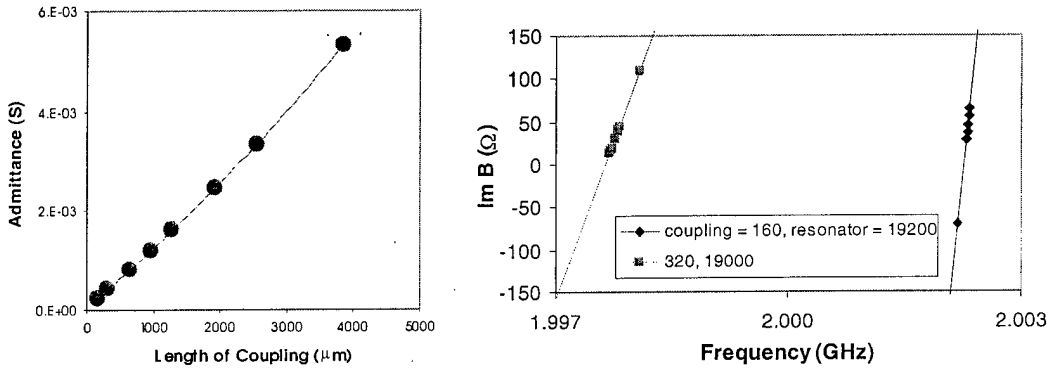

Figure 7.1.(a). Calculated admittance of coupling segment at 2 GHz versus its length; **(b)** calculated slope of resonators' admittance near 2 GHz; any change in coupling changes the resonant length at a particular frequency.

recently implemented by Kanaya *et al.*[2] Briefly, we start by finding the admittances of the coupling sections and the slope of the admittance of the resonators at the desired center frequency using Sonnet™. Sample calculations are shown in Figure 7.1.(a) & (b). Using these values in conjunction with the tabulated lumped element values obtained from network synthesis, the dimensions of the resonators and coupling segments can be calculated with analytic formulas.

To make the electromagnetic analyses tractable, we chose a simple two finger interdigital coupling scheme which was symmetric around the propagation axis. We also split the entire filter into separately analyzed sections, the results of which were joined at the last step to

---

[1] G. Matthaei, L. Young, E. M. T. Jones, *Microwave Filters, Impedance-matching Networks, and Coupling Structures*, Artech House (Norwood, MA), 1980.

[2] H. Kanaya, T. Shinto, K. Yoshida, T. Uchiyama, and Z. Wang, Miniaturized HTS Coplanar Waveguide Bandpass Filters with Highly Packed Meanderlines, to be published in the proceedings of the 2000 Applied Superconductivity Conference.

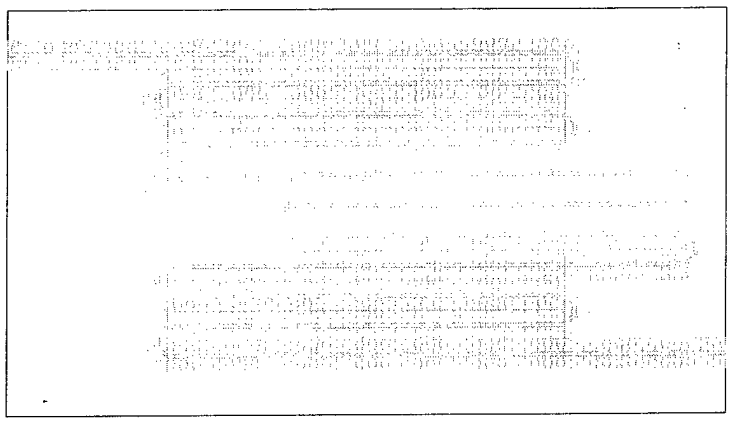

Figure 7.2. Layout of 3 pole coplanar bandpass filter centered at 2 GHz, 1% bandwidth. The chip size is 9.25 x 5.12 mm.

produce the filter S-parameters. The resulting filter layout and its calculated performance are shown below in Figures 7.2. and 7.3. The layout is compact and easy to fabricate, however, the calculated performance is not to our desired specifications. The design is nominally a Chebyshev bandpass filter centered at 2.0 GHz with 1% bandwidth and 0.01 dB ripple. The ripple is much larger than 0.01 dB! We believe this reflects the inadequacies of both our electromagnetic simulation and semi-analytic techniques: splitting the filter layout into smaller sections makes the electromagnetic calculations faster, but leads to some inaccuracies because long range coupling is no longer taken into account. Also, the analytic formulas for the filter design are approximations for very small bandwidths.

We are currently focussing on using more advanced filter synthesis tools (like Agilent's Advanced Design System) in conjunction with full electromagnetic analysis to produce a better filter design.

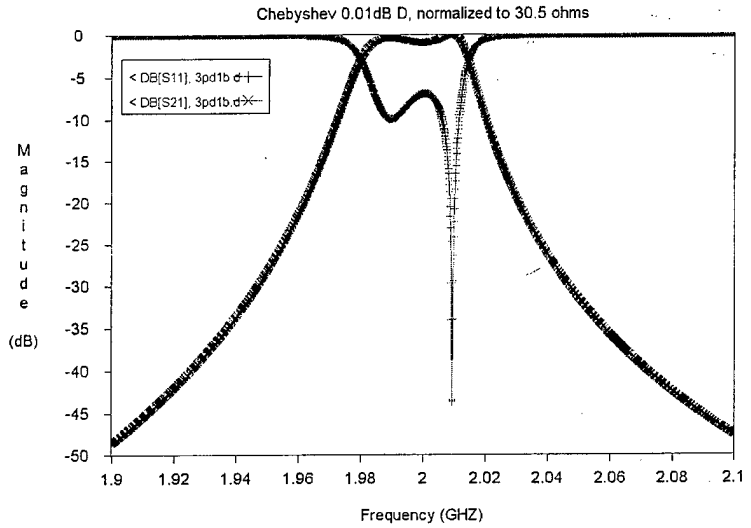

Figure 7.3. Performance of filter in Figure 7.2. Although the center frequency and bandwidth are good, the in band ripple is not to desired specifications. This reflects the limitations of the initial design technique.

Frequency Agile Materials for Electronics

Quarterly Report 11

Date: 06/21/01

Period covered in this report: 1/1/01 through 3/31/01

Program Title: Novel Ferroelectric Materials for Satellite Communications

Contract # DABT63-98-C-0046

Performing Organization: DuPont Superconductivity

Subcontractor: University of Colorado at Boulder

Progress By Task

Task 2. Large Area Sputtered Film Manufacturing & Task 3. Multilayer Film Development and Manufacturing

In Q11, we continued to investigate thicker films (> 0.5 μm) of BSTO for ultimate incorporation in a tunable filter. We deposited twelve additional BSTO films on 51 mm diameter Si and LAO substrates. We also deposited 350 nm of YBCO on top of two of the thicker films in order to look at the epitaxy and microwave properties of the superconducting layer.

Synchrotron Measurements at the APS

We began our analysis of the diffraction measurements made at the Advanced Photon Source at Argonne National Lab in Q10. We looked at the transmission diffraction patterns of a number of samples (both thin film and bulk) from 5-350 K. An example of this data is shown in

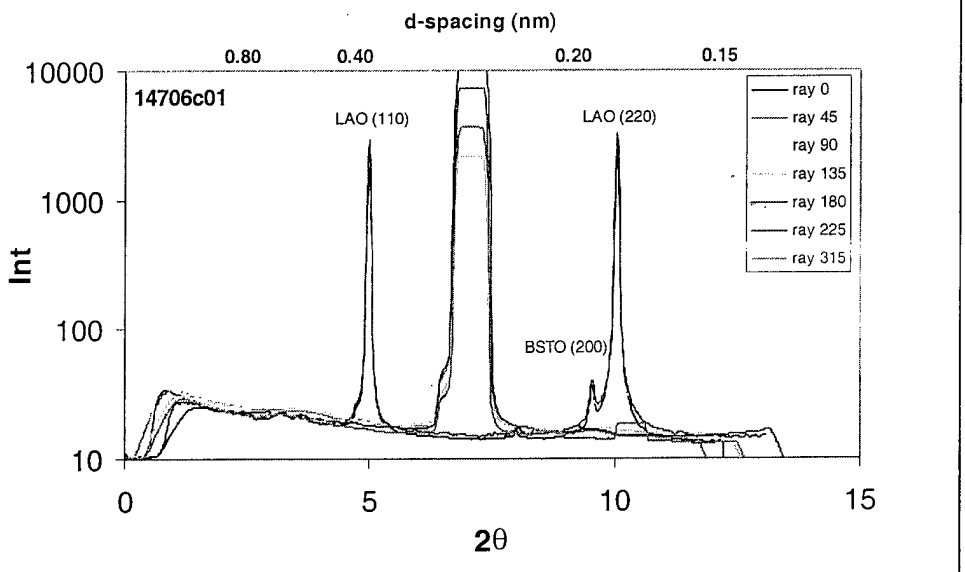

Figure 2-1. X-ray diffraction scans extracted from CCD data for a BSTO06 film on LAO at 300 K. Each trace is a slice through the image in a different direction.

figure 2-1. Using software developed at DuPont, we extracted peak positions and intensities. Analyses of bulk and thin film sample diffraction patterns indicate we do not have the resolution necessary to see small tetragonal distortions ($\Delta a/a < 10^{-3}$) in this initial dataset. Improvements in the image processing software are being pursued.

Thick Film Deposition

We continued our characterization of thicker BSTO films for use in tunable filters. AFM images (an example is shown in figure 2-2) show that these films are very smooth (R_{avg} ~ 1 nm). We resumed the deposition and characterization of YBCO films on top of these thick ferroelectric films in Q11. Earlier, we demonstrated that we could grow high quality YBCO on thinner (~ 200 nm) BSTO films. X-ray diffraction data on these two YBCO/BSTO bilayers show good epitaxy consistent with earlier results. In Q12, we will characterize the microwave properties of these films.

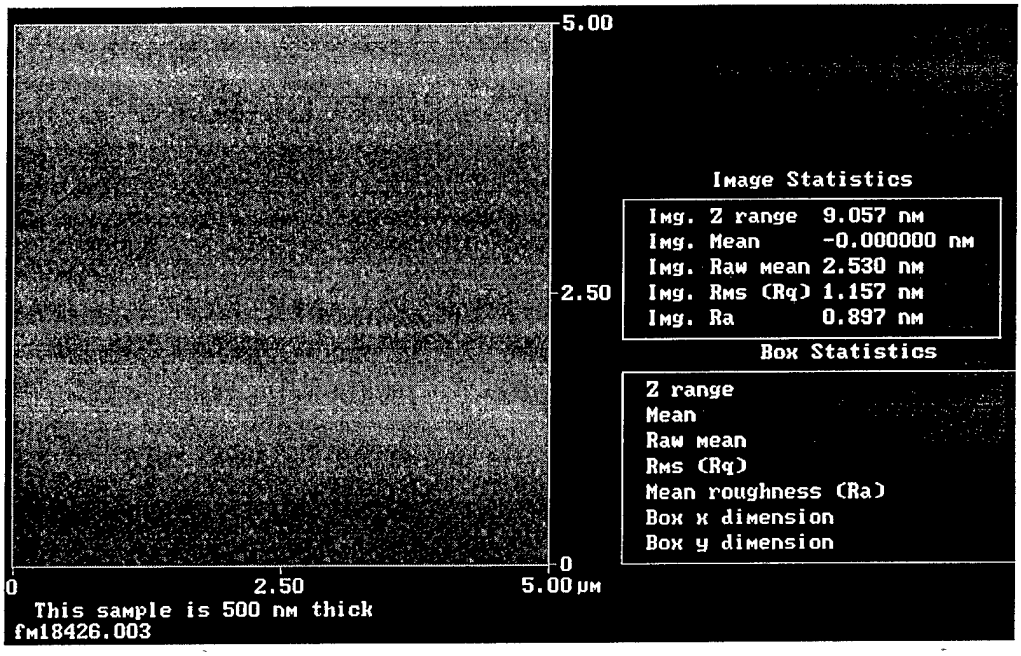

Figure 2-2. AFM image of 25 μm^2 area of 500 nm BSTO on LAO. The film is surprisingly smooth: R_{avg} = 0.9 nm. This bodes well for multilayer growth.

Task 4. Exploratory Laser Ablation Processing (University of Colorado)

In this quarterly progress, we report the preparation of some new bulk materials, deposition and dielectric characterization of epitaxial films of doped-$Ca_{0.05}Sr_{0.95}TiO_3$ materials. We also report preparation of Pechini solution for spin coating of Pb-doped STO materials.

4.1. Synthesis of $Ba_{0.05}Sr_{0.95}Ti_{1-x}M_xO_3$ and $Ca_{0.05}Sr_{0.95}Ti_{1-x}M_xO_3$ bulk materials

Bulk materials with the following compositions were prepared by standard solid state reaction.

$Ca_{0.05}Sr_{0.95}Ti_{0.98}M_{0.02}O_3$ (M = Mn, W, Fe)

$Ba_{0.05}Sr_{0.95}Ti_{0.98}M_{0.02}O_3$ (M = W, Fe)

The materials were sintered at 1550 °C to make high density targets for PLD. The phase formation of the materials was confirmed by powder X-ray diffraction. Typical powder XRD pattern for the composition, $Ca_{0.05}Sr_{0.95}Ti_{0.98}Mn_{0.02}O_3$ is shown in figure 4.1-1.

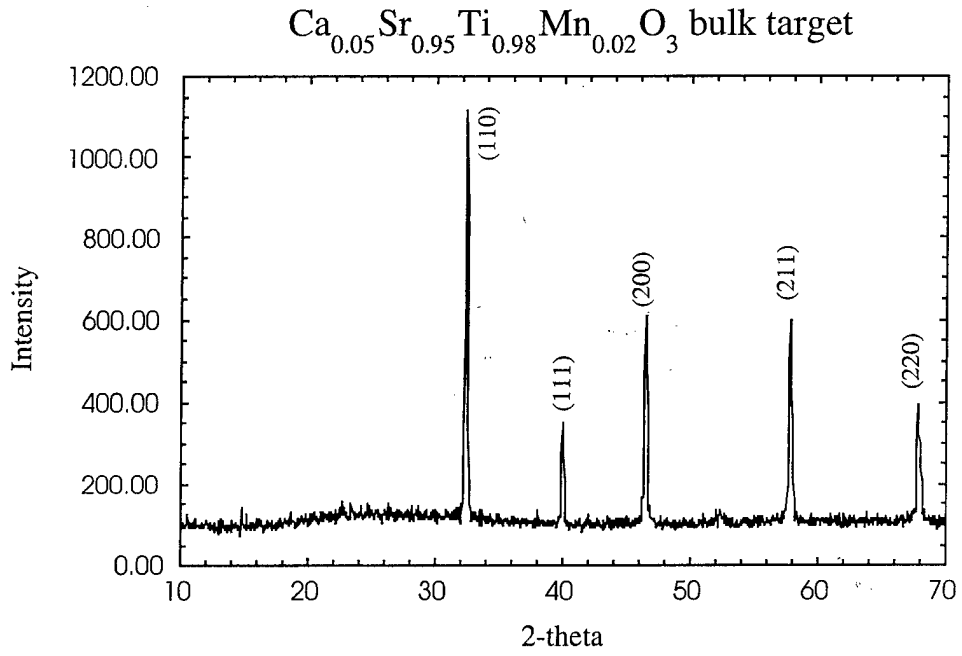

Fig. 4.1-1. Powder X-ray diffraction pattern of Mn- doped CSTO bulk material

We also prepared bulk materials of $K_{1-x}Li_xTaO_3$ (x = 0.1, 0.2, 0.5), since Li doping is reported to increase the Tc of the incipient ferroelectric material, $KTaO_3$. Structural and dielectric characterization of these materials is underway.

4.2. Deposition of doped- BSTO and CSTO films and their dielectric characterization.

Epitaxial films of doped- BSTO and CSTO materials were grown on $LaAlO_3$ (LAO) single crystal substrates using pulsed laser deposition. The deposition was carried out at reduced

oxygen partial pressure of 50 mTorr instead of the usual 300 mTorr, since it is reported that deposition at higher oxygen partial pressures results in interstitial Ti sites and consequently higher dielectric loss. The substrate temperature was maintained at 700 °C during deposition. The films were post-annealed in a controlled manner to compensate for the reduced oxygen content during deposition. The heating and cooling rates for the annealing treatment was maintained at 2 °C/min. The annealing was carried out in flowing oxygen at a final temperature of 950 °C for 6 h. Epitaxial nature of the annealed films was confirmed by the presence of only (h00) reflections in the powder X-ray diffraction patterns.

Dielectric measurements were carried out on doped CSTO epitaxial films using interdigitated capacitor configuration. The measurements were done at 1 MHz. The dielectric properties of $Ca_{0.05}Sr_{0.95}Ti_{0.98}Fe_{0.02}O_3$ epitaxial film are shown in figure 4.2-1. The film does not show a well-defined ferroelectric transition. While the material shows negligible tunability, the moderately low dielectric loss offers promise.

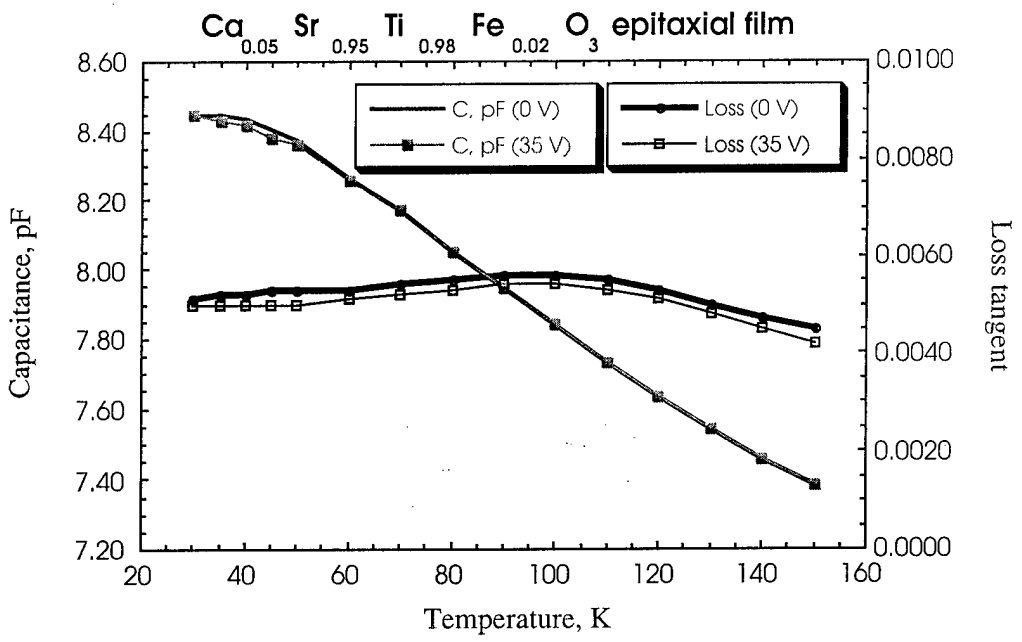

Figure 4.2-1 Capacitance and dielectric loss as a function of temperature for $Ca_{0.05}Sr_{0.95}Ti_{0.98}Fe_{0.02}O_3$ epitaxial film

Figure 4.2.2 shows the dielectric properties of $Ca_{0.05}Sr_{0.95}Ti_{0.98}Mn_{0.02}O_3$ epitaxial film. This material showed a Tc of ~60 K, with a broad ferroelectric-to-paraelectric transition. The tunability behavior of this material is promising and is better than the pristine material reported by us earlier. The observed loss was ~8 x 10^{-3} at 70 K.

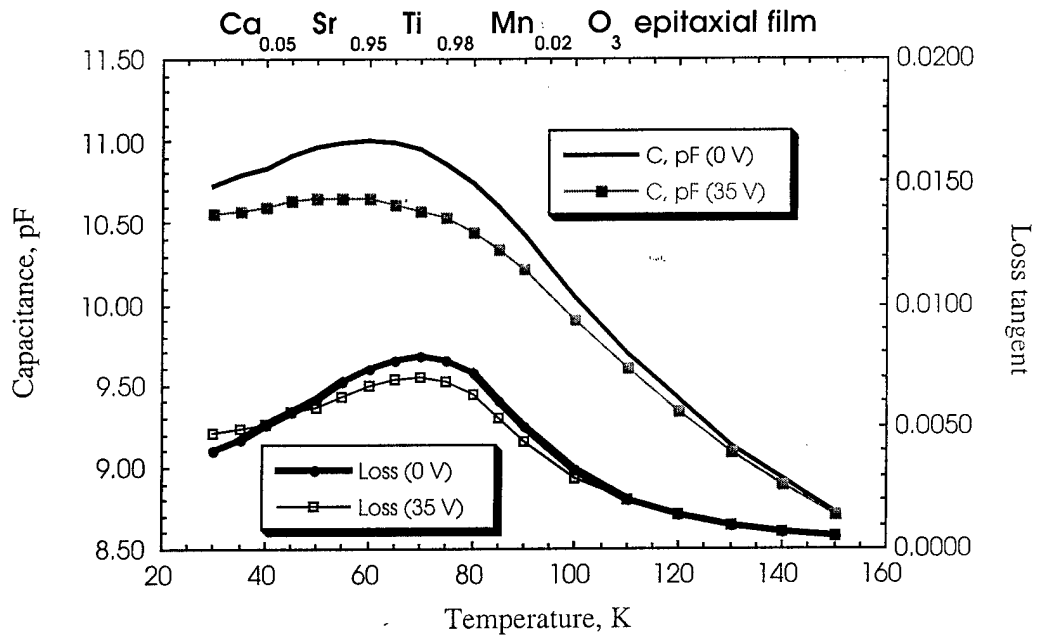

Fig. 4.2-2 Capacitance and loss tangent as a function of temperature of Mn-doped CSTO epitaxial thin film on LAO substrate

4.3 Preparation of Pechini solution for $(Sr,Pb)TiO_3$ films

Bulk samples of $(Sr,Pb)TiO_3$ were reported to exhibit very low dielectric loss. However, deposition of epitaxial films of this material using PLD is difficult owing to the high volatility of Pb. Spin coating from a Pechini solution is a viable method to grow films of this material without Pb-loss. We prepared a solution for titanium oxide using Titanium isopropoxide, ethylene glycol, and citric acid. To this, we added appropriate amounts of lead acetate and strontium acetate solutions to prepare precursor solutions for varying compositions of $(Sr,Pb)TiO_3$. These Pechini solutions will be used for spin coating of the materials.

Task 5. Materials Discovery Research

$KTaO_3$-$BaTiO_3$ solid solutions were prepared. Their tunability, T_C and loss properties at low temperature were measured. As shown in figures 5-1 and 5-2, it seems the T_C can be shifted due to the doping of $BaTiO_3$. However due to the relaxation, the peaks are too broad. No tunabilities are observed.

Studied materials:

$K_{1-x}Ba_xTa_{1-x}Ti_xO_3$: (x=0.01, 0.02, 0.04, 0.05, 0.06, 0.08, 0.1, 0.2)

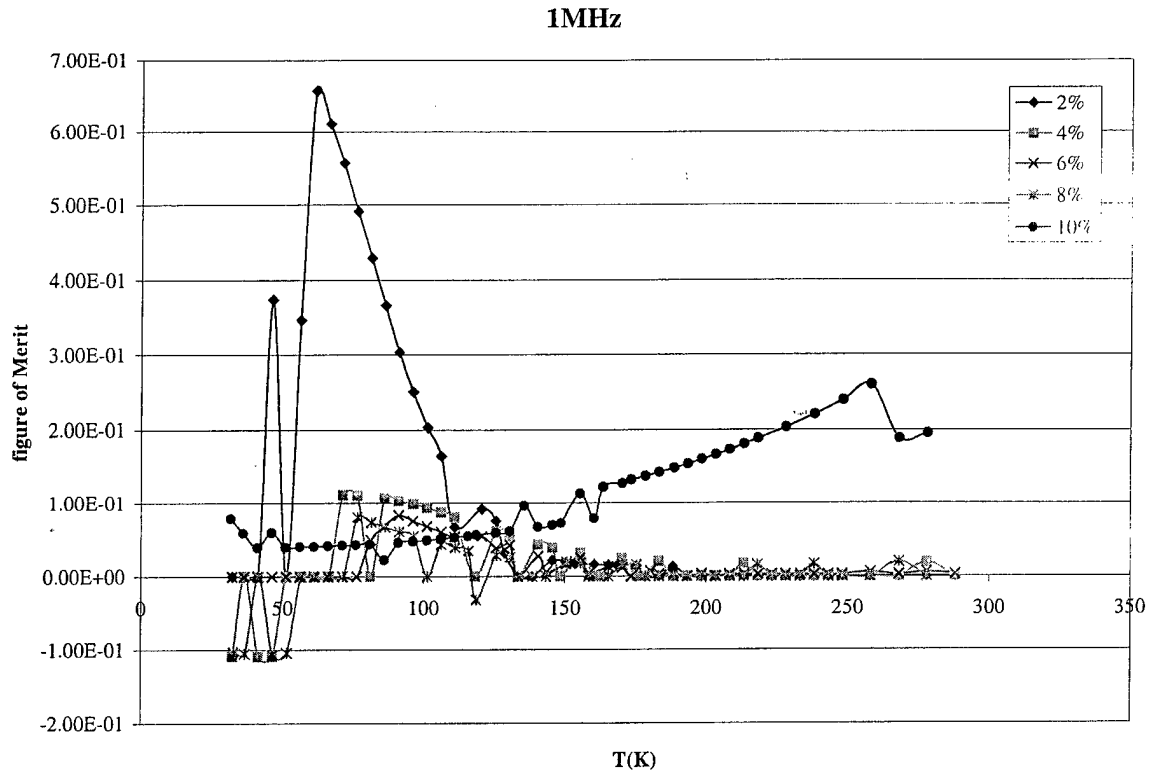

Figure 5-1: Figure of Merit of $KTaO_3$:x%$BaTiO_3$

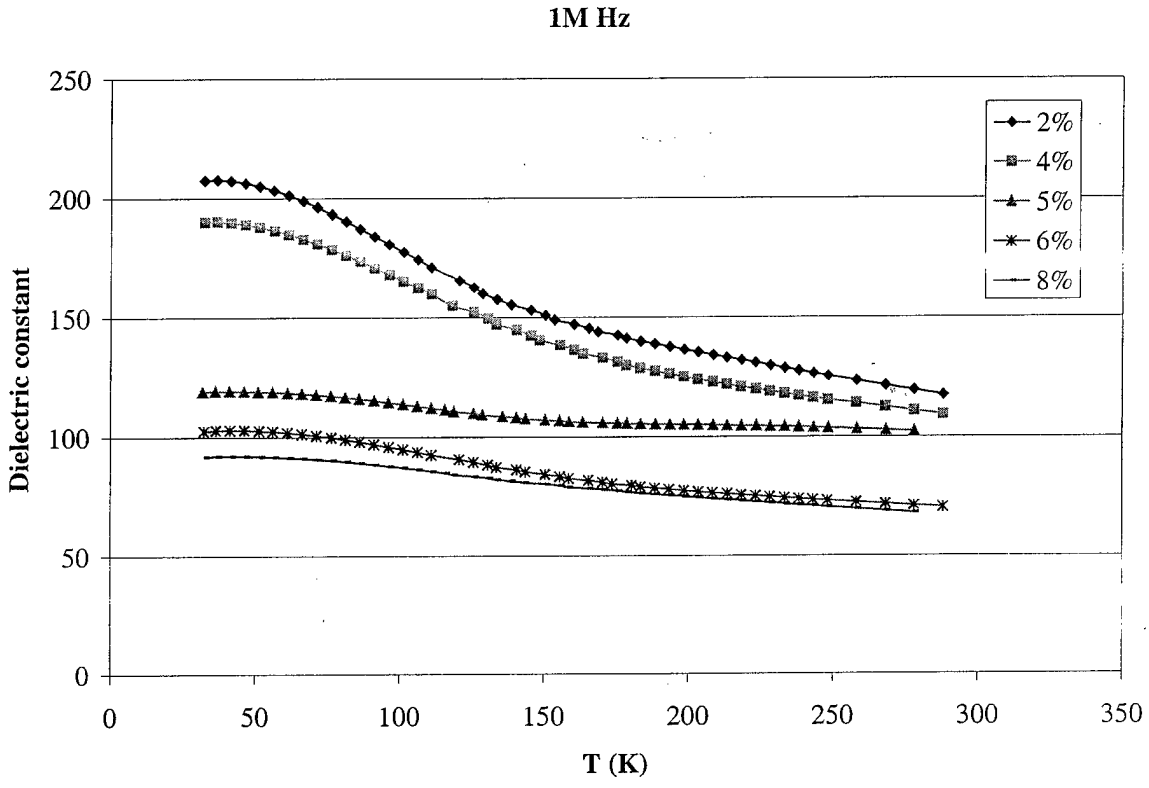

Figure 5-2: Dielectric constant of $KTaO_3$:x%$BaTiO_3$

Task 7. Demonstration Device Design and Test

In Q11, we concentrated much of our efforts on improving and understanding the design of tunable filters. We used the results of our full-wave EM solver, Sonnet, to make simple models for coplanar transmission line and coupling structures for use in Agilent's Advanced Design System. ADS allowed us to optimize and explore various multipole filter designs quickly and accurately. We designed and fabricated a photolithography mask set using a filter designed using ADS with input from Sonnet (see Figure 7-3) to complete milestone 7A. We also put a number of test resonators on the mask to verify and improve our modeling of tunable resonators. We will continue developing our designs through Q12. A number of issues remain. Our creation of models using Sonnet is not entirely accurate: for example, only nearest neighbor interactions are considered. This may necessitate further optimization of the full structure in Sonnet, which can be very slow. An additional area we would like to investigate is self-equalized tunable filters: heretofore, tunable multipole filters have generally required the adjustment of the individual poles or coupling between poles to maintain filter performance. We would like to move toward designs that require a minimum number of tuning inputs.

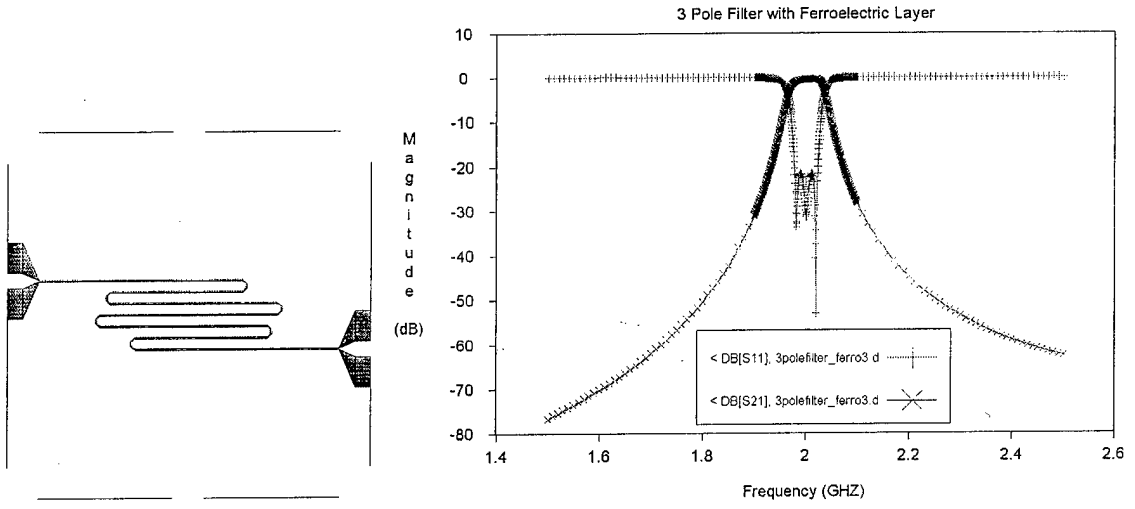

Figure 7-3. A 3 pole coplanar waveguide filter. Left: the layout of the filter on a 12 mm x 12 mm x 0.5 mm LAO chip. The filter is designed for a 1.5 μm thick ferroelectric layer with an average relative permittivity of 500. The dark areas indicate the gaps between the center conductor and the coplanar grounds. Right: the simulated performance (S_{11} and S_{21}) of the filter. The filter is centered at 2 GHz with a 3% bandwidth.

Frequency Agile Materials for Electronics

Quarterly Report 12

Date: 08/28/01

Period covered in this report: 4/1/01 through 7/31/01

Program Title: Novel Ferroelectric Materials for Satellite Communications

Contract # DABT63-98-C-0046

Performing Organization: DuPont Superconductivity

Subcontractor: University of Colorado at Boulder

Summary

Progress By Task

Task 1. Large Area Sputtered Film Manufacturing & Task 3. Multilayer Film Development and Manufacturing

In Q12, we finished our depositions of thick, large area, 3rd generation ferroelectric films to complete milestone 1.H. A total of eleven BSTO06 films between 400 and 900 nm thick were deposited on LAO substrates. We characterized some of them by AFM. We found that we could grow thick films of BSTO which were quite smooth (RMS roughness < 1.5 nm for a 0.87 μm thick film). We plot the increase in surface roughness versus film thickness for a number of recent BSTO06 films on LAO in Figure 1-1. Four thick BSTO films were sent to our colleagues at NIST for independent testing of the microwave losses; if time permits, the results will be included in the final report.

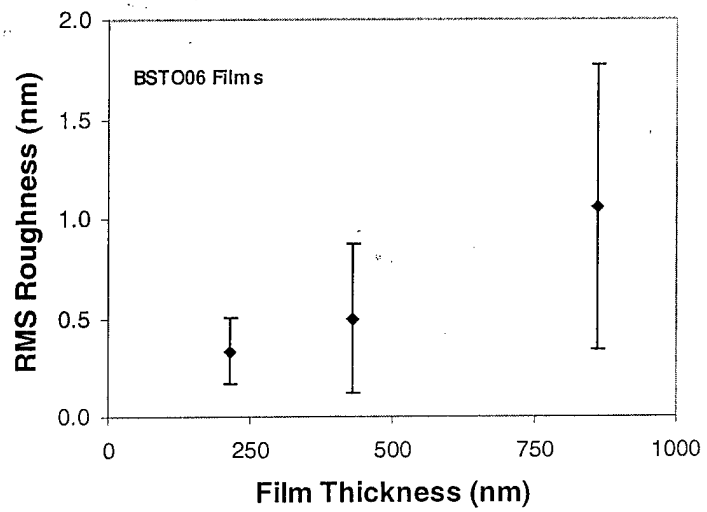

Figure 1-1. Increase of surface roughness of BSTO06 grown on LAO for different film thicknesses. We expect an increase in roughness with the film thickness, but these films are surprisingly smooth.

We deposited an additional 350 nm of YBCO on top of seven of the BSTO films to fabricate into

filters. The YBCO films were much rougher than the underlying BSTO, in some cases by an order of magnitude or more. We checked the superconducting quality of 2 of the YBCO/BSTO films prior to patterning: both had microwave surface resistances at 77 K and 10 GHz of less than 530 μΩ (DuPont's commercial specification is 600 μΩ). This is in line with our measurements of thinner YBCO/BSTO bilayers in Q4 and completes milestone 3.G.

Task 4. Exploratory Laser Ablation Processing (University of Colorado)

In this quarterly progress, we report the preparation of some new bulk and thin film materials, for strain-dielectric loss correlations. We also report our attempts to prepare films of Pb-doped strontium titanate by spin coating.

4.1. Synthesis of 5% Mn and Yb doped BSTO materials

Bulk materials of 5% Mn and Yb doped $Ba_{0.6}Sr_{0.4}TiO_3$ were prepared by standard solid state reaction. The materials were sintered at 1550 °C to make high density targets for PLD. The phase formation of the bulk materials was confirmed by powder X-ray diffraction. While the 5% Mn doped BSTO formed single phase, 5% Yb doping led to phase segregation of Yb_2O_3. This is probably because of the limited solid solubility of Yb_2O_3 in BSTO. The XRD patterns of the bulk materials are shown in figure 4.1-1 and 4.1-2.

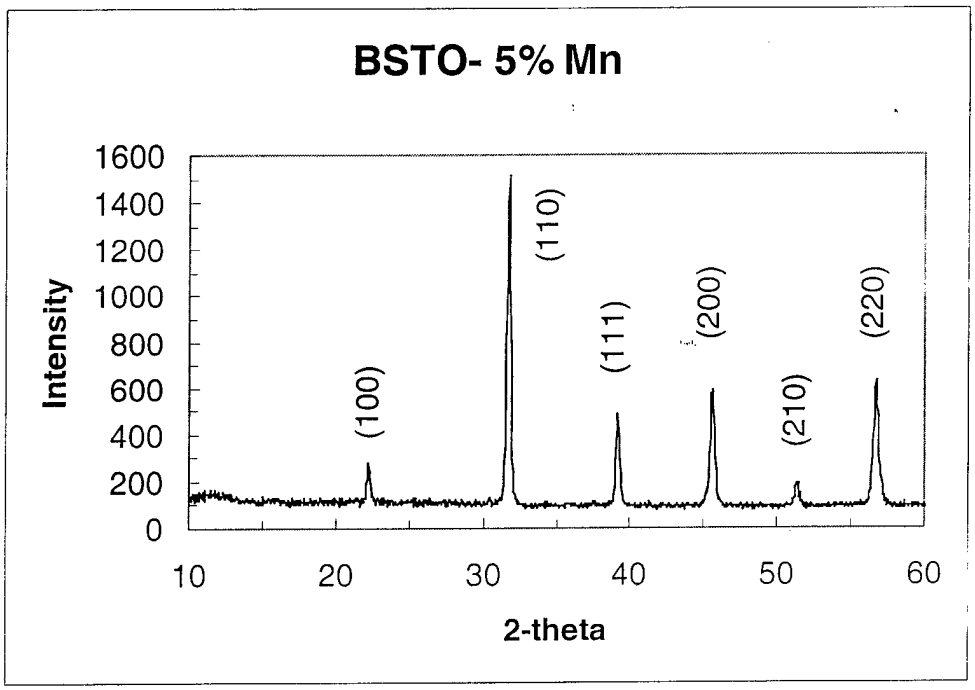

Fig. 4.1-1. Powder X-ray diffraction pattern of 5% Mn- doped BSTO bulk material

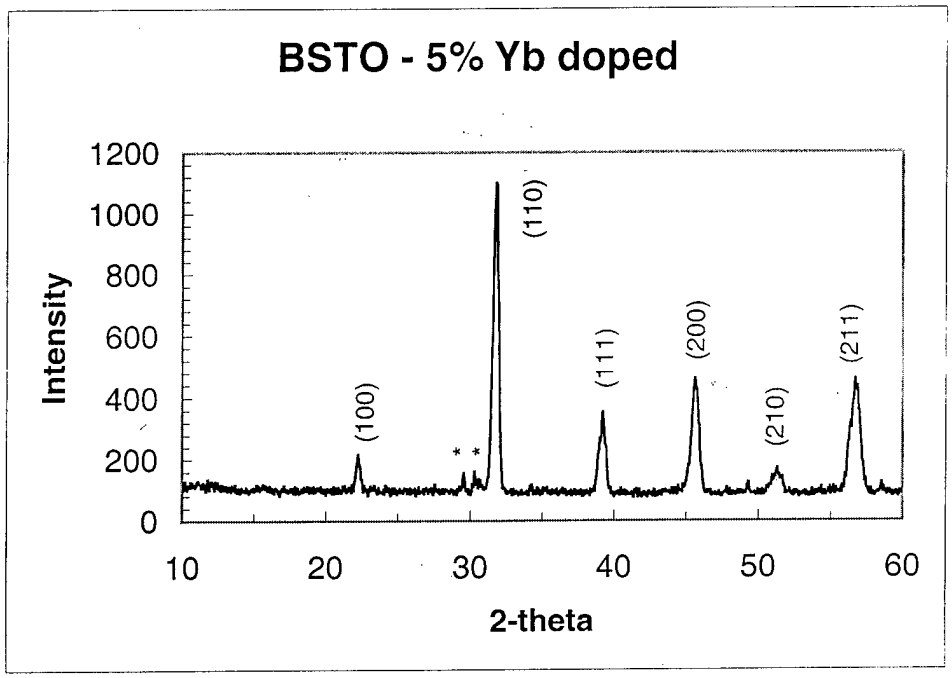

Fig. 4.1-2. Powder XRD pattern of 5% Yb doped BSTO bulk material. Asterisks show impurity peaks due to phase segregation.

4.2. Deposition of doped- BSTO films on MgO substrates

Our earlier studies on strain-dielectric loss correlations focused on LAO substrates, which induce a in-plane compressive stress on the film, due to the lattice mismatch. Presently, we deposited epitaxial films on MgO substrates, which induce a in-plane tensile stress on the ferroelectric films. This will provide insight on the effect of substrate-film interaction on dielectric properties.

Epitaxial films of the doped- BSTO materials were grown on MgO single crystal substrates with (100) orientation using pulsed laser deposition. The deposition was carried out at reduced oxygen partial pressure of 300 mTorr. The substrate temperature was maintained at 700 °C during deposition. The films were post-annealed in flowing oxygen content at 950 °C for 6 h, with the heating and cooling rates of 2 °C/min. Routine XRD measurements showed only (h00) reflections, confirming the overall epitaxy of the films. Further detailed XRD measurements to understand the effect of strain on dielectric properties are underway.

4.3 Preparation of $(Sr,Pb)TiO_3$ films by spin coating.

The spin coating of $(Sr,Pb)TiO_3$ films was carried out using the precursor solution containing the metal ions in the appropriate proportions. Three layers of coating was carried out on single crystalline LAO substrates, with intermittent drying at 150 °C. This was followed by a final annealing at a temperature of 700 °C (to avoid Pb evaporation). However, after the annealing treatment, the surface coverage of the film was found to be poor. Also, the thickness of the film was not uniform. Increasing the spin speed did not improve the film quality.

Task 7. Demonstration Device Design and Test

The seven films manufactured under tasks 1 and 3 were patterned into tunable ferroelectric/superconductor filters using the designs and masks developed in Q11 (one of the designs is shown in Figure 2). However, we were unable to test these filters because of time constraints. We will present the performance data in the final report (if time is available) to complete milestone 7.B.

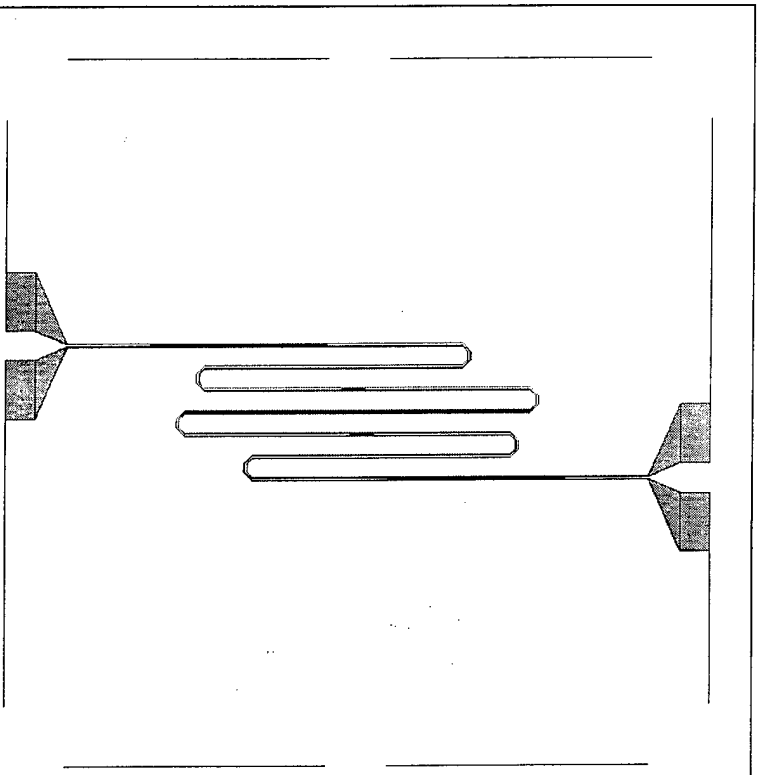

Figure 2. Mask layout of a 3 pole end-coupled coplanar waveguide bandpass filter. The dark areas are the gap in the superconducting layer.

REPORT DOCUMENTATION PAGE

Form Approved
OMB No. 0704-0188

1. AGENCY USE ONLY (Leave blank)	2. REPORT DATE	3. REPORT TYPE AND DATES COVERED
	11-Nov-02	Final Report; 7 May 1998 - 14 June 2001

4. TITLE AND SUBTITLE
Novel Ferroelectric Materials for Satellite Communications
Fequency Agile Materials for Electronics

5. FUNDING NUMBERS

6. AUTHOR(S)
Dr. Dean Face and Dr. James McCambridge

7. PERFORMING ORGANIZATION NAMES(S) AND ADDRESS(ES)
DuPont Superconductivity
Chestnut Run Plaza
P O Box 80708
Wilmington, DE 19880-0708

8. PERFORMING ORGANIZATION REPORT NUMBER
Final Report

9. SPONSORING / MONITORING AGENCY NAME(S) AND ADDRESS(ES)
DARPA
3701 N. Fairfax Drive
Arlington, VA 22203-1714

10. SPONSORING / MONITORING AGENCY REPORT NUMBER

11. SUPPLEMENTARY NOTES

12a. DISTRIBUTION / AVAILABILITY STATEMENT
Approved for Public Release; distribution is unlimited

12b. DISTRIBUTION CODE

13. ABSTRACT (Maximum 200 words)
This report summarizes work performed by DuPont and the University of Colorado.
The work was divided into seven key task areas: 1) Large Area Sputtered Film Manufacturing for Cryogenic Temperature, 2) Large Area Sputtered Film Manufacturing for Ambient Temperature, 3) Multilayer Film Development and Manufacturing, 4) Exploratory Laser Ablation Processing (University of Colorado), 5) Materials Discovery Research, 6) Rapid Test Method Development, and 7) Demonstration Device Design and Test.
A wide range of ferroelectric materials and related compounds were explored for use in tunable microwave devices: the best figures of merit of thin films for cryogenic operation were in the range 15-20; the best results for room temperature were lower, generally less than 5. Tunable filters and devices were designed which frequency tunabilities in the range of 5-10% with low Q.

14. SUBJECT TERMS	15. NUMBER OF PAGES
Large Area Sputtered Film Manufacturing, Multilayer film development Exploratory laser ablation, ferroelectric compounds, characterizing dielectric properties	148
	16. PRICE CODE N/A

17. SECURITY CLASSIFICATION OF REPORT	18. SECURITY CLASSIFICATION OF THIS PAGE	19. SECURITY CLASSIFICATION OF ABSTRACT	20. LIMITATION OF ABSTRACT
N/A	N/A	N/A	None